

1-1-2011

# Modeling of advanced fossil fuel power plants

Farshid Zabihian  
*Ryerson University*

Follow this and additional works at: <http://digitalcommons.ryerson.ca/dissertations>



Part of the [Mechanical Engineering Commons](#)

---

## Recommended Citation

Zabihian, Farshid, "Modeling of advanced fossil fuel power plants" (2011). *Theses and dissertations*. Paper 658.

This Dissertation is brought to you for free and open access by Digital Commons @ Ryerson. It has been accepted for inclusion in Theses and dissertations by an authorized administrator of Digital Commons @ Ryerson. For more information, please contact [bcameron@ryerson.ca](mailto:bcameron@ryerson.ca).

# **MODELING OF ADVANCED FOSSIL FUEL POWER PLANTS**

By

**Farshid Zabihian**

B.Sc., Amirkabir University of Technology, Tehran, Iran, 1996.

M.A.Sc., Iran University of Science and Technology, Tehran, Iran, 1998

**A dissertation  
presented to Ryerson University  
in partial fulfillment of the  
requirement for the degree of**

**Doctor of Philosophy**

**in the Program of  
Mechanical Engineering in**

Toronto, Ontario, Canada, 2011

**© Farshid Zabihian, 2011**

## **AUTHOR'S DECLARATION**

I hereby declare that I am the sole author of this thesis.

I authorize the Ryerson University to lend this thesis to other institutions or individuals for the purpose of scholarly research.

-----

Farshid Zabihian

I further authorize the Ryerson University to reproduce this thesis by photocopying or by other means, in total or in part, at the request of other institutions or individuals for the purpose of scholarly research.

-----

Farshid Zabihian

# **ABSTRACT**

## **Modeling of Advanced Fossil Fuel Power Plants**

Doctor of Philosophy, 2011

Farshid Zabihian

Mechanical Engineering

Ryerson University

The first part of this thesis deals with greenhouse gas (GHG) emissions from fossil fuel-fired power stations. The GHG emission estimation from fossil fuel power generation industry signifies that emissions from this industry can be significantly reduced by fuel switching and adaption of advanced power generation technologies.

In the second part of the thesis, steady-state models of some of the advanced fossil fuel power generation technologies are presented. The impacts of various parameters on the solid oxide fuel cell (SOFC) overpotentials and outputs are investigated. The detail analyses of operation of the hybrid SOFC-gas turbine (GT) cycle when fuelled with methane and syngas demonstrate that the efficiencies of the cycles with and without anode exhaust recirculation are close, but the specific power of the former is much higher. The parametric analysis of the performance of the hybrid SOFC-GT cycle indicates that increasing the system operating pressure and SOFC operating temperature and fuel utilization factor improves cycle efficiency, but the effects of the increasing SOFC current density and turbine inlet temperature are not favourable. The analysis of the operation of the system when fuelled with a wide range of fuel types demonstrates that the hybrid SOFC-GT cycle efficiency can be between 59% and 75%, depending on the inlet fuel type. Then, the system performance is investigated when methane as a reference fuel is replaced with various species that can be found in the fuel, i.e.,  $H_2$ ,  $CO_2$ ,  $CO$ , and  $N_2$ . The results point out that influence of various species can be significant and different for each case. The experimental

and numerical analyses of a biodiesel fuelled micro gas turbine indicate that fuel switching from petrodiesel to biodiesel can influence operational parameters of the system. The modeling results of gas turbine-based power plants signify that relatively simple models can predict plant performance with acceptable accuracy. The unique feature of these models is that they are developed based on similar assumptions and run at similar conditions; therefore, their results can be compared.

This work demonstrates that, although utilization of fossil fuels for power generation is inevitable, at least in the short- and mid-term future, it is possible and practical to carry out such utilization more efficiently and in an environmentally friendlier manner.

## ACKNOWLEDGEMENTS

First and foremost, my deepest thanks go to Dr. Alan Fung to whom I owe much of my achievements during the past five years. He was a major contributor to my professional activity in the course of my PhD studies. His contribution to this work by thoughtful advice, fruitful discussions, and helpful comments have benefited me greatly. His contribution to my career was not limited to academia. He helped my professional development by supporting my attendance in numerous conferences and events. I was able to get my professional engineering licence with his support. I got my first real teaching experience in Canada because of his recommendation and support. I can continue this list on and on but I just want to add one more case. Without his support I would not have been able to start my academic career even before finishing my PhD. He gave me courage to believe that I was ready for my career in academia. Beyond professional relationship, his support was invaluable in my personal life. He helped my family and me to peacefully go through early cultural shock after our landing in Canada. I will not forget the first day after our landing in Canada when he comforted my family and me on that stressful day by taking us a restaurant and giving us a ride to find an apartment. Thanks Alan for everything!

In addition, I am thankful to Dr. Wey Leong and Dr. David Naylor for their understanding and accepting the challenge of reviewing this dissertation in a tight schedule and for their valuable advice during my comprehensive exam toward my proposal. Further, thanks to Dr. Leong for his support by serving as my referee on various occasions. I learned a lot from Dr. Leong while I was working as his teaching assistant in my early years at Ryerson and during our joyful discussions. My special thanks to Dr. Feridun Hamdullahpur and Dr. Ali Lohi for being on the defence committee as external examiners.

My sincere appreciation goes to Mr. Fabio Schuler (P.Eng.), the manager of the Whitby cogeneration power plant for giving me the opportunity to visit the power plant and providing comprehensive explanation during the visit and particularly for providing all the data I required for my models with no hesitation.

My special thanks go to Dr. Hsiao-Wei Chiang, Professor and Director of the Power Mechanical Engineering Department at National Tsing Hua University, Taiwan, for his generous support during my stay in Taiwan during the summer of 2010. His hospitality provided me a very

pleasant time in Taiwan. He also generously gave me an opportunity to conduct research in his Turbogenerator Lab. I also would like to thank the members of his research team without whose help this research would not have been possible. These include Dr. Chih-Neng Hsu, Dr. Pai-Yi Wang, Mrs. Lee Cheng-Shin, Wu-Bin Huang, Chung-Wei Yang, Yu-Lung Chen, Hsing-Lei Yuan, David Chung, and many others.

I sincerely appreciate Dr. Robert (Bob) Roseberry for his significant help and patience in the past two years in revising this manuscript.

Further, I would like to thank many individuals who helped me during the past five years, including Dr. Murat Köksal, Associate Professor, Department of Mechanical Engineering, Hacettepe University, Turkey for his comments regarding our publications; Mr. Torgeir Suther; Dr. Ali Behdashti, Mrs. Hamid Ebrahim Pour, and Hosein Sharifi for providing operational data for gas turbine-based power plants; Dr. Ismet Ugursal, Professor, Department of Mechanical Engineering Dalhousie University; and Dr. Saeed Zolfaghari.

The financial support of the Ontario Government in the forms of Ontario Graduate Scholarship (OGS, 2009) and Graduate Scholarship in Science and Technology (OGSST, 2006, 2008, and 2010); MITACS Accelerate Internship Program (2010); Natural Sciences and Engineering Research Council (NSERC) through Dr. Fung's Discovery Grant and through the Summer Program in Taiwan scholarship (2010); the Department of Mechanical and Industrial Engineering, Ryerson University through Ryerson Graduate Scholarship (RGS, 2007), Ryerson Graduate Award (RGA, 2006 and 2007), and various travel grants (2007, 2009, and 2010); and Taiwan National Science Foundation (NSF) through the Summer Program in Taiwan scholarship (2010) are greatly appreciated.

Last but certainly not least, my deepest gratitude goes to my beloved family, my wife Niloufar and my little Diana. I have no doubt that without their support, encouragement, patience, and sacrifices I would not have been able to accomplish any of my achievements. They patiently accompanied and supported me during all the moments and ups and downs. Their love, presence, and support are my most valuable resource.

Farshid Zabihian, 2011

# TABLE OF CONTENTS

AUTHOR’S DECLARATION .....	II
ABSTRACT .....	III
ACKNOWLEDGEMENTS .....	V
TABLE OF CONTENTS.....	VII
LIST OF TABLES .....	XIX
NOMENCLATURE .....	XXIII
CHAPTER ONE .....	1
INTRODUCTION .....	1
1.1 OBJECTIVE OF THE THESIS.....	2
CHAPTER TWO .....	5
GREENHOUSE GAS EMISSIONS OF FOSSIL FUEL-FIRED POWER PLANTS: CURRENT STATUS AND REDUCTION POTENTIALS, CASE STUDY OF CANADA AND IRAN .....	5
2.1 INTRODUCTION .....	5
2.2 CAUSES OF THE GREENHOUSE EFFECT .....	8
2.3 CURRENT STATUS OF GHG EMISSIONS IN POWER GENERATION INDUSTRY.....	9
2.4 GHG EMISSION SOURCES AND ELECTRICITY GENERATION SECTOR .....	12
2.5 DIFFERENT METHODOLOGIES TO ESTIMATE GHG EMISSIONS.....	13
2.6 GHG EMISSIONS IN FOSSIL FUEL-FIRED POWER GENERATION INDUSTRY IN CANADA.....	18
2.7 GHG EMISSIONS IN IRANIAN FOSSIL FUEL-FIRED POWER GENERATION SECTOR .....	19
2.8 COMPARISON OF GHG EMISSIONS IN FOSSIL FUEL-FIRED POWER GENERATION IN CANADA AND IRAN .....	25
2.9 GHG EMISSION REDUCTION SCENARIOS.....	26
2.10 GHG EMISSION REDUCTION POTENTIALS IN CANADA .....	28
2.11 GHG EMISSION REDUCTION POTENTIALS IN IRAN .....	35
2.12 COMPARISON OF GHG EMISSION REDUCTION POTENTIALS IN CANADA AND IRAN.....	40



2.13	COST OF DIFFERENT SCENARIOS .....	42
2.14	CONCLUSION.....	45
FUEL CELL TECHNOLOGY AND HYBRID SOLID OXIDE FUEL CELL CYCLE MODELING .....		47
3.1	INTRODUCTION TO FUEL CELLS .....	47
3.1.1	FUEL CELL BASIC OPERATION.....	49
3.1.2	CONFIGURATION OF FUEL CELLS .....	50
3.1.3	BALANCE OF PLANT .....	51
3.1.4	FUEL CELL CLASSIFICATION .....	52
3.2	SOLID OXIDE FUEL CELLS .....	54
3.2.1	SOFC COMPONENTS.....	56
3.2.2	CONFIGURATIONS OF SOFCs.....	56
3.2.3	HYBRID SOFC CYCLES .....	59
3.2.4	BALANCE OF PLANT IN HYBRID SOFC SYSTEMS .....	61
3.2.4.1	FUEL PROCESSING .....	61
3.2.4.1.1	STEAM REFORMING.....	62
3.2.4.1.2	PARTIAL OXIDATION (POX).....	63
3.2.4.1.3	AUTOTHERMAL REFORMING.....	64
3.2.4.2	INTERNAL REFORMER.....	65
3.2.4.3	COMBUSTOR .....	65
3.2.4.4	HEAT EXCHANGERS .....	66
3.3	FUEL CELL MODELING.....	66
3.3.1	MODELING STEPS .....	67
3.4	REVIEW ON MODELING OF HYBRID SOLID OXIDE FUEL CELL SYSTEMS.....	71
3.4.1	HYBRID SOFC SYSTEMS MODELING CATEGORIZATION.....	72
3.4.2	EARLY MODELS.....	77
3.4.3	PARAMETRIC STUDIES .....	78
3.4.4	2-DIMENSIONAL MODELS.....	83
3.4.5	MODELS FOR COMPARISON OF CONFIGURATIONS .....	85
3.4.6	OPTIMIZATION .....	90

3.4.7	EXERGY ANALYSIS.....	91
3.4.8	CO <sub>2</sub> CAPTURE .....	93
3.4.9	FUEL FLEXIBILITY .....	95
3.4.10	DIFFERENT APPLICATIONS (NON-STATIONARY ELECTRICITY GENERATION) .....	97
3.4.11	TRANSIENT AND OFF-DESIGN CONDITION MODELING .....	98
3.4.12	THERMOECONOMIC STUDIES .....	104
3.4.13	COMBINATION OF MODELING AND EXPERIMENTAL WORK.....	105
3.5	CONCLUSION.....	106
CHAPTER FOUR.....		111
SOFC MODEL DEVELOPMENT.....		111
4.1	MODELING APPROACH .....	111
4.2	MODELING SOFTWARE .....	113
4.3	SOFC MODEL .....	114
4.3.1	ASSUMPTIONS .....	114
4.3.2	MATHEMATICAL FORMULATIONS OF SOFC.....	115
4.3.2.1	SOFC OUTLET COMPOSITION .....	116
4.3.2.1.1	FUEL REFORMING.....	116
4.3.2.1.2	ELECTROCHEMICAL REACTIONS.....	117
4.3.2.1.3	MATHEMATICAL FORMULATION TO DETERMINE SOFC EXHAUST COMPOSITION.....	119
4.3.2.2	ESTIMATION OF SOFC OUTPUT POWER.....	124
4.3.2.2.1	REVERSIBLE OPEN CIRCUIT POTENTIAL DIFFERENCE.....	124
4.3.2.2.2	ACTUAL POTENTIAL DIFFERENCE.....	126
4.3.2.2.3	LOSSES DUE TO INTERNAL CURRENT AND FUEL CROSSOVER.....	127
4.3.2.2.4	ACTIVATION LOSSES.....	128
4.3.2.2.5	OHMIC LOSSES.....	134
4.3.2.2.6	CONCENTRATION LOSSES.....	137
4.3.2.3	OUTPUT POWER OF THE SOFC .....	142
4.3.2.4	CALCULATION OF THE HEAT OUTPUT FROM THE STACK AND OUTLET TEMPERATURE.....	143
4.3.3	MODEL CONSTANTS AND PARAMETERS.....	144
4.3.4	VALIDATION .....	147

4.4	HYBRID CYCLE MODEL .....	149
4.4.1	SYSTEM CONFIGURATIONS .....	151
4.4.2	INPUT AND OUTPUT PARAMETERS .....	157
4.5	CONCLUSION AND FUTURE WORK .....	160
CHAPTER FIVE .....		163
PERFORMANCE OF METHANE FUELLED HYBRID SOFC-GT CYCLE .....		163
5.1	VARIATION OF OPERATIONAL PARAMETERS THROUGHOUT THE CYCLE IN THE METHANE FUELLED HYBRID SOFC-GT SYSTEM.....	163
5.2	PARAMETRIC ANALYSIS OF METHANE FUELLED HYBRID SOFC-GT CYCLE.....	172
5.2.1	IMPACTS OF SYSTEM OPERATING PRESSURE AND SOFC OPERATING TEMPERATURE .....	173
5.2.2	IMPACTS OF CURRENT DENSITY AND FUEL UTILIZATION FACTOR .....	178
5.2.3	IMPACTS OF TIT AND SOFC OPERATING TEMPERATURE.....	182
5.2.4	IMPACTS OF ISENTROPIC EFFICIENCY OF GT AND ISENTROPIC EFFICIENCY OF AIR COMPRESSOR.....	182
5.3	CONCLUSION AND FUTURE WORK .....	187
CHAPTER SIX.....		189
EFFECTS OF INLET FUEL TYPE AND COMPOSITION ON HYBRID SOFC-GT CYCLE PERFORMANCE .....		189
6.1	VARIATION OF OPERATING PARAMETERS OF SYNGAS FUELLED HYBRID SOFC-GT CYCLE.....	190
6.2	PERFORMANCE OF HYBRID SOFC-GT CYCLE FUELLED WITH VARIOUS FUELS .....	198
6.3	EFFECTS OF FUEL COMPOSITION ON PERFORMANCE OF HYBRID SOFC-GT CYCLE.....	204
6.3.1	REFERENCE CASE .....	205
6.3.2	EFFECT OF HYDROGEN CONCENTRATION IN INLET FUEL ON CYCLE PERFORMANCE.....	205
6.3.2.1	HYDROGEN CONCENTRATION AT VARIOUS STREAMS .....	206
6.3.2.2	OUTPUT POWER.....	207
6.3.2.3	SPECIFIC WORK .....	212
6.3.2.4	EFFICIENCY .....	215
6.3.2.5	SOFC-TO-GT WORK RATIO .....	216

6.3.2.6 TEMPERATURE OF EXHAUST STREAM.....	217
6.3.3 EFFECT OF CARBON DIOXIDE CONCENTRATION IN INLET FUEL ON CYCLE PERFORMANCE.	219
6.3.3.1 OUTPUT POWER.....	220
6.3.3.2 SPECIFIC WORK .....	224
6.3.3.3 EFFICIENCY .....	226
6.3.3.4 SOFC-TO-GT OUTPUT WORK RATIO .....	227
6.3.4 EFFECT OF CARBON MONOXIDE CONCENTRATION IN INLET FUEL ON CYCLE PERFORMANCE .....	228
6.3.4.1 OUTPUT POWER.....	228
6.3.4.2 SPECIFIC WORK .....	235
6.3.4.3 EFFICIENCY .....	236
6.3.5 EFFECT OF NITROGEN CONCENTRATION IN INLET FUEL ON CYCLE PERFORMANCE.....	237
6.3.5.1 OUTPUT POWER.....	238
6.3.5.2 SPECIFIC WORK .....	241
6.3.5.3 EFFICIENCY .....	243
6.4 CONCLUSIONS AND FUTURE WORK.....	243
CHAPTER SEVEN .....	246
PERFORMANCE ANALYSIS OF MICRO GAS TURBINES FUELLED BY BLENDS OF BIODIESEL AND PETROLEUM-BASED DIESEL: EXPERIMENTAL AND MODELING APPROACH .....	246
7.1 INTRODUCTION .....	247
7.2 DESCRIPTION OF MICRO GAS TURBINE SET .....	249
7.3 INSTRUMENTATION .....	253
7.4 RECORDED DATA .....	258
7.5 DISCUSSION OF EXPERIMENTAL RESULTS.....	261
7.6 MODELING OF MICRO GAS TURBINE .....	271
7.6.1 MODELING APPROACH .....	271
7.6.2 MODEL VALIDATION .....	273
7.7 MODELING RESULTS AND DISCUSSION .....	275
7.8 CONCLUSION.....	277

7.9	FUTURE WORK .....	278
CHAPTER EIGHT .....		280
ENERGY ANALYSIS OF GAS TURBINE-BASED POWER PLANTS.....		280
8.1	INTRODUCTION .....	280
8.2	COGENERATION .....	282
8.2.1	MODEL DESCRIPTION .....	283
8.2.2	MODEL VALIDATION AND MODELING RESULTS .....	288
8.3	COMBINED CYCLE POWER PLANT (CCPP).....	288
8.3.1	CCPP MODEL IN ASPEN PLUS® .....	291
8.4	AUGMENTATION OF GAS TURBINE OUTPUT POWER.....	297
8.4.1	EVAPORATIVE COOLING SYSTEMS.....	297
8.4.1.1	MEDIA EVAPORATIVE COOLING SYSTEMS .....	298
8.4.1.2	INLET AIR FOGGING SYSTEMS.....	298
8.4.2	MECHANICAL REFRIGERATION SYSTEM COOLING .....	300
8.4.3	COMPRESSOR INLET AIR EVAPORATIVE COOLING SYSTEM OF WHITBY COGENERATION POWER PLANT .....	300
8.4.4	MODELING RESULTS OF COMPRESSOR INLET AIR COOLING SYSTEM OF WHITBY COGENERATION PLANT.....	302
8.5	FUTURE WORK .....	303
8.5.1	INTEGRATED GASIFICATION COMBINED CYCLE (IGCC) .....	304
8.5.2	CO <sub>2</sub> CAPTURE AND STORAGE TECHNOLOGIES.....	305
8.5.2.1	CO <sub>2</sub> CAPTURE AFTER COMBUSTION (POST-COMBUSTION) .....	306
8.5.2.2	CO <sub>2</sub> CAPTURE AFTER CONCENTRATION IN THE FLUE GAS (OXY-FUEL POWER PLANTS).....	307
8.5.2.3	CO <sub>2</sub> CAPTURE BEFORE COMBUSTION (PRE-COMBUSTION) .....	307
8.5.2.4	CO <sub>2</sub> LIQUEFACTION AND SEQUESTRATION .....	308
8.6	CONCLUSION.....	308
CHAPTER NINE.....		309
CONCLUSION.....		309
REFERENCES .....		312

## LIST OF FIGURES

Figure 1: Industrial CO <sub>2</sub> emission of large point sources (Gale, 2002; Bauer, 2005) .....	10
Figure 2: Average GHG intensity in Canada's electricity generation sector between 1995 and 2006 (based on the raw data provided by Environment Canada (2008)) .....	19
Figure 3: GHG intensity for Iran's thermal and all power plants from 1995 to 2005 .....	22
Figure 4: Comparison of the average GHG intensity in Iran and Canada's electricity generation sectors between 1995 and 2005 .....	25
Figure 5: Canada greenhouse gas emission projection and the Kyoto Protocol (based on the raw data provided by Environment Canada (2005)).....	31
Figure 6: Natural gas prices in Canadian market from 2002 to 2008 (Natural gas, 2009) .....	44
Figure 7: Sketch of the basic operation of a typical fuel cell fuelled by hydrogen and oxygen (Suther, 2006) .....	50
Figure 8: Schematic of a typical planar SOFC (Suther, Fung, Koksall, and Zabihian, 2010b).....	57
Figure 9: Different polarization curves for chemical composition of the gases based on inlet, outlet or an average in a 0-D model (Bove et al., 2005).....	70
Figure 10: Performance parameter symbolic curves (Suther, 2006) .....	79
Figure 11: Influence of pressure ratio on system performance (Palsson et al., 2000).....	81
Figure 12: Effect of pressure on SOFC-GT-CHP power system efficiency (Chan et al., 2002a)	82
Figure 13: Tubular SOFC discretization along longitudinal direction for quasi-two dimensional model (Song et al., 2005).....	84
Figure 14: Distributions of cell temperature along longitudinal direction of tubular SOFC with different number of segments for quasi-two dimensional model (Song et al., 2005).....	85
Figure 15: Influences of TIT and PR on overall efficiency in SOFC-GT with HSR ( $T_{\text{steam,max}} = 823 \text{ K}$ ) (Kuchonthara et al., 2003a) .....	89
Figure 16: Rate of destroyed exergy for different components in SOFC-GT cycle (Calise et al., 2006b) .....	93
Figure 17: Steady-state performance of SOFC and GT hybrid cycle (power, efficiency, and shaft speed) (Stiller et al., 2006a) .....	101
Figure 18: Control volume of SOFC system model .....	113

Figure 19: Dependency of the activation loss on the constants in Equations 44 and 45 (3-D curves).....	132
Figure 20: Dependency of activation loss on the constants in Equations 44 and 45 (2-D curves) .....	134
Figure 21: Dependency of the total ohmic loss on the constants in Equations 48 and 50 (3-D curves) a) A and b) B .....	136
Figure 22: Dependency of the total ohmic loss on the constants in Equations 48 and 50 (2-D curves) a) A and b) B (Suther et al., 2010a) .....	137
Figure 23: Dependency of concentration loss on the constants in Equations 53 and 54 (3-D curves) a) limiting current density b) correction factor .....	140
Figure 24: Dependency of concentration loss on the constants in Equations 53 and 54 (2-D curves) a) limiting current density b) correction factor (Suther et al., 2010a).....	141
Figure 25: Reversible voltage (a) and actual voltage (b) of the SOFC as functions of the current density and operating temperature .....	142
Figure 26: SOFC power density versus current density for various operating temperatures (°C) .....	143
Figure 27: The model validation using current density versus voltage curves: a) dependency on operating temperature b) dependency on operating pressure (Suther et al., 2010a).....	149
Figure 28: Hybrid SOFC-GT cycle configuration .....	152
Figure 29: A schematic diagram of an actual SOFC module (Siemens, 2010) .....	153
Figure 30: Actual implemented configuration of the hybrid SOFC-GT cycle model with anode recirculation .....	154
Figure 31: Actual implemented configuration of the hybrid SOFC-GT cycle model without anode recirculation.....	156
Figure 32: Hybrid SOFC-GT cycle configuration in this study .....	165
Figure 33: Influence of system operating pressure and SOFC operating temperature on specific works a) SOFC specific work b) GT specific work c) cycle net specific work d) SOFC-to-GT work ratio .....	175
Figure 34: Influence of system operating pressure and SOFC operating temperature on air-to-fuel ratio .....	176

Figure 35: Influence of system operating pressure and SOFC operating temperature on cycle total efficiency (based on LHV) a) 3D graph b) 2D graph .....	177
Figure 36: Influence of current density and fuel utilization factor on specific works .....	180
Figure 37: Influence of current density and fuel utilization factor on cycle efficiency .....	181
Figure 38: Influence of current density and GT isentropic efficiency on cycle efficiency .....	182
Figure 39: Influence of TIT and SOFC operating temperature on specific works .....	184
Figure 40: Influence of TIT and SOFC operating temperature on cycle efficiency .....	185
Figure 41: Influence of isentropic efficiency of GT and air compressor on specific works .....	187
Figure 42: Influence of isentropic efficiency of GT and air compressor on cycle efficiency ....	187
Figure 43: Hydrogen molar flow rate in the inlet fuel, anode inlet (reformer outlet), anode outlet, and combustor inlet streams for the cycle with anode recirculation versus $H_2$ concentration in the inlet fuel .....	207
Figure 44: Output power of GT, SOFC, and whole system for different configurations versus $H_2$ concentration in the inlet fuel .....	208
Figure 45: Inlet fuel's LHV, mass flow rate, and energy content versus $H_2$ concentration .....	209
Figure 46: GT mass flow rate for both configurations and the anode recirculation mass flow rate in the cycle with anode recirculation with respect to $H_2$ concentration in the fuel .....	210
Figure 47: Steam molar and mass flow rate required for fuel reforming process for both configurations .....	211
Figure 48: Molar flow rate of $H_2$ in anode exhaust .....	212
Figure 49: GT, SOFC, and system specific works versus $H_2$ concentration in the inlet fuel .....	213
Figure 50: Inlet air mass flow rate and air-to-fuel ratio versus $H_2$ concentration for different configurations .....	214
Figure 51: Efficiency of the SOFC, GT, and cycle for both configurations versus $H_2$ concentration.....	215
Figure 52: SOFC-to-GT work ratio for two configurations.....	217
Figure 53: Temperature of several outlet streams at the cycle with anode recirculation .....	218
Figure 54: Temperature of several outlet streams at the cycle without anode recirculation .....	218
Figure 55: Output power of the GT, SOFC, and whole cycle for different configurations versus the $CO_2$ concentration in the fuel.....	220



Figure 56: GT mass flow rate for different configurations and anode recycle mass flow rate in cycle with anode recirculation versus CO <sub>2</sub> concentration in fuel .....	221
Figure 57: Molar flow rate of H <sub>2</sub> and CO in anode exhaust .....	222
Figure 58: Input fuel's LHV, mass flow rate, and energy content with respect to CO <sub>2</sub> concentration.....	223
Figure 59: Specific work of GT, SOFC and whole cycle for different configurations versus CO <sub>2</sub> concentration.....	224
Figure 60: Inlet air mass flow rate and air-to-fuel ratio for different configurations versus CO <sub>2</sub> concentration.....	225
Figure 61: Reformate temperature for the cycle with anode recirculation versus CO <sub>2</sub> concentration in fuel .....	226
Figure 62: Efficiency of SOFC, GT, and whole cycle for different configurations versus CO <sub>2</sub> concentration in fuel .....	227
Figure 63: SOFC-to-GT output work ratio for two configurations versus CO <sub>2</sub> concentration in the fuel .....	228
Figure 64: Output power of SOFC, GT, and system as a whole for different configurations versus CO concentration in fuel.....	229
Figure 65: Inlet fuel's LHV, mass flow rate, and energy content with respect to CO concentration in inlet fuel .....	229
Figure 66: GT mass flow rate for both configurations and anode recycle mass flow rate in cycle with anode recirculation versus CO concentration .....	230
Figure 67: Molar flow rate of H <sub>2</sub> and CO in anode inlet for both configurations with respect to CO concentration .....	231
Figure 68: Molar flow rate of H <sub>2</sub> and CO in anode outlet for both configurations with respect to CO concentration .....	232
Figure 69: LHV, mass flow rate, and energy content of anode inlet stream for both configurations with respect to fuel CO concentration .....	233
Figure 70: LHV, mass flow rate, and energy content of anode outlet stream for both configurations .....	233
Figure 71: Inlet air mass flow rate and air-to-fuel ratio for both configurations versus CO concentration in inlet fuel .....	234

Figure 72: Specific work of SOFC, GT, and system as a whole for two configurations versus CO concentration in fuel .....	235
Figure 73: Efficiency of SOFC and cycle as a whole for both configurations versus CO concentration.....	237
Figure 74: Output power of SOFC, GT, and system as a whole for different configurations versus N <sub>2</sub> concentration in fuel.....	238
Figure 75: Inlet fuel's LHV, mass flow rate, and energy content with respect to N <sub>2</sub> concentration in inlet fuel .....	239
Figure 76: GT mass flow rate for both configurations and anode recycle mass flow rate in cycle with anode recirculation versus N <sub>2</sub> concentration.....	240
Figure 77: Molar flow rate of H <sub>2</sub> in the anode outlet for both configurations with respect to N <sub>2</sub> concentration.....	241
Figure 78: Specific work of SOFC, GT, and the system as a whole for two configurations versus N <sub>2</sub> concentration in fuel .....	242
Figure 79: Inlet air mass flow rate and air-to-fuel ratio for both configurations versus N <sub>2</sub> concentration.....	242
Figure 80: Efficiency of SOFC and cycle as a whole for both configurations versus N <sub>2</sub> concentration.....	243
Figure 81: Regenerative micro turbine generator set.....	250
Figure 82: Flow pattern for twin rotating disk regenerator micro gas turbine (Chiang et al., 2009) .....	250
Figure 83: Major components of the micro gas turbine: a) compressor b) compressor turbine c) compressor diffuser d) combustion chamber e) ceramic regenerator disk f) generator .....	252
Figure 84: Schematic of the micro gas turbine components and material streams (Chiang et al., 2007) .....	253
Figure 85: a) The micro gas turbine set testing facility b) The load bank .....	255
Figure 86: Measuring instrument locations (Li, 2010): (cont.) .....	257
Figure 87: Compressor, power turbine, and generator shaft rotational speeds; air mass flow rate; and compressor outlet pressure for various output powers when the system was fuelled by B10 (Chiang, 1995) .....	259

Figure 88: Turbine inlet temperature, exhaust stream temperature, compressor inlet air mass flow rate, and ambient temperature for various output powers when the system was fuelled by B10 (Chiang, 1995) .....	260
Figure 89: Diagrams to investigate the variation of the inlet fuel flow rate a) the inlet fuel volumetric flow rate b) the fuel lower heating value and density vs. the biodiesel content of fuel blend c) the energy content of inlet fuel .....	263
Figure 90: Uncertainty of fuel flow rate measurement at the output power of 89 kW .....	263
Figure 91: Diagrams to investigate the variation of the inlet air flow rate: a) the air mass flow rate b) the compressor rotational speed c) the ambient pressure d) the ambient temperature ....	265
Figure 92: Uncertainty of measurements at the output power of 89 kW: a) the compressor rotational speed b) the ambient pressure c) the ambient temperature .....	267
Figure 93: The variation of the MGT performance parameters when the system is fuelled by B10, B20, and B30 a) turbine inlet temperature b) exhaust temperature c) compressor pressure ratio .....	268
Figure 94: Uncertainty of measurements at the output power of 89 kW: a) turbine inlet temperature b) exhaust temperature c) compressor pressure ratio.....	270
Figure 95: MGT electrical efficiency vs. fuel type for constant output powers .....	271
Figure 96: MGT cycle model configuration .....	272
Figure 97: Comparison of modeling results with experimental data.....	275
Figure 98: MGT modeling results for electrical efficiency vs. fuel type for constant output powers .....	276
Figure 99: Variation of the MGT performance parameters when the system is fuelled by B10, B20, and B30 a) TIT b) exhaust temperature .....	277
Figure 100: Schematic of a simple gas turbine cycle model in Aspen Plus® .....	281
Figure 101: General overview of the Whitby cogeneration power plant.....	283
Figure 102: Schematic of gas turbine cogeneration plant model studied in this chapter .....	284
Figure 103: Schematic of a simple steam power generation (Rankine) cycle .....	290
Figure 104: Schematic of a simple combined cycle power plant .....	290
Figure 105: Schematic of an Aspen Plus® model of a two-pressure CCPP.....	292
Figure 106: Zahedan gas turbine power plant (Iran) compressor inlet air cooling system.....	299

## LIST OF TABLES

Table 1: Electricity generation capacity and generated electricity for various types of power stations in the Iranian electricity generation sector during the period from March 2005 to February 2006 (based on the raw data provided by Iran Power Generation Co. (2007)).....	11
Table 2: Electricity generation in Canada for different types of consumed fuels in 2006 (based on the raw data provided by Environment Canada (2008)).....	12
Table 3: Default emission factors in Tier 1 (kg of GHG per TJ on net calorific basis) (IPCC, 2006) .....	14
Table 4: Country-specific CO <sub>2</sub> emission factors of various types of coal (for Ontario), petroleum oils, and natural gas (for Canada) (Environment Canada, 1997).....	15
Table 5 : Default emission factors used in Tier 3 (kg of GHG per TJ of input fuel on net calorific basis) (IPCC, 2006).....	16
Table 6: Country-specific CH <sub>4</sub> and N <sub>2</sub> O emission factors of various types of coal, petroleum oils, and natural gas for Canada (Environment Canada, 1997) .....	16
Table 7: GHG emissions and intensity, estimated by using Tier 3, in Iran's thermal power plants from March 2005 to February 2006.....	20
Table 8: GHG emissions and intensity, estimated by using Tier 1, in Iran's electricity generation sector from 1995 to 2005 .....	22
Table 9: GHG intensity for local electricity companies for 2004 and 2005 in Iran .....	23
Table 10: GHG intensity (gCO <sub>2</sub> eq/kWh) for all Iranian thermal power plants in 2005 .....	24
Table 11: Fuel consumption, electricity production, GHG emission reduction potentials, and GHG intensity (estimated by using Tier 3) in Canada.....	29
Table 12: GHG emissions as well as reduction potentials for each scenario in different provinces in Canada, estimated by using Tier 3.....	31
Table 13: Fuel consumption, electricity production, and GHG emissions for both the reference case (existing conditions) and each GHG reduction scenario in Ontario, estimated by using Tier 3.....	33

Table 14: Fuel consumption, electricity production, and GHG emissions for both the reference case (existing conditions) and each GHG reduction scenario in Alberta, estimated by using Tier 3 .....	34
Table 15: Fuel consumption, electricity production, and GHG emissions for both the reference case (existing conditions) and each GHG reduction scenario in Saskatchewan, estimated by using Tier 3.....	35
Table 16 : Energy consumption, electricity generation, and GHG emission reduction potentials, estimated by using Tier 3, in Iran's electricity generation sector for the period of March 2005 to February 2006 .....	36
Table 17: GHG emissions and intensity of Iran's electricity generation sector for different scenarios from 1995 to 2005, estimated by using Tier 1 .....	38
Table 18 : GHG emissions reduction potentials for local electricity companies in 2004 and 2005 (Tier 1) .....	39
Table 19: GHG reduction potential for all Iranian thermal power plants by first scenario in 2005 .....	40
Table 20: Age of fossil fuel power stations in the Iranian power generation industry based on the share of each category for different age ranges (based on the raw data provided by Iran Power Generation Co. (2007)) .....	42
Table 21: Summary of reported costs for a new power plant with and without CO <sub>2</sub> capture based on current technologies in studies published prior to 2004 (Rubin et al., 2007) .....	43
Table 22: Summary of recent study (after 2004) for costs of a new power plant with and without CO <sub>2</sub> capture unit based on current technologies (Rubin et al., 2007).....	43
Table 23: Summary of the characteristics of various types of fuel cells .....	55
Table 24: Categorization of sample papers in the open literature .....	75
Table 25: Summarized characteristics of some selected models in the open literature .....	109
Table 26: Composition of the SOFC outlet streams .....	124
Table 27: SOFC model constants .....	146
Table 28: Output electrochemical properties of the model.....	147
Table 29: Hybrid SOFC-GT model constants .....	158
Table 30: Pressure drops in the system equipment.....	161

Table 31: Properties of streams in the hybrid SOFC-GT system with anode recirculation fuelled by methane .....	167
Table 32: Properties of streams in the hybrid SOFC-GT system without anode recirculation ..	167
Table 33: Power, specific work, and efficiency of mechanical systems in the hybrid SOFC-GT system with anode recirculation.....	168
Table 34: Power, specific work, and efficiency of mechanical systems in the hybrid SOFC-GT system without anode recirculation .....	169
Table 35: Heat duty of heat exchangers in the hybrid SOFC-GT system (both configurations)	171
Table 36: Molar composition of a syngas used in this analysis (Kee et al., 2008).....	191
Table 37: Properties of streams in the hybrid SOFC-GT system with anode recirculation fuelled with syngas.....	191
Table 38: Power, specific work, and efficiency of mechanical systems in the hybrid SOFC-GT system with anode recirculation.....	194
Table 39: Heat duties of heat exchangers in the hybrid SOFC-GT system (both configurations) .....	194
Table 40: Properties of streams in the hybrid SOFC-GT system without anode recirculation ..	196
Table 41: Power, specific work, and efficiency of mechanical systems in the hybrid SOFC-GT system without anode recirculation .....	197
Table 42: Performance of the hybrid SOFC-GT system fuelled by methane, natural gas, and farm and sewage biogas.....	200
Table 43: Performance of hybrid SOFC-GT system fuelled by coal and biomass syngas, biofuel, and gasified biomass .....	201
Table 44: Range of variation of fuel composition and cycle operational parameters .....	202
Table 45: Variation of methane and hydrogen concentration in some fuels .....	206
Table 46: Rate of variation of the inlet air mass flow rate and output power and specific work of different components .....	215
Table 47: Rate of variation of the inlet fuel energy content, output power, and efficiencies of different components .....	216
Table 48: Variation of methane and carbon dioxide concentration in some fuels.....	219
Table 49: Properties of typical diesel and biodiesel fuels (Borbely and Kreider, 2001) .....	249
Table 50: Micro gas turbine (RGT-3600) measured specifications.....	254

Table 51: Instrument specifications (Chiang et al., 2009) .....	258
Table 52: The summary of experimental results from the micro gas turbine system (Chiang, 1995; Li, 2010).....	261
Table 53: Input parameters for macro gas turbine model .....	273
Table 54: Constants for the gas turbine cogeneration plant model.....	285
Table 55: Natural gas composition delivered to Whitby cogeneration power plant (mass-based) .....	286
Table 56: Important thermodynamic properties of the major streams in gas turbine cogeneration system .....	287
Table 57: Comparison of modeling results with operational data from Whitby cogeneration power plant.....	289
Table 58: Model constants for the steam cycle of the CCPP .....	293
Table 59: Important thermodynamic properties of the major streams in the steam cycle at the ambient temperature of 10°C .....	294
Table 60: Summary of results of model of compressor inlet air cooling system of Whitby cogeneration plant.....	303

# NOMENCLATURE

<b>Acronym</b>	<b>Definition</b>
AC	Alternating Current
AFC	Alkaline Fuel Cell
APU	Auxiliary Power Unit
ASU	Air Separation Unit
BoP	Balance of Plant
CCHP	Combined Cooling, Heating, and Power
CCPP	Combined Cycle Power Plant
CCS	CO <sub>2</sub> Capture and Storage
CHP	Combined Heat and Power
COE	Cost of Electricity
CPT	Cost Pay-Back Time
CPOX	Catalytic Partial Oxidation
D	Dimensional
DAFC	Direct Alcohol Fuel Cell
DC	Direct Current
DCFC	Direct Carbon Fuel Cell
DG	Distributed Generation
DIR	Direct Internal Reforming
DMFC	Direct Methanol Fuel Cells
EPT	Energy Pay-Back Time
Ex	Exergy Analysis
FCCC	Framework Convention on Climate Change
GA	Genetic Algorithm
GCV	Gross Calorific Value
GHG	Greenhouse Gas
GT	Gas Turbine
GWP	Global Warming Potential



HAT	Humid Air Turbine
HHV	Higher Heating Value
HR	Heat Recuperation
HRSG	Heat Recovery Steam Generator
HSR	Heat and Steam Recuperation
HT-SOFC	High Temperature Solid Oxide Fuel Cell
Hyper	Hybrid Performance
IEA	International Energy Agency
IG	Integrated Gasification
IGCC	Integrated Gasification Combined Cycle
IGFC	Integrated Gasification Fuel Cell
IGV	Inlet Guide Vane
IIR	Indirect Internal Reforming
IPCC	Intergovernmental Panel on Climate Change
IP-SOFC	Integrated Planar Solid Oxide Fuel Cell
IT-SOFC	Intermediate Temperature Solid Oxide Fuel Cell
LHV	Lower Heating Value
LT-SOFC	Low Temperature Solid Oxide Fuel Cell
MCFC	Molten Carbonate Fuel Cells
MGT	Micro Gas Turbine
MHI	Mitsubishi Heavy Industries, Ltd.
MSOFC	Monolithic Solid Oxide Fuel Cells
NCV	Net Calorific Value
NETL	National Energy Technology Laboratory
NG	Natural Gas
NGCC	Natural Gas Combine Cycle
NRC	Natural Resources Canada
OAG	Office of the Auditor General of Canada
PAFC	Phosphoric Acid Fuel Cell
PEFC	Polymer Electrolyte Fuel Cell
PEM	Proton Exchange Membrane

PF	Pulverized Coal Fuel-Fired
POX	Partial Oxidation
PR	Pressure Ratio
PSOFC	Pressurized Solid Oxide Fuel Cells
SCR	Steam-to-Carbon Ratio
SOFC	Solid Oxide Fuel Cells
ST	Steam Turbine
STIG	Steam Injected Gas Turbine
STP	Standard Temperature and Pressure
TER	Thermal-to-Electrical load Ratio
TIT	Turbine Inlet Temperature
UNCED	United Nations Conferences on Environment and Development
UNFCCC	United Nations Framework Convention on Climate Change.
WCED	World Commission on Environment and Development

<b>Symbol</b>	<b>Definition</b>
a, b, c, and d	stoichiometric coefficients
A	dimensional constant, $\Omega\text{-m}^2$
B	dimensional constant, K
$C_{\text{corr}}$	limiting current density correction factor
E	voltage or voltage losses, V
$\dot{E}$	energy rate, J/s
$\varepsilon$	activation energy, kJ/mole
F	Faraday's constant ( $96,485 \times 10^3 \text{ C/kmole}$ )
$\bar{g}$	Gibbs free energy, C/kmole
h	specific enthalpy, kJ/kg
I	current, A
i	current density, $\text{A/m}^2$
$i_0$	exchange current density, $\text{A/m}^2$
$i_L$	limiting current density, $\text{A/m}^2$

$i_{L,adj}$	pressure adjusted limiting current density, $A/m^2$
$K$	equilibrium constant
$\dot{m}$	mass flow rate, kg/s
$\dot{n}$	total number of moles in a stream
$n_e$	number of electrons transferred in the electrochemical reaction
$N_T$	total number of moles, mole
$P$	pressure, Pa/ bar
$P_1$	pressure for the limiting current density, Pa
$P_i$	partial pressures of species i, Pa
$Q$	heat, J
$\dot{Q}$	heat rate, W
$r$	area-specific resistance, $\Omega m^2$
$R$	resistance, $\Omega$
$R_u$	universal gas constant (8,314.6 J/kmole K)
$T$	operating temperature, K/°C
$U_f$	fuel utilization factor
$V$	voltage, V
$\dot{V}$	volumetric flow rate, $m^3/s$
$\dot{W}$	power, W
$X$	stream heat factor
$[]$	concentration of each species per molar flow

<b>Greek Symbol</b>	<b>Definition</b>
$\alpha$ , $\beta_1$ , $\beta_2$ , and $\beta$	transfer coefficients
$\rho$	molecular weights, kg/kmole
$\gamma$	pre-exponential factor, $A/m^2$

<b>Subscripts</b>	<b>Definition</b>
act	actual
activ	activation

adj	adjusted
conc	concentration
corr	correction
I	internal
in	inlet
ohm	ohmic
op	operating
out	outlet
react	reacted
ref	reference
rev	reversible

# **CHAPTER ONE**

## **Introduction**

We owe our sophisticated society and current standard of living to energy infrastructure development and its consequences in the last century. This dependency is going to continue in the future. According to the World Energy Outlook published by the International Energy Agency (IEA), the world's total electricity consumption will be doubled between 2003 and 2030 (IEA, 2006). Conventionally, the majority of electricity is generated from thermal fossil fuel power stations. However, global climate change and natural resource pollution cause significant worldwide concerns about the current trend in energy system development. It has been shown that more than half of the CO<sub>2</sub> emission of industrial large point sources are from the power production industry (Gale, 2002; Bauer, 2005, p. 13). Also, it is predicted that the global energy-related CO<sub>2</sub> emission will increase by 55% between 2003 and 2030 (IEA, 2006). This shows that conventional power plants using current technologies cannot address current environmental constraints, and they should be replaced by new and more environmentally benign technologies. Therefore, sustainability considerations should be involved in all major energy development plans all over the world. There are various definitions for sustainability. Probably the simplest one is that "sustainable development is development that meets the needs of the present without compromising the ability of future generations to meet their own needs" (WCED, 1987).

Ultimately, renewable energies are the most environmentally friendly candidates for sustainable electricity generation. But their applications have been limited by some major drawbacks, such as low availability and reliability, and high cost, at least in the short- and mid-term future. According to the IEA, the share of electricity production from renewable energy resources in the world-installed electricity generation capacity will experience a slight decrease from 23% in

2003 to 22% in 2030 (IEA, 2006). On the other hand, the same report predicted that the share of fossil fuels as energy supplies for electricity generation will remain constant at nearly 65%.

Thus, both fossil and non-fossil forms of energy will be needed in the foreseeable future to meet global energy requirements. That is why the IEA has commented that “numerous technology solutions offer substantial CO<sub>2</sub>-reduction potentials, including renewable energies, more efficient power generation, fossil-fuel use with CO<sub>2</sub> capture and storage, nuclear fission, fusion energy, hydrogen, biofuels, fuel cells, and efficient energy end use. No single technology can meet this challenge by itself. Different regions and countries will require different combinations of technologies to best serve their needs and best exploit their indigenous resources. The energy systems of tomorrow will rely on a mix of different advanced, clean, efficient technologies for energy supply and use” (IEA, 2003b, p. 5).

Despite the problems with fossil fuel power plants, fossil fuels are available on a mid- and long-term basis, and their continued large-scale and widespread applications in the power generation industry are essential in order to maintain current economic growth throughout the world. That means it is very unlikely that the current trend of fossil fuel consumption for electricity generation will be changed drastically in the near future. It is, therefore, important that alternative technologies are commercialized to permit the consumption of fossil fuels with significantly reduced greenhouse gas (GHG) emissions and other pollutants.

This thesis is about how to make power generation by fossil fuels less harmful to the environment.

## **1.1 Objective of the thesis**

The primary objective of this project is to develop comprehensive, detailed, and accurate models (as required by the applications) of advanced power generation technologies for both single and hybrid cycle power plants. In this project, the purpose of modeling is beyond just investigating performance of a specific power plant or technology. Instead, the objective is to have a comprehensive library of steady-state advanced power plant models. The results of the modeling can be helpful for scientific community as well as policy makers and plant designers. This is a major project in which the following models are covered in this thesis:

- Solid oxide fuel cell (SOFC);
- Hybrid SOFC-gas turbine (GT);
- Micro gas turbine (MGT, biodiesel fuelled);
- GT, cogeneration, and combined cycle power plant (CCPP).

These hybrid cycle models, then, can be used for different purposes. For instance, new advanced technologies can be applied to existing technologies to realize effects of the new technologies on the overall performance of the cycles and compare these cycles to recognize the most suitable ones.

Different phases of the project can be summarized as follows:

*Phase 1.* The influence of various technologies to reduce GHG emissions was investigated. In order to perform this investigation, first the methodology to estimate GHG emissions in the electricity generation sector with the example of Iran was explained. Then, eight different scenarios to reduce GHG emissions by fuel switching and adoption of advanced power generation systems were evaluated for two countries: Canada and Iran. The results demonstrated that there are great potentials for GHG emission reduction in both countries.

*Phase 2.* In this phase, the SOFC model in Aspen Plus<sup>®</sup> was used for evaluation of the impact of various parameters on the fuel cell overpotentials and output power.

*Phase 3.* The hybrid SOFC-GT model in Aspen Plus<sup>®</sup> was then used to investigate the variation of operational parameters throughout the cycle in the methane fuelled hybrid SOFC-GT system. Also, the parametric analysis of the methane fuelled hybrid SOFC-GT cycle was performed to investigate the effects of SOFC operating temperature, fuel utilization factor, current density; system operating pressure; turbine inlet temperature (TIT); and isentropic efficiencies of the GT and air compressor on the performance of the cycle.

*Phase 4.* In this phase, the hybrid SOFC-GT model was employed to explain the variation of operational parameters throughout the cycle in the syngas fuelled hybrid SOFC-GT system. Then, the system performance was presented when fuelled with pure methane, natural gas, farm biogas, sewage biogas, dry coal syngas, dry biomass syngas, biofuel, and gasified biomass. Finally the effects of fuel composition on the performance of the hybrid SOFC-GT cycle were

evaluated when methane as an inlet fuel was partially replaced by  $H_2$ ,  $CO_2$ ,  $CO$ , and  $N_2$ , the chemical species that can be found in fuels. In order to monitor the performance of the system, parameters such as SOFC and system thermal efficiencies; net and specific works of SOFC, GT, and cycle; air-to-fuel ratio; air and fuel mass flow rates, and so on were investigated in detail for each case.

*Phase 5.* The performance of a micro gas turbine was experimentally and numerically evaluated when the system was fuelled with various blends of biodiesel and petrodiesel.

*Phase 6.* Finally, the models of the gas turbine-based power plants, namely single gas turbine, cogeneration plant, and combined cycle power plant, were developed in Aspen Plus<sup>®</sup>. In this phase, it was essential to determine real world cycles with equipment specifications to model a specific power plant. Furthermore, performance results of these real power plants were required to validate the models. For this work, the data from the Whitby cogeneration power plant were used. The gas turbine model was also used to determine the effect of the compressor inlet air evaporative cooling system on the cycle performance.

These models were utilized to compare the performance of the hybrid cycles under similar conditions. This is an important feature because there are plenty of simulations for different types of power generation technologies with a wide range of assumptions and configurations in the open literature. However, due to different assumptions and inputs, it is not possible to compare performance of these power generation technologies. Therefore, in this work these technologies were compared based on similar conditions, in terms of different operational parameters such as efficiency and output power.



## **CHAPTER TWO**

### **Greenhouse Gas Emissions of Fossil Fuel-Fired Power Plants: Current Status and Reduction Potentials, Case Study of Canada and Iran**

This chapter first presents the methodology to estimate greenhouse gas (GHG) emissions from the electricity generation sector using Iran as an example. Then different scenarios to reduce GHG emissions by fuel switching and adoption of advanced power generation systems (based solely on fossil fuels) are evaluated for two countries: Canada and Iran. The results demonstrate that there are great potentials for GHG emission reduction in both countries. These potentials are evaluated by introducing eight different scenarios. In the first scenario, the existing power stations' fuel is switched to natural gas. The existing power plants are replaced by natural gas combined cycle (NGCC), integrated gasification combined cycle (IGCC), solid oxide fuel cell (SOFC), hybrid SOFC, and hybrid SOFC-IGCC power stations in scenario numbers 2 to 6, respectively. In the last two scenarios, CO<sub>2</sub> capture systems are installed in the existing power plants and in the second scenario, respectively.

#### **2.1 Introduction**

Recently, the negative environmental impacts associated with fossil fuel consumption such as greenhouse gas emissions and their effects on the global climate change have been a worldwide concern. Greenhouse gases are the most important contributor to the global climate deterioration. It has been proven that there is a direct relation between GHG concentrations in the atmosphere and global warming (IPCC, 1996, 2007a).

In order to address the climate change challenge, there were three major United Nations Conferences on Environment and Development (UNCED) in 1992, 1997, and 2009 in Rio de Janeiro, Kyoto, and Copenhagen, respectively. The first conference resulted in an international environmental treaty known as the United Nations Framework Convention on Climate Change (UNFCCC or FCCC). In the second conference, 160 countries agreed to reduce GHG emissions to the target levels set out by the Kyoto Protocol. This agreement also explained the options available to achieve these targets (UNFCCC, 1998).

The objective of the Kyoto Protocol is the “stabilization of greenhouse gas concentrations in the atmosphere at a level that would prevent dangerous anthropogenic interference with the climate system” (UNFCCC, 1992, p. 4). There are two groups of signatories to the UNFCCC: Annex I Parties and Non-Annex I Parties. Annex I countries are mostly developed countries and are required to decrease their GHG emissions to target levels below their 1990 emission levels. They are also required to submit an accounting of the GHG emissions and removals known as the annual greenhouse gas inventory report according to the UNFCCC reporting guidelines. The reduction percentages of the target levels below 1990 GHG emission levels are varied for different countries, from 8% for the European Union and some others to 7% for the USA, 6% for Canada and Japan, 0% for Russia, and permitted increases of 8% for Australia and 10% for Iceland (UNFCCC, 1998).

In order for the Kyoto Protocol to become legally binding, it had to be ratified by at least 55 countries. In addition, at least 55% of the emissions addressed by the Protocol should be covered by these countries. These conditions were satisfied on February 16, 2005. As of April 09, 2010, 190 countries as well as the European Union accepted the Protocol, covering about 64% of the emissions addressed by the Protocol (Status of Ratification, 2010).

Due to the expected failure of most countries to meet Kyoto Protocol objectives, the latest United Nations Climate Change Conference, commonly known as the Copenhagen Summit, was held in Copenhagen in December 2009. The objective was to agree on the climate change mitigation after 2012, the final year of the Kyoto Protocol. The summit did not result in a concrete agreement but a general political statement which was called a “meaningful agreement” by the United States government. Although the document was not legally binding and did not provide any GHG reduction commitments to the participants, it underlined climate change as one of the

greatest challenges of the present time and the necessity of limiting the global temperature increase to below 2°C (UNFCCC, 2009). However, some countries proposed actions they would take if a binding agreement was achieved. Canada proposed to reduce its carbon emissions to 20% below 2006 levels by 2020 which is equivalent to 3% below 1990 GHG emission levels. But provincial governments of Quebec, Ontario, and British Columbia disagreed with the federal government target and proposed stricter goals, 20%, 15% and 14% reductions, below their 1990 levels, respectively (Canada inactive, 2009). The United States target is to cut its GHG emissions by 17% below 2005 levels by 2020, 30% by 2025, 42% by 2030, and 83% by 2050 (Obama vows, 2009). Similarly, the European Union and Japan announced plans to cut GHG emissions by 30% (EU climate package, 2009) and 25% (Japan vows, 2009) below 1990 levels by 2020, respectively. Finally, China and India proposed to cut their GHG intensity (and not GHG emissions), respectively, by 40–45% and 20–25% below 2005 levels by 2020 (Where countries stand, 2009).

The objectives of this chapter are to evaluate the current status of GHG emissions in the fossil fuel-fired electricity generation industry and then to introduce and evaluate several scenarios to reduce these GHG emissions. In order to achieve these objectives, first, the methodology to estimate GHG emissions to prepare the annual greenhouse gases inventory report based on UNFCCC reporting guidelines with the example of Iran is explained. Then, different scenarios to reduce GHG emissions by fuel switching and adoption of advanced power generation systems (based solely on fossil fuels) are evaluated and compared for two countries: Canada and Iran.

The main reason to select Canada and Iran for case studies is availability of raw data for the two countries. Moreover, these two countries have unique characteristics that make them suitable candidates. They are both fossil fuel producers and exporters, but they are from Annex I and Non-Annex I Parties, respectively. The two countries are also different in their incomes and weather conditions. Moreover, their population size and total and per capita electricity consumption are very different. Canada with the population of almost 34,000,000 (Canada's population, 2010) had annual electricity consumption of approximately 536,100 GWh/year and average power per capita of 1,910 W (The world factbook: Canada, n.d.). On the other hand, Iran with the population of more than 70,500,000 (A glance at Iran, n.d.) and annual electricity consumption and average power per capita of 153,800 GWh/year and 224 W (The world

factbook: Iran, n.d.), respectively, had very different conditions. Therefore, they can be considered to be reasonable representatives of developed and developing countries, respectively.

As noted earlier, Annex I Parties are committed to submit an annual greenhouse gas inventory report. But since most of the developing countries, including Iran, are among Non-Annex I Parties, they are not required to submit an annual GHG inventory report, and they have no GHG emission reduction obligations. However, it is necessary to prepare such a report, at least unofficially, to facilitate reporting in the future when it becomes necessary, and to develop a solid foundation for future GHG emission reduction success.

According to the Kyoto Protocol, developing countries can join Annex I Parties as soon as they believe they are sufficiently developed. Therefore, eventually all countries will be required to submit the annual greenhouse gas inventory report and accept the GHG emission reduction obligations. Thus, it is essential for these countries to be ready for that time and reduce their GHG emissions. Also, more importantly, global climate change is a worldwide phenomenon, so all countries should be involved to face such an enormous challenge. Moreover, this report can be used as an indication of performance of electricity generation sectors in terms of their environmental impacts. This approach will lead to a more sustainable society, which means enough resources for everybody at anytime.

In addition, the Kyoto Protocol includes a "flexible mechanism" to encourage Non-Annex I Parties to implement GHG emission reduction projects ("GHG Projects"). These countries can receive a Carbon Credit for the projects which can be sold to Annex I economies to meet their GHG emission limitation (UNFCCC, 1998). Therefore, for Non-Annex I countries, reducing GHG emissions is beneficial both environmentally and economically.

## **2.2 Causes of the greenhouse effect**

The earth both absorbs solar energy and emits energy in the form of radiation. Since the earth's temperature is much lower than the sun's temperature, its radiation has much longer wavelengths. Greenhouse gases in the atmosphere, such as carbon dioxide (CO<sub>2</sub>), methane (CH<sub>4</sub>), and nitrous oxide (N<sub>2</sub>O), are transparent for short wave radiant energy but they absorb some of the longer wavelengths before they are lost to space. This phenomenon results in an

increase in the atmospheric temperature, which in turn causes the atmosphere to emit long wave radiation both upward and downward to space and surface, respectively. The downward part of this radiation is the greenhouse effect. The detailed and exact causes of global warming are an active field of research; however, the increase in the GHG level in the atmosphere is accepted as the primary cause of the recent global warming by scientific consensus. One of the earlier reports of the Intergovernmental Panel on Climate Change (IPCC) concluded that: “our ability to quantify the human influence on global climate is currently limited because the expected signal is still emerging from the noise of natural variability, and because there are uncertainties in key factors. ... Nevertheless, the balance of evidence suggests that there is a discernable human influence on global climate” (IPCC, 1996, p. 8). However, a more recent report was more specific in this matter “most of the observed increase in globally averaged temperatures since the mid-20th century is very likely (greater than 90% probability) due to the observed increase in anthropogenic greenhouse gas concentrations” (IPCC, 2007b). The major greenhouse gases are water vapour, carbon dioxide, methane, ozone, nitrous oxide, sulfur hexafluoride, hydrofluorocarbons, perfluorocarbons, and chlorofluorocarbons. Carbon dioxide, methane, and nitrous oxide are the subject of the Kyoto Protocol.

### **2.3 Current status of GHG emissions in power generation industry**

In this subsection, current and expected future status of the electricity generation sector as well as its contribution to the global GHG emissions throughout the world, in Iran, and in Canada are investigated.

According to *World Energy Outlook* published by the International Energy Agency (IEA), the world’s total net electricity consumption will increase dramatically. The world electricity generation was 14,781 billion kWh in 2003 and is expected to increase to 21,699 and 30,116 billion kWh in 2015 and 2030, respectively, which means 2.7% average increase rate per year (IEA, 2006). The same report predicted that the global energy-related GHG emissions would increase by 1.7% per year, and they would reach 40 Gt in 2030. During this period, coal and oil are the leading contributors to global energy-related CO<sub>2</sub> emissions (IEA, 2006).

Figure 1 shows CO<sub>2</sub> emission of large point sources by industry. As the chart illustrates, the power production industry is responsible for 54% of the industrial CO<sub>2</sub> emissions (Gale, 2002; Bauer, 2005, p. 13). This is confirmed by the IEA, where it is stated that power generation contributes half of the increase in global emissions (IEA, 2006).

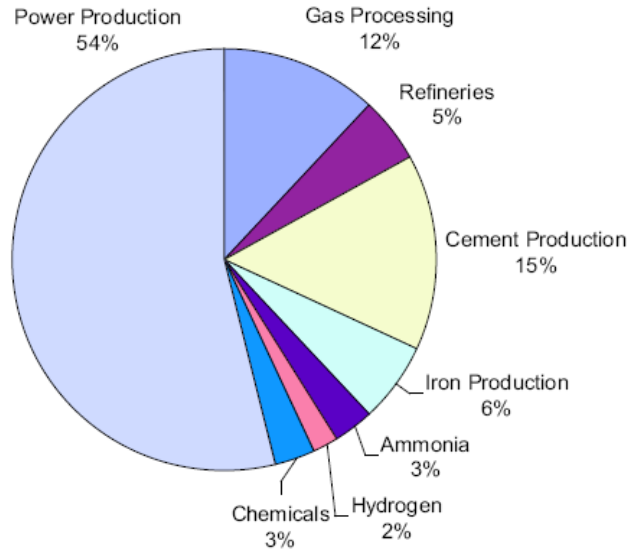


**Figure 1: Industrial CO<sub>2</sub> emission of large point sources (Gale, 2002; Bauer, 2005)**

Iran's electricity generation sector requires 54 GW of new capacity to increase its electricity generation from 153 TWh in 2003 to 359 TWh by 2030, growing at an average rate of 3.2% per year over the period. This new capacity needs about a \$92 billion investment and is dominated by natural gas-fired plants, mostly combined cycle power plants (CCPP). More than 75% of the electricity would be generated in natural gas-fired power plants (IEA, 2005). Table 1 reflects the status of the Iranian electricity generation sector in terms of the resources and technologies (Iran Power Generation Co., 2007). The table shows the distribution of electricity generation capacity and generated electricity for various types of power stations and their percentage of contribution in the Iranian electricity generation industry during the period from March 2005 to February 2006. As the table illustrates, more than 90% of generated electricity and 84% of electricity generation capacity are from fossil fuel-fired power plants. It should be noted that the capacity of

electricity generation and the actual electricity production are different, and better matching of electricity demand and production can reduce this difference, so greater use of installed capacity can be made.

**Table 1: Electricity generation capacity and generated electricity for various types of power stations in the Iranian electricity generation sector during the period from March 2005 to February 2006 (based on the raw data provided by Iran Power Generation Co. (2007))**

Type of power plant	Capacity (MW)	Percent (%)	Electricity generation (GWh)	Percent (%)
Steam cycle	15,554	37.9	93,383	52.4
Gas turbine	12,050	29.4	32,128	18.0
Combined cycle	6,832	16.7	36,194	20.3
Hydro-electric	6,037	14.7	16,085	9.0
Wind and diesel	530	1.3	281	0.3
<b>Total</b>	<b>41,003</b>	<b>100</b>	<b>178,071</b>	<b>100</b>

According to *Canada's Energy Outlook* published by Natural Resources Canada, electricity consumption in Canada will increase to 593 TWh by 2020, growing at an average rate of 1.2% annually. By 2004, CO<sub>2</sub> emissions in Canada had risen to 27% above 1990 levels, which compares unfavourably to the 16% increase in emissions by the United States during the same period (OAG, 2006). The GHG emissions of electricity generation industry are expected to increase slightly, from 130 Mt in 2004 to 131 Mt in 2010 (NRC, 2006).

According to *Canada's National GHG Inventory Report* published by Environment Canada, Canada's total GHG emissions were 721,000 ktCO<sub>2</sub>eq in 2006. The energy sector was responsible for almost 81% of the GHG emissions, and stationary combustion sources emitted 324,000 ktCO<sub>2</sub>eq GHGs. The GHG emissions of the electricity generation industry were 110,540 ktCO<sub>2</sub>eq, which was equal to approximately 15% of the total GHG emissions in 2006 (Environment Canada, 2008).

Table 2 shows the status of the Canadian electricity generation sector based on the type of consumed fuels for electricity generation (Environment Canada, 2008). Comparison of Tables 1 and 2 points out that in these two countries, the electricity generation sectors cannot be directly compared. This is because of different data collection procedures used in the two countries. This

is one of the major challenges when different countries' electricity generation sectors have to be compared.

**Table 2: Electricity generation in Canada for different types of consumed fuels in 2006 (based on the raw data provided by Environment Canada (2008))**

<b>Fuel type</b>	<b>Generated electricity (GWh)</b>	<b>Percent (%)</b>
<b>Hydro</b>	314,230	58.4
<b>Coal</b>	95,050	17.6
<b>Nuclear</b>	92,420	17.2
<b>Natural gas</b>	25,780	4.8
<b>Refined petroleum products</b>	5,140	1.0
<b>Renewables</b>	3,770	0.7
<b>Other</b>	1,870	0.3
<b>Total</b>	538,260	100

These statistics show that the electricity generation sector is, and will remain, a major source of GHG emissions, and in order to achieve a sustainable environment, it is essential to reduce these emissions.

## **2.4 GHG emission sources and electricity generation sector**

The IPCC published a guideline for greenhouse gas inventory report preparation. The first guideline, issued in 1997 was titled *Revised 1996 IPCC Guidelines for National Greenhouse Gas Inventories* (IPCC, 1997). The *2006 IPCC Guidelines for National Greenhouse Gas Inventories* provides methodologies for estimating national inventories of anthropogenic greenhouse gas emissions and removals by GHG sources and sinks. This guideline categorized GHG emission sources into five categories (IPCC, 2006): energy; industrial processes and product use; agriculture, forestry and other land use; waste; and others.

Based on the 2006 IPCC Guidelines, the electricity generation sector is considered to be in category 1-A-1-a-i. The definition of these categories is as follows (IPCC, 2006):



*1- Energy:* Comprises emissions from combustion and fugitive releases of fuels for energy uses. All GHG emissions from the non-energy consumption of fuels are commonly included under Industrial Processes and Product Use.

*1 A - Fuel combustion activities:* GHG emissions from the intentional oxidation of fuels within a device to generate either heat, mechanical work, or both.

*1 A 1 - Energy industries:* Sum of emissions from fuel consumption for power generation industries.

*1 A 1 a - Main activity, electricity and heat production:* All emissions from electricity generation, combined heat and power generation, and heat plants whose products are supplied to the public. These plants can be in public or private ownership and include on-site use of fuel.

*1 A 1 a i – Electricity generation:* GHG emissions from all fuel combustion to generate electricity, excluding those from combined heat and power plants.

## **2.5 Different methodologies to estimate GHG emissions**

In this subsection different methods to estimate GHG emissions are investigated, and the estimation for the Iranian electricity generation sector is presented as a case study. The *2006 IPCC Guidelines for National Greenhouse Gas Inventories* (IPCC, 2006) is used to provide methodologies for estimating GHG emissions for category 1-A-1-a-i.

Generally, emission of each GHG is estimated by multiplying fuel consumption by the corresponding emission factors. There are three tiers presented in the *2006 IPCC Guidelines* for estimating the emissions from fossil fuel combustion for electricity generation. In these tiers, fuel consumption and emission factors are considered as follows (IPCC, 2006):

Tier 1: The Tier 1 approach is a fuel-based method to estimate GHG emissions. In this tier, the quantities of consumed fuel and average emission factors for all relevant direct greenhouse gases are used for GHG analysis. The Tier 1 emission factors are available in the IPCC guidelines. Table 3 shows the Tier 1 default emission factors for three fuels (natural gas, diesel, and residual oil) (IPCC, 2006).

**Table 3: Default emission factors in Tier 1 (kg of GHG per TJ on net calorific basis) (IPCC, 2006)**

Fuel type	Default emission factors		
	CO <sub>2</sub>	CH <sub>4</sub>	N <sub>2</sub> O
Natural gas	56,100	5	0.1
Diesel	74,100	10	0.6
Residual oil	77,400	10	0.6

Tier 2: In Tier 2, similar to Tier 1, the quantities of consumed fuel from fuel statistics are used to estimate GHG emissions. But instead of the Tier 1 default emission factors, country-specific emission factors are used. In order to develop country-specific emission factors, information such as fuel carbon content, fuel quality, and the state of technological development (particularly for non-CO<sub>2</sub> emissions) for a given country should be taken into account.

Other parameters to be considered are the variation of emission factors over time and the amount of carbon retained in the ash (for solid fuels). The data used in this tier are more applicable to a specific country's conditions. Therefore, it is expected that the results of applying this method are more accurate (IPCC, 2006).

Table 4 shows the country-specific CO<sub>2</sub> emission factor for some solid, liquid, and gaseous fuels for Canada. It should be noted that due to the variable nature of characteristics of the various types of coal in different regions, CO<sub>2</sub> emission factors of coal are provided for all provinces individually. The coal emission factors listed in Table 4 are for Ontario (Environment Canada, 1997).

**Table 4: Country-specific CO<sub>2</sub> emission factors of various types of coal (for Ontario), petroleum oils, and natural gas (for Canada) (Environment Canada, 1997)**

<b>Fuel type</b>	<b>CO<sub>2</sub> emission factors</b>
<b>Coals*</b>	<b>(g/ kg<sub>fuel</sub>)</b>
Lignite	1,490
Sub-bituminous	2,520
Low volatile bituminous	2,520
Medium volatile bituminous	2,500
<b>Petroleum Oils**</b>	<b>(g/ L<sub>fuel</sub>)</b>
Heavy distillate	3,090
Light distillate	2,830
Diesel	2,730
<b>Gaseous fuels**</b>	<b>(g/ L<sub>fuel</sub>)</b>
Natural gas	1.880

\* Average for Ontario

\*\* Average for Canada

Tier 3: The Tier 1 and Tier 2 approaches of estimating GHG emissions described in the previous sections necessitate using average emission factors, either default emission factors in Tier 1 or country-specific emission factors in Tier 2. In reality, GHG emissions depend upon fuel type, combustion technology, operating conditions, control technology, quality of maintenance, and age of equipment. In the Tier 3 approach, these parameters are taken into account by using different emission factors for each case (Table 5). The emission of CO<sub>2</sub> highly depends on the carbon content of the fuel and not the combustion technology. Therefore, it is not required to use the Tier 3 approach to estimate emissions of CO<sub>2</sub>, and the CO<sub>2</sub> emission factors from Table 3 or the country-specific CO<sub>2</sub> emission factors (such as Table 4) are sufficient (IPCC, 2006). Table 5 shows the Tier 3 methane and nitrous oxide default emission factors for three fuels (natural gas, diesel, and residual oil) (IPCC, 2006). Similarly, Table 6 illustrates the country-specific CH<sub>4</sub> and N<sub>2</sub>O emission factors for some solid, liquid, and gaseous fuels for Canada (Environment Canada, 1997).

**Table 5 : Default emission factors used in Tier 3 (kg of GHG per TJ of input fuel on net calorific basis)  
(IPCC, 2006)**

Fuel and technology type	Emission factors	
	CH <sub>4</sub>	N <sub>2</sub> O
<b>Natural gas</b>		
Boilers	1	1
Gas-fired gas turbines (>3 MW)	4	1
Combined cycle	1	3
<b>Diesel</b>		
Boilers	0.9	0.4
<b>Residual oil</b>		
Residual oil normal firing	0.8	0.3

**Table 6: Country-specific CH<sub>4</sub> and N<sub>2</sub>O emission factors of various types of coal, petroleum oils, and natural gas for Canada (Environment Canada, 1997)**

Fuel and technology type	Emission factors	
	CH <sub>4</sub>	N <sub>2</sub> O
<b>Coals</b>	<b>(g/kg<sub>fuel</sub>)</b>	
Conventional utility boilers	0.015	0.05
Fluidized bed combustors	0.015	2.11
Conventional industrial boilers	0.015	0.11
<b>Petroleum oils</b>	<b>(g/ L<sub>fuel</sub>)</b>	
<i>Utility applications</i>		
Heavy distillate boilers	0.03	0.013
Light distillate boilers	0.006	0.013
Diesel	0.26	0.40
<i>Industrial applications</i>		
Heavy distillate boilers	0.12	0.013
Light distillate boilers	0.006	0.013
Diesel	0.26	0.40
<b>Gaseous fuels</b>	<b>(g/ L<sub>fuel</sub>)</b>	
<i>Utility applications</i>		
Natural gas boiler and combustor	0.0000048	0.00002

All these tiers use the amount of combusted fuel as the activity data. In the power production sector, the activity data are typically the fuel consumption to generate electricity. These data are sufficient for Tier 1 analysis. In higher tier approaches, additional data are required on fuel characteristics and the power generation technologies.

In most national energy statistics used for GHG emission estimation, fuel consumption is specified in physical units, such as in tonnes or cubic metres. But in the above mentioned tiers, the default emission factors are given based on the energy content of fuel (Tables 3 and 5); therefore, the energy content of consumed fuels is required to estimate GHG emissions. Thus, the mass or volume units of fuel consumption should be first converted to fuel energy content. The fuel energy content can be expressed by two definitions: net calorific value (NCV) or lower heating value (LHV), and gross calorific value (GCV) or higher heating value (HHV).

The difference between NCV and GCV is the latent heat of vaporization of the water content of the exhaust stream. The NCV for coal and oil is about five percent, and for natural gas about 10 percent, less than the GCV. The *IPCC Guidelines* use NCV, expressed in SI units or multiples of SI units. In this work the net calorific values provided by the Iran Power Generation, Transmission, Distribution, and Management Co. (Iran Power Generation Co., 2007) are used. In the case of Canada, since country-specific emission factors are based on physical units of fuels, such a conversion is not required (Tables 4 and 6).

Another parameter that plays an important role in GHG estimation is Global Warming Potential (GWP). GWP is the ability of each greenhouse gas to trap heat in the atmosphere relative to another gas (usually carbon dioxide). By definition, “a GWP is a relative measure of the warming effect that the emission of a radiative gas might have on the troposphere” (Environment Canada, 2006, p. 18). In the estimation of GWP of a GHG, both the instantaneous and the lifetime effect of the gas are considered. The 100-year GWPs recommended by the IPCC and required for inventory reporting are used in this work. According to the IPCC, the GWP of CH<sub>4</sub> and N<sub>2</sub>O are 21 and 310, respectively. This means the contribution of 1 kg CH<sub>4</sub> and N<sub>2</sub>O to the warming of the atmosphere are 21 and 310 times higher than 1 kg CO<sub>2</sub>, respectively, for a 100-year time frame (Environment Canada, 2006).

The next step is to select tier(s) for estimation of GHG emissions in Canadian and Iranian thermal power stations. The estimation of GHG emissions for the Canadian electricity generation

industry in this work is based on Tier 2. The country-specific emission factors and activity data are provided by Environment Canada (Environment Canada, 1997).

Since country-specific emission factors for Iran's power plants do not exist, Tier 2 cannot be used. On the other hand, due to the fact that fuel consumption for each power generation technology has been recorded for the national energy statistics, Tier 3 is used for estimation of GHG emissions for 2005. However, for years before 2005, Tier 1 is more suitable. The activity data for GHG estimation is provided by the Iran Power Generation, Transmission, Distribution, and Management Co. (Iran Power Generation CO., 2007).

## **2.6 GHG emissions in fossil fuel-fired power generation industry in Canada**

Being one of the Annex I Parties, Canada's annual national greenhouse gas inventory report has been prepared and published by Environment Canada. Figure 2 illustrates average GHG intensity in Canada's fossil fuel-fired electricity generation sector between 1995 and 2006. According to the figure, Canada experienced a 6% increase in average GHG intensity in this period. In this diagram, the GHG intensity is the ratio of greenhouse gas emissions to generated electricity. This parameter is used to evaluate the electricity generation performance in terms of GHG emissions. The GHG intensity is greatly influenced by the electricity generation technology and the source of energy. For instance, Figure 2 shows that there was a sharp increase in GHG intensity between 1996 and 1998. This can be explained based on the fact that the share of coal in electricity generation increased from 15% to 18% and the share of nuclear power generation decreased from 17% to almost 12% in this period (Environment Canada, 2008).

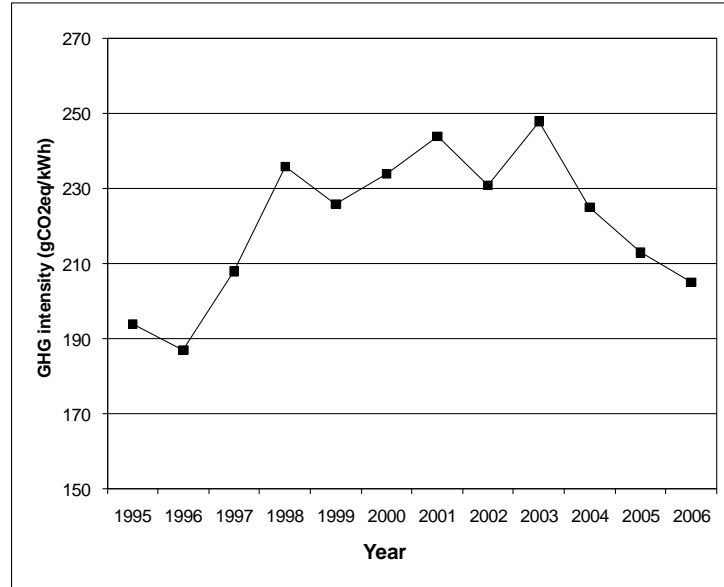


**Figure 2: Average GHG intensity in Canada's electricity generation sector between 1995 and 2006 (based on the raw data provided by Environment Canada (2008))**

## 2.7 GHG emissions in Iranian fossil fuel-fired power generation sector

In this section, the previously described methods are used to estimate GHG emissions in the Iranian fossil fuel-fired electricity generation sector. Table 7 shows the electricity generation, fuel consumption, GHG emissions, and GHG intensity for thermal power stations in Iran for the period of March 2005 to February 2006. As shown in the table, the GHG intensity for steam power plants, gas turbines, and combined cycle power plants are 617, 773, and 462 gCO<sub>2</sub>eq/kWh, respectively, with the overall intensity of 610 gCO<sub>2</sub>eq/kWh for all thermal power plants.

**Table 7: GHG emissions and intensity, estimated by using Tier 3, in Iran's thermal power plants from March 2005 to February 2006**

Power plant type	Electricity generation (GWh)	Fuel consumption			GHG emissions (kt/year)			GHG intensity (gCO <sub>2</sub> eq/kWh)
		Natural gas (10 <sup>6</sup> m <sup>3</sup> )	Diesel (10 <sup>6</sup> L)	Residual oil (10 <sup>6</sup> L)	NG	Diesel	Residual oil	
Steam cycle	89,574	17,211	43	6,329	35,074	123	20,104	617
Gas turbine	29,023	8,444	1,819	0	17,227	5,220	0	773
Combined cycle	36,194	7,204	660	0	14,841	1,894	0	462
<b>Total/Ave</b>	154,791	32,859	2,522	6,329	67,143	7,237	20,104	610

It should be noted that combined cycle power plants emit 25% and 40% less GHG compared to steam power plants and gas turbines, respectively. This result is expected because combined cycle power plants have much higher efficiency. In this case, the efficiency of steam power plants, gas turbines, and combined cycle power plants are 36.5%, 27.8%, and 45.5%, respectively, during the same period. This means 25% and 64% higher efficiency for combined cycles in comparison to steam power plants and gas turbines, respectively.

If these GHG intensities are compared with similar data for Canada, it can be seen that the results are comparable. For instance, in 2006 GHG intensity for the electricity generation sector in Canada for different fuels was as follows: coal 907 gCO<sub>2</sub>eq/kWh, refined petroleum products 790 gCO<sub>2</sub>eq/kWh, and natural gas 490 gCO<sub>2</sub>eq/kWh (Environment Canada, 2008).

As can be seen, from comparing Table 7 and the numbers in the previous paragraph, it is not possible to directly compare GHG intensity between two countries. Based on the current activity data collection procedure in Iran, it is not possible to calculate total GHG intensity for each fuel. The reason is that although the consumption of each fuel and total generated electricity in each power station were recorded, the breakdown of the generated electricity by consumption of each fuel is not known. In order to follow the IPCC guideline, the data collection procedure should be adjusted so that this type of calculation could be carried out.

Regarding average GHG intensity, it should be noted that the value shown in Table 7, 610 gCO<sub>2</sub>eq/kWh, is just for thermal power plants, and if the total electricity generation is considered (including hydro-electric power plants), this intensity will be reduced to 570 gCO<sub>2</sub>eq/kWh.



When this overall average GHG intensity is compared with the equivalent data for Canada, a huge difference can be observed: Canada 205 (Environment Canada, 2008) versus Iran 570 gCO<sub>2</sub>eq/kWh. The reason is that a considerable portion of electricity in Canada is generated by hydro-electric and nuclear power plants (Table 2), from which no significant amounts of GHGs are emitted.

Using the same method, a wide variety of analyses can be carried out. Investigation can be performed and results can be compared for different levels of electricity generation, for example for individual power stations, different provinces, and even countries. Also, the time variation of GHG emissions can be estimated to evaluate progress in a certain sector in a given period of time. The following subsection presents some of these analyses carried out in this work for the Iranian electricity generation industry.

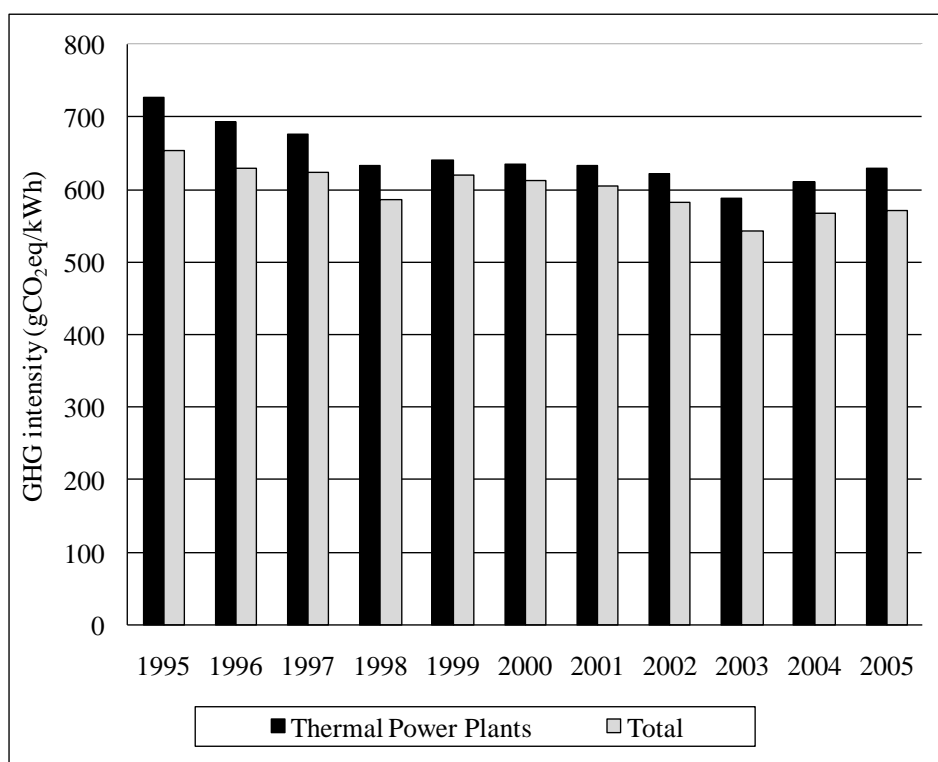
Table 8 shows the electricity generation, GHG emissions and intensity (total and thermal power plants) for Iran's electricity generation sector from 1995 to 2005. The table indicates that GHG emission intensity has been reduced in recent years and 2003, with total intensity of 542 gCO<sub>2</sub>eq/kWh, was the best year in terms of GHG emission intensity.

Figure 3 shows the diagram for average GHG intensity for thermal and all power plants from 1995 to 2005 in Iran.

Table 9 shows the electricity generation, GHG emissions, and thermal power plants' and total GHG intensity for local electricity companies in Iran for 2004 and 2005.

**Table 8: GHG emissions and intensity, estimated by using Tier 1, in Iran's electricity generation sector from 1995 to 2005**

Year	Electricity generation (GWh)		GHG emissions (kt)	GHG intensity (gCO <sub>2</sub> eq/kWh)	
	Thermal	Total		Thermal	Total
2005	157,181	173,547	98,991	630	570
2004	149,103	160,029	90,958	610	568
2003	135,574	146,988	79,631	587	542
2002	126,740	135,177	78,844	622	583
2001	118,890	124,306	75,099	632	604
2000	111,697	115,708	70,863	634	612
1999	101,845	105,187	65,137	640	619
1998	90,474	97,862	57,222	632	585
1997	84,926	92,310	57,470	677	623
1996	77,839	85,825	53,959	693	629
1995	72,046	80,044	52,299	726	653



**Figure 3: GHG intensity for Iran's thermal and all power plants from 1995 to 2005**

**Table 9: GHG intensity for local electricity companies for 2004 and 2005 in Iran**

Local electricity companies	Year	Electricity generation (GWh)		GHG emissions (kt)	GHG intensity (gCO <sub>2</sub> eq/kWh)	
		Thermal	Total		Thermal	Total
Azarbaijan	2005	9,005	9,199	5,980	664	650
	2004	6,742	6,946	4,303	638	619
Isfahan	2005	16,680	17,010	10,396	623	611
	2004	16,932	17,183	10,690	631	622
Bakhtar	2005	13,634	13,644	7,730	567	567
	2004	12,562	12,575	7,268	579	578
Tehran	2005	34,061	34,501	20,607	605	597
	2004	29,764	30,194	17,878	601	592
Khorasan	2005	13,674	13,674	7,716	564	564
	2004	13,620	13,620	7,274	534	534
Khozestan	2005	11,409	26,047	5,997	526	230
	2004	14,703	24,077	7,725	525	321
Zanjan	2005*	-	-	-	-	-
	2004*	-	-	-	-	-
Semnan	2005	7	7	10	1,451	1,451
	2004	5	5	8	1,625	1,625
Sistan and Balouchestan	2005	2,401	2,401	2,599	1,082	1,082
	2004	2,207	2,207	2,439	1,105	1,105
Gharb	2005	4,364	4,364	2,718	623	622
	2004	4,218	4,218	2,671	633	633
Fars	2005	11,255	11,313	6,337	563	560
	2004	11,518	11,583	6,723	584	580
Kerman	2005	4,934	5,030	3,589	727	713
	2004	5,029	5,040	3,603	716	715
Gilan	2005	9,116	9,435	4,361	478	462
	2004	9,200	9,478	4,319	469	456
Mazandaran	2005	11,828	11,828	7,264	614	614
	2004	12,537	12,537	7,466	596	596
Hormozgan	2005	10,556	10,556	7,393	700	700
	2004	8,253	8,253	5,255	637	637
Yazd	2005	1,513	1,513	2,708	1,790	1,790
	2004	1,502	1,502	2,534	1,687	1,687
Kish	2005	355	355	489	1,379	1,379
	2004	312	312	432	1,384	1,384
Private Sector	2005	2,391	2,391	1,387	580	580
	2004*	-	-	-	-	-
Industry	2005	4,524	4,524	3,230	714	714
	2004	2,841	2,841	1,823	642	642

\* No fossil fuel power generation.

In terms of the GHG emission intensity of total electricity generation, Khozestan with 321 and 230 gCO<sub>2</sub>eq/kWh, respectively, for 2004 and 2005 had the best performance. This was expected because in this province 39% and 56% of electricity was generated by hydro power stations in 2004 and 2005, respectively. But regarding the thermal power plants, Gilan with GHG emissions intensity of 469 and 478 gCO<sub>2</sub>eq/kWh in 2004 and 2005, respectively, was the best. The range of intensity (from 478 to 1,451 gCO<sub>2</sub>eq/kWh) proves that regardless of progress in the reduction of GHG emissions in recent years there are opportunities for further improvement.

Table 10 illustrates the GHG emission intensity in Iran's major power plants (with annual electricity generation of more than 100,000 MWh) in 2005.

**Table 10: GHG intensity (gCO<sub>2</sub>eq/kWh) for all Iranian thermal power plants in 2005**

Power plant	GHG intensity	Power plant	GHG intensity	Power plant	GHG intensity	Power plant	GHG intensity
<b>Steam</b>		Rajaei	565	Shirvan	879	Sanandaj	893
Tarasht	931	Bistoon	617	Shariati	940	Kish	1,346
Besat	768	Gharb	615	Sofian	988	Rest	1,209
Eslam Abad	626	Iranshahr	941	Zahedan	1,252	Ave.	774
Montazer Ghaem	670	Shazand	538	Salimi	716	<b>CCPP</b>	
Loshan	562	Sahand	695	Kazeron	608	Montazer Ghaem	467
Zarand	1,125	Ave.	617	Kangan	1,004	Gilan	449
Mashhad	703	<b>GT</b>		Zanbagh (Yazd)	1,059	Ghom	459
Neka	606	Shiraz	1,029	Yazd (GT)	827	Rajaei	484
Ramin	515	Mashhad	827	Yazd (CCPP)	682	Fars	428
Bandar Abbass	696	Loshan	729	Kerman	705	Khoi	513
Montazeri	622	Rey	915	Abadan	584	Neishaboore	482
Toos	595	Chabahar	1,318	Damavand	777	Shariati	455
Tabriz	665	Oroumie	1,093	Hormozgan	694	Ave.	462

For 2005, the GHG intensity for steam power plants ranged from 515 to 1,125 gCO<sub>2</sub>eq/kWh. The ranges for gas turbines and combined cycles were 584-1,346 gCO<sub>2</sub>eq/kWh and 428-513 gCO<sub>2</sub>eq/kWh, respectively. Again, this implies that still there are great potentials for GHG emission reduction in Iran's electricity generation sector.

## 2.8 Comparison of GHG emissions in fossil fuel-fired power generation in Canada and Iran

Figure 4 compares average GHG intensity in all electricity generation sectors of Iran and Canada between 1995 and 2005. According to the diagram, in Iran average GHG intensity was reduced by 13% from 1995 to 2005, whereas Canada experienced a 6% increase in the same period.

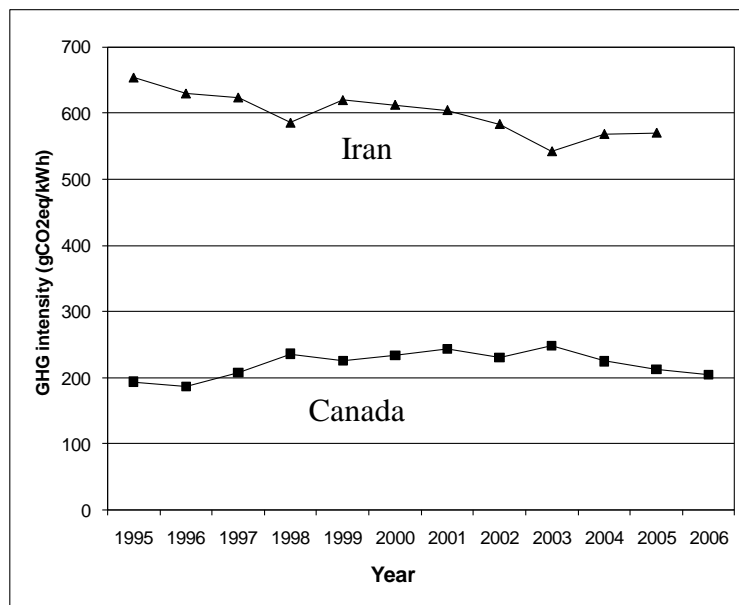


**Figure 4: Comparison of the average GHG intensity in Iran and Canada's electricity generation sectors between 1995 and 2005**

One of the reasons for this GHG emission reduction in the Iranian electricity generation sector was that in recent years many combined cycle power plants were installed in the country. In fact,

in 1999 there was no electricity generation using combined cycles, but in 2005, more than 20% of total electricity was generated by using these power plants. Moreover, fuel switching from diesel and residual oil to natural gas was another factor for the reduced GHG emissions.

Thus far the results demonstrated that Iran's electricity generation sector did a reasonably good job in reducing the GHG intensity in the past 10 years. However, detailed calculation (Tables 9 and 10) proved that still there are power plants with extremely high GHG intensity. This indicates that there are great potentials for further GHG intensity reduction in the sector. The GHG emissions for Canadian fossil fuel-fired power plants point to the same conclusion. In the rest of this chapter some of these potentials are discussed.

## **2.9 GHG emission reduction scenarios**

As noted, the electricity production industry is responsible for a considerable portion of total GHG emissions. Therefore, in the remainder of this chapter, GHG emission reduction potentials under various scenarios are investigated. Then, Canadian and Iranian electricity generation industries are examined to evaluate the potential effects of these scenarios on the GHG emissions.

For this work, different scenarios to reduce GHG emissions are defined as follows:

*Scenario 1:* In this scenario, GHG emission reduction potentials by fuel switching are investigated. Based on this scenario, all power plants use natural gas as the primary fuel instead of their original fuel. But the technology of power stations remains unchanged.

*Scenario 2:* In the second scenario, there is fuel switching as well as technology changes. According to this scenario, all power stations are replaced by a natural gas combined cycle (NGCC). The size of the alternative NGCC power plant is 505 MW. The plant configuration consists of two gas turbines, a three-pressure heat recovery steam generator, and a reheat steam turbine. In this work, the efficiency of the power plant is considered to be 49% (based on higher heating value, HHV) (Spath and Mann, 2000).

*Scenario 3:* In this scenario, it is assumed that all existing coal-fired power stations are replaced by an integrated gasification combined cycle (IGCC). Based on IGCC technology, the gas

turbine and steam cycle are incorporated with a modern coal gasification plant to use coal for electricity generation, which results in greatly improved efficiency and environmental performance. The advantages of this technology can be summarized as it has greater than 40 percent thermal efficiency, high fuel flexibility, and very low pollutant emissions. The efficiency of IGCC is considered to be 43% (HHV) (Ratafia-Brown, Manfredo, Hoffmann, and Ramezan, 2002; Topper, 2006) in this work.

*Scenarios 4 and 5:* In order to implement these scenarios, all existing power stations are replaced by a solid oxide fuel cell (SOFC) for the fourth scenario and hybrid SOFC power plants for the fifth scenario. In both cases, the power plants are fuelled by natural gas. These systems are explained in detail in Chapter 3.

There are many demonstrational and semi-commercial units of SOFCs with different sizes and configurations installed around the world (Singhal and Kendall, 2003; Singhal, 2002; Fuel Cell Handbook, 2004; Williams, Strakey, Surdoval, and Wilson, 2006). But so far, there have been few proof-of-concept hybrid SOFC power plants installed in the world (Veyo, Shockling, Dederer, Gillett, and Lundberg, 2002a; Veyo, Vora, Litzinger, and Lundberg 2002b; MHI, 2006). Therefore, these two technologies are in the development phase, and there is no commercial product in the market yet. Thus, there is no universally accepted configuration for them. For SOFC power generation units, efficiency of 50% to 60% has been reported (Petruzzi, Cocchi, and Fineschi, 2003; Shimada, Kato, and Tanaka, 2007; Campanari, 2001, 2002). In the case of the hybrid SOFC cycle, the efficiency is higher and its range is wider, from 57% to 75% (Calise, Dentice d'Accadia, Palombo, and Vanoli, 2006b; Campanari, 2002; Fuel Cell Handbook, 2004; Kuchonthara, Bhattacharya, and Tsutsumi, 2003a; Palsson, Selimovic, and Sjunnesson, 2000; Song, Sohn, Kim, Kim, Ro, and Suzuki, 2005). For this work the average efficiencies of 55% for the fourth scenario and 65% for the fifth scenario are considered.

*Scenario 6:* This scenario is a combination of the third and fourth scenarios. In this case, all existing coal-fired power stations are replaced by hybrid SOFC and IGCC cycles. The efficiency of the cycle is considered to be 50% (Kuchonthara, Bhattacharya, and Tsutsumi, 2005; Jansen, van der Laag, Oudhuis, and Ribberink, 1994).

*Scenarios 7 and 8:* CO<sub>2</sub> capture and storage (CCS) systems are technologies that can be used by different industries to reduce CO<sub>2</sub> emission where combustion is part of the process. A major

problem of CCS utilization in power plants is their high efficiency penalty. For different types of power plants fuelled by oil, natural gas, and coal, there are two main techniques that can be applied (Metz, Davidson, de Coninck, Loos, and Meyer, 2005; Riahi, Rubin, and Schrattenholzer, 2003):

- CO<sub>2</sub> capture after combustion (post-combustion);
- CO<sub>2</sub> capture after concentration of flue gas by using pure oxygen in boilers and furnaces (oxy-fuel power plants).

In the seventh scenario, the CCS system is installed in the existing power plants with the current technologies. For the last scenario, all existing power plants are replaced by the NGCC plants equipped with the CO<sub>2</sub> capture system. The CCS system in these scenarios is capable of removing 90% of CO<sub>2</sub> from flue gas, but because of consumption of more fuel to compensate the plants' efficiency reduction, overall, the percentage of the captured CO<sub>2</sub> is slightly lower.

## **2.10 GHG emission reduction potentials in Canada**

In this subsection, GHG emission reduction potentials in Canada under eight previously explained scenarios are investigated.

Table 11 shows the different fuel consumption, electricity production for each fuel, and the GHG emissions for both the reference case (existing conditions) and the eight GHG emission reduction scenarios. It also shows the reduction potentials as well as the GHG intensity for each scenario in the Canadian fossil fuel-fired thermal power plants.

In order to perform these calculations, the fuel consumption, electricity production, and emission factors for different fuels for each province were used to estimate GHG emission reduction potentials. The latest data publicly available from Environment Canada that has been used in this paper is for 1996 (Environment Canada, 1997). It should be noted that some recent data for electricity generation sectors and their GHG emissions is available for some provinces. However, for those provinces that power plants are privately owned, the only publicly available data is electricity generation, which is not sufficient for GHG emission estimation with reasonable accuracy. In order to estimate GHG emissions, at least the fuel consumption to generate certain



amount of electricity is required. When only generated electricity is available, to estimated consumed fuel, the efficiency of the electricity generation is required. Since this minimum required information is not available, those recent data cannot be used for GHG emission evaluation.

**Table 11: Fuel consumption, electricity production, GHG emission reduction potentials, and GHG intensity**  
(estimated by using Tier 3) in Canada

	<b>Fuel</b>	<b>Existing</b>	<b>Scenario 1</b>	<b>Scenario 2</b>	<b>Scenario 3</b>	<b>Scenario 4</b>	<b>Scenario 5</b>	<b>Scenario 6</b>	<b>Scenario 7</b>	<b>Scenario 8</b>
<b>Fuel consumption</b>	Coal (kt)	46,927	0	0	35,259	0	0	30,322	51,620	0
	Petroleum (ML)	1,692	0	0	1,692	0	0	1,692	1,861	0
	Natural gas (BL)	4,061	34,690	21,368	4,061	18,960	16,043	4,061	4467	23,505
<b>Electricity production (GWh)</b>	Coal	86,150	0	0	86,150	0	0	86,150	86,150	0
	Petroleum	7,115	0	0	7,115	0	0	7,115	7,115	0
	Natural gas	14,577	107,841	107,841	14,577	107,841	107,841	14,577	14,577	107,841
	Total	107,841	107,841	107,841	107,841	107,841	107,841	107,841	107,841	107,841
<b>GHG emissions (kt/year)</b>	Coal	85,421	0	0	66,147	0	0	56,886	12,215	0
	Petroleum	5,202	0	0	5,202	0	0	5,202	744	0
	Natural gas	7,662	65,436	40,138	7,662	35,609	30,131	7,662	1,096	5,740
	Total	98,285	65,436	40,138	79,011	35,609	30,131	69,750	14,055	5,740
<b>Reduction potential (%)</b>	Coal	-	-	-	23	-	-	33	86	-
	Petroleum	-	-	-	0	-	-	0	86	-
	Natural gas	-	33	59	0	64	69	0	86	94
	Total	-	33	59	20	64	69	29	86	94
<b>GHG intensity (gCO<sub>2</sub>eq/ kWh)</b>	Total	911	607	372	733	330	279	647	130	53

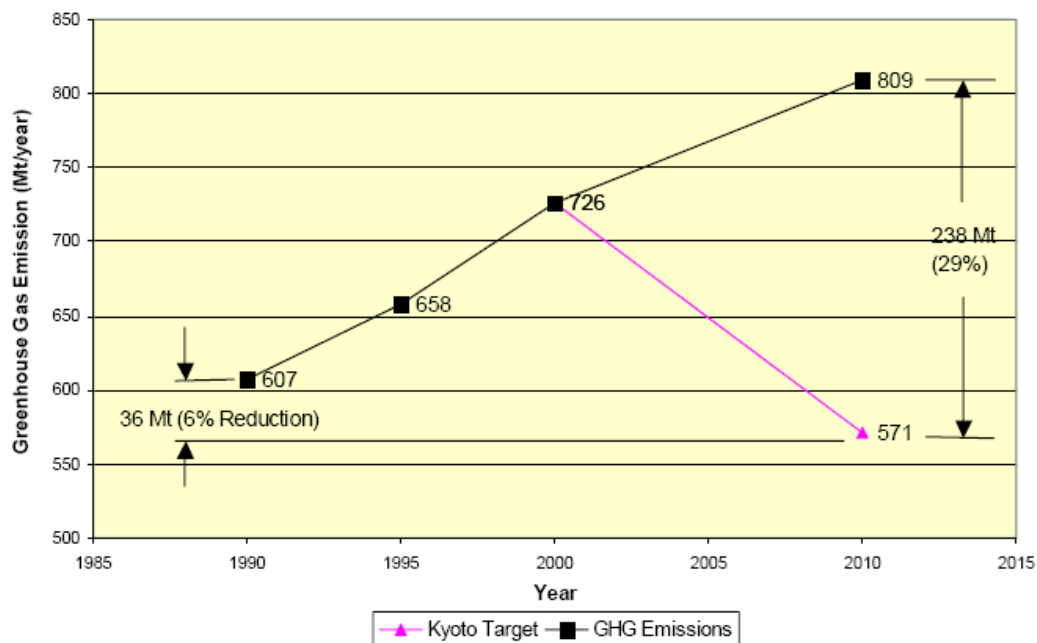
It should be noted that the focus of this work is on the GHG emission reduction potentials in fossil fuel-fired thermal power plants. Therefore, other power generation technologies (e.g. nuclear, hydro, renewables, etc.) are not considered in the estimation of GHG emissions.

Table 11 shows that Canada's GHG emissions can be reduced from almost 100 Mt/year in the base case (existing case) to 65, 40, 79, 36, 30, 70, 14, and 6 Mt/year based on the first to eighth scenarios, respectively. This means 33%, 59%, 20%, 64%, 69%, 29%, 86%, and 94% reduction potentials in GHG emissions, respectively.

The best solutions are the eighth (NGCC and CCS), seventh (CCS), and fifth (hybrid SOFC) scenarios, in order of reduction potential. On the other hand, the second scenario (NGCC) is the most practical one, and its technology has already matured and is available. This scenario can reduce GHG emissions by almost 60%.

Figure 5 illustrates Canada's GHG emission projection and its commitment to the Kyoto Protocol (Environment Canada, 2005). According to the Kyoto Protocol, Canada should reduce its GHG emissions to 6% below 1990 GHG emission levels by 2012 (UNFCCC, 1998). The diagram points out that Canada's GHG emissions in 1990 were 607 Mt/year and should be reduced by 36 Mt/year to 571 Mt/year by 2012. On the other hand, it is predicted that the GHG emissions in 2012 will be approximately 809 Mt/year. Therefore, in order to meet the Kyoto Protocol commitment, Canada should reduce its emissions by 238 Mt/year. This means that just by replacing existing power plants by NGCC plants (second scenario), which results in a 60 Mt/year emission reduction, Canada can achieve more than 25% of its commitment of GHG emission reduction to the Kyoto Protocol.

Table 12 shows the summary of estimations of GHG emission reduction potentials for some Canadian provinces, including Alberta, Ontario, Saskatchewan, Nova Scotia, New Brunswick, British Columbia, and Newfoundland as well as Canada as a whole. Other provinces are not included in the table since they, together, are responsible for only approximately 1% of Canada's GHG emissions from electricity generation. Based on this table, Alberta, Ontario, and Saskatchewan are the biggest producers of GHG in Canada's electricity generation sector, emitting 49%, 21%, and 14% of this sector's GHGs, respectively. Therefore, they have higher potentials to reduce GHG emissions.



**Figure 5: Canada greenhouse gas emission projection and the Kyoto Protocol (based on the raw data provided by Environment Canada (2005))**

**Table 12: GHG emissions as well as reduction potentials for each scenario in different provinces in Canada, estimated by using Tier 3**

	Existing	Scenario 1		Scenario 2		Scenario 3	
	GHG emissions (kt/year)	GHG emissions (kt/year)	Reduction potential %	GHG emissions (kt/year)	Reduction potential %	GHG emissions (kt/year)	Reduction potential %
<b>Canada</b>	98,285	65,436	33	40,138	59	79,011	20
<b>Alberta</b>	48,070	31,870	33	18,200	62	37,368	22
<b>Ontario</b>	20,784	13,590	35	10,710	48	19,978	4
<b>Saskatchewan</b>	13,661	9,517	30	3,486	74	7,482	45
<b>Nova Scotia</b>	7,282	4,675	36	3,304	55	6,260	14
<b>New Brunswick</b>	6,055	3,716	39	2,627	57	5,491	9
<b>British Columbia</b>	1,277	1,286	-	1,260	1.5	1,277	-
<b>Newfoundland</b>	1,155	782	32	552	52	1,155	-

**Table 12: GHG emissions as well as reduction potentials for each scenario in different provinces (Cont.)**

	Existing	Scenario 4		Scenario 5		Scenario 6	
	GHG emissions (kt/year)	GHG emissions (kt/year)	Reduction potential %	GHG emissions (kt/year)	Reduction potential %	GHG emissions (kt/year)	Reduction potential %
<b>Canada</b>	98,285	35,609	64	30,131	69	69,750	29
<b>Alberta</b>	48,070	16,146	66	13,662	72	32,529	32
<b>Ontario</b>	20,784	9,501	54	8,040	61	17,712	15
<b>Saskatchewan</b>	13,661	3,092	77	2,617	81	6,504	52
<b>Nova Scotia</b>	7,282	2,931	60	2,480	66	5,475	25
<b>New Brunswick</b>	6,055	2,330	62	1,972	67	5,099	16
<b>British Columbia</b>	1,277	1,117	12	946	26	1,277	-
<b>Newfoundland</b>	1,155	490	58	415	64	1,155	-

**Table 12: GHG emissions as well as reduction potentials for each scenario in different provinces (Cont.)**

	Existing	Scenario 7		Scenario 8	
	GHG emissions (kt/year)	GHG emissions (kt/year)	Reduction potential %	GHG emissions (kt/year)	Reduction potential %
<b>Canada</b>	98,285	14,055	86	5,740	94
<b>Alberta</b>	48,070	6,874	86	2,603	95
<b>Ontario</b>	20,784	2,972	86	1,532	93
<b>Saskatchewan</b>	13,661	1,954	86	498	97
<b>Nova Scotia</b>	7,282	1,041	86	472	94
<b>New Brunswick</b>	6,055	866	86	376	94
<b>British Columbia</b>	1,277	183	86	180	86
<b>Newfoundland</b>	1,155	165	86	79	93

Furthermore, Table 12 points out that the level of GHG reduction potentials is greatly influenced by the share of coal in electricity generation. For instance, the shares of coal in electricity generation from fossil fuels in Alberta, Ontario, and Saskatchewan are 87%, 70%, and 92%, respectively (Environment Canada, 2008). Accordingly, results show that Saskatchewan, Alberta, and Ontario have the highest levels of GHG emission reduction potentials, respectively, especially in the third and sixth scenarios.

Tables 13 to 15 show details of GHG estimations, including consumption of different fuels, electricity production, and GHG emissions for both the reference case (existing conditions) and each reduction scenario in Ontario, Alberta, and Saskatchewan, respectively. Since effects of the seventh and eighth scenarios are similar for all provinces, only the first to sixth scenarios are considered in these tables.

In Ontario, for the first scenario (fuel switching to natural gas) there is a 35% reduction potential, which is slightly higher than the national average of 33%. For the second, fourth, and fifth scenarios, GHG reduction potentials in Ontario are considerably lower than the Canadian average with 48%, 54%, and 61% in comparison with 59%, 64%, and 69%, respectively. This could be as a result of high efficiency of both natural gas and coal fuelled power stations in Ontario. Same is true for the third and sixth scenarios where Ontario's GHG emission reduction potentials are significantly lower than the national average.

**Table 13: Fuel consumption, electricity production, and GHG emissions for both the reference case (existing conditions) and each GHG reduction scenario in Ontario, estimated by using Tier 3**

	<b>Fuel</b>	<b>Existing</b>	<b>Scenario 1</b>	<b>Scenario 2</b>	<b>Scenario 3</b>	<b>Scenario 4</b>	<b>Scenario 5</b>	<b>Scenario 6</b>
<b>Fuel consumption</b>	Coal (kt)	7,192	-	-	6,851	-	-	5,892
	Oil (ML)	117	-	-	117	-	-	117
	Natural Gas (BL)	1,825	7,205	5,702	1,825	5,059	4,281	1,825
<b>Electricity production (GWh)</b>	Coal	20,928	-	-	20,928	-	-	20,928
	Oil	557	-	-	557	-	-	557
	Natural Gas	7,290	28,775	28,775	7,290	28,775	28,775	7,290
	Total	28,775	28,775	28,775	28,775	28,775	28,775	28,775
<b>GHG emissions (kt/year)</b>	Coal	16,993	-	-	16,187	-	-	13,920
	Oil	348	-	-	348	-	-	348
	Natural Gas	3,443	13,590	10,710	3,443	9,501	8,040	3,443
	Total	20,784	13,590	10,710	19,978	9,501	8,040	17,712
<b>Reduction</b>	<b>%</b>	-	35	48	4	54	61	15

For Ontario, it can be concluded that although the power generation sector is emitting less GHG in comparison to the national average, there are still considerable potentials for using the technologies proposed in these scenarios. In addition, the first scenario tends to be the most suitable one in the short term.

In Alberta (Tables 14 and 12), reduction potentials for eight scenarios are 33%, 62%, 22%, 66%, 72%, 32%, 86% and 95%, respectively. These are very close to the average values for Canada. This means the consumed fuel distribution and efficiency of electricity generation in Alberta is very close to the average values of these parameters in Canada.

**Table 14: Fuel consumption, electricity production, and GHG emissions for both the reference case (existing conditions) and each GHG reduction scenario in Alberta, estimated by using Tier 3**

	<b>Fuel</b>	<b>Existing</b>	<b>Scenario 1</b>	<b>Scenario 2</b>	<b>Scenario 3</b>	<b>Scenario 4</b>	<b>Scenario 5</b>	<b>Scenario 6</b>
<b>Fuel consumption</b>	Coal (kt)	25,794	-	-	19,696	-	-	16,939
	Oil (ML)	16	-	-	16	-	-	16
	Natural Gas (BL)	1,458	16,896	9,689	1,458	8,597	7,274	1,458
<b>Electricity production (GWh)</b>	Coal	44,577	-	-	44,577	-	-	44,577
	Oil	99	-	-	99	-	-	99
	Natural GAS	4,221	48,897	48,897	4,221	48,897	48,897	4,221
	Total	48,897	48,897	48,897	48,897	48,897	48,897	48,897
<b>GHG emissions (kt/year)</b>	Coal	45,272	-	-	34,569	-	-	29,730
	Oil	47	-	-	47	-	-	47
	Natural gas	2,752	31,870	18,200	2,752	16,146	13,662	2,752
	Total	48,071	31,870	18,200	37,368	16,146	13,662	32,529
<b>Reduction</b>	%	-	33	62	22	66	72	32

Table 15 shows the GHG reduction potentials in Saskatchewan. It is obvious that GHG emission reduction potentials are the highest in Saskatchewan among all other provinces for all scenarios except the first one. As noted earlier, the reason is the high share of coal in the power generation of this province. In the first scenario, it is assumed that the efficiency of power plants is maintained, and that is why the emission reduction potential is not high.

**Table 15: Fuel consumption, electricity production, and GHG emissions for both the reference case (existing conditions) and each GHG reduction scenario in Saskatchewan, estimated by using Tier 3**

	<b>Fuel</b>	<b>Existing</b>	<b>Scenario 1</b>	<b>Scenario 2</b>	<b>Scenario 3</b>	<b>Scenario 4</b>	<b>Scenario 5</b>	<b>Scenario 6</b>
<b>Fuel consumption</b>	Coal (kt)	9,706	-	-	5,149	-	-	4,428
	Oil (ML)	6	-	-	6	-	-	6
	Natural gas (BL)	255	5,045	1,856	255	1,647	1,393	255
<b>Electricity production (GWh)</b>	Coal	8,856	-	-	8,856	-	-	8,856
	Oil	36	-	-	36	-	-	36
	Natural gas	474	9,365	9,365	474	9,365	9,365	474
	Total	9,365	9,365	9,365	9,365	9,365	9,365	9,365
<b>GHG emissions (kt/year)</b>	Coal	13,160	-	-	6,981	-	-	6,004
	Oil	20	-	-	20	-	-	20
	Natural gas	481	9,517	3,486	481	3,092	2,617	481
	Total	13,661	9,517	3,486	7,482	3,092	2,617	6,504
<b>Reduction percent</b>	%	-	30	74	45	77	81	52

## 2.11 GHG emission reduction potentials in Iran

In the Iranian power generation industry, the third and sixth scenarios cannot be considered because there is no coal-fired power plant. Therefore, in this case, only six scenarios are investigated.

Table 16 shows the energy of consumed fuel, electricity generation, GHG emissions, and intensity for both the reference case (existing conditions) and six alternative scenarios and reduction potentials in each scenario in Iran's electricity generation sector for the period of March 2005 to February 2006. Unlike the tables for the Canadian electricity generation industry, in this table the energy of consumed fuel (and not consumed fuel itself) is reported. The reason is that, in the case of Iran, default emission factors have been used, and as Tables 3 and 5 show, these emission factors are based on fuel energy content, not physical units of fuels. Therefore, in this table physical units of consumed fuels are converted to consumed fuel energy content.

**Table 16 : Energy consumption, electricity generation, and GHG emission reduction potentials, estimated by using Tier 3, in Iran's electricity generation sector for the period of March 2005 to February 2006**

	<b>Power plant type</b>	<b>Existing</b>	<b>Scenario 1</b>	<b>Scenario 2</b>	<b>Scenario 4</b>	<b>Scenario 5</b>	<b>Scenario 7</b>	<b>Scenario 8</b>
<b>Energy of consumed fuel (TJ)</b>	Steam PP	882	882	0	0	0	970	0
	GT	375	375	0	0	0	413	0
	CCPP	285	285	1,137	0	0	314	1,251
	SOFC	0	0	0	1,013	0	0	0
	Hybrid SOFC	0	0	0	0	857	0	0
	Total	1,543	1,543	1,137	1,013	857	1,697	1,251
<b>Electricity generation (GWh)</b>	Steam PP	89,574	89,574	0	0	0	89,574	0
	GT	29,023	29,023	0	0	0	29,023	0
	CCPP	36,194	36,194	154,791	0	0	36,194	154,791
	SOFC	0	0	0	154,791	0	0	0
	Hybrid SOFC	0	0	0	0	154,791	0	0
	Total	154,791	154,791	154,791	154,791	154,791	154,791	154,791
<b>GHG emissions (kt/year)</b>	Steam PP	55,300	49,804	0	0	0	7,908	0
	GT	22,447	21,199	0	0	0	3,210	0
	CCPP	16,736	16,297	64,354	0	0	2,393	9,203
	SOFC	0	0	0	57,333	0	0	0
	Hybrid SOFC	0	0	0	0	48,513	0	0
	Total	94,483	87,300	64,354	57,333	48,513	13,511	9,203
<b>Reduction potential (%)</b>	Steam PP	-	9.9	-	-	-	86	-
	GT	-	5.6	-	-	-	86	-
	CCPP	-	2.6	31.9	-	-	86	90
	SOFC	-	-	-	39.3	-	-	-
	Hybrid SOFC	-	-	-	-	48.7	-	-
	Total	-	7.6	31.9	39.3	48.7	86	90
<b>GHG intensity (gCO<sub>2</sub>eq/kWh)</b>	Total	610	564	416	370	313	87	59



Table 16 shows how fuel consumption can be decreased in different scenarios. For instance, the energy of consumed fuel can be reduced in the fifth scenario from the reference case (existing case) of 1,543 TJ to 857 TJ, which means a 44% reduction. This is due to higher efficiency of the introduced scenarios in comparison to current conditions.

Scenario 8 (NGCC and CCS) with almost 90% GHG emission reduction potential is the best option. Scenarios 2 (NGCC), 4 (SOFC), 5 (hybrid SOFC), and 7 (CCS) have about 32%, 39%, 49%, and 86% reduction potentials, respectively. In the first scenario, there are 9.9%, 5.6%, and 2.6% GHG emission reduction potentials for steam power plants, gas turbines, and combined cycle power plants, respectively, with an overall reduction potential of 7.6%. Also, GHG emission intensity can be reduced from the current 610 gCO<sub>2</sub>eq/kWh to 564, 416, 370, 313, 87, and 59 gCO<sub>2</sub>eq/kWh in the first to eighth scenarios, respectively.

In order to show the variety of possible analyses, timely variations of GHG reduction potentials are presented for the Iranian thermal power plants. Table 17 shows the GHG emissions and intensity for the existing situation and six alternative scenarios and reduction potentials for each scenario in Iran's electricity generation sector between 1995 and 2005. The table shows that the GHG reduction potentials decreased from 1995 to 2005. The reasons stem from the installation of many combined cycle power plants and fuel switching from diesel and residual oil to natural gas in recent years. It should be mentioned that, as the table shows, the net amount of GHG emissions has increased. This is due to the commissioning of new power stations and an increase in electricity generation capacity.

Table 18 shows the GHG emissions in current conditions and two alternative scenarios and reduction potential for each scenario for all local electricity companies in 2004 and 2005. Due to the space limitation, only the first and second scenarios are presented in this table.

Table 18 illustrates that, in the first scenario, GHG reduction potential ranges from almost 0% for provinces that use natural gas in all their power stations all the time to 24% and 26% in Kish and Sistan and Balouchestan, respectively, where there is no natural gas for electricity generation. For the second scenario, the reduction potential can be as low as 12% or as high as 77%. This depends on the share of CCPPs in electricity generation of the province, current efficiency of power plants, and natural gas consumption.

**Table 17: GHG emissions and intensity of Iran's electricity generation sector for different scenarios from 1995 to 2005, estimated by using Tier 1**

Year	Existing		Scenario 1			Scenario 2			Scenario 4		
	GHG emissions (kt/year)	Intensity (gCO <sub>2</sub> eq/kWh)	GHG emissions (kt/year)	Intensity (gCO <sub>2</sub> eq/kWh)	Reduction potential (%)	GHG emissions (kt/year)	Intensity (gCO <sub>2</sub> eq/kWh)	Reduction potential (%)	GHG emissions (kt/year)	Intensity (gCO <sub>2</sub> eq/kWh)	Reduction potential (%)
2005	98,991	630	91,847	584	7.2	65,166	415	34.2	58,057	369	41.4
2004	90,958	610	84,638	568	6.9	61,817	415	32.0	55,074	369	39.5
2003	79,631	587	74,515	550	6.4	56,208	415	29.4	50,077	369	37.1
2002	78,844	622	72,415	571	8.2	52,546	415	33.4	46,814	369	40.6
2001	75,099	632	68,185	574	9.2	49,291	415	34.4	43,914	369	41.5
2000	70,863	634	64,444	577	9.1	46,309	415	34.6	41,257	369	41.8
1999	65,137	640	59,340	583	8.9	42,224	415	35.2	37,618	369	42.2
1998	57,222	632	52,539	581	8.2	37,510	415	34.4	33,418	369	41.6
1997	57,470	677	50,607	596	11.9	35,210	415	38.7	31,369	369	45.4
1996	53,959	693	46,826	602	13.2	32,272	415	40.2	28,751	369	46.7
1995	52,299	726	45,541	632	12.9	29,870	415	42.9	26,611	369	49.1

**Table 17: GHG emissions and intensity of Iran's electricity generation sector for different scenarios from 1995 to 2005 (Cont.)**

Year	Scenario 5			Scenario 7			Scenario 8		
	GHG emissions (kt/year)	Intensity (gCO <sub>2</sub> eq/kWh)	Reduction potential (%)	GHG emissions (kt/year)	Intensity (gCO <sub>2</sub> eq/kWh)	Reduction potential (%)	GHG emissions (kt/year)	Intensity (gCO <sub>2</sub> eq/kWh)	Reduction potential (%)
2005	49,125	313	50.4	14,156	90	85.7	9,319	59	85.7
2004	46,601	313	48.8	13,007	87	85.7	8,840	59	85.7
2003	42,372	313	46.8	11,387	84	85.7	8,035	59	85.7
2002	39,611	313	49.8	11,275	89	85.7	7,514	59	85.7
2001	37,158	313	50.5	10,739	90	85.7	7,049	59	85.7
2000	34,910	313	50.7	10,133	91	85.7	6,622	59	85.7
1999	31,831	313	51.1	9,315	92	85.7	6,038	59	85.7
1998	28,277	313	50.6	8,183	90	85.7	5,364	59	85.7
1997	26,543	313	53.8	8,218	97	85.7	5,035	59	85.7
1996	24,328	313	54.9	7,716	99	85.7	4,615	59	85.7
1995	22,517	313	56.9	7,479	104	85.7	4,271	59	85.7

**Table 18 : GHG emissions reduction potentials for local electricity companies in 2004 and 2005 (Tier 1)**

Local electricity companies	Year	Existing	Scenario 1		Scenario 2	
		GHG emissions (kt/year)	GHG emissions (kt/year)	Reduction potential (%)	GHG emissions (kt/year)	Reduction potential (%)
Azarbaijan	2005	5,980	5,156	13.8	3,733	37.6
	2004	4,303	3,780	12.2	2,795	35.0
Isfahan	2005	10,396	9,428	9.3	6,915	33.5
	2004	10,690	9,566	10.5	7,020	34.3
Bakhtar	2005	7,730	6,979	9.7	5,653	26.9
	2004	7,268	6,402	11.9	5,208	28.3
Tehran	2005	20,607	19,193	6.9	14,122	31.5
	2004	17,878	16,417	8.2	12,340	31.0
Khorasan	2005	7,716	7,586	1.7	5,669	26.5
	2004	7,274	7,202	1.0	5,647	22.4
Khozestan	2005	5,997	5,857	2.3	4,730	21.1
	2004	7,725	7,537	2.4	6,096	21.1
Zanjan	2005*	-	-	-	-	-
	2004*	-	-	-	-	-
Semnan	2005	10	10	0.3	3	71.4
	2004	8	8	0.3	2	74.5
Sistan and Balouchestan	2005	2,599	1,919	26.1	995	61.7
	2004	2,439	1,802	26.1	915	62.5
Gharb	2005	2,718	2,421	10.9	1,809	33.4
	2004	2,671	2,319	13.2	1,749	34.5
Fars	2005	6,337	6,255	1.3	4,666	26.4
	2004	6,723	6,678	0.7	4,775	29.0
Kerman	2005	3,589	3,253	9.4	2,046	43.0
	2004	3,603	3,337	7.4	2,085	42.1
Gilan	2005	4,361	4,269	2.1	3,779	13.3
	2004	4,319	4,255	1.5	3,814	11.7
Mazandaran	2005	7,264	6,810	6.2	4,904	32.5
	2004	7,466	7,194	3.6	5,198	30.4
Hormozgan	2005	7,393	6,593	10.8	4,376	40.8
	2004	5,255	4,947	5.9	3,422	34.9
Yazd	2005	2,708	2,241	17.3	627	76.8
	2004	2,534	2,100	17.1	623	75.4
Kish	2005	489	371	24.2	147	69.9
	2004	432	327	24.2	129	70.0
Private Sector	2005	1,387	1,383	0.3	991	28.5
	2004*	-	-	-	-	-
Industry	2005	3,230	3,223	0.2	1,876	41.9
	2004	1,823	1,823	0.0	1,178	35.4

\* No fossil fuel power generation.

Table 19 demonstrates the GHG reduction potentials in Iran's major power plants (with electricity generation of more than 100,000 MWh) via the first scenario in 2005. Again the reduction potentials depend on natural gas consumption in a particular power station. For instance, in the Tarasht power plant, all burned fuel is natural gas, so there is no potential to reduce GHG emissions by employing this scheme.

**Table 19: GHG reduction potential for all Iranian thermal power plants by first scenario in 2005**

Power plant	Reduction Percent (%)	Power plant	Reduction Percent (%)	Power plant	Reduction Percent (%)	Power plant	Reduction Percent (%)
<b>Steam</b>		Rajaei	11.5	Shirvan	0.1	Sanandaj	23.9
Tarasht	0.0	Bistoon	10.5	Shariati	1.0	Kish	23.9
Besat	9.2	Gharb	7.2	Sofian	6.6	Rest	12.5
Eslam Abad	10.5	Iranshahr	27.2	Zahedan	23.9	Ave.	5.6
Montazer Ghaem	12.0	Shazand	11.4	Salimi	0.0	<b>CCPP</b>	
Loshan	1.6	Sahand	16.2	Kazeron	0.7	Montazer Ghaem	4.5
Zarand	27.2	Ave.	9.9	Kangan	0.0	Gilan	2.5
Mashhad	0.0	<b>GT</b>		Zanbagh (Yazd)	3.7	Ghom	2.9
Neka	7.1	Shiraz	6.9	Yazd (GT)	0.0	Rajaei	2.4
Ramin	2.7	Mashhad	0.1	Yazd (CCPP)	6.5	Fars	0.5
Bandar Abbass	15.1	Loshan	2.3	Kerman	7.7	Khoi	7.3
Montazeri	8.8	Rey	4.6	Abadan	2.0	Neishaboor	2.3
Toos	2.2	Chabahar	23.9	Damavand	7.1	Shariati	0.6
Tabriz	14.8	Oroumie	11.5	Hormozgan	2.3	Ave.	2.6

## 2.12 Comparison of GHG emission reduction potentials in Canada and Iran

The comparison of GHG emission reduction potentials in Iran and Canada shows that there are higher potentials in Canada. For the first scenario, the GHG reduction potential is 7.6% and 33%

for Iran and Canada, respectively. The reason is that most Iranian thermal power plants are equipped with dual fuel burners and use natural gas most of the time. In fact, 77% of energy consumed in Iran's thermal power plants comes from natural gas.

For the second scenario the pattern is similar; 32% versus 59% for Iran and Canada, respectively. The reason is that in 2005, as noted earlier, more than 20% of the total electricity generated in Iran was produced by CCPPs, whereas most fossil fuel-fired thermal power plants in Canada are coal-fired steam cycles. In fact, almost 73% of electricity in Canadian thermal power stations is generated by coal. The same trend is observed for the fourth and fifth scenarios with 39% and 49% for Iran and 64% and 69% for Canada, respectively. This is due to the higher efficiency of natural gas fuel power plants, especially NGCCs. In the last two scenarios, however, both countries have similar potentials. This is because of the absorption of most of the CO<sub>2</sub> by the CO<sub>2</sub> capture system, regardless of power plant technology.

Obviously these scenarios cannot be entirely implemented in the short term, and they require long-term plans. The best option is to apply appropriate scenario(s) as old power plants retire, and new plants are built to replace them.

Table 20 categorizes the capacity of power stations in Iran's fossil fuel electricity generation industry based on the age of the plants. The table shows that more than 40% of Iran's electricity generation capacity was installed more than 20 years ago. Also, approximately 11% of the capacity is more than 30 years old, and these older plants should be retiring in a few years (Iran Power Generation Co., 2007). Although similar data for the Canadian power generation sector is not available, it is expected that the ages of fossil fuel-fired power plants, especially coal-fired plants, are high, and many of them are in their final years of effective life. Also, the fact that ownership of all power plants in Iran and some power stations in Canada belongs to the government can be helpful, because the decision about technology of new power plants will not be based solely on economic considerations, and environmental considerations should be taken into account as well. This opportunity can be used to apply the aforementioned scenarios and effectively reduce GHG emissions from this industry.

**Table 20: Age of fossil fuel power stations in the Iranian power generation industry based on the share of each category for different age ranges (based on the raw data provided by Iran Power Generation Co. (2007))**

Technology	Less than 20 years (%)	20-30 years (%)	30-40 years (%)	More than 40 years (%)
Steam plants	32	57	8	3
GT	74	6	20	<0.1
CCPP	100	0	0	0
Total	60	29	10	1

## 2.13 Cost of different scenarios

Inevitably, the first question raised about these scenarios is their impacts from an economic point of view. The cost of the first scenario is not considerable, and the main issue is availability of natural gas at a reasonable price. Since SOFC technology and thus Scenarios 4, 5, and 6 are not commercialized yet, it is not possible to assess their cost accurately. Therefore, in the remainder of this section economic effects of Scenarios 2 (NGCC), 3 (IGCC), 7 (CCS), and 8 (NGCC and CCS) are investigated mostly based on Rubin, Chen, and Rao (2007).

Table 21 summarizes the range of costs reported for new power plants using available commercial power generation and CO<sub>2</sub> capture technologies in studies published prior to 2004 (IPCC, 2005; Rubin et al., 2007; IEA, 2000, 2003a, 2004; Parsons, Shelton, and Lyons, 2002; Nsakala, Liljedahl, Marion, Bozzuto, Andrus, and Chamberland, 2003; Rao and Rubin, 2002; Rubin, Rao, and Chen, 2005; Simbeck, 2002; Stobbs and Clark, 2005).

The table reveals considerable variation in both capital cost and cost of electricity (COE) of power generation and CO<sub>2</sub> capture unit for all three power generation technologies, namely, NGCC, pulverized coal fuel-fired (PF), and IGCC, due to different assumptions about key parameters (such as fuel properties, fuel cost, plant size, plant efficiency, plant capacity factor, plant financing, and performance of the CO<sub>2</sub> capture unit) (Rubin et al., 2007).

The general conclusion from these studies is that the COE, for both configurations with and without CO<sub>2</sub> capture, is the lowest for NGCC plants. For coal-based plants, pulverized coal fuel-fired plants for configuration without CO<sub>2</sub> capture and IGCC plants for configuration with CO<sub>2</sub> capture have the lowest COE.

**Table 21: Summary of reported costs for a new power plant with and without CO<sub>2</sub> capture based on current technologies in studies published prior to 2004 (Rubin et al., 2007)**

Performance and cost measures	NGCC plant	PF plant	IGCC plant
GHG intensity (without CCS) (gCO <sub>2</sub> eq/kWh)	344–379	736–811	682–846
GHG intensity (with CCS) (gCO <sub>2</sub> eq/kWh)	40–66	92–145	65–152
Total capital cost (without CCS) (\$/kW)	515–724	1,161–1,486	1,169–1,565
Total capital cost (with CCS) (\$/kW)	909–1,261	1,894–2,578	1,414–2,270
Percentage increase in capital cost (when CCS installed) (%)	64–100	44–74	19–66
COE (without CCS) (\$/MWh)	31–50	43–52	41–61
COE (with CCS) (\$/MWh)	43–72	62–86	54–79
Increase in COE (when CCS installed) (\$/MWh)	12–24	18–34	9–22
Percentage increase in COE (when CCS installed) (%)	37–69	42–66	20–55
Cost of captured CO <sub>2</sub> (\$/t CO <sub>2</sub> )	37–74	29–51	13–37

A more recent study showed a different pattern because of an increase in the price of several items. Table 22 summarizes the major results of this analysis (Rubin et al., 2007). The table shows that PF and IGCC have the lowest COE for configurations without and with a CO<sub>2</sub> capture system, respectively. These results are not in agreement with the studies in Table 21. The reason is that, at the time of this analysis, the price of natural gas (\$3–4.5/GJ in Table 21 vs. \$6/GJ in Table 22) as well as many raw materials had increased significantly.

**Table 22: Summary of recent study (after 2004) for costs of a new power plant with and without CO<sub>2</sub> capture unit based on current technologies (Rubin et al., 2007)**

Performance and cost measures	NGCC plant		PF plant		IGCC plant	
	Without CCS	With CCS	Without CCS	With CCS	Without CCS	With CCS
GHG intensity (gCO <sub>2</sub> eq/kWh)	367	43	811	107	822	97
CO <sub>2</sub> captured (g/kWh)	-	387	-	959	-	850
CCS plant derating (% output loss)	-	14.7	-	23.9	-	13.4
CCS energy penalty (% fuel input/kWh)	-	17.3	-	31.4	-	15.5
Total capital cost (\$/kW)	671	1,091	1,442	2,345	1,567	2,076
COE (\$/MWh)	60.3	80.6	53.0	88.0	55.5	71.9
Cost of captured CO <sub>2</sub> (\$/t CO <sub>2</sub> )	-	62.6	-	49.7	-	22.6

In order to have a clear idea of natural gas price variations, Figure 6 shows natural gas price in Canadian \$/GJ in the Canadian market (Natural gas, 2009). As the graph indicates, although \$6/GJ in Table 22 is somewhat less than the price of natural gas at the time of this analysis (2008), it is closer than the \$3–4.5/GJ assumed in Table 21.

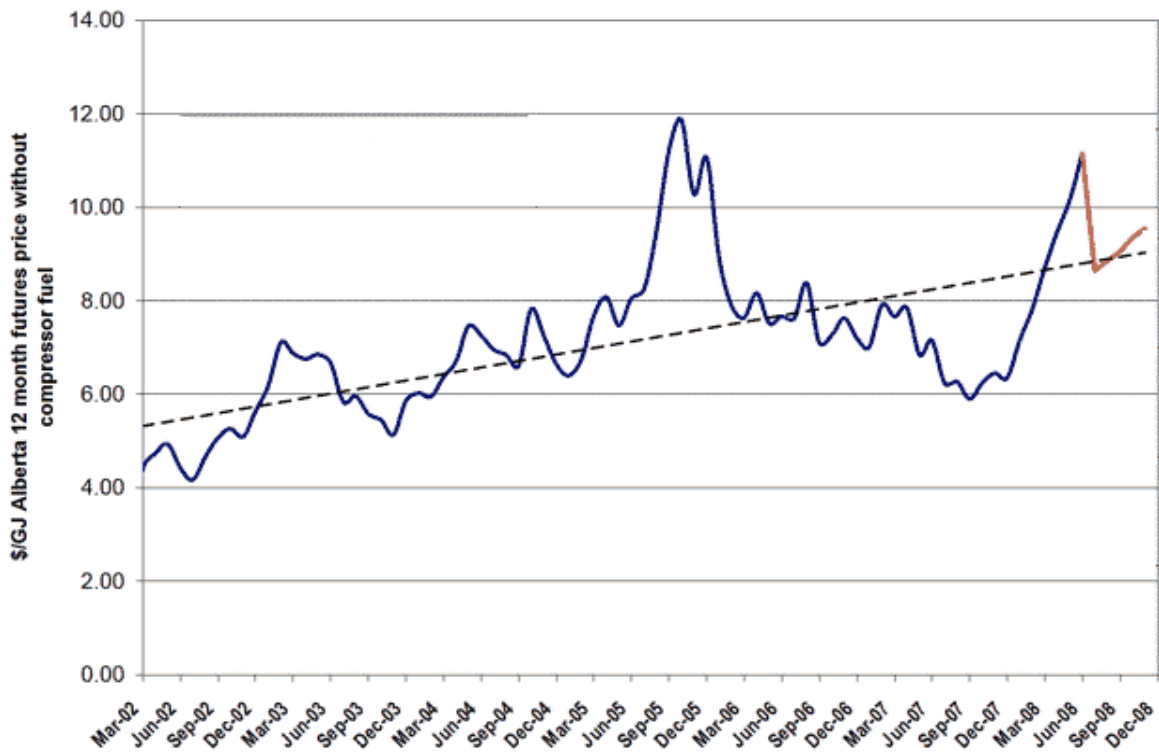


**Figure 6: Natural gas prices in Canadian market from 2002 to 2008 (Natural gas, 2009)**

To conclude this subsection, Scenarios 2 and 3 can compete with existing power plants, especially using IGCC technology when the increase in the natural gas price is considered. Therefore, when a new power station is to be built, these technologies should be considered as main candidates. For Scenarios 7 and 8, CO<sub>2</sub> capture from power plants is still too expensive but its cost is expected to lower as a consequence of technological improvements.



## 2.14 Conclusion

The first part of this chapter showed the importance of preparation of the GHG inventory report for the electricity generation sector. The results demonstrated that Iran's electricity generation sector did a reasonably good job in reducing the GHG intensity in the past 10 years with 13% overall reduction. However, the detailed estimations showed that still there are power plants with extremely high GHG intensity. This indicated that there are great potentials for further GHG intensity reduction in the sector. Moreover, some minor adjustments are required in the data collection procedure for the Iranian power plants in order to follow the IPCC guidelines for the GHG inventory report. A similar conclusion can be arrived at about the GHG emission reduction potentials in the Canadian thermal fossil fuel power generation industry.

In the remainder of the chapter, the GHG reduction potentials were investigated through eight scenarios. The results for Canadian power stations showed that there were very high GHG emission reduction potentials. The estimation for GHG emission reduction potentials for different provinces revealed that Alberta, Ontario, and Saskatchewan were responsible for more than 84% of GHG emissions in the electricity generation sector in Canada. Therefore, they had the highest GHG emission reduction potentials. The results pointed out that, despite acceptable performance of the power generation sector in some provinces, there are considerable potentials to reduce GHG emissions. For instance, the second scenario (NGCC), being the most practical scenario, can reduce GHG emissions by almost 60%, which is more than 25% percent of Canada's commitment of GHG emission reduction to the Kyoto Protocol.

In the case of Iran, the results illustrated that the GHG reduction potentials are lower than the potentials for Canada. One of the reasons is that 77% of energy consumed in Iran's thermal power plants comes from natural gas. However, implementation of the scenarios can help the country in sustainable development. Moreover, it could be economically beneficial due to the possibility of selling the Carbon Credit to Annex I Parties of the Kyoto Protocol.

The economic analysis showed that when a new power station is to be built, different scenarios should be considered, particularly Scenarios 2 (NGCC) and 3 (IGCC). CO<sub>2</sub> capture from power plants is still too expensive, but its costs are expected to decrease.

Furthermore, the results of various estimations were presented to show a wide variety of possible analyses in this field. This included estimation of GHG emissions and reduction potentials in different levels, for example, individual power plants, local electricity companies, and provincial and national electricity generation sectors. The time variations of GHG emissions and reduction potentials were also taken into account to evaluate progress in a certain sector.

## **CHAPTER THREE**

### **Fuel Cell Technology and Hybrid Solid Oxide Fuel Cell Cycle Modeling**

Fuel cell technology is a promising technology for electricity generation with high efficiency and minimal environmental impacts. The idea is to directly convert fuel chemical energy to electrical and thermal energy via electrochemical reactions. This section outlines the basic operation of a fuel cell and its essential components, as well as the main subsystems of fuel cell plants. Then, the solid oxide fuel cell (SOFC), as a main candidate for stationary power generation, is investigated in detail. Finally, SOFC and hybrid SOFC cycle computer modeling are presented. For this purpose, a comprehensive literature survey on different types of hybrid SOFC system modeling is presented. It begins with a general discussion on roles of the fuel cell and hybrid SOFC system modeling in this field. Then, key features of the fuel cell models are highlighted and model selection criteria are explained. After that, the models in the open literature are categorized and discussed based on the selected criteria. Finally, in the last subsection, key features of selected models are summarized and suggestions for areas that require further studies are presented.

#### **3.1 Introduction to fuel cells**

Fuel cells are an interesting alternative for conventional power generation technologies because of their high efficiency and very low environmental impacts. In conventional power generation systems, fuel is to be combusted to generate heat and then heat is converted to mechanical energy before it can be used to produce electrical energy. The maximum efficiency that a thermal engine can achieve is when it operates in a Carnot cycle. On the other hand, fuel cell operation is

based on electrochemical reactions and not fuel combustion. Bypassing this conversion of chemical energy to thermal and then mechanical energy enables fuel cells to achieve efficiency potentially much higher than that of conventional power generation technologies.

A fuel cell can be considered as a “cross-over” of a battery and a thermal engine. It resembles an engine because theoretically it can operate as long as fuel is fed to it. However, similar to a battery, its operation is based on electrochemical reactions. This combination provides significant advantages for fuel cells. On the other hand, batteries are energy storage devices, and when their chemical energy is depleted, they need to be replaced or recharged, whereas fuel cells can generate electricity continuously. Actually, in principle, a fuel cell resembles an instantly rechargeable battery. Mench (2008) explained the differences between a fuel cell and a battery based on the thermodynamics definition of a closed system and control volume. According to his description, a battery is a thermodynamically closed system, whereas a fuel cell is a thermodynamically control volume, and fuel and oxidizer can flow across the system’s boundaries.

The main advantages of fuel cells can be summarized as follows: direct energy conversion (no combustion), potential for high efficiency, lower pollution, scalability, no moving parts in the energy converter, quiet operation, fuel flexibility, easier carbon capture, possibility for water production, and possibility for hybrid systems and cogeneration. It should be noted that this list is not exhaustive and just enumerates general attributes of most types of fuel cells. Moreover, at least some types of fuel cells have demonstrated the following characteristics: fast response to load changes, unattended operation, good off-design load operation, reliability, and high availability.

All these attributes and characteristics make fuel cells ideal candidates for some major applications. However, before the commercialization of fuel cells can be realized, some significant improvements are required. The most important barrier is cost. In order to reduce the cost of fuel cells, new construction methods and materials must be developed. Mass production and the economy of scale can reduce cost significantly, but some mass markets have to be in place to support it. Also for each application, suitable durability, endurance, reliability, longevity, specific power, and power density need to be achieved, especially for high temperature fuel cells. This includes transient operation and operation in extreme ambient

conditions. In addition, the performance of the balance of plant (ancillary system) should be improved to meet the technical and economic requirements of fuel cell systems. Other obstacles to overcome can be enumerated as follows: lack of familiarity of markets with fuel cell technology (especially the power generation industry) and the lack of certain elements of infrastructure, including hydrogen production, storage, and distribution for hydrogen fuelled fuel cells.

Fuel cell technology is highly multidisciplinary and its development requires engagement of most of the engineering fields, from electrochemistry to manufacturing and from thermodynamic to material science and control, and is experiencing a tremendous growth. For instance, it has been shown that the number of registered patents related to fuel cells has increased exponentially in the United States in recent years (Mench, 2008). However, any claim regarding the future of fuel cells should be considered cautiously, because a quick review of the literature over the past few decades shows that fuel cells have always been seen, and still are being seen, as being a few years away from commercialization.

### **3.1.1 Fuel cell basic operation**

In a fuel cell, the reductant (fuel) flows across the anode and is oxidized by the removal of electrons. Similarly, the oxidant (usually oxygen from air) flows across the cathode, where it is reduced by gaining electrons. Then either positively-charged or negatively-charged ions, depending on the fuel cell type, flow through the electrolyte to participate in electrochemical reactions. The excess electrons in the anode and lack of electrons in the cathode generate the desired product of the system, electricity. The electrons are conducted from or to the electrodes by interconnections. Figure 7 illustrates a sketch of the basic operation of a typical fuel cell fuelled by hydrogen and oxygen. The exact reactions in the electrodes and the type of ions transferred through the electrolyte depend on the fuel cell type and the type of inlet fuel.

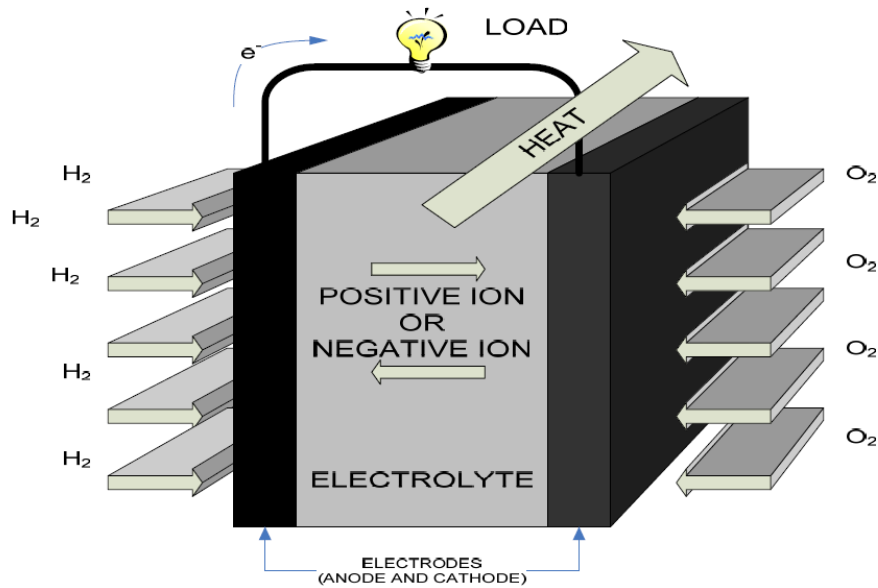


**Figure 7: Sketch of the basic operation of a typical fuel cell fuelled by hydrogen and oxygen (Suther, 2006)**

### 3.1.2 Configuration of fuel cells

Although current and output power of a fuel cell, to some extent, can be controlled by its size and reactants flow rate, the voltage of electricity that can be generated by a single fuel cell unit is limited to a theoretical maximum of about 1.2 V at 298 K and 0.9 V at 1273 K for hydrogen oxidation (Campanari and Macchi, 1998). This is due to the limited electrochemical potential of the reacting agents. Since actual operating voltage is generally lower than 1 V, several fuel cell units should be connected to generate a considerable amount of electricity. The combination of fuel cells is known as a fuel cell stack and gives the fuel cell size flexibility. The fuel cell stacking is one of the reasons for the development of various fuel cell configurations, which are the subject of the rest of this subsection.

The common configuration of fuel cells can be categorized into two main groups: the planar and the tubular configurations. At the beginning of fuel cell development, there was a monolithic design as well but due to its high fabrication costs, its development was not pursued (Singhal, 2000b).

**Planar fuel cells:** In this design, the fuel cell's flat plate electrolyte and electrodes are located parallel to each other and the individual cells are connected in series (bipolar plates). The planar

fuel cells enjoy high power density, and their fabrication is simpler. But their structural integrity and sealing at high operating temperatures are serious challenges.

In solid state electrolyte fuel cells, in order to provide mechanical strength for a planar cell, each cell should be self-supported or supported by an external support. In a self-supported cell, either the electrodes or electrolyte should be thick enough to support other components. The three types of self-supported fuel cells are electrolyte-supported, anode-supported, and cathode-supported. The problem with electrolyte-supported cells is the high ionic resistance in the electrolyte due to its greater thickness, requiring a high operating temperature of the system. In electrode-supported cells, due to their thinner electrolyte and lower ionic resistance, the operating temperature can be reduced significantly. Alternatively, cells can be externally supported by the interconnections, which results in stronger structure and thinner cell components, but cell support requirements may impose some limitations in flow channel design. Recently, anode-supported fuel cells have been receiving the most attention due to their better thermal and electrical conductivity, mechanical strength, and minimal chemical interaction with the electrolyte (Singhal, 2002).

**Tubular fuel cells:** In this design, a whole cell is in the form of a tube, the cathode being the inner layer, and the electrolyte and anode are deposited on top of the cathode. Since this configuration is mainly used in solid oxide fuel cells, the detailed description of the design will be presented in Subsection 3.2.2.

### 3.1.3 Balance of plant

The balance of plant (BoP) is a significant portion of a fuel cell system's weight, volume, and cost. The fuel processor is required to provide fuel in proper conditions for the fuel cell and increase the fuel flexibility of the system. Also, the generated electricity in the fuel cell cannot be directly used by end users and has to be adjusted to meet the load requirements. The inlet fuel type, system application, and operating conditions can affect the type and configuration of the balance of plant. The BoP can include all or some of the following subsystems:

- Feed stream conditioning: fuel preparation and storage, and fuel and oxidant supply (compressors or blowers and pumps as well as filters);
- Thermal management equipment (to manage the fuel cell stack temperature);

- Water management;
- Electric power conditioning (to convert variable direct current (DC) fuel cell output to usable electricity);
- Residual fuel recirculation and/or consumption (due to a lower than 100% fuel utilization factor in fuel cells, residual fuel should be recycled and/or combusted before being discharged to the environment);
- Start-up equipment (to initiate start of components and preheating of the system);
- Cooling subsystem;
- Control subsystem.

Some of these subsystems will be discussed in more detail in Subsection 3.2.4.

#### **3.1.4 Fuel cell classification**

Fuel cells can be classified based on various parameters. The most popular categorization is based on the type of electrolyte. The electrolyte can be either solid or liquid with the operating temperatures ranging from 80°C to over 1000°C. According to this classification, fuel cells can be categorized into five groups: polymer electrolyte fuel cell (PEFC), alkaline fuel cell (AFC), phosphoric acid fuel cell (PAFC), molten carbonate fuel cell (MCFC), and solid oxide fuel cell (SOFC).

Fuel cells can also be grouped based on the charge of ions that are carried between the electrodes. In some fuel cells, positive ions move from the anode to the cathode to produce water and heat by reacting with oxygen (such as PEFC and PAFC). In others, however, negative ions move from the cathode to the anode (such as AFC, MCFC, and SOFC). Some fuel cells are classified by their fuel. The most important and well known fuel cells in this categorization are direct methanol fuel cells (DMFC) and direct carbon fuel cells (DCFC).

The type of electrolyte determines the operating temperature of a fuel cell, which in turn dictates the material for other components. Different operating temperatures provide characteristics for each type of fuel cell, making them suitable for various applications.

**Low temperature fuel cells:** The low operating temperature of this type of fuel cells, usually lower than 200°C, including PEFC, AFC, and PAFC, provides them with some advantages, most



important of which are faster start-up and usually higher efficiency. However, the low temperature fuel cells require expensive electro-catalysts (mostly platinum). Therefore, they should be fuelled with hydrogen with high purity (with some exceptions, such as DMFC), since some fuel gases, like carbon monoxide, can poison platinum.

**High temperature fuel cells:** The operating temperature of high temperature fuel cells, SOFC and MCFC, is between 500°C and 1000°C. Unlike low temperature fuel cells, they can operate with less expensive electro-catalysts and require minimal processing of conventional fuels. Some fuel components, like CO and CH<sub>4</sub>, not only do not poison the fuel cell, but also can be internally reformed to produce hydrogen-rich streams or even directly participate in the electrochemical reactions. The high temperature fuel cells are particularly suitable for stationary power generation, although they have been proposed for other applications as well. In addition, the high temperature exhaust stream of this type of fuel cells contains a considerable amount of energy, which can be used to generate further power and/or thermal energy by integrating bottoming cycles, such as a gas turbine or a waste heat recovery subsystem.

Fuel cells can be classified based on their applications. There are many potential applications for fuel cells. In order to recognize the specific fuel cell type for each application, the attribute of the desired system should match the specifications required for particular applications. Most likely, it is not possible to find a system that perfectly satisfies all preferences for an application; therefore, the parameters should be ranked based on their priorities. The desired attributes can be one or several of the following characteristics: cost, efficiency, durability, power density, simplicity, rapid start-up, compactness, robustness, etc. This list is not exhaustive, and for every application other parameters may be added.

Stationary and distributed power generation are one of the main applications of fuel cells. For the stationary electricity generation, the main desired characteristics are high efficiency and long lifetime. Therefore, compactness, simplicity, and weight are not major constraints for this application. Their power generation capacity ranges from a few hundred kW to several MW.

Fuel cells are particularly suitable for distributed power generation, because the capital costs and efficiency are almost unaffected by the plant size. This means the cost of generated electricity for small power generation plants is close to that of the larger ones and is relatively insensitive to scale. With a well developed natural gas distribution network in urban and industrial regions, this

characteristic provides a unique opportunity for residential and industrial on-site and distributed power generation. Fuel cells' modular nature can help them to match demand load specifications. In addition, high efficiency at partial loads, low air pollution, and quiet operation are other important positive attributes of fuel cells, especially for residential applications. Also, coal gasifier requirements closely match the high temperature fuel cell operating conditions. Thus, an integrated system can be developed to use inexpensive coal to generate electricity with high efficiency.

Fuel cells are potential candidates wherever electricity is required; however, some applications fit the characteristics of fuel cells more closely. A few of these applications are: transportation applications, portable applications, auxiliary power units (APUs) for vehicles, electricity storage by regenerative (reversible) fuel cells, space applications, and military applications.

Table 23 summarizes the characteristics of various types of fuel cells, including the suitable material for different components, operating temperature, and potential applications.

Although fuel cells were invented in the 19<sup>th</sup> century, it took more than a century before the first operational fuel cell was made. Over the past two decades, there have been tremendous R&D activities and dramatic improvements in this field. As noted in Table 23, most types of fuel cells, especially SOFC and MCFC, can be used for stationary power generation. For this work, the SOFC will be further investigated for the power generation application, which reflects the present level of interests in the field.

### **3.2 Solid oxide fuel cells**

In the 1890s, Walther Nernst, a German scientist, was the first to observe the ion conductivity of stabilized zirconia at a high temperature. His observation was used to build the first SOFC in the 1930s. The SOFC's actual development started in the 1950s, which gave SOFC the longest continuous development period among different types of fuel cells.

In SOFCs, the electrolyte is a solid ceramic (nonporous metal oxide), which demonstrates sufficient ionic conduction for oxygen ions at a high operating temperature, between 500°C and 1000°C. The electro-catalyst is non-noble metal or other less expensive material, and the

electrolyte, cathode, and anode are typically made of  $Y_2O_3$ -stabilized  $ZrO_2$ , Sr-doped  $LaMnO_3$ , and Ni- $ZrO_2$  cermet, respectively.

**Table 23: Summary of the characteristics of various types of fuel cells**

	<b>PEFC</b>	<b>AFC</b>	<b>PAFC</b>	<b>MCFC</b>	<b>SOFC</b>
<b>Electrolyte material</b>	Acidic solid proton exchange membrane	Potassium hydroxide (KOH)	Phosphoric acid	Molten alkali carbonates	Ceramic
<b>Electrodes material</b>	Porous carbon	Metals	Porous carbon or graphite	Nickel or nickel oxide	Ceramic
<b>Catalyst material</b>	Platinum	Nickel, metal oxides, or noble metals	Platinum	Electrode material	Electrode material
<b>Interconnections material</b>	Carbon or metals	Metal	Graphite	Nickel or stainless steel	Nickel, ceramic, stainless steel
<b>Prime cell components</b>	Carbon	Carbon	Graphite	Stainless steel	Ceramic
<b>Mobile ion</b>	$H^+$	$OH^-$	$H^+$	$CO_3^{=}$	$O^-$
<b>Operating temperature</b>	60°C to 100°C	50°C to 220°C	200°C to 220°C	600°C to 700°C	500°C to 1000°C
<b>Electrolyte poisons</b>	CO	CO, $CH_4$ , $CO_2$ , $H_2S$	CO, $H_2S$	$H_2S$	$H_2S$
<b>Internal fuel reforming</b>	No	No	No	Yes	Yes
<b>Applications</b>	Vehicles, mobile, small CHPs (DMFC: portable electronic systems)	Space vehicles	Medium-scale stationary and CHPs	Medium- and large-scale stationary, hybrid, and CHPs	All sizes of stationary stand alone and hybrid systems, CHPs, and APUs

Major technical challenges are the cost of materials and manufacturing, system life, thermal cycling, limited power density, mismatches of thermal expansion coefficient of different components and sealing problem in planar configuration, materials selection at a high temperature especially metal interconnections (Williams et al., 2006), and corrosion in some components. Some of these problems can be intensified at higher temperatures. That is why a

lower operating temperature is desired, and there have been numerous studies to reduce the operating temperature even as low as around 500°C by using a thinner electrolyte. Stationary power generation, mobile power, and auxiliary power for vehicles are considered as potential applications of SOFCs, the latter being most likely the first real market. SOFCs can be integrated to bottoming cycles or heat and power cogeneration plants to increase the overall efficiency of the plant (Calise et al., 2006b). An excellent historical and technical review of SOFCs can be found in Singhal and Kendall (2003), Williams et al. (2006), and Singhal (2002). Moreover, Dokiya (2002) studied materials and fabrication technologies deployed for manufacturing of different cell components, investigated the performance of the fuel cells manufactured using these materials, and reviewed efforts to reduce fuel cell costs.

In the following subsections, SOFC components, stack configurations, and balance of plant will be briefly introduced.

### **3.2.1 SOFC Components**

Figure 8 illustrates the schematic of a typical planar SOFC, including its components and flow paths. Similar to other fuel cells, an SOFC can be broken down into four main components: the electrolyte, anode, cathode, and interconnections.

In SOFCs, oxygen is reduced and gains electrons to produce free negatively charged oxygen ions in the cathode. The electrons required for oxygen reduction are provided from the anode and via external electric load. The oxygen ions immigrate across the oxide-ion conducting electrolyte to the anode. In the anode, the negative ions participate in reactions with fuel to generate steam or carbon dioxide. The actual electrochemical reactions and the products depend on the reductant agents: hydrogen, carbon monoxide, or even methane (these reactions are presented in Figure 8 for hydrogen as fuel). The reactions in the anode release electrons, which in turn are collected and transferred by the interconnections to generate external electric current.

### **3.2.2 Configurations of SOFCs**

Due to the solid state electrolyte in SOFCs, there are fewer limitations in their design in comparison to other types of fuel cells. That is why a wide range of cell and stack geometries

have been proposed for SOFCs. As noted earlier, the configuration of SOFCs can be categorized into two main groups: the flat plate and the tubular configurations.

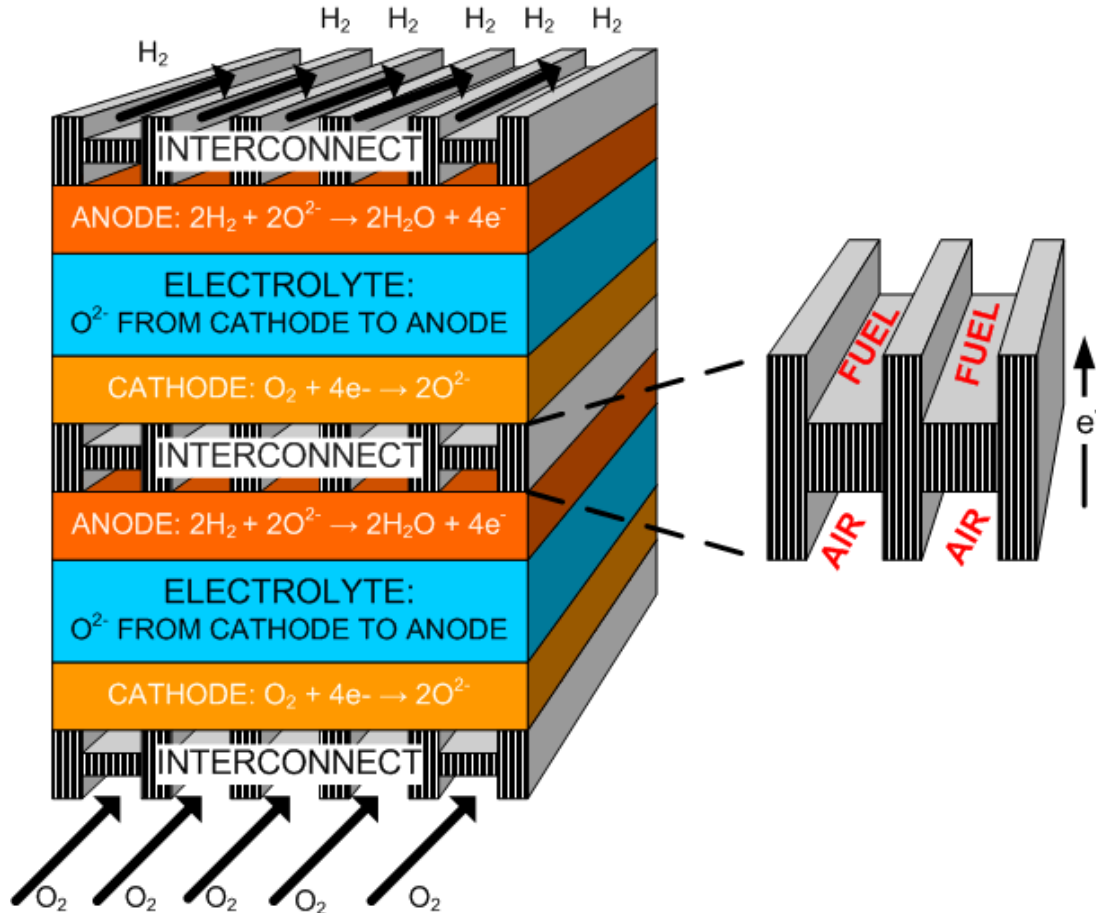


Figure 8: Schematic of a typical planar SOFC (Suther, Fung, Koksai, and Zabihian, 2010b)

Tubular fuel cells were specifically designed for SOFC and most progress in SOFC design has been achieved for this type (Singhal, 2000b). This design solved the sealing problem and provides excellent mechanical integrity for the stack. In this design, the electrodes and electrolyte are in the form of different layers on a tube. In earlier designs, these layers were deposited over a cylindrical tube that did not participate in the electrochemical process (Bevc, 1997). But in current designs, the tube is made of lanthanum manganite and functions as the cathode as well as mechanical support (Singhal and Kendall, 2003). In any case, for operation of this type of SOFC, fuel is passed outside the tube, while air is passed inside the inner cathode

tube. Siemens Westinghouse has been historically the pioneer in the tubular SOFC design and manufacturing since 1984 (Singhal, 2000a). The latest development in this design is the flat-tube design, which is less expensive and has higher power density (Young, 2007). This design is similar to the tubular design but with flattened tubes which incorporates ribs inside the cell. The ribs reduce the current path, like a bridge for electrons, decreasing the cell internal resistance. They can also help to reduce the thickness of cathode and its overpotential (Singhal, 2000a). Another innovative design, developed by Rolls-Royce and called integrated-planar SOFC (IP-SOFC), is a combination of the two aforementioned designs. This type of SOFC enjoys the lower fabrication cost of the planar SOFC and thermal-mechanical strength of the tubular SOFC (Young, 2007).

However, the tubular SOFCs suffer both low specific power density ( $\text{W}/\text{cm}^2$ ) and volumetric power density ( $\text{W}/\text{cm}^3$ ) due to a longer current path and thus higher electrical resistance (Singhal, 2002). Also, their fabrication cost is high, and there is not much potential to reduce this cost. Last but not least, due to the relatively high thickness of the electrolyte, their operating temperature is high. These problems are partially solved in planar SOFCs. They can achieve high power density. Their manufacturing cost is relatively lower due to the possibility of using a broader set of materials, and can be significantly reduced by mass production and the economy of scale. Also, the electrode-supported planar SOFCs can be made of a very thin electrolyte, which means they can operate at lower temperature (as low as  $500^\circ\text{C}$ ). This is very important for some applications such as APUs for vehicles. Furthermore, a lower operating temperature results in simpler BoP, easier thermal management, less degradation of the components, and faster start-up and cool down. However, the temperature gradient and heat cycles as well as a slight mismatch in the thermal expansion coefficient between cell components can cause huge thermal stress, as high as several tens of MPa (Yakabe, Ogiwara, Hishinuma, and Yasuda, 2001), which makes the sealing of the stack more challenging.

For the tubular SOFC, a power density of about  $0.3 \text{ W}/\text{cm}^2$  with degradation rate of less than 0.1% per 1000 hours of operation and a fuel utilization factor of about 85% and for the planar SOFC, a power density of about  $2 \text{ W}/\text{cm}^2$  with fuel utilization factor of about 95% has been reported (Singhal, 2000a, 2002; Williams et al., 2006).

### 3.2.3 Hybrid SOFC cycles

As mentioned earlier, one of the advantages of high temperature fuel cells is their capability to be integrated to a bottoming cycle, so that exhaust thermal energy can be used to generate further useful energy in the form of electricity and/or heat. Singhal (2000a) reported that due to higher efficiency and availability as well as low maintenance costs, the hybrid SOFC plants could compete with conventional power generation systems. In a fuel cell hybrid cycle, both SOFC and MCFC can be utilized in the fuel cell stack, but the focus of this work is only on hybrid SOFC cycles, which reflects current trends in the field.

The high temperature of SOFC products provides very good potential for hybrid SOFC systems, especially for distributed generation (DG). The outlet temperature of SOFCs perfectly matches the requirement of modern gas turbines (Calise, Dentice d' Accadia, Vanoli, and Von Spakovsky, 2007). Rajashekara (2005) classified the hybrid fuel cell systems as Type-1 and Type-2 systems. They are mainly suited for combined cycles power generation and backup or peak shaving power systems, respectively. An example of Type-1 hybrid systems is hybrid fuel cell and gas turbine (GT) cycle, where high temperature of fuel cell off-gas is used in the GT to increase the efficiency of the combined system. Another example of this type of combined cycle is designs that combine different fuel cell technologies. Examples of Type-2 hybrid systems are designs that combine a fuel cell with wind or solar power generation systems which integrate the operating characteristics of the individual units such as their availability of power.

By definition, proposed by Winkler, Nehter, Williams, Tucker, and Gemmen (2006), any combination of a fuel cell and a heat engine can be considered as a fuel cell hybrid system. Therefore, an SOFC-based hybrid system can be any combination of SOFC and gas turbine, steam and gas turbine combined cycle power plant (CCPP), steam turbine, coal integrated gasification (IG), integrated gasification combined cycle (IGCC), application in combined cooling and/or heating and power (CCHP/CHP) cycles, and other power generation systems.

The operating pressure of SOFC affects the types of bottoming cycle that can be integrated into the system. In Type-1 hybrid systems, if the fuel cell is operated at atmospheric pressure, the exhaust gases can be passed through series of heat exchangers to generate hot water and/or low pressure steam for industrial applications (Riensch and Fedders, 1993) or high-pressure steam for a Rankine power cycle. The latter scheme was proposed as early as 1990 (Dunbar, Lior, and

Gaggioli, 1990). The fuel cell may also be operated at an elevated pressure. In this case, the pressurized hot combustion gases exiting the combustor at the bottom of SOFC can be used to drive a gas turbine with or without a bottoming steam cycle. This scheme was proposed in 1991 (Donitz, Erdle, Schafer, Schamm, and Spah, 1991).

Among various hybrid schemes proposed for pressurized fuel cells, probably hybrid SOFC-GT cycles are the most popular systems being studied theoretically and the only one being studied experimentally. This configuration is the best way to use thermal energy of the SOFC exhaust because the SOFC exhaust temperature matches the required temperature of the gas turbine inlet (Calsie et al., 2007). There are two main designs to combine SOFC and GT. The difference between these designs is how they extract heat from fuel cell exhaust. In the first design, fuel cell off-gas directly passes through the GT. That means the gas turbine combustor is replaced by the fuel cell stack. But in the second scheme, the fuel cell off-gas passes through a high temperature recuperator, which in fact replaces the combustor of the gas turbine cycle (Roberts, Brouwer, Jabbari, Junker, and Ghezel-Ayagh, 2006). From an operational point of view, these designs are distinguished by the operating pressure of the fuel cell. Their operating pressure is equal to the operating pressure of the gas turbine and slightly above atmospheric pressure, respectively. It should be mentioned that in all cases a steam cycle (Campanari and Macchi, 1998) and CHP plants (Palsson et al., 2000) can be integrated into the hybrid system to recover more energy from exhaust.

So far, to the author's best knowledge, there have been three proof-of-concept and demonstration SOFC-GT power plants installed in the world. Siemens Westinghouse claimed that it successfully demonstrated its pressurized hybrid SOFC-GT system and has two units, a 220 kW at the University of California, Irvine and a 300 kW unit in Pittsburgh (Veyo et al. 2002a). Also, in 2006 Mitsubishi Heavy Industries, Ltd. (MHI, Japan) claimed that it succeeded in verification testing of a 75 kW SOFC-Micro gas turbine (MGT) hybrid cycle (MHI, 2006). These experiences prove the possibility of integrating SOFC and gas turbine. However, they showed that this integration was not necessarily straightforward, and finding a GT with operational conditions close to the SOFC exhaust condition and coupling them could be extremely challenging (Calise et al., 2007).



### **3.2.4 Balance of plant in hybrid SOFC systems**

In Section 3.1.3, the general BoP for fuel cell systems was briefly presented. In this subsection, some of these subsystems that are more important for hybrid SOFC systems' performance will be considered in more detail. It should be noted that a great number of configurations have been proposed in the literature for hybrid SOFC systems. These layouts have combined some of the following equipment: various SOFC stacks with different configurations, gas turbines, fuel and air compressors, heat exchangers, anode recirculation, a water pump, heat recovery steam generators, pre-reformers, internal reformers, mixers, (catalytic) burners, bypasses, electric generators, invertors, etc.

#### **3.2.4.1 Fuel processing**

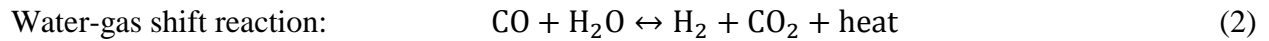
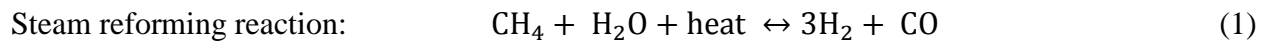
Theoretically, every fluid that can be chemically oxidized can be used as fuel in a fuel cell (Appleby and Foulkes, 1989). SOFCs can be directly fuelled by hydrogen, methanol, and some other fuels. In these cases, the fuel processing system consists of only fuel storage and handling systems. For fuels other than hydrogen, generally the first step in the fuel preparation process is removal of harmful species, such as sulfur and ammonia, which can degrade the fuel cell and/or auxiliary systems. Sometimes it is required to remove some components at the end of the fuel processing, such as removal of CO in PEFCs, but this is not the case for SOFCs. The fuel cleaning is a well-developed process and existing technologies can be employed for this purpose.

An SOFC can directly use conventional fuels, such as methane, in electrochemical reactions, at least theoretically. However, this is not currently feasible (Peters, Riensche, and Cremer, 2000). Therefore, in order to increase fuel flexibility, a fuel cell system should be able to use commercially available fuels to produce a hydrogen-rich stream, a chemically preferred fuel for fuel cells. Depending on the fuel cell and the inlet fuel type, one or more of these steps are required for fuel processing in a specific system. Since the fuel cleaning is a mature industry, in this section only fuel conversion to a hydrogen-rich stream is explained in detail.

At present, three fuel conversion technologies are commercially available, namely, steam reforming, partial oxidation, and autothermal reforming, which are explained in following subsections.

### 3.2.4.1.1 Steam reforming

In this technique, the vaporized hydrocarbon fuel and superheated steam react to create hydrogen and carbon monoxide. To increase the concentration of hydrogen, CO participates in the water-gas shift reaction, where carbon monoxide and steam react to create hydrogen and carbon dioxide. Steam reforming has the highest efficiency and hydrogen concentration at the product among various fuel preparation techniques. For methane, the steam reforming and water-gas shift reactions are as follows:



For higher hydrocarbons, the steam-reforming reaction produces a stream of a combination of hydrogen, methane, and carbon oxides. This reaction can be simplified in Equation 3 (total reaction including the steam reforming of generated methane but not water-gas shift reaction):



where  $n$  and  $m$  define the composition of the fuel and  $\text{SCR}$  represents the steam-to-carbon ratio of the mixture.

Although the steam reforming reaction does not require a catalyst, a catalyst can improve reaction efficiency at a lower temperature. The steam reforming process is endothermic, and the reaction is slow by nature; therefore, it needs a large reactor. Also, this technology is not suitable for rapid start-up, and its response to load change is slow.

The water-gas shift reaction is exothermic; however, the overall reaction, both steam reforming and water-gas shift simultaneous reactions, is endothermic. In a fuel cell system, the required heat can be provided from either the electrochemical reactions in the fuel cell (which can help to cool down the cell), from a furnace that burns some of the inlet fuel, or the fuel effluent from the fuel cell.

In a steam reforming process, there is possibility of carbon formation by the following reactions (Van herle, Marechal, Leuenberger, and Favrat, 2003; Achenbach, 1994):





The carbon formation can be suppressed by providing sufficient steam (Young, 2007). The steam-to-carbon molar ratio of higher than 2 is common to prevent soot formation and to force the reaction toward completion (Fuel Cell Handbook, 2004; Achenbach, 1994).

As Equations 1 and 2 show, these reactions require steam. This steam can be provided from an external water or steam source. In the case of water, water can be converted to steam in a heat recovery steam generator (HRSG) by recovering the waste heat of the system exhaust. Alternatively, the steam can be provided by recycling steam-rich anode products. The mixing of the fuel and anode exhaust streams can be performed by means of an ejector. Obviously, during the start-up, the plant requires an external boiler that produces steam for the reactions.

#### **3.2.4.1.2 Partial oxidation (POX)**

Unlike the steam reforming reaction, the partial oxidation does not require any steam. In this process, the fuel is partially combusted with a substoichiometric amount of air or oxygen:

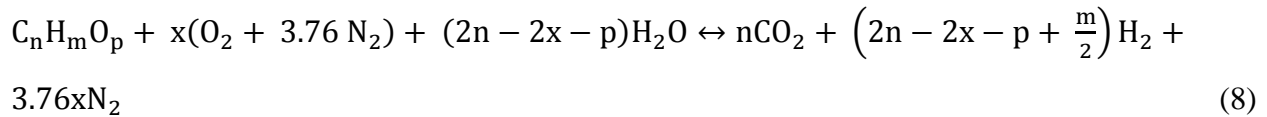


Due to the exothermic fuel combustion, the temperature of the reaction is high, but can be reduced by steam injection during the water-gas shift reaction. Since there is no need for indirect heat, the equipment is simpler, lighter, and smaller. Its response to load change is fast, and start-up time is shorter. However, the concentration of hydrogen in the products is lower. There are different opinions regarding its efficiency. Some references, like Fuel Cell Handbook (2004), reported higher efficiency for the partial oxidation process, but the widely-held opinion is that the efficiency of the steam reforming process is higher. Due to the higher temperature of POX, most liquid fuels are reformed in POX reformers (Petruzzi et al., 2003). If air is used for the process (opposed to pure oxygen), nitrogen from air is introduced to the product, which reduces the partial pressure of hydrogen in the product stream and thus the fuel cell power output. In addition, since available heat from the fuel cell is not used in this system and the fuel is directly combusted for this purpose, the effectiveness of the system is lower.

### 3.2.4.1.3 Autothermal reforming

The autothermal reforming is a combination of steam reforming and partial oxidation reactions, where the heat generated by the latter reaction is consumed by the former reaction, resulting in a slightly exothermic reaction. The technique results in a simpler, smaller, and faster responding system compare to the steam reformer, and in higher hydrogen concentration and lower temperature than those of the partial oxidation processor.

A generic equation that covers all aforementioned techniques (the total reaction including water-gas shift reaction) can be summarized as follows (Fuel Cell Handbook, 2004):



For instance, for  $x=0$ ,  $p=0$ ,  $n=1$ , and  $m=4$ , this equation reduces to the steam reforming of methane (Equations 1 and 2). The efficiency of a fuel processor can be defined based on Equation 9 (Fuel Cell Handbook, 2004):

$$\text{Efficiency} = \frac{\text{LHV of produced fuel}}{\text{LHV of inlet fuel}} \quad (9)$$

Both steam reforming and partial oxidation can be utilized in SOFC plants. However, only a few experimental and modeling works, such as Finnerty, Tompsett, Kendall, and Ormerod (2000), Petruzzzi et al. (2003), and Van herle et al. (2003) used POX and a majority of the SOFC systems in the literature applied the steam reformer. It is suggested that, for small units, where compactness is important, POX process is applied and for applications, where high efficiency is desired, steam reformer is used (Peters, Dahl, Kluttgen, Palm, and Stolten, 2002). Also, POX is used when the fuel cell is fuelled with liquid fuel, for example, for auxiliary power units (APUs) in vehicles, where the system should use the same fuel as the vehicle to avoid a second fuel tank (Petruzzzi et al., 2003; Steffen, Freeh, and Larosiliere, 2005).

In high temperature fuel cells, the fuel, especially methane, can be internally reformed. Although a few SOFC systems with the external reformer have been reported in the literature (Harvey and Richter, 1994a, 1994b; Palsson et al., 2000; Massardo and Lubelli, 2000; Van herle et al., 2003), due to the considerable benefits of internal reformers, most systems make use of this capability

of high temperature fuel cells. The internal reforming of fuel can significantly decrease the system cost and increase its efficiency. Also, the endothermic internal steam reforming process can help to provide additional cooling for the cells, which otherwise should be provided by flowing excess air through the cathode (Achenbach, 1994). This can cause even distribution of hydrogen, which can potentially result in more even temperature distribution in the stack (Ahmed and Foger, 2000). However, the complete internal reforming can result in some problems, such as carbon formation in the anode and the exposure of stack to large temperature gradients as a result of the cooling effects of the endothermic reforming reaction (Peters et al., 2000). Existence of heavier hydrocarbons in natural gas, which at high temperatures have a tendency to produce unwanted materials, such as carbon, can intensify the problem. Therefore, to avoid aforementioned problems, it is suggested that the fuel cell system should be equipped with a compact pre-reformer (Peters et al., 2000, 2002; Ahmed and Foger, 2000; Calise et al., 2007; Achenbach, 1994; Dicks, Pointon, and Siddle, 2000; Stiller, Thorud, Seljeb, Mathisen, Karoliussen, and Bolland, 2005).

#### **3.2.4.2 Internal reformer**

As noted earlier, the high operating temperature of SOFCs can eliminate or at least minimize the fuel reforming process by internal reforming of the fuel. There are two designs for internal reforming in SOFCs; direct internal reforming (DIR) and indirect internal reforming (IIR). The difference between these two techniques is the actual place that fuel reforming takes place. In DIR, the fuel is reformed while it flows over the catalyst particles in the anode, whereas in IIR, the reforming reactions take place over the paths close to the stack before the fuel reaches the anode. In both cases, the reformer is integrated to the stack and the heat required for the reforming reaction is provided by the electrochemical reactions in the fuel cell. Some kind of catalyst, such as material with nickel content, is required to promote the reforming reaction.

#### **3.2.4.3 Combustor**

The fuel cannot be completely consumed in a fuel cell, and the fuel utilization factor of fuel cell is always less than 100%. Therefore, in order to avoid unnecessary air pollution and the loss of fuel energy, the remaining fuel should be burned before the SOFC exhaust can be discharged

into the environment or a bottoming cycle. This can be done by combusting the anode exhaust with depleted air in the cathode outlet stream. The available fuels in the combustor are hydrogen and a lower percentage of carbon monoxide and methane. The cathode air mass flow rate is much higher than the fuel flow rate in order to control stack temperature. Thus, there is enough air in the cathode outlet for the combustion process. The extra heat generated in the combustor can help improve the performance of the bottoming cycle and/or heating inlet air as well as fuel to the fuel cell.

#### **3.2.4.4 Heat exchangers**

Heat exchangers are an important part of a hybrid fuel cell system. Although electrochemical reaction in the fuel cell is highly exothermic, the inlet air and fuel should be preheated before they are fed to the fuel cell to prevent a high temperature gradient and thermal stress in the stack.

### **3.3 Fuel cell modeling**

Simulation and mathematical models are certainly helpful for the development of various power generation technologies; however, they are probably more important for fuel cell development. This is due to the complexity of fuel cells and systems based on them, and the difficulty in experimentally characterizing their internal operation. This complexity can be explained based on the fact that within the fuel cell, tightly coupled electrochemical reactions, electrical conduction, ionic conduction, and heat transfer take place simultaneously. Modeling can help to understand what is really happening within the fuel cells (Fuel Cell Handbook, 2004). Understanding the internal physics and chemistry of fuel cells is often difficult. This is due to the great number of physical and chemical processes in the fuel cells, difficulty in independent controlling of the fuel cell parameters, and access limitations to inside of the fuel cells (Bove and Ubertini, 2006). In addition, fuel cells simulation can help focus experimental research and improve accuracy of interpolations and extrapolations of the results. Furthermore, mathematical models can serve as valuable tools to design and optimize fuel cell systems. Also, dynamic models can be used to design and test fuel cell systems' control algorithms. Finally, models can

be developed to evaluate whether characteristics of a specific type of fuel cell can meet the requirements of an application and its cost-effectiveness (Fuel Cell Handbook, 2004).

Due to its importance, in the past two decades, there has been tremendous progress on numerical and computational tools for fuel cells and energy systems based on them, and virtually an unlimited number of papers have been published on fuel cell modeling and simulation. With this large amount of literature, it is very difficult to keep track of the developments in the field. This problem can be intensified for new researchers as they can be easily overwhelmed by this sheer volume of resources. That is why there have been many review papers on the modeling of different types of fuel cells, especially for modeling and simulation of PEFC (Biyikoglu, 2005; Haraldsson and Wipke, 2004; Sousa and Gonzalez, 2005; Tao et al., 2006; Young, 2007; Wang, 2004), SOFC (Young, 2007; Wang, 2004; Kakac, Pramuanjaroenkij, and Zhou, 2007; Bove and Ubertini, 2006) and to a lesser extent, MCFC (Baker, 1984).

As mentioned previously, although both SOFC and MCFC can be used in hybrid cycles, due to the cell reactions, the molten nature of the electrolyte, and lower efficiency of MCFC (Song et al., 2005), the vast majority of research in this field is in hybrid SOFC cycles. There have been some steady-state (Massardo and Bosio, 2002; Iora and Campanari, 2007) and dynamic (Ghezel-Ayagh, Lukas, and Junker, 2004) modeling on the hybrid MCFC-GT cycles. However, the number of papers and their diversity are not comparable with papers on the hybrid SOFC cycle modeling.

The complex nature of interaction between the already complicated fuel cell and bottoming cycle makes simulation and modeling an essential tool for researchers in this field. In the next section, the ways to categorize the modeling of hybrid SOFC cycles will be discussed.

### **3.3.1 Modeling steps**

Before starting the modeling of a hybrid system, it is very important to define the purpose of the desired model and then determine the key features of the model. The best modeling approach and the characteristics of the model are dependent on the application. Although this is a vital step, there is a high tendency for it to be overlooked. After finalizing these criteria, details of the model can be identified (Haraldsson and Wipke, 2004).

Similar to modeling other thermal systems, the first step in the modeling of a hybrid SOFC system is to understand the system and translate it into mathematical equations and statements.

The common steps for model development are as follows:

- specifying a control volume around desired system;
- writing general laws (including conservation of mass, energy, and momentum; second law of thermodynamics; charge balance; and so on);
- specifying boundary and initial conditions;
- solving governing equations by considering boundary and initial conditions (analytical or numerical solution);
- validating the model.

Unlike the actual fuel cell operation which is three-dimensional and time dependent, fuel cell simulation can be simplified to a steady-state, 2-D, 1-D, or 0-D problem by proper assumptions, based on the application of the modeling. Many of the hybrid SOFC system simulations in the open literature are 0-D models. In this type of modeling, a series of mathematical formulations are utilized to define output variables based on input ones. In this approach, a fuel cell is treated as a dimensionless box, and that is why some authors referred to it as box modeling. Despite the large numbers of assumptions and simplifications in this method, it is useful to analyze the effects of various operational parameters on the cycles' overall performance, perform sensitivity analysis, and compare different configurations. When the objective of modeling is to investigate the inner working of SOFC, the 0-D approach is not appropriate. However, for hybrid SOFC system simulation, where emphasis is placed on the interaction of the fuel cell and the rest of the system and how the fuel cell can affect the overall performance of the system, this approach can be suitable. In this level of system modeling, there are a variety of assumptions and simplifications. For instance, Winkler et al. (2006) developed a hybrid fuel cell cycle model and assumed that the fuel cell was operated reversibly, representing any fuel cell type, and the heat engine was a Carnot cycle, representing any heat engine.

Different software and programming languages have been used in hybrid SOFC system simulation. Since there is no commercially available model for the SOFC stack, all modelers should prepare their own model with appropriate details and assumptions. Therefore, from this point of view, what differentiates models is how they simulate the other components of the



system. Generally, they can be divided into two categories. In the first approach, whole models can be developed in programming languages such as Fortran or high level software such as MATLAB/Simulink<sup>®</sup> platform to solve governing equations of the system. In the second approach, the modelers can take advantage of commercial software such as Aspen Plus<sup>®</sup> to model conventional components of the cycle.

Due to the nature of numerical modeling, its results should be used carefully. In every modeling, the physical realities of the system should be translated into mathematical equations and the solution of these equations is used to express behaviour of the system. In the case of fuel cells, the physical realities are extremely complex, some of which are completely unknown. Therefore, in order to extract these governing equations, a high level of assumptions and simplifications should be considered, which in turn introduce inaccuracy to the final results. This means fuel cell models are a simplified representation of real systems and even with appropriate validation, the accuracy of their results cannot be guaranteed (Bove and Ubertini, 2006). For instance, one should be aware of the possible problems that can arise when local equations are considered as global. Bove, Lunghi, and Sammes (2005) highlighted this problem in their paper. They described that the main problem of using 0-D approach for modeling was the negligence of variation in the fuel, air, and exhaust gas compositions through the fuel cell. As a result of this problem, when the inlet, outlet, or an average value of the gas composition was used in the modeling, different results could be obtained. In particular, it was shown that it was impossible to evaluate effects of fuel utilization variation through the fuel cell when inlet gas composition was considered. On the other hand, considering output streams composition could result in underestimating cell voltage and power output. Figure 9 shows such a variation in simulated characteristic curves.

However, Magistri, Bozzo, Costamagna, and Massardo (2004) studied simplified versus detailed SOFC models and how this simplification affected the predictions of the design-point performance of the hybrid systems. They emphasized the usefulness of the simplified model for hybrid system design and off-design analyses and a detailed model for the complete description of the SOFC internal behaviour.

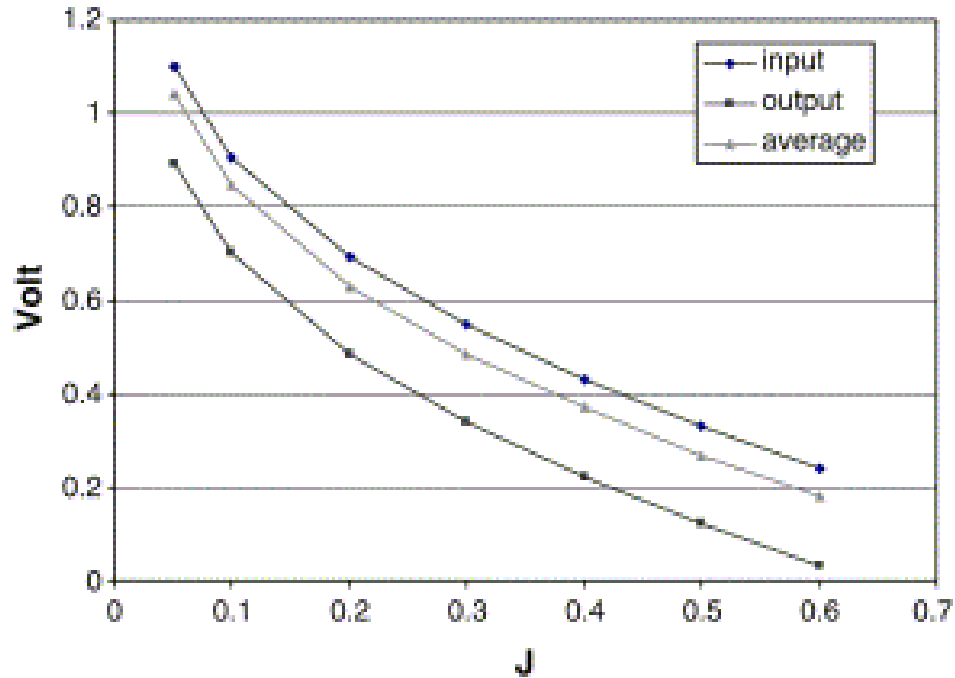


**Figure 9: Different polarization curves for chemical composition of the gases based on inlet, outlet or an average in a 0-D model (Bove et al., 2005)**

Finally, the validation of a model is important because a model must be validated to be a credible tool. Appropriate data are needed for validation. With limited resources, this can be difficult because most data cannot be found in the open literature. Although performance data from an entire hybrid power generation system are usually proprietary and are not available in the literature, this information from a single system is easier to find. Therefore, a way to resolve the problem of limited performance data is to develop and validate well-defined subsystem models, and then integrate them to have a complete model of a large hybrid power generation system.

Judkoff and Neymark (1995) classified the sources of simulation errors into three groups (these were provided for building simulation programs, but they were equally applicable to hybrid SOFC system simulation):

- Errors introduced due to assumptions and simplifications;
- Errors or inaccuracies in solving mathematical equations;
- Coding errors.

They also proposed a pragmatic, three-step approach to identify these errors. In the first approach, comparative testing, the results of the model should be compared with the results of other models for the same problem with similar initial and boundary conditions. If the results of the models match with acceptable error, it means the implementations are acceptable. However, this does not guarantee the correctness of the results because they all can be incorrect. In the second approach, analytical validation, the results of the model for a simple case are compared with the results of available analytical solutions. Last but not least, in empirical validation, the results of the simulation are compared with real data from the actual system under laboratory or field conditions.

### **3.4 Review on modeling of hybrid solid oxide fuel cell systems**

Although SOFC is considered as the heart of these hybrid cycles, its detailed mathematical modeling and simulation methodology is not included in this review. The focus here is on the evaluation of overall system performance and not its components performance. One can refer to Young (2007), Wang (2004), Colpan, Dincer, and Hamdullahpur (2008), Kakac et al. (2007), and Bove and Ubertini (2006) for review papers on SOFC modeling. In addition, some good examples of such simulations can be found in Yakabe et al. (2001) and Petruzzi et al. (2003) for steady-state and Padulle's, Ault, and McDonald (2000) and Achenbach (1994) for transient and dynamic modeling. Since the focus of this thesis is on hybrid SOFC cycles, in this review a comprehensive literature survey on different type of hybrid SOFC systems modeling are presented. The purpose of this review is to summarize the present status of the worldwide research efforts in this field. Thus, the unresolved problems can be identified, and they can be addressed in this work as much as possible.

This review will be started with a general discussion on key features of the fuel cell models. Then, the models in the open literature will be categorized and discussed based on these features. This part includes discussion on early models, models with different objectives such as parametric analysis, comparison of configurations, transient and off-design analysis, and so on. Objectives of some papers in this field are not directly addressed in this thesis such as optimization, non-stationary power generation, and thermoeconomic analysis. However, in order to make this review extensive and exhaustive, these papers are included as well. Finally, in the

last section selected models' key features will be summarized and suggestions for areas that require further studies will be presented.

### **3.4.1 Hybrid SOFC systems modeling categorization**

Haraldsson and Wipke (2004) summarized the key features of the fuel cells models as follows:

- modeling approach (theoretical or semi-empirical);
- model state (steady-state or transient);
- system boundary (atomic/molecular, cell, stack, or system);
- spatial dimension (zero to three dimensions);
- complexity/details (electrochemical, thermodynamic, or fluid dynamic relationships);
- speed, accuracy, and flexibility;
- source code (open or proprietary);
- graphical representation of model;
- library of models, components, and thermodynamic properties;
- validation.

Although they provided the above list for PEFC, it could equally be applicable for SOFC modeling. They described the approach of a model as being either theoretical (mechanistic) or semi-empirical. The mechanistic models are based upon electrochemical, thermodynamic, and fluid dynamic relationships, whereas the semi-empirical models use experimental data to predict system behaviours. The state of the model, either steady-state or transient, shows whether the model can simulate system only at single operating condition, or it can be used in dynamic conditions, including start-up, shut-down, and load changes too. Spatial dimension of a model can be zero to three dimensions. Zero-dimension models only consider current-voltage (I-V) curves. On the other hand, multi-dimensional mechanistic models address governing laws, including mass, momentum, and energy balances, and the electrochemical reactions and need the explicit treatment of geometry (Beausoleil-Morrison, Weber, Marechal, and Griffith, 2004).

Singhal and Kendall (2003) categorized the resolution of SOFC models in four levels: atomic/molecular, cell, stack, and system. As Singhal and Kendall pointed out, the proper

modeling approach and modeling level depends upon the objectives of the modeling. For instance, the recommended approach for IEA Annex 42, model specifications for a fuel cell cogeneration device, is system level approach. It is because the Annex 42 cogeneration models include the models of associated plant components, such as hot-water storage, peak-load boilers and heaters, pumps, fans, and heat exchangers. In addition, the system models should be able to couple to the building models. These models simulate the building to predict its thermal and electrical demands (Beausoleil-Morrison et al., 2004).

On the other hand, the models can be categorized based on their SOFC type rather than modeling approach. For instance,

- Fuel cell type:
  - Planar;
  - Tubular;
  - Monolithic (MSOFC);
  - Integrated Planar (IP-SOFC);
- Cell and stack design (anode-, cathode-, electrolyte-supported and co-, cross-, and counter-flow types);
- Temperature level:
  - Low temperature (LT-SOFC, 500–650°C);
  - Intermediate temperature (IT-SOFC, 650–800°C);
  - High temperature (HT-SOFC, 800–1000°C);
- Fuel reforming type:
  - External steam reforming;
  - Internal steam reforming;
  - Partial oxidation (POX);
- Anode recirculation;
- Fuel type.

They can even be categorized by the cycles, such as GT, CCPP, IGCC, and CHP, which are used to form a hybrid system with the SOFC. Alternatively, the purpose of modeling such as parametric sensitivity analysis, optimization, exergy analysis, economical analysis, configuration analysis, feasibility studies, and partial load and transient condition analyses can be considered

for categorizing hybrid SOFC models. In this review, papers will be categorized and explained based on one of the aforementioned categories whenever appropriate.

Table 24 categorizes some of the papers in the open literature based on the criteria discussed in this section. In this table, the purposes of the papers are divided into parametric, configuration, partial load, optimization, and economical analyses. They can be identified based on the intersection of rows and columns. Also, the system or cycle that is combined with the SOFC to form the hybrid cycle can be identified by shape of each icon. For example, a square represents the hybrid SOFC-GT cycle. Line type and line thickness of each icon are used to recognize the number of geometrical axes through which the flow parameters vary, and the time dependency of the model, respectively. For instance, a circle with solid thin line represents a hybrid SOFC-CHP steady-state 0-D model. Finally, the direction of the shading shows fuel cell type, i.e., tubular or planar.

There are a few points about this table that should be mentioned. First, when the spatial dimension of the model is not mentioned in the paper, it is shown in solid line (similar to the 0-D model). Also, papers concerning feasibility study and conceptual design are considered as configuration analysis. Monolithic SOFCs (MSOFC) and integrated planar SOFCs (IP-SOFC) are considered as planar and tubular fuel cells, respectively.

**Table 24: Categorization of sample papers in the open literature**

	Parametric analysis	Configuration analysis	Partial load	Optimization	Economical analysis
Parametric analysis			<p>Shades:</p> <div>  GT  Steam Turbine  CO<sub>2</sub> Capture  IG  CHP  0-D  &gt;0-D  Steady-State  Transient or Both </div> <div>  Tubular  Planar  Both  Unknown </div>		
Configuration analysis					
Partial load					
Optimization					
Economical analysis					

1. Roberts et al. (2006) and Mueller et al. (2007)
2. Song et al. (2005)
3. Harvey and Richter (1994a, 1994b)
4. Suther, Fung, Koksai, and Zabihian (2010a, 2010b) and Zabihian, Fung, Koksai, Malek, and Elhebshi (2008)
5. Palsson et al. (2000)
6. Chan, Ho, and Tian (2002a, 2003a)
7. Calise et al. (2006a, 2006b, 2007)
8. Stiller et al. (2005)
9. Selimovic and Palsson (2002)
10. Magistri et al. (2005)
11. Granovskii, Dincer, and Rosen (2007a, 2007b, 2008)
12. Pangalis, Martinez-Botas, and Brandon (2002) and Cunnell et al. (2002)
13. Kuchonthara, Bhattacharya, and Tsutsumi (2003a, 2003b)
14. Tanaka, Wen, and Yamada (2000)
15. Lundberg, Veyo, and Moeckel (2003)
16. Rao and Samuelson (2003)
17. Song, Sohn, Kim, and Ro (2006)
18. Möller, Arriagada, Assadi, and Potts (2004)
19. Riensche et al. (2000)
20. Franzoni, Magistri, Traverso, and Massardo (2008)
21. Massardo and Lubelli (2000)
22. Inui, Yanagisawa, and Ishida (2003)
23. Campanari and Chiesa (2002)
24. Lobachyov and Richter (1996)
25. Kivisaari et al. (2004)
26. Kuchonthara et al. (2005)
27. Van herle et al. (2003)
28. Braun, Klein, and Reindl (2006)
29. Winkler and Lorenz (2002)
30. Steffen et al. (2005) and Freeh, Steffen, and Larosiliere (2005)
31. Costamagna, Magistri, and Massardo (2001)
32. Stiller, Thorud, Bolland, Kandepu, and Imsland (2006a) and Stiller, Thorud, and Bolland (2006b, 2006c)
33. Chan, Ho, and Tian (2003b)
34. Zhang, Li, Li, and Feng (2006)
35. Zhu and Tomsovic (2002)
36. Kemm, Hildebrandt, and Assadi (2004)
37. Lin and Hong (2006)
38. Riensche, Stimming, and Unverzagt (1998a) and Riensche, Meusinger, Stimming, and Unverzagt (1998b)
39. Fontell, Kivisaari, Christiansen, Hansen, and Pålsson (2004)



### 3.4.2 Early models

The SOFC development started in the late 1950s, the longest continuous development period among various types of fuel cells (Fuel Cell Handbook, 2004). However, it was not until the mid 1980s that results of the first simple SOFC models were published in the open literature. For the hybrid SOFC cycles, the first papers were published in the early 1990s.

Dunbar and Gaggioli have been considered as pioneers in the field of the SOFC modeling and their integration with the Rankine cycle. They published their first paper on the results of mathematical modeling of the performance of solid electrolyte fuel cells as early as 1988 (Dunbar and Gaggioli, 1988). In 1990 (Dunbar et al., 1990), they proposed integrating SOFC units into the conventional Rankine steam cycle power plant. That study revealed a significant efficiency increase, up to 62%, compared to the maximum conventional plant efficiency of about 42% in those days (Dunbar et al., 1990). They found that the main reason for this efficiency improvement was higher exergetic efficiency of SOFC as contrasted with the combustion process in conventional fossil fuel-fired power plants (Dunbar, Lior, and Gaggioli, 1991). They also investigated (Dunbar et al., 1991) the exergetic effects of the major plant components as a function of fuel cell unit size. The results showed that specific fuel consumption might be reduced by as much as 32% in the hybrid cycle.

Harvey and Richter, who proposed a hybrid thermodynamic cycle combining a gas turbine and a fuel cell, were the pioneers in this area. Harvey and Richter (1993) first proposed the idea in 1993 by conducting one of the earliest modeling works in the hybrid SOFC-GT cycle. They developed a model (Harvey and Richter, 1994b) to simulate MSOFC combined with an intercooled GT in Aspen Plus<sup>®</sup> and a fuel cell simulator developed by Argonne National Laboratory (Ahmed, McPheeters, and Kumar, 1991). They found that for a power plant with net electricity generation of 100 MW, about 61 MW were produced by the SOFC with a thermal efficiency of 77.7% (LHV). In addition, their second law analysis noted the large exergy destruction in the SOFC, combustor, and air mixer. They concluded that internal reforming could improve both system efficiency and its simplicity.

In their following paper (Harvey and Richter, 1994a), they improved the model by incorporating an internal reformer to the cycle and taking into account all major cycle overpotentials. This time the cycle efficiency was 68%. Moreover, they noted that the system efficiency increased with

cycle pressure. They determined that maximum efficiency could be achieved at system operating pressure equal to 15 bar while satisfying the system constraints. They also compared efficiency of the cycle with internal and external reforming and surprisingly found that their efficiencies were almost identical. The thermodynamics second law analysis showed that exergy destructions in a cycle with internal reforming were marginally higher than those of a cycle with external reforming (275 versus 273 MJ/s).

For the successful integration of the SOFCs with other power generating technologies, such as gas turbines, models that can accurately address steady-state and dynamic behaviour of systems with different configurations, optimization, fluctuating power demands, and techno-economic evaluation are required. In the following subsections, models that addressed these objectives will be discussed.

### **3.4.3 Parametric studies**

One of the primary aims of any system simulation is to evaluate the effects of various parameters on system performance. By doing so, the most influential parameters can be identified. In turn, these parameters should be considered for system optimization within system constraints.

The curves in Figure 10 are presented to quickly summarize the results of these parametric studies in the literature. For instance, if a performance parameter is linearly increasing, Curve 2 will be referred to describe the trend (Suther, 2006).

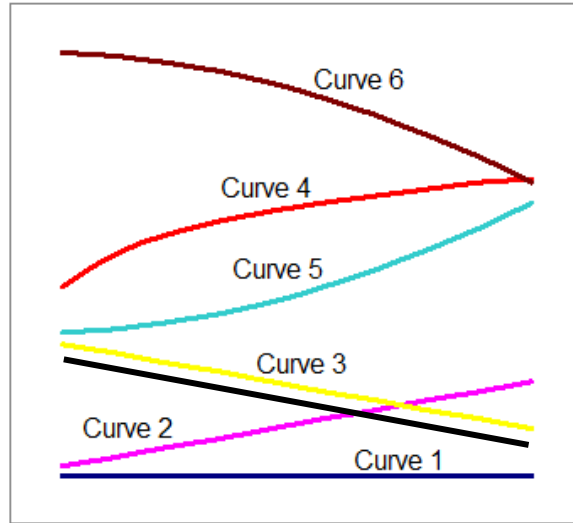


**Figure 10: Performance parameter symbolic curves (Suther, 2006)**

The first study to be reviewed in this subsection is presented by Suther et al. (2010a, 2010b). They studied the effects of system pressure, SOFC operating temperature, turbine inlet temperature (TIT), steam-to-carbon ratio (SCR), SOFC fuel utilization factor, and GT isentropic efficiency on the specific output work and efficiency of two generic hybrid cycles, with and without anode off-gas recirculation. They chose specific output work (actual work divided by air mass flow rate) and cycle efficiency as two main performance parameters. They found cycle specific work and thermal efficiency with respect to system parameters to follow curves in Figure 10 as follows:

- Specific work and efficiency with respect to system pressure followed Curve 4 and Curve 5 for the system with anode off-gas recirculation and Curve 4 and Curve 2 for the system without anode off-gas recirculation, respectively.
- Specific work and efficiency with respect to SOFC operating temperature followed Curve 3 and Curve 2, respectively, for both systems, with and without anode off-gas recirculation.
- Specific work and efficiency with respect to TIT followed Curve 2 and Curve 3, respectively, for both configurations.

- Specific work and efficiency with respect to SOFC current density followed Curve 3 for both configurations.
- Specific work and efficiency with respect to SCR followed Curve 2 and Curve 3, respectively, for both configurations.
- Specific work and efficiency with respect to SOFC fuel utilization factor followed Curve 5 and Curve 2 or 3 (depending on GT isentropic efficiency), respectively, for both configurations.

The results showed that the cycle efficiencies with and without anode off-gas recirculation were very close with variation in many of the system parameters.

Palsson et al. (2000) developed a steady-state model for a combined SOFC-GT system featuring external pre-reforming and recirculation of anode gases in Aspen Plus<sup>®</sup> by using their SOFC model as a user-defined unit and other components modeled as standard unit operation models. In order to model SOFC, they used a 2-D model of planar electrolyte-supported SOFC.

The finite volume method was used to discretize cell geometry by considering resistance and activation polarisation. Their system size was 500 kW because they believed this was the proper size for demonstration and market entry purposes. It should be noted that they added primary fuel to increase TIT but they maintained a constant fuel flow rate to the system. Furthermore, in order to provide heat for a district heating system, they added a cooler to the cycle exhaust stream. This simple cooler limited the exhaust temperature to a specific value (80°C). They studied various system parameters, including the electrical efficiency, specific work, TIT, and SOFC temperature with respect to the pressure ratio. Their sensitivity studies revealed that these parameters varied according to Curve 6, Curve 4, Curve 2, and Curve 1, respectively. Moreover, the electrical efficiency and SOFC temperature varied with respect to the cycle inlet air flow rate according to Curve 3 and Curve 2, respectively. They found that increasing TIT did not improve system efficiency and specific work. The reason was that in order to increase TIT, more fuel should be combusted at the GT combustion chamber; thus, less fuel remained to be consumed in the SOFC unit. Their analysis showed that the system operating pressure had great impact on hybrid system performance, as shown in Figure 11. At lower pressure ratios (PRs), the efficiency increased slightly to an optimum point and then sharply decreased for higher PRs. A maximum

efficiency of 65% could be achieved at a pressure ratio of 2. At this point the GT output was almost zero; therefore, this efficiency was equal to the SOFC efficiency. The slight improvement in the system efficiency stemmed from increased efficiency of the SOFC. At higher PRs, more output power from the gas turbine and less from the SOFC decreased system overall efficiency. In addition, they pointed out that cell voltage had no impact on system performance. Similarly, they investigated the performance improvement of the system when the intercooling of air compressor and gas turbine reheat were added and found that their application would not be worthwhile because of their relatively small impact, particularly for the reheat case.

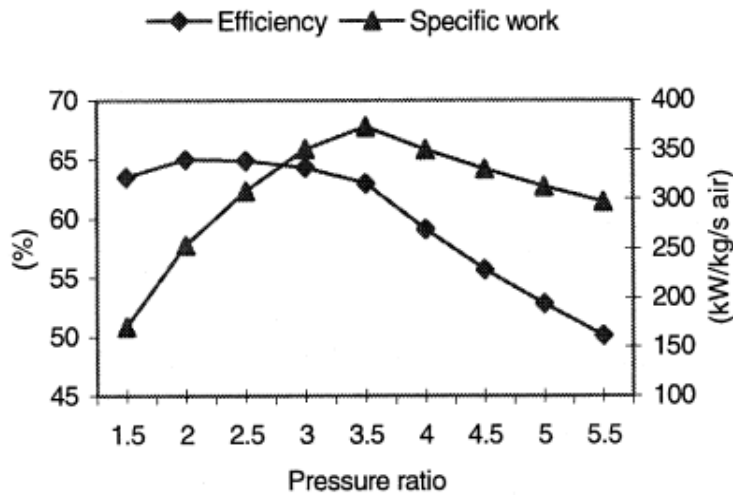
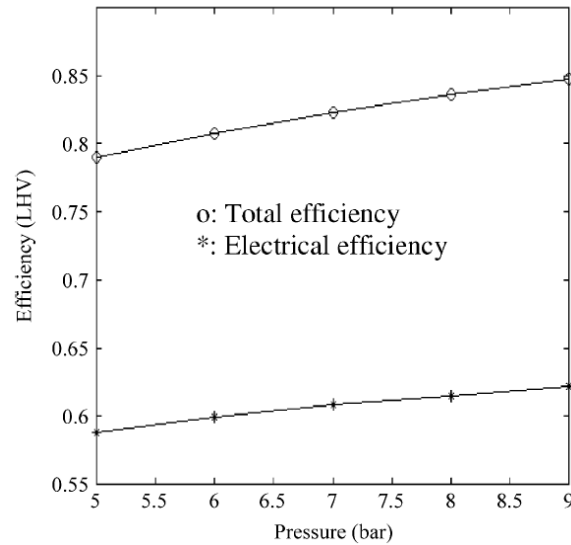


Figure 11: Influence of pressure ratio on system performance (Palsson et al., 2000)

The discrepancy between the results of Suther et al. (2010b) and Palsson et al. (2000) is due to the different control strategies of the two systems. In the former, the fuel molar flow rate was kept constant when varying the system operating pressure. But in the latter, as mentioned earlier in this subsection, although the total fuel flow rate was held constant, part of this fuel was fed to the gas turbine combustor to sustain the turbine exhaust temperature in a specified range. Therefore, in the case of Palsson et al. (2000), at high system operating pressures more fuel was combusted in the GT combustor resulting in more work to be generated in the GT at lower efficiency, which in turn lowered cycle overall efficiency.

Chan et al. (2002a, 2003a) developed a model of a simple SOFC-GT-CHP power system and performed the first law of thermodynamics analysis on the model. Their model achieved electrical and total efficiencies of over 62% and 83%, respectively. Then, they investigated the effects of system operating pressure and fuel flow rate on the system overall performance. They showed that system efficiency with respect to pressure and fuel flow rate followed Curves 2 and 3, respectively. Their results and those of Palsson et al. (2000) do not show the same trend, as can be seen by comparing Figures 11 and 12. The reason is similar to what was explained in the previous paragraph.



**Figure 12: Effect of pressure on SOFC-GT-CHP power system efficiency (Chan et al., 2002a)**

Calise et al. (2006b) investigated the impacts of current density, system operating pressure, fuel-to-oxygen ratio, water-to-methane ratio, and fuel utilization factor on the electrical efficiency of a hybrid SOFC-GT system and found the electrical efficiency to follow Curve 3, Curve 4, Curve 4, Curve 1, and Curve 2, respectively, when varying these parameters. They also showed that increasing the fuel utilization factor of the SOFC could slightly improve cycle performance. In contrast with the fuel utilization factor, the effect of SCR was not favourable. It was stated that this was as a result of more energy being used to generate steam in the heat recovery steam

generator and less energy for power generation. These results are in agreement with those of Suther et al. (2010b).

#### **3.4.4 2-Dimensional models**

As noted earlier, one method to categorize SOFC models is based on the number of geometrical axes through which the flow parameters vary, namely, 0-D, 1-D, 2-D, or 3-D models. It should be noted that, in this review, dimension of the model is defined by the SOFC model dimension not the other components. Due to the objective and complexity of the hybrid SOFC cycle modeling, most of the simulations in the open literature were 0-D. However, there are some papers that used a multi-dimensional approach to model the SOFC stack, such as Palsson et al. (2000), which was discussed previously, and Stiller et al. (2005), which will be explained later in Subsection 3.4.5. In this section, one example of such models will be reviewed.

Song et al. (2005) developed a model to evaluate the impacts of system parameters on the performance of the hybrid tubular SOFC-micro gas turbine (MGT) system. They used quasi-two dimensional approach in their model. In this approach, in order to achieve a two-dimensional model, the fuel cell was discretized into a number of one-dimensional sections, and they were dynamically coupled (input of  $i^{\text{th}}$  section = output of  $(i-1)^{\text{th}}$  section) (Bove and Ubertini, 2006), as shown in Figure 13. To implement this approach, they divided the fuel cell tubes into segments, considering control volumes around air and fuel streams for each segment. For each control volume, heat and mass transfer, electrochemical reactions, reforming, and steam shifting were considered. The heat transfer was assumed to be in the longitudinal direction through the walls that separate the streams. In addition, the mass transfer and electrochemical reactions were considered in the longitudinal and perpendicular directions, respectively.

The most important parameter influencing the accuracy of this approach was proper selection of the number of segments along the longitudinal direction of the SOFC tubes. Figure 14 shows that the distributions of cell temperature along the longitudinal direction tended to converge to a specific pattern when the number of segments increased. This, again, shows the importance of reasonable and accurate assumptions, in this case the number of geometrical axes through which the flow parameters vary. For instance, in the lumped model (when the number of segments is

equal to one), the mean value of the cell temperature was underestimated in comparison to the converged quasi-2-D model (about 900°C vs. 930°C). Also, in the lumped model the temperature difference along the length of the SOFC (74°C) was neglected.

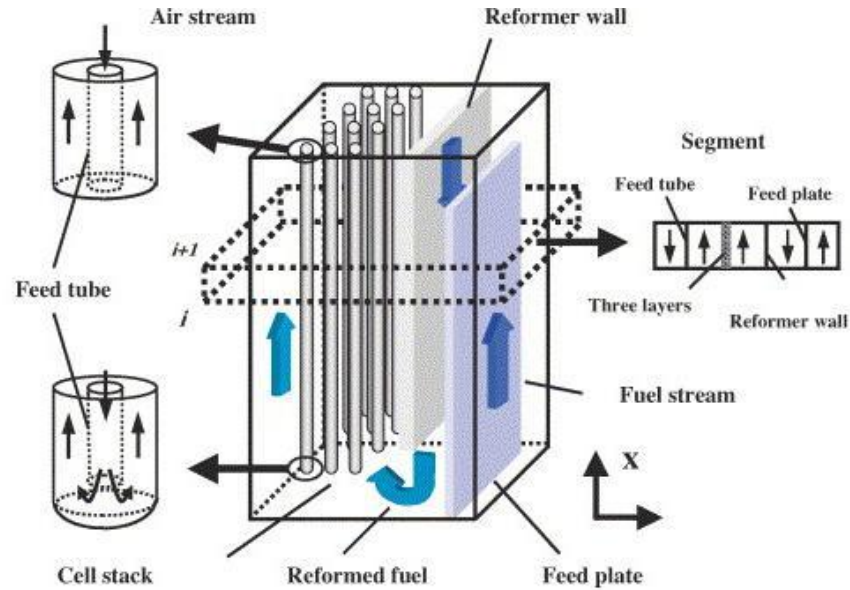


**Figure 13: Tubular SOFC discretization along longitudinal direction for quasi-two dimensional model (Song et al., 2005)**



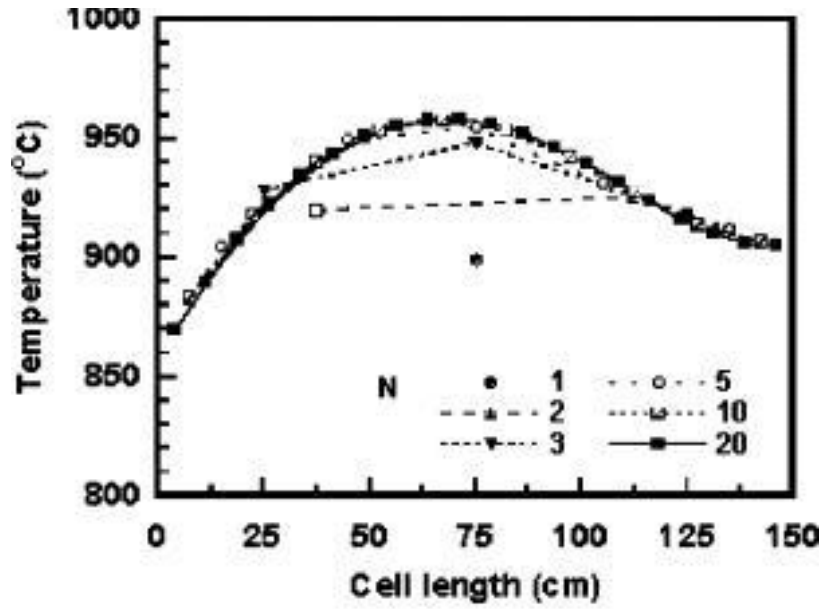


**Figure 14: Distributions of cell temperature along longitudinal direction of tubular SOFC with different number of segments for quasi-two dimensional model (Song et al., 2005)**

Furthermore, they evaluated and compared system performance for different configurations, including co- and counter-flow SOFC systems with and without pre-reformer, and various catalyst densities of reformer. They found that, for instance, although flow direction did not have significant impact on SOFC efficiency, the hybrid system efficiency for co-flow SOFC was higher than that of counter-flow SOFC (about 60% vs. 58%, respectively). As a result, they concluded that the system configuration and its component characteristics could significantly influence hybrid system performance.

### 3.4.5 Models for comparison of configurations

As stated, an important objective of hybrid SOFC system modeling is to predict system performance for different configurations. There has been a huge number of proposed hybrid SOFC system configurations in the open literature that combined SOFC stacks with heat exchangers, compressors, GTs, pre-reformers, mixers, heat recovery steam generators (HRSGs), CCS systems, combustors, and so on (such as Campanari and Macchi (1998)). However, there have been no universally accepted configuration(s) yet, and scientists are still trying to propose

innovative cycles for hybrid SOFC systems. In this section, various configurations proposed in the open literature for the stack and equipment will be reviewed.

Stiller et al. (2005) developed the 2-D planar and 1-D tubular SOFC models to simulate the hybrid SOFC-GT cycle. They investigated effects of different parameters, such as pressure ratio, air inlet temperature, and so on, to compare the performance of two cycles. It was shown that hybrid systems could achieve efficiencies above 65% with both planar and tubular SOFCs. The main difference between the planar and the tubular SOFC cycles was the internal pre-heating of the air in the tubular system, which allowed a lower air inlet temperature to the stack. This reduced the amount of required high temperature heating in the pre-heating. This effect was compensated by lower efficiency of the tubular fuel cell stack, due to its higher ohmic loss.

Selimovic and Palsson (2002) investigated the effect of networked SOFC stacks, i.e. using two smaller stacks in series (in terms of fuel and air flows) instead of a conventional one stage stack. They used the same model as (Palsson et al., 2000), with minor modifications. They showed that for a stand-alone SOFC, fuelled by hydrogen or 30% pre-reformed methane, dividing the single stage stack into two smaller stacks in series (staged stacks) increased the output power by 2.7% and 0.6%, respectively. The reason stemmed from increased uniformity of current density in the staged system. Then, they examined the hybrid SOFC-GT cycle fuelled by natural gas (NG) for two options, both the air and fuel streams in series (network A) or only the fuel stream in series and air stream divided (network B). The results signified that there was a performance improvement in the network A, whereas efficiency was reduced for the network B. They concluded that for relatively small stacks, networked stacks could reduce the cooling demand of the cells, so they were preferred.

Magistri et al. (2005) developed a model to investigate the performance of a hybrid system consisting of an integrated planar SOFC (IP-SOFC), GT, and district heating. They found that overall efficiency of an atmospheric hybrid system was 10% lower than that of a pressurized system.

In 2007, Granovskii et al. (2007a) presented results of their simulation of a combined SOFC-GT system for two possible configurations to provide required steam-to-methane ratio (in all cases higher than 2 (Hengyong and Stimming, 2004)), a cycle with anode exhaust recirculation and a cycle with HRSG for steam generation. They also added a Rankine steam cycle at the bottom of

the GT for the configuration with anode exhaust recirculation. They performed energy and exergy analyses on the models and determined that the suitability of these schemes depended on the application of the power generation system. For example, although configuration with anode off-gas recirculation had higher exergy and energy efficiencies, the other scheme was associated with a higher power generation capacity.

Pangalis et al. (2002) and Cunnell, Pangalis, and Martinez-Botas (2002) modeled and compared six different configurations of hybrid SOFC-GT systems by considering a variety of features in each system, including combustion chamber, recuperator, intercooler, and reheat SOFC stack. They showed that both thermal efficiency and net specific power versus compression ratio for most of the configurations followed Curve 4. They found that the optimal configuration in terms of efficiency could be achieved when the GT with an intercooler and recuperator was integrated to primary SOFC (ahead of the combustor) and reheat SOFC (between high- and low- pressure GT) with an efficiency of 76%. Also, they showed that in configuration with intercooler and recuperator integrated to the primary SOFC, the net specific power was maximized. Again, they concluded that the most important factor for selecting hybrid SOFC system configuration was the application of the power plant. For example, a recuperated GT with SOFC ahead of the combustor with a thermal efficiency of 64% at a relatively low pressure ratio of 14 and the specific power of 520 kW/kg<sub>air</sub> was probably the most suitable configuration for small and medium scale power generation.

Kuchonthara et al. (2003a) developed their hybrid SOFC model by writing a Fortran code for the SOFC and running it in Aspen Plus<sup>®</sup>. They conducted a parametric analysis on two hybrid SOFC system configurations: hybrid SOFC-GT with a heat recuperation (HR) system and hybrid SOFC-GT with a heat and steam recuperation (HSR) system. In the former, heat from the GT exhaust was recovered by an air preheating system, whereas, in the latter, an air preheating system and an HRSG were used for this purpose. In the HSR system, in order to increase the net mass flow rate and output power of the GT, the generated steam was directly injected into the combustor. They found that GT output power and system overall thermal efficiency were higher in the HSR configuration, due to a higher energy recuperation rate in this configuration. Also, they illustrated that higher pressure ratios increased the effect of steam recuperation. Furthermore, their parametric analysis showed that the SOFC work, GT work, TIT, and thermal

efficiency with respect to the SOFC fuel utilization factor varied according to Curve 2, Curve 3, Curve 3, and Curve 4, respectively. Also, the cycle specific work and thermal efficiency with respect to the TIT followed Curve 5 and Curve 6, respectively.

They evaluated the overall efficiency of the cycle against TIT for different pressure ratios. As shown in Figure 15, they found that, at low TITs, the thermal efficiency decreased when the pressure ratio increased. This was due to a lower fuel utilization factor in the SOFC for higher PRs. In contrast, higher PRs led to thermal efficiency improvement at high TITs due to larger GT power output. As a result, they suggested that the optimal system (simultaneously high output power and high efficiency) could be achieved when the system operated at a high TIT with an optimal pressure ratio. It seemed that their results completed previous studies (Suther et al., 2010b; Palsson et al., 2000; Tanaka et al., 2000) on the effect of TIT on the cycle's overall performance.

Similarly, they published another paper (Kuchonthara et al., 2003b) to evaluate performance of hybrid systems when the SOFC cycle integrated with various enhanced gas turbine cycles, namely, steam injected gas turbine (STIG) cycle (including additional air preheating), GT-steam turbine (ST) combined cycle, and humid air turbine (HAT). They assessed effects of operating conditions, such as TIT and PR, on the overall efficiency and specific output work of the system. They concluded that the SOFC–HAT system, operating at a high TIT and PR, not only could significantly improve system performance, but also could lessen the problem of water supply by reducing water consumption.

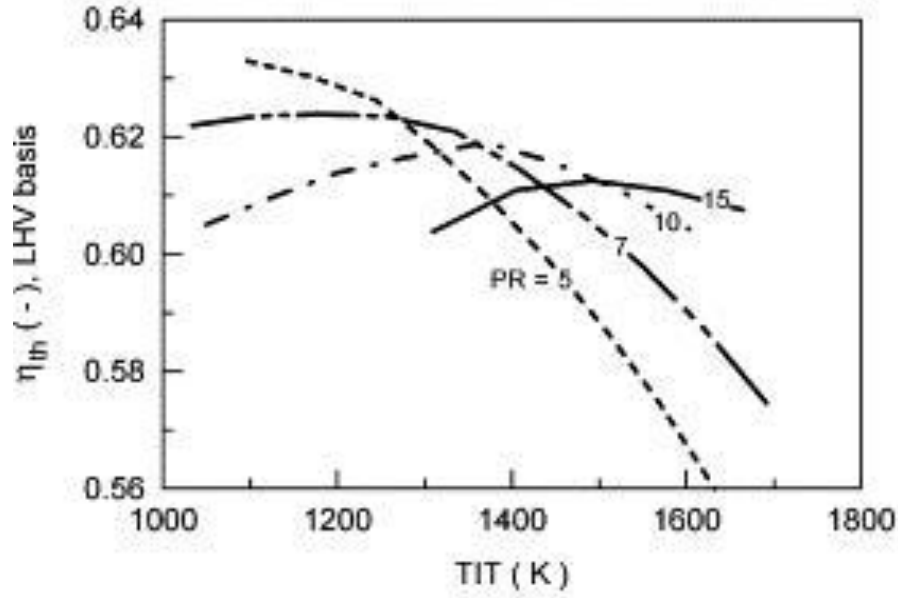


**Figure 15: Influences of TIT and PR on overall efficiency in SOFC-GT with HSR ( $T_{\text{steam,max}} = 823 \text{ K}$ )**  
(Kuchonthara et al., 2003a)

One of the challenges in hybrid SOFC system development is to find a gas turbine that matches the requirements of the hybrid cycle. Lundberg et al. (2003) studied the possibility of a hybrid system that integrated a pressurized SOFC with a Mercury 50 gas turbine. The Mercury 50 GT was chosen due to its unique characteristics, including high thermal efficiency, power rating, modular design, reliability, and low cost of maintenance. They determined the optimal size of the pressurized SOFC (PSOFC) in a hybrid system with a single Mercury 50 gas turbine using the cost of electricity (COE) as the optimizing parameter. Minimum COE was achieved when four PSOFC modules and one Mercury 50 gas turbine were integrated to generate approximately 12.5 MW at an efficiency of nearly 60% (net alternating current (AC)/LHV). They also explained the required modification on commercially available GTs. Furthermore, they studied different bottoming cycle options (i.e. combined cycle power plant and ammonia-water cycle) to utilize thermal energy at the GT exhaust.

On the other hand, most of the works performed on the modeling of hybrid SOFC and GT cycles concentrated on the fuel cell operation using the performance characteristics of existing GTs. However, different operating conditions of the GT (i.e., the increased pressure losses) in the hybrid cycle shifts the operating point of the compressor and GT to off-design areas. Sieros and

Papailiou (2007) examined the optimal fitting of a small GT in a hybrid SOFC-GT cycle for both design-point and part-load operation conditions. They proposed variable geometry components to avoid compressor surge and increase part-load efficiency. They concluded that further work should be performed for the detailed design of these devices.

Rao and Samuelsen (2003) introduced an SOFC cycle coupled with an intercooled-reheat GT as a reference power generation system for their thermodynamic modeling. Then, they formed their alternative cases by incorporating the HAT system to their reference case and also replacing the reheater with the second SOFC (dual SOFC-HAT). They found that efficiency of the reference case and its alternatives were 66%, 69%, and 76%, respectively. In addition, they showed that the second scenario could achieve the lowest COE.

Song et al. continued their previously explained work, Subsection 3.4.4, (2005) in another research (2006). They extended their model to find optimal matching between a commercially available GT (Mercury 50) and an SOFC unit. The parameters to be matched included: operating temperature, pressure, and control strategies. The maximum allowable cell temperature was considered as a limiting parameter. Based on the selected conditions, the total system power at the design-point condition was 11.5 MW at a system efficiency of about 59%. In comparison to the power ratio of the SOFC and GT in kW-class cases described in Veyo et al. (2002b), the power ratio of this system was very low. Their results agreed with results found by Lundberg et al. (2003).

### **3.4.6 Optimization**

A quick survey of the literature in the modeling of hybrid SOFC systems shows that little has been done for optimization of these systems. In most of those few works, such as Yi, Rao, Brouwer, and Samuelsen (2004), sensitivity analysis of various parameters was performed to develop an optimal hybrid SOFC power generation system. For example, Riensche et al. (1998a) optimized the efficiency and cost of electricity of a 200 kW planar self-supported cross-flow SOFC cogeneration plant by investigating parameters, such as fuel utilization factor, cell voltage, air temperature increase in the stack, and degree of internal reforming. They found that the electric and total efficiencies can be increased from 43% and 67% in the reference case to 49%

and 76% in the optimized case, respectively. In another paper (Riensch et al. 1998b), they used the same method to find optimal configuration of the cycle. However, due to the large number of parameters involved and the complex nature of their interrelation and correlation, the suitability of this optimization method is controversial.

In optimization of a typical hybrid SOFC cycle five to ten (or even more) (Möller et al., 2004) independent variables should be considered, depending on how complex the system and model are. Therefore, it is vital to find methods that can optimize these non-linear multi-dimensional systems.

In a considerable development in the optimization of SOFC-GT systems, Möller et al. (2004) deployed the genetic algorithm (GA) to optimize an SOFC-GT configuration with and without a CO<sub>2</sub> separation plant. In order to model the SOFC stack, they used the same model as in Palsson et al. (2000). In their optimization, the electrical efficiency was selected as the objective function. Also, the air flow, fuel flow, cell voltage in the stack, air temperature at the stack inlet, reformer duty, and pressure ratio were selected as decision parameters. The optimization procedure resulted in an SOFC-GT system with above 60% efficiency when equipped with CO<sub>2</sub> capture. The results showed that the system efficiency was greatly influenced by SOFC temperature. Furthermore, a low air flow rate and no or little supplementary fuel could improve the system efficiency. Later, Calise et al. (2007) used the same method to optimize an SOFC-GT cycle to reduce the cost of electricity.

### **3.4.7 Exergy analysis**

According to Dincer and Rosen (2004), exergy analysis is a method that can be applied to design, improve, and analyze energy systems. This technique considers the second law of thermodynamics as well as the conservation of mass and energy, simultaneously.

Granovskii et al. (2008) evaluated the importance of exergy analysis in applying the “principles of industrial ecology” for integrating different technologies. For instance, they performed exergy analysis on a hybrid SOFC-GT system and found that the depletion number of a stand-alone SOFC and GT was much higher than that of the hybrid system. This confirmed that the hybrid SOFC-GT system was more environmentally friendly. The depletion number, proposed by

Connelly and Koshland (2001), is a concept to describe the efficiency of fossil fuel consumption according to exergy analysis and is defined based on how exergy destruction within a system is related to total exergy input.

Calise et al. (2006b) in a previously mentioned paper (see Subsection 3.4.3) and in another paper (Calise et al., 2006a) (with a few changes in the system configuration) performed the second law of thermodynamics analysis on a gas turbine cycle integrated with an SOFC. Their exergy analysis illustrated (Figure 16) that the SOFC stack and the catalytic burner were responsible for most of the exergy destruction, respectively, when the hybrid system operated at the design-point. This high rate of exergy destruction stemmed from inefficiencies of chemical reactions occurring in those pieces of equipment. Despite the high efficiency of the SOFC, fuel cell stacks are the greatest source of exergy losses due to the number of chemical and electrochemical reactions, such as steam reforming and electrochemical oxidation, taking place simultaneously. Similarly the catalytic burner, where the anode off-gas stream was combusted, demonstrated a significant exergy destruction rate. On the other hand, the exergy destruction rate of turbomachinery was not remarkable because of its high isentropic efficiency and low energy flow. They also performed exergy analysis on partial load operation and found that although exergy destruction generally increased, its rate depended on the selected control scheme. Finally, they concluded that in the hybrid energy system design, particular emphasis should be placed on the component with the highest exergy losses, i.e. SOFC stacks.

In another paper, Granovskii et al. (2007b) presented exergetic performance analysis of a hybrid SOFC-GT cycle. They found that the SOFC stack and combustion chamber were the components with the highest rate of exergy destruction, respectively, similar to the results of Calise et al. (2006a). But in their model, the difference in exergy losses of the SOFC stack and combustion chamber was less than 5%.



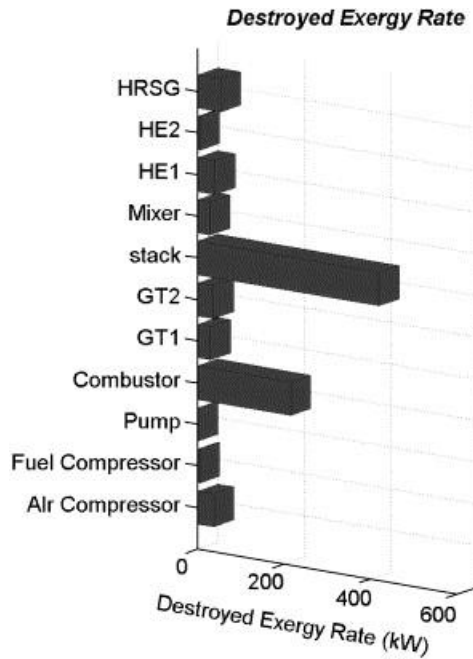


Figure 16: Rate of destroyed exergy for different components in SOFC-GT cycle (Calise et al., 2006b)

### 3.4.8 CO<sub>2</sub> capture

Although hybrid SOFC power plants are considered to be the cleanest technology to generate electricity from fossil fuels (due to their high efficiency and minimal fuel combustion), still there is a considerable amount of CO<sub>2</sub> in their exhaust. Therefore, integrating CO<sub>2</sub> separation technologies to hybrid SOFC plants is an active field of research. In this section, some of the models for such plants will be discussed.

Riensch et al. (2000) developed a model to simulate a near-zero CO<sub>2</sub> emission hybrid SOFC-GT power plant. Their adiabatic tubular air electrode-supported fuel cell model was based on one of the earliest planar SOFC models (Achenbach, 1994). There are two approaches to separate CO<sub>2</sub> in the exhaust stream of power plants. In one of these approaches, the spent fuel is combusted with pure oxygen, instead of air, to avoid introducing nitrogen to the plant's off-gas stream. Riensch et al. (2000), in their proposed model, made use of one of the unique characteristics of SOFC cycles that other technologies cannot easily compete with. They modeled a bank of oxygen ion conducting tubes (very similar to SOFC tubes) and passed the unused fuel over them to oxidize the fuel. They found that system operation was optimal when

the system was pressurized. It was concluded that a gross electric efficiency of about 50% to 60% for the tubular SOFC and 60% to 70% for the SOFC-GT combination were achievable in this configuration.

Franzoni et al. (2008) developed a model to simulate a 1.5 MW hybrid SOFC-GT system based on the model explained in Massardo and Lubelli (2000). They compared performance of the hybrid plant when it was integrated with two CO<sub>2</sub> capture technologies, namely, by separation of CO<sub>2</sub> in exhaust by chemical absorption, and combustion of spent fuel with pure oxygen. In the former approach, they observed 17% efficiency penalty, from 62% to 45% with 0.15 kgCO<sub>2</sub>/kWh in the exhaust. In the second approach, the system was equipped with an air separation unit to provide oxygen for the GT combustor. The efficiency loss in this case was much lower at 3.6% with near-zero CO<sub>2</sub> at the exhaust stream. The thermoeconomic analysis showed that the cost of the second plant was significantly lower.

Using the same method, Inui et al. (2003) used the second approach (pure oxygen as the oxidant gas in the GT combustion chamber) for CO<sub>2</sub> capture. They found that the efficiency of the cycle could reach as high as 71% (LHV) indicating that the proposed system could satisfy both expectations of high efficiency and ultra clean power generation.

Campanari and Chiesa (2002) compared performance of an SOFC-GT cycle with two configurations for the CO<sub>2</sub> capture process. In the first scheme, steam and CO<sub>2</sub> in the anode exhaust were separated from the mixture by condensation and chemical absorption, respectively. Then, 30% of the remaining fuel was combusted in the GT combustor, and the rest was recycled to the anode to be consumed in the SOFC. In the second scheme, CO in the anode exhaust was converted to H<sub>2</sub> in the shift reactor. Then, the existing CO<sub>2</sub> was chemically absorbed, and the hydrogen-rich gas was combusted in the GT combustion chamber. The SOFC model for this plant was explained in Campanari (2001). The results showed that both plants exceeded 71% (LHV) efficiency and removed 90% of CO<sub>2</sub> in the exhaust stream. Although utilization of the shift reactor increased complexity of the second scheme, it took advantage of a lower energy consumption of the auxiliaries (5.5% vs. 8.2% of the net output), and better potential for CO<sub>2</sub> sequestration.

### 3.4.9 Fuel flexibility

So far, in all models either natural gas or hydrogen was considered as fuel. However, hybrid SOFC systems enjoy the advantage of being able to utilize other fuel sources. In this subsection, some models that use fuels other than hydrogen, methane, and natural gas will be discussed.

In one of the earliest works in this field, Lobachyov and Richter (1996) presented results of their theoretical study on the system that incorporated a coal gasification process into a hybrid SOFC-GT cycle. The SOFC-GT part of this model was proposed by Harvey and Richter (1994b). They suggested recycling part of the hot cathode off-gas to provide the heat required for gasification. They performed energetic and exergetic analysis on the model. They found that the cycle could achieve up to 60% efficiency (energetic). Exergy analysis revealed that the gasifier, SOFC, and steam generator were responsible for most of the exergy destruction. In addition, the integration of a two-stage GT with reheater and steam turbine at the bottom of the GT resulted in 0.5% and 3.2% improvement in the system's overall efficiency, respectively.

Kivisaari et al. (2004) performed a feasibility study for integration of a high temperature fuel cell (either MCFC or SOFC), a gas production unit based on coal gasification, and existing networks of heat distribution among residential users (CHP plant). They considered a thermal input of 50 MW with and without anode off-gas recirculation for the SOFC. They employed a 0-D model to reduce calculation times and model complexity. They found that the introduction of the anode off-gas recirculation resulted in a 12% increase of the output power from the SOFC because of the almost 10% increase in overall fuel utilization. They observed that the final system, which was a combination of a gasifier, a standard low temperature gas cleanup, and SOFC, could achieve electrical and overall efficiencies of about 47% and 85%, respectively.

Another study on the combination of the coal gasification and fuel cell for power generation was presented by Kuchonthara et al. (2005). They considered the integrated power generation cycle combined with thermochemical recuperation, brown coal gasification, and an SOFC. In order to model the SOFC, they used the same model as in Kuchonthara et al. (2003a, 2003b). Their simulation indicated that the cycle efficiency could be increased from 39.5% (HHV) without the SOFC to about 45% with the SOFC.

Rao et al. (2005) performed thermoeconomic analysis of an integrated gasification fuel cell (IGFC) plant and compared it with an integrated gasification combined cycle (IGCC). They showed that the cost of electricity of the IGFC plant was compatible with that of the IGCC plant (based on \$400/kW installation cost for the SOFC stack).

Sucipta, Kimijima, and Suzuki (2007) used a similar model as Song et al.'s (2005) and added different biomass gasification processes, namely, air-, oxygen- and steam-blown, to analyze the effects of the biomass fuel composition on the SOFC-GT performance. They found that the efficiency levels for all three cases were reasonably high (although lower than the reference case fuelled with pure methane) and concluded that the biomass fuelled SOFC–MGT hybrid system was a suitable alternative for conventional power plants. They pointed out that air- and steam-blown biomass fuel had the lowest and highest efficiency, respectively, for both the SOFC module and for the entire hybrid system.

Van herle et al. (2003) performed the energy balance analysis on an existing biogas production unit, equipped with a 1 kW SOFC demonstrational stack as a small CHP system. The fact that they used some real data for their model and, to some extent, compared the results with the measurement from the site made this paper one of the few exceptions in this respect. They achieved almost 34% and 58% electrical and cogeneration thermal efficiency, respectively. The results were validated by the natural gas fuelled Sulzer Hexis 1 kW systems with an electrical efficiency of 35% (DC, LHV) (Raak, Diethelm, and Riggensbach, 2002). They also compared two reformer technologies, i.e., steam reforming and partial oxidation reforming with air (POX). They also investigated the impacts of water addition for the steam reforming process and observed that cogeneration thermal efficiency significantly decreased with water addition. This was due to the fact that there was no condensation in the exhaust to recover the evaporation heat consumed at the inlet.

They also indicated that electrical efficiency reduced when the system was pressurized. Clearly, this was in contrast with other studies such as Suther et al. (2010b) and Chan, Low, and Ding (2002b). The reason was that their model did not consider two positive impacts of higher system operating pressure: more output work when high pressure hot exhaust passed through GT and improved mass transfer which led to a lower electrode overpotentials. On the other hand, more compression work to pressurize inlets streams reduced net output work.

#### **3.4.10 Different applications (non-stationary electricity generation)**

Stationary power generation plants are not the only application of hybrid SOFC cycles. The residential CHP, mobile application, and auxiliary power units for vehicles and aircrafts are considered as potential applications of hybrid SOFC cycles. In this subsection, a few simulations that addressed these applications will be presented.

Nowadays, distributed generation (DG) of combined heat and power (CHP) cycles is gaining increasing attention. This is due to the deregulation of the electricity market and widespread residential utilization of natural gas as a primary energy source. Although some authors proposed application of PEFCs for CHP (Ellis and Burak Gunes, 2003; Obara and Kudo, 2005), hybrid SOFC cycles are the most promising candidates in this application.

Braun et al. (2006) developed a model to evaluate the energetic and exergetic performance of various configurations of residential-scale SOFC-CHP hybrid systems, including hydrogen- and methane-fuelled systems with external and internal catalytic steam reforming, and cathode and anode off-gas recirculation. They investigated the parameters influencing suitability of this system to match residential demands and found that one of the most important parameters was the thermal-to-electrical load ratio (TER) of the residential unit. The TER is defined as the ratio of the thermal energy demand of the home to its base electrical load. Their results indicated that the optimal system included the cathode and anode off-gas recirculation and internal reforming of methane. The electrical and combined heat and power efficiencies of this system were 40% and 79% (based on HHV), respectively.

In 2002, Winkler and Lorenz (2002) investigated the potential utilization of hybrid SOFC-GT cycles in mobile applications. They first proposed a reheat SOFC-GT with an efficiency of more than 70%. They also showed that by incorporating a bottoming steam cycle to a reheat hybrid SOFC-GT system, an electrical efficiency of more than 80% would be possible. They illustrated that the electrical efficiency with respect to the SOFC pressure followed Curve 4. Their results agreed well with the results of Yi et al. (2004) and Suther et al. (2010b). Finally, they investigated the possibility of deployment of the SOFC-GT in a mid-size car with a capacity of 75 kW and efficiency of 55%. They concluded that the results of their modeling proved the

feasibility of utilization of the hybrid SOFC–GT system in unconventional applications, which required further and more detailed investigations.

Steffen et al. (2005) developed a model of an SOFC-GT cycle to provide auxiliary power for a 300-passenger commercial transport aircraft to be built in 2015. They stated that 440 kW was an adequate unit size for this application. Unlike the ground stationary power plants, in aerospace systems, power density (power/volume) and system specific power (power/mass) were the most important parameters to consider. Another remarkable difference in this application was fuel source, which was jet fuel. This led to using catalytic partial oxidation (CPOX) for the fuel reforming process. Their proposed system resulted in an efficiency of about 63% (LHV), which was significantly higher than the efficiency of conventional systems at about 42%. However, the proposed system was much heavier (1,396 kg versus 331 kg) mainly because of the metallic interconnect mass in the fuel cell stack. They suggested that by applying some innovative techniques (e.g. corrugated flow channels) the system's mass could considerably be reduced. They completed this study in another paper (Freeh et al., 2005) by considering system partial load operation. In this case, system total mass increased considerably to 1,912 kg.

#### **3.4.11 Transient and off-design condition modeling**

In every energy system, dynamic and part-load behaviour and load following characteristics are critical factors to consider. This is especially important for hybrid SOFC systems, since they have been considered as forerunner technology in the market of distributed and residential power supply, and mobile applications. Since these types of power stations operate in isolated conditions, their load demand following characteristic is extremely important. Thus, part-load performance, operational stability, and safety are key issues that should be addressed for SOFC-based energy systems before they can be commercialized. The main objective of these studies is to design a control strategy that can maintain SOFC and GT inlet temperatures during load changes (Roberts et al., 2006). These aspects of the hybrid SOFC system have been studied extensively in the literature. In this subsection, some of these papers will be reviewed.

Costamagna et al. (2001) evaluated design and off-design performance of an SOFC and MGT hybrid system. For the design-point operation, they found the overall efficiency to be higher than

60%, and the MGT-to-SOFC output work ratio to be 0.19. In off-design operation, they considered two control strategies: constant and variable turbine rotational speed. In the former scheme, the load was controlled by varying the overall fuel flow, which resulted in reduced system efficiency (from efficiency of 61% to 56% at 70% of the power at the design-point). The latter involved variation of the MGT rotational speed. However, the operation mode of conventional large size GT plants generally did not provide such opportunity. The rotational speed of these plants was dictated by alternating current (AC) frequency required by the end user or electrical grid. Since typical plants were not equipped with an inverter, their rotational speed was fixed and could not be used as a control parameter. However, an inverter was one of the essential components for hybrid SOFC-GT systems to convert electricity generated by the SOFC to AC required by the electrical grid. Thus, in these hybrid systems, it was possible to operate the GT at variable rotational speeds (variable frequency).

In variable MGT rotational speed control mode, they found that it was possible to obtain very high overall efficiency (always higher than 50%) even at very low part-load conditions (up to 30% of nominal power). It was interesting that the power ratio of the MGT and SOFC dropped for variable rotational speed control and increased for constant speed in comparison to that of design-point. They concluded that the hybrid system controlled by the variable rotational speed strategy operated with higher efficiency and flexibility. In addition, this scheme could control the tubular SOFC stack temperature more accurately.

Roberts et al. (2006) also investigated two control strategies for an atmospheric hybrid SOFC-GT system, variable versus fixed speed gas turbine operation. In the case of the constant GT speed, in order to maintain the SOFC stack operating temperature, they considered two mechanisms: cathode exhaust bypass or additional combustor. They found that none of these strategies was satisfactory because the former resulted in very high oxygen utilization in the cathode and low recuperator temperature, and the latter significantly reduced system efficiency. On the other hand, the variable rotational speed gas turbine control design satisfied all operational constraints, including high efficiency and sufficient control of the SOFC stack temperature.

In their next paper (Mueller et al., 2007), they further expanded their work by limiting the gas turbine's minimum operating speed to 65,000 rpm and adding an auxiliary combustor to the

system. The combustor was used to protect the SOFC from excessive cooling by combusting extra fuel to maintain the cathode inlet temperature, when the GT minimum rotational speed was reached. By applying this control strategy, hybrid system efficiency higher than 60% could be achieved. However, excessive burning of supplementary fuel in the auxiliary combustor, particularly at partial load conditions, considerably reduced the system efficiency. Then, they evaluated the dynamic behaviour of the hybrid cycle output power when the system was controlled by the designed control strategy. They concluded that this strategy was stable, safe, and robust over a wide range of output powers.

Similarly, Kimijima and Kasagi (2002) pointed out that the variable rotational speed operation strategy was superior to the constant rotational speed operation strategy for a 30 kW SOFC-MGT cycle.

Magistri et al. (2005), in their previously explained paper (see Subsection 3.4.5), investigated off-design behaviour of the hybrid cycle for three system sizes, namely 250 kW, 2 MW, and 20 MW with over 60% to 65% efficiencies at the design-point and always over 55% at part-load conditions. They also evaluated fixed and variable gas turbine rotational speed strategies as off-design control strategies. They stated that varying the rotational speed of the gas turbine could be considered as an appropriate control strategy for small and medium size systems. However, for large hybrid systems, it was not possible to apply this strategy. In this case, they suggested bypassing the SOFC to maintain stack operating temperature in an acceptable range. Moreover, they estimated the influence of ambient conditions on cycle performance and noted that due to their significant impact on the system performance, they should be taken into account in the system design and operation. Finally, they studied the transient behaviour of the system as a result of a fuel step reduction. They concluded that it took about 300 seconds for the SOFC and the heat exchanger to adapt to transient conditions due to their high thermal inertia.

Stiller et al. (2006a, 2006b) developed a model to investigate steady-state and transient conditions for an SOFC and GT hybrid cycle. They used different approaches for modeling of various components. For instance, gas flows were modeled by a 1-D scheme, whereas solid structures and recuperator heat exchanger were treated as 2-D components in axial and radial directions, and finally, the burner was simulated non-dimensionally. For off-design steady-state operation, the fuel and air flow rates (controlled by a flow control valve and GT shaft speed



variation, respectively) were used as controlling parameters. They illustrated the steady-state off-design behaviour of the hybrid system by providing a performance map of different parameters, such as net power, net electricity, pressure, and SCR, as a function of fuel flow and air flow relative to their design values. Figure 17 shows an example of such a graph. At high fuel flow and low air flow, there is no steady-state condition (unstable regime) and at high air flow and low fuel flow, the SOFC temperature is lower than the acceptable range.

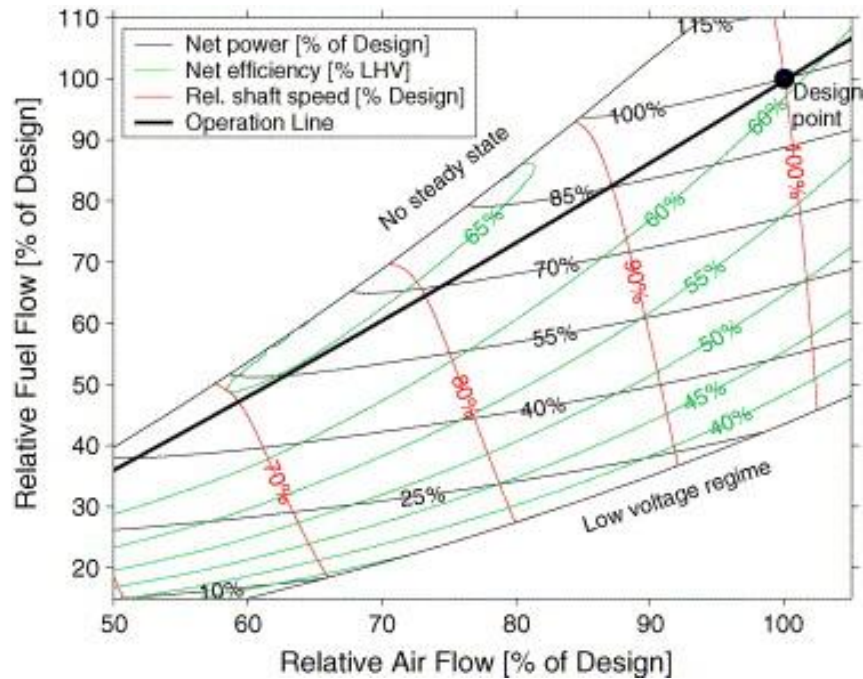


**Figure 17: Steady-state performance of SOFC and GT hybrid cycle (power, efficiency, and shaft speed)**  
(Stiller et al., 2006a)

In the next step, based on these findings, they designed a multi-loop feedback control scheme for the hybrid cycle with the following objectives: safe and long lifetime operation, high efficiency, fast load following, and governing external influences. They controlled the system output power by adjusting the SOFC current, fuel utilization, air flow, and the SOFC stack temperature. They investigated how the system responded to variations in several system parameters, such as load changes, load curve following, ambient air condition changes, and system malfunction and degradation. They concluded that by using this control scheme, the system's safe and stable

operation was guaranteed during all tests. In addition, the system was able to follow small and large load changes in time scales of below 1 and 10-60 seconds, respectively.

Song et al. (2006) in previously explained work (see Subsections 3.4.4 and 3.4.5) analyzed impacts of the system operating characteristics at part-load conditions on the hybrid system performance. They found that when a supplied fuel reduction strategy was utilized as the only load control parameter, the efficiency drop in both the SOFC (due to the decrease of cell temperature) and the GT (due to the decrease in TIT) were unacceptable. Therefore, they suggested simultaneous reduction of supplied air and fuel in order to maintain the SOFC stack temperature and the TIT as close to the design-point conditions as possible as the best control strategy. The air flow rate could be adjusted by manipulating the angles of the inlet guide vanes (IGVs) located in front of the compressor inlet. The results of this simulation revealed that the performance characteristics of MW-class systems in this study were very close to those of the multi-kW systems with a variable rotating speed of the gas turbine proposed by Campanari (2000).

Calise et al. (2006a) deployed the same approach to test partialization strategies. Similarly, they found that the best partialization strategy could be achieved by maintaining the air to fuel ratio. However, the technique did not demonstrate high flexibility of operating range. By applying this scheme, the plant net electrical output power could be reduced to a minimum of 80% of its rated value. Further reduction in load led the air compressor to approach its surge line. They stated that in such limited range of load change, none of the strategies resulted in a considerable efficiency penalty. They suggested that using fuel flow rate as a load control parameter could result in a better behaviour of the off-design operation of the system, provided that the turbomachinery design was optimized.

Chan et al. (2003b) proposed a strategy for system start-up, part-load, and full-load operational control based on the model developed in Chan et al. (2002a, 2003a). In their control scheme, in order to reduce system electrical load, part of the fuel was directly injected into the GT combustor (bypassing SOFC stacks). Although this scheme was safe and simple, it reduced the total efficiency of the system.

Tanaka et al. (2000) developed a model to perform technical and economical sensitivity analysis on an SOFC-GT combined cycle. They studied system performance as well as cost and energy

pay-back times (CPT and EPT). In their model, additional combustion in the GT combustor, similar to Palsson et al. (2000), was considered for the anode off-gas stream. But, unlike Palsson et al. (2000), the SOFC-to-GT output power ratio was controlled by supplementary fuel flow rate. They illustrated the electrical efficiency and TIT versus this ratio for different values of operating pressure, temperature, SCR, fuel and air utilization ratios, and load following characteristic (partial load performance). Their finding for the latter was interesting. The SOFC cycle could operate in part load condition to provide lower power demands without reducing its electrical efficiency below the nominal value. However, in the hybrid SOFC-GT system total efficiency dropped. This was due to the compressor's constant rotational speed, which meant more air should be compressed than really required resulting in a higher compression work and lower TIT. Nevertheless, they concluded that system load following capability was higher than that of conventional power plants. Moreover, they mentioned similar results as Palsson et al. (2000) for the influence of TIT on overall efficiency.

Therefore, generally speaking, based on the aforementioned studies it can be concluded that a variable rotational speed gas turbine control strategy increases the efficiency and the range of operation of both pressurized and atmospheric hybrid SOFC-GT systems.

Zhang et al. (2006) developed a dynamic model to simulate a simple hybrid SOFC-GT cycle. Their model required to define a disturbance variable and then to evaluate the responses of the system's vital parameters to this disturbance. They chose the current density of the SOFC as disturbance and the SOFC air inlet temperature, SOFC outlet temperature, TIT, the output voltage, and the gas species molar fractions at the outlet of SOFC as system parameters. They found that the response of the SOFC outlet temperature was directly proportional to the magnitude of disturbance. But the SOFC air inlet temperature and TIT were inversely proportional to current density. They also compared the response time constant of some system parameters and pointed out that this time for temperature to reach stable condition was much greater than the time required for species molar fraction to reach stable condition. They concluded that their model was able to follow the disturbance accurately.

Zhu and Tomsovic (2002) developed a slow dynamic model of an SOFC-MGT system to analyze the load-following performance of the system. They showed that the system could

follow a total load increase of 5% of the base load with a rate of about 10 kW/s. They concluded that the system's load-following capability was suitable for application in the DG sector.

Another important issue in this type of modeling is protection of the hybrid SOFC-GT system and its components from critical incidents, such as anode oxygen exposure; excessive cell temperature gradients; and carbon deposition during severe load changes, shut-down, or start-up. The simulations that addressed these conditions might be able to provide information for the development of control strategies for operation of the systems in these situations. A few published papers investigated hybrid system behaviour in shut-down and start-up trips (Stiller et al., 2006c; Kemm et al., 2004; Lin and Hong, 2006). They concluded that the SOFC stack sensitivity to thermal stress resulted in their slow characteristics, which limited the optimal time required for start-up and shut-down (Kemm et al., 2004). The start-up time varied from 1.3 (Lin and Hong, 2006) to 5.5 hours (Stiller et al., 2006c) for different configurations and control strategies.

#### **3.4.12 Thermoeconomic studies**

Riensch et al. (1998a, 1998b) developed a model for a 200 kW SOFC-CHP plant and conducted a technical and economic sensitivity analyses on the effects of system parameters on efficiency and COE. They assumed a lifetime of 10 years (40,000 hours) for the system. They found that net COE could be reduced by nearly 50%, when external reforming was replaced by internal reforming. Also, the electrical efficiency could be increased up to 50% at a fuel utilization factor of about 95%. But for optimal COE, the fuel utilization factor should be set to 65%. They also studied the effects of different plant configurations. They found that with anode off-gas recirculation, the stack one-pass fuel utilization factor could be reduced to about 60%, while the plant's net fuel utilization factor remained fixed at 80%, which resulted in 25% reduction in the cell area. In addition, steam concentration in the system exhaust stream was lower; thus, the unrecoverable latent heat was lower and afterburner temperature was higher. Both effects resulted in higher total system efficiency.

Fontell et al. (2004) performed a conceptual study of a 250 kW planar SOFC plant for CHP application. They set some performance targets for their design. They were able to meet some of

these targets. For instance, their design exceeded the aimed electrical and total efficiencies (LHV) of 47% and 80% by achieving about 56% and 85% efficiencies, respectively. However, their system's specific mass, about 49 kg/kW, could not satisfy the desired specific mass of 15–20 kg/kW. Finally, they conducted an economic analysis assuming stack lifetime of 40,000 hours (similar to Riensche et al. (1998a, 1998b)) and system lifetime of 20 years (similar to Tanaka et al. (2000)). Also, the degradation rate (percentage decline of the cell voltage per 1000 hours) was considered 0.25%/1000h. They listed relative cost of major components based on total cost as follows: stacks: 31%, power electronics: 15%, control system: 17%, and labour and overheads: 15%.

Tanaka et al. (2000), in a previously explained paper (see Subsection 3.4.11), conducted economic analysis to investigate the effects of system parameters on CPT and EPT. Unlike Riensche et al. (1998a, 1998b), in their model, total plant life was assumed to be 20 years and fuel cells and catalyst were replaced every five years. They concluded that although the unit initial capital costs were higher than those of a large-scale conventional coal power plant, the SOFC-GT was still a competitive alternative technology.

Calise et al. (2007) added thermoeconomic evaluations to their previously explained model (Calise et al., 2006b) and used genetic algorithm (GA) for optimization purposes. The model included 19 fixed parameters and 48 synthesis and design decision variables. The system initial investment was selected as an optimization objective. The results showed that the optimized plant investment was 45% lower than that of the reference case. However, the system suffered an efficiency loss, from 67.9% to 67.5%. Some system parameters, such as turbomachinery designs as well as SOFC geometric parameters, were remarkably adjusted by the optimization process. For instance, the number, diameter, and length of the tubes in the cell stacks were decreased, resulting in a dramatic reduction of the cell's active area.

### **3.4.13 Combination of modeling and experimental work**

Lai, Hsiao, Lee, Chyou, and Tsai (2007) introduced a new method to evaluate the performance of the hybrid SOFC and GT cycle under various operational conditions without using an actual SOFC. They stated that the cost of SOFC experimental equipment was still too high for

university researchers. Therefore, the authors designed an SOFC-GT system by replacing the SOFC by a traditional furnace to simulate fuel cell off-gas conditions. Also, in order to simulate a real hybrid SOFC-GT plant, their system was equipped with another burner (to allow additional hydrogen injection for complete combustion of spent gas from the SOFC), a turbocharger, and a water injection system. Their system proved that such a system could simulate real SOFC-GT behaviours with reasonable approximation. They found that, for example, no particular device was required to combust residual fuel for high temperature SOFCs. But for mid and low temperature SOFCs, some devices were required to provide better mixing and to maintain the flame.

With similar approach, Tucker, Lawson, and Gemmen (2005) used the Hybrid Performance (Hyper) hardware simulation facility at the National Energy Technology Laboratory (NETL), U.S. Department of Energy to evaluate the possibility of using air flow as the process control variable in the hybrid SOFC-GT system. The Hyper facility was able to simulate the SOFC-GT system with an electricity generation capacity of 300 kW to 900 kW by its hardware and software simulator. The hardware portion consisted of a natural gas burner, a modified GT, an off-gas recuperator, several tanks representing the volumes and flow impedances of real components, and required piping. The purpose of a real time fuel cell simulator was to control the burner to resemble the thermal output and temperature of the SOFC. Their objective was to test the feasibility of using compressor bleed air and cold air by-pass as system control variables through air flow management.

### **3.5 Conclusion**

In order to have a clear idea about the current status of hybrid SOFC system modeling in the open literature, the summarized characteristics of some selected models are presented in Table 25. In this table, characteristics, such as the purpose of the studies (parametric, configuration, partial load, and economic analysis, as well as optimization), the system or cycle which combined with SOFC to form the hybrid cycle, fuel type, fuel cell type (tubular or planar, fuel and air flow direction, temperature level), reformer type (taking into account anode off-gas recirculation), plant capacity, number of geometrical axes through which the flow parameters vary, time dependency of the model, simulation software, and model validation are considered.

Some keys about this table should be mentioned. First of all, when several papers used the same model for different analyses, they are considered as one entry. When none of the boxes is marked, it means that there was no information about that specific parameter in the paper(s). For anode recirculation, Y/N means both cycles (with and without anode recirculation) were investigated. But for validation of the model with experiments, Y/N means the model was partially validated. Most likely this indicates that the SOFC model was validated but the whole cycle was not. Also, the feasibility studies and conceptual design papers were considered as configuration analysis.

This table shows that many models concentrate on studying the effect of various parameters on system performance as well as examining and comparing different configurations. Also, the majority of the models have been on internal reforming SOFC-GT systems fuelled by methane or natural gas with a vast range of plant capacity from a few hundred kilowatts to multi-hundred megawatts. In terms of the SOFC stack, the majority of the models were based on the high temperature tubular SOFC both with and without anode recirculation. It is possible to find 1-D and 2-D modeling approaches in the literature. However, it should be noted that even though authors called their model 1-D or 2-D, some components, such as gas turbine or heat exchangers, might be modeled as 0-D. Many models were steady-state, and they were not fully validated against experimental data. A few of them were partially validated by validating the SOFC part. And finally, many modelers used Aspen Plus<sup>®</sup> as the simulation software.

Some key findings of this review work to identify areas that require further studies may be summarized as follows:

1. Most of the studies used well established tubular type SOFCs. However, recently, the planar type has proved to have more potential for cost reduction. Therefore, future studies should be focused on this type of SOFC, especially the low temperature (LT-SOFC) type.
2. The 0-D modeling approach for hybrid system simulation has been well developed. But further investigation is required to assess the influence of this approach. In other words, the question of how realistic it is to assume the SOFC as a box should be investigated. In order to do this, an extensive study to compare 0-D and a higher dimensional approach for the same system is required.

3. As Table 25 shows, most of the models were not validated. More demonstration sites and experimental studies are crucial in this respect so that researchers will be able to validate their model according to the results of these experimental works.
4. As mentioned, most models emphasized parametric and configuration analyses. The next logical step is to use different optimization methods to optimize the hybrid system with the objective of improving system efficiency and lowering cost.
5. Although numerous configurations have been proposed for hybrid systems in the literature, a well established and accepted configuration is still lacking. Existing proposed configurations should be compared with similar specifications and assumptions so that selection of the best configuration for different conditions and applications can be achieved.
6. Dynamic models are extremely important to study system performance and establish suitable control strategies in transient conditions, such as start up, shut down, and severe load changes. Thus, further investigations are required in this area.
7. More studies are needed on the indirect internal reformer to evaluate its effect on system overall performance.
8. A hybrid SOFC with an integrated gasification combined cycle is considered as the ultimate SOFC-based power generation cycle, and its different aspects should be studied in detail.
9. Effects of fuel composition variation on system design and operation of the existing systems should be investigated.

This review shows that in spite of tremendous improvements in the modeling of hybrid SOFC systems, there are areas that need further studies. They include planar SOFCs, transient and off-design conditions, and coal- and biogas-fed hybrid cycle modeling, and model validation. In this thesis, notes number 5 and 9 (above) will be addressed. In addition, although notes 1, 2, 4, 6, and 8 are not within the scope of this work, they are considered as future work of this thesis.



**Table 25: Summarized characteristics of some selected models in the open literature**

			1	2	3	4	5	6	7	8	9	10	11	12	13	14	15	16	17	18	19	20	21	22	23	24	25	26	27	28	29	30	31	32	33	34	35	36	37	38	39	
Purpose of paper	Parameter analysis			×	×	×	×	×	×	(Ex)	×		×	(Ex)	×	×	×		×				×			×	(Ex)			×		×	×		×							
	Configuration analysis			×	×						×	×	×	×	×	×		×	(Ex)			×	×	×	×	×	×	×	×	×												
	Partial load		×							×			×							×												×	×	×	×	×	×	×	×	×		
	Optimization									×											×																			×		
	Economical analysis									×								×	×	×				×																×	×	
Hybrid cycle	GT	HR	×	×	×	×	×	×	×	×	×	×	×	×	×	×	×	×	×	×	×	×	×	×	×	×		×			×	×	×	×	×	×	×	×	×			
		SHR			×	×		×	×		×		×		×			×					×			×						×	×		×		×					
	Steam turbine											×											×			×					×				×				×			
	CHP						×	×				×								×							×		×	×				×					×	×		
	IG																									×	×	×												×	×	
CO <sub>2</sub> capture																				×	×	×		×	×																	
Fuel type	Hydrogen										×				×																						×					
	Methane/ NG		×	×	×	×	×	×	×	×	×	×	×	×		×	×	×	×	×	×	×	×	×	×					×	×		×	×	×	×	×		×	×	×	×
	Coal																									×	×	×														
	Biogas/others																										×	×			×											
FC type	Tubular			×	M	×		×	×	×		I	×	×		×	×	×	×		×	×	×		×	M							×	×	×		×	I				
	Planar	E					×			×	×									×															×			×	×			
		A	×																										×	×		×								×		
		C																																								
FC type (temperature)	LT-SOFC		×																																						×	
	IT-SOFC											×				×														×	×		×									
	HT-SOFC			×	×	×	×	×	×	×	×		×	×	×	×	×	×	×	×	×	×	×	×	×	×	×	×	×				×	×	×	×	×	×	×	×		
Flow configuration	Co-flow		×	×		×		×	×	×			×	×		×	×	×	×	×	×	×	×	×	×	×								×	×	×	×		×	×		
	Counter-flow																													×										×		
	Cross-flow				×		×			×	×	×								×							×										×		×			
Reforming type	Internal		×	×	×	×		×	×	×	×	×	×	×	×	×	×	×	×		×	×	×	×	×	×	×	×	×		×		×	×	×	×	×	×	×	×	×	
	External				×		×													×		×	×						×	×		×							×			
Anode recirculation			N	Y	N	Y/N	Y	N	Y/N	N	N	Y	Y/N	Y		Y	Y	N	Y	N	Y			Y		N	Y/N	N	Y/N		N	Y	Y	N	N		Y	N	Y/N	Y		
Plant Capacity (MW)			0.25	0.22	100		0.5	1.3	1.5		0.3	2				20		11	15	1.5	640	70		50			0.0015	0.44	0.3		1.3		19	0.55	0.25	0.2	0.25					
Model Dimension	0-D					×		×	×						×							×	×		×		×	×	×			×	×		×				×			
	>0-D			×			×				×	×	×						×	×							×						×		×							
Dependency to time	Steady-state		×	×	×	×	×	×	×	×	×	×	×	×	×	×	×	×	×	×	×	×	×	×	×	×	×	×	×	×	×	×	×	×	×	×	×	×	×	×		
	Transient		×									×																						×		×	×	×				
Validation with experiments			N	N	N	Y/N	N	N	N	Y/N	N	Y/N	N	Y/N	N	N	N	N	N	Y/N	N	N	N	N	Y	N	N	N	Y	N	N	N	N	N	N	N	N	N	N	N	N	
Simulation software			M		AP	AP	AP	M	M	PR	AP				AP					IP	PR	T	T		AP	AP	AP	AP	V			AP	M	g	M	ACM			M	PR	AP	

Abbreviation:

GT+HR: Gas turbine + Heat recuperation  
GT+HSR: Gas turbine + Heat recuperation  
+ Steam recuperation  
Ex: Exergy analysis  
NG: Natural gas  
E: Electrolyte supported SOFC  
A: Anode supported SOFC  
C: Cathode supported SOFC  
M: Monolithic SOFC (MSOFC)  
I: Integrated planar SOFC (IP-SOFC)  
AP: Aspen Plus<sup>®</sup>  
M: MATLAB/Simulink<sup>®</sup>  
PR: PRO/II  
IP: IPSEpro<sup>™</sup>  
T: Thermo Economic Modular Program  
(TEMP)  
V: VALI<sup>™</sup>  
g: gPROMS  
ACM: Aspen Custom Modeler<sup>®</sup>

Selected papers:

1. Roberts et al. (2006) and Mueller et al. (2007)
2. Song et al. (2005)
3. Harvey and Richter (1994a, 1994b)
4. Suther et al. (2010a, 2010b) and Zabihian et al. (2008)
5. Palsson et al. (2000)
6. Chan et al. (2002a, 2003a)
7. Calise et al. (2006a, 2006b, 2007)
8. Stiller et al. (2005)
9. Selimovic and Palsson (2002)
10. Magistri et al. (2005)
11. Granovskii et al. (2007a, 2007b, 2008)
12. Pangalis et al. (2002) and Cunnell et al. (2002)
13. Kuchonthara et al. (2003a, 2003b)
14. Tanaka et al (2000)
15. Lundberg et al. (2003)
16. Rao and Samuelsen (2003)
17. Song et al. (2006)
18. Möller et al. (2004)

19. Riensche et al. (2000)
20. Franzoni et al. (2008)
21. Massardo and Lubelli (2000)
22. Inui et al. (2003)
23. Campanari and Chiesa (2002)
24. Lobachyov and Richter (1996)
25. Kivisaari et al. (2004)
26. Kuchonthara et al. (2005)
27. Van herle et al. (2003)
28. Braun et al. (2006)
29. Winkler and Lorenz (2002)
30. Steffen et al. (2005) and Freeh et al. (2005)
31. Costamagna et al. (2001)
32. Stiller et al. (2006a, 2006b, 2006c)
33. Chan et al. (2003b)
34. Zhang et al. (2006)
35. Zhu and Tomsovic (2002)
36. Kemm et al. (2004)
37. Lin and Hong (2006)
38. Riensche et al. (1998a, 1998b)
39. Fontell et al. (2004)

## **CHAPTER FOUR**

### **SOFC Model Development**

As already explained, simulation is a vital tool for fuel cell development (see Subsection 3.3). The system simulation models that can accurately predict steady-state and transient operation of systems and can address optimization, heat management, fluctuating power demands, and techno-economic evaluation of systems can be valuable assistance for the successful integration of the systems. This section presents the steps undertaken to develop a mathematical model and computerized simulation of a solid oxide fuel cell model, including assumptions, mathematical formulations, determination of constants and system parameters, and model validation. Then, the integration of the developed SOFC model to a gas turbine as a bottoming cycle is presented.

#### **4.1 Modeling approach**

As noted in Subsections 3.3.1 and 3.4.1, it is very important to determine the modeling approach and the model characteristics and features based on the application of the model, before developing an actual model. This subsection outlines the approach used in this work to develop a model of an SOFC-GT cycle based on the information provided in Subsection 3.4.1.

The modeling approach in this work was theoretical and mechanistic (and not semi-empirical) because the model was developed based on the electrochemical, thermodynamic, and chemical equations (and not experimental data). In the SOFC theoretical modeling, depending on the model objective and application, the three-dimensional and time-dependent operation of the system can be simulated as 3-D, 2-D, 1-D, or 0-D models and the steady-state model by proper assumptions and simplifications. Models with a higher number of geometrical axes are more suitable for investigating the internal operation and complex behaviour of the SOFC and the

effects of the material of the components and their microscopic properties on the system operation. Examples of this approach in the literature are: Yakabe et al. (2001), Achenbach (1994) (3-D models); Palsson et al. (2000), Möller et al. (2004), Stiller et al. (2005) (2-D models); Song et al. (2005) (quasi-2-D models); and Calise, Dentice d'Accadia, Palombo, and Vanoli (2008), Pfafferodt, Heidebrecht, Stelter, and Sundmacher (2005), Magistri et al. (2005) (1-D models). On the other hand, if the modeling objective is to investigate the SOFC operation as a part of a hybrid system and how it interacts with other equipment in the overall system, a 0-D model can be sufficient (Costamagna et al., 2001). It has been reported that the gradients of properties (both thermodynamic and electrochemical properties) are commonly not significant in the SOFC stack (Calise et al., 2006a), which means, at least for some applications, these gradients can be neglected for the sake of simplicity. As shown in Tables 24 and 25, this approach is very popular and many researchers employed this approach for modeling hybrid SOFC cycles (such as Calise et al. (2006a), Chan et al. (2002a, 2003a), Kuchonthara et al. (2003a, 2003b), Franzoni et al. (2008), Massardo and Lubelli (2000), Campanari and Chiesa (2002), Van herle et al. (2003), Costamagna et al. (2001), Riensche et al. (1998a), Freeh et al. (2004)), which shows the suitability of the approach for some applications. In this approach, the mathematical equations are used to transform available input parameters to the desired outputs. Since the system boundary for this work was the entire power plant, the electrochemical and thermodynamic laws were employed to develop the required zero-dimensional model. Further discussions on the modeling approach in terms of the number of geometrical axes can be found in Subsections 3.3.1, 3.4.1, and 3.4.4.

The SOFC in this work was tubular, co-flow, high temperature, and with internal reforming. Both cycles with and without anode recirculation were considered. Also, fuel composition was not fixed. In fact, how it affected cycle performance was one of the objectives of this modeling. Figure 18 shows the control volume of the SOFC system model which will be used for the first law thermodynamics analysis in this work.

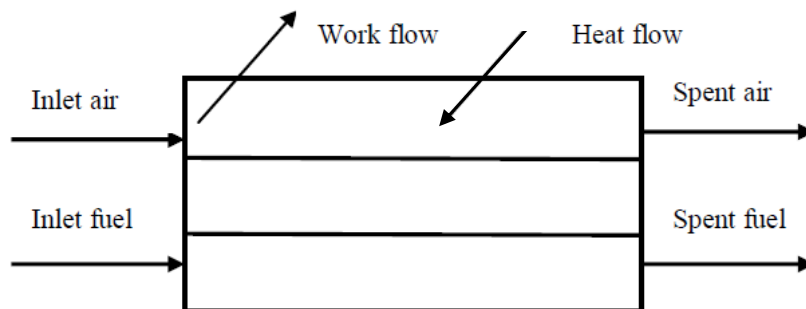


Figure 18: Control volume of SOFC system model

## 4.2 Modeling software

In this research, steady-state thermodynamic models of the SOFC-based cycles were developed using commercial process simulation software, Aspen Plus<sup>®</sup>. Aspen Plus<sup>®</sup> is a process simulation tool that can be utilized to develop a realistic steady-state model of thermodynamic cycles, and as Table 25 shows, has been commonly used in the modeling of hybrid SOFC cycles (such as Harvey and Richter (1994a), Palsson et al. (2000), Kuchonthara et al. (2003a), Lobachyov and Richter (1996), Kivisaari et al. (2004), Van herle et al. (2003), Fontell et al. (2004)). In this software, to develop a model, built-in thermodynamic models, such as compressor, gas turbine, fuel reformer, combustor, material stream mixer and splitter, heat exchanger, and user-defined models can be connected with material, work, and heat streams to form a model of an actual system. The user-defined models can be developed in Fortran, Aspen Custom Modeler<sup>®</sup>, or Microsoft Excel. The thermodynamic and physical properties required for the flow sheet calculations can be estimated by choosing one of the various existing physical property models in the software. One of the inherent characteristics of Aspen Plus<sup>®</sup> is its sequential modular approach to modeling. That means each component, either built-in or user-defined, is treated independently and calculation results for each block are considered the input for the next block (Bove and Ubertini, 2006).

The developed models consisted of two main parts: the cycle model with various built-in equipment and the SOFC model. As mentioned, there is no built-in SOFC model available in this software; therefore, first the SOFC stack model was developed using fundamental equations of thermodynamics, chemical reactions, and electrochemistry in Fortran as the user-defined model

in Aspen Plus<sup>®</sup>. Most model constants were determined by using the available data from Siemens Westinghouse SOFC systems as well as considering the variations in the open literature. All other necessary system equipment, such as fuel reformer, compressor, combustor, heat exchanger, mixing chamber, pump, etc. were modeled by available built-in models in Aspen Plus<sup>®</sup>. These individual unit operations were connected with material and energy streams (work and heat) to form the hybrid SOFC system model.

### **4.3 SOFC model**

The first step towards developing the hybrid system models is to have a modular fuel cell model that can predict the performance characteristics of an SOFC with reasonable accuracy under varying operating and design conditions. In the following subsections, the model is outlined, including the assumptions and simplifications, mathematical formulation, along with a sensitivity analysis of the input parameters, and the model validation with experimental results.

#### **4.3.1 Assumptions**

The general considerations and the assumptions in the model were (the references in parentheses are examples of the modeling works in the literature that used similar assumptions):

- The developed model was steady-state and 0-dimensional.
- The model simulated a high temperature tubular co-flow SOFC system.
- Chemical components behaved as ideal gases at the operating temperature and pressure of the SOFC (Jiang, Fang, Dougal, and Khan, 2008; Sucipta, Kimijima, and Suzuki, 2008a).
- Every cell within the SOFC stack operated at uniform temperature and pressure (Kuchonthara et al., 2003a; Costamagna et al., 2001).
- The operating voltage is equal for all cells and is uniform over each cell (Sucipta et al., 2007; Petruzzi et al., 2003; Palsson et al., 2000).

- The distribution of inlet gases among the tubes was uniform (Jiang et al., 2008; Palsson et al., 2000).
- No pressure losses occurred within the SOFC. This is a common assumption for macro-level thermodynamic models, such as Cunnell et al. (2002), Palsson et al., (2000), Calise et al. (2006b).
- Heat losses from the SOFC were negligible (adiabatic external walls). This assumption is also very common in the SOFC modeling, such as Jiang et al. (2008), Calise et al. (2006b), Magistri et al. (2005), Stiller et al. (2005).
- Both methane reforming and water-gas shift reactions were assumed to be at chemical equilibrium (Calise et al., 2006 a; Achenbach, 1994; Palsson et al., 2000; Campanari, 2001; Massardo and Lubelli, 2000; Chan et al., 2002a; Sucipta et al., 2007; Costamagna et al., 2001).
- The inlet fuel to the SOFC was a mixture of gases at ambient temperature and pressure, which consisted of any combination of  $\text{CH}_4$ ,  $\text{H}_2$ ,  $\text{H}_2\text{O}$ ,  $\text{CO}$ ,  $\text{CO}_2$ ,  $\text{O}_2$ , and  $\text{N}_2$ . This assumption implied that the inlet fuel was sulfur free and no desulfurization equipment was required.
- The air supplied to the fuel cell consisted of 21%  $\text{O}_2$  and 79%  $\text{N}_2$ , neglecting its argon, water, and carbon dioxide content.
- There was no gas leakage to the outside of the system (Jiang et al., 2008).
- The kinetic and gravitational terms in the balance equations were negligible (Calise et al., 2006b; Cunnell et al., 2002).

#### **4.3.2 Mathematical formulations of SOFC**

In this subsection, the macro-level model of SOFC developed for this work using fundamental equations of thermodynamics, chemical reactions, and electrochemistry is explained. The SOFC model was written in FORTRAN 77, and executed from within Aspen Plus<sup>®</sup>.

#### 4.3.2.1 SOFC outlet composition

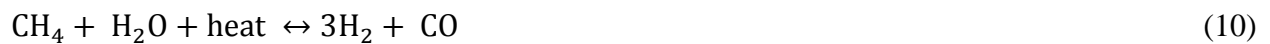
The first step in the SOFC modeling was to find exhaust stream composition. The objective was to find a relationship between the system inlet and outlet stream composition. This required investigating the chemical and electrochemical reactions in the SOFC. The following subsections describe how the fuel reforming processes and electrochemical reactions were modeled in this work.

##### 4.3.2.1.1 Fuel reforming

As noted in Subsection 3.2.4.1, three fuel conversion technologies, namely, steam reforming, partial oxidation, and autothermal reforming are commercially available. Steam reforming is the most common technology to convert conventional fuels to a hydrogen-rich stream suitable for the SOFC operation. Therefore, the steam reforming process was considered for the fuel reforming within the cells and pre-reformer.

Few studies can be found in the literature related to the kinetics of steam reforming of methane in the SOFC. Even worse, there is little agreement among these published data. This could be partially as a result of difficulty in conducting experimental studies due to limitations in the measuring and recording parameters in the SOFC. Also, the availability of data for commercial methane reforming plants can be another reason for this shortage of data for the reforming process in the SOFC. But the problem with these available data for commercial reformers is that the operational conditions of the commercial methane reforming plants have little similarity to the SOFC steam reformers (Dicks et al., 2000).

In this work, it was assumed that the fuel cell was fuelled with a pre-reformed gas stream consisting of a user-defined combination of CH<sub>4</sub>, H<sub>2</sub>, H<sub>2</sub>O, CO, CO<sub>2</sub>, O<sub>2</sub>, and N<sub>2</sub>. As noted earlier, due to the high operating temperature of the SOFC, methane in the inlet fuel can be internally reformed within the cells. This process involves the methane steam reforming, where the endothermic reaction of CH<sub>4</sub> and H<sub>2</sub>O creates H<sub>2</sub> and CO.



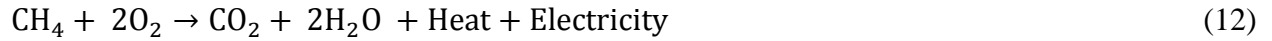
Furthermore, CO created in the methane steam reforming and existing in the inlet fuel react with H<sub>2</sub>O in an exothermic water-gas shift reaction to produce CO<sub>2</sub> and H<sub>2</sub>.





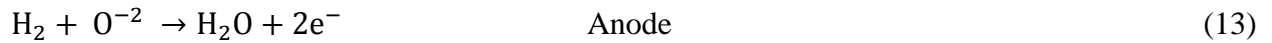
#### 4.3.2.1.2 Electrochemical reactions

The electrochemical reactions are where the desired product of the system, electricity, is generated. Theoretically, every fluid that can be chemically oxidized can be used as a fuel in a fuel cell (Appleby and Foulkes, 1989). Thus, theoretically, methane can be electrochemically oxidized in the following reaction:

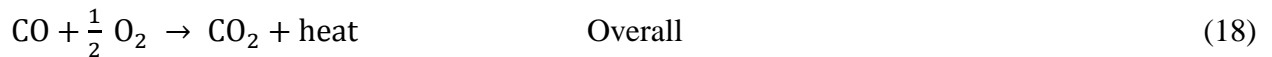
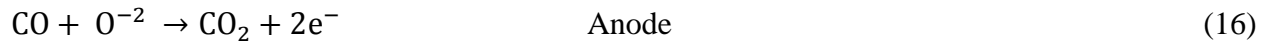


The entropy loss in the electrochemical reaction of methane is very small, which results in extremely high thermodynamic efficiency (Achenbach and Riensche, 1994). Due to this reason, the direct participation of methane in the electrochemical reactions in the SOFC is not possible in the current SOFC technology, and, in fact, is a great challenge (Peters et al., 2000; Achenbach and Riensche, 1994; Kakac et al., 2007). However, in current SOFCs both hydrogen and carbon monoxide can participate in the following electrochemical reactions (Yakabe et al., 2001; Petruzzi et al., 2003):

Hydrogen:



Carbon monoxide:



The electrochemical oxidation takes place at the anode side, and the required oxygen ions are released by the reduction reaction of oxygen taking place at the cathode side of the SOFC.

Although these net reactions are well understood, there may be some intermediate reactions that are not known yet (Noren and Hoffman, 2005). Equations 10, 11, and 15 show that  $H_2O$  as the product of hydrogen electrochemical oxidation is, in fact, a reactant for both steam reforming and water-gas shift reactions and will shift their equilibrium.

For modeling of the SOFC, two approaches have been established in the literature. In the first approach only hydrogen is electrochemically oxidized, and carbon monoxide just participates in the water-gas shift reaction. But in the second approach, the electrochemical reactions of both hydrogen and carbon monoxide are taken into account. Some models in the literature deployed the first approach (such as Palsson et al., 2000; Calise et al., 2006a; Omosun, Bauen, Brandon, Adjiman, and Hart, 2004; Campanari, 2001; Massardo and Lubelli, 2000; Chan et al., 2002a; Kuchonthara et al., 2003a; Costamagna et al., 2001; Freeh et al., 2004), some the second approach (such as Yakabe et al., 2001; Achenbach, 1994; Sucipta et al., 2007), and some both (Petruzzi et al., 2003).

Haberman and Young (2006) showed that the rate of consumption of CO in the water-gas shift reaction is higher than its consumption in the electrochemical reaction. Also, Matsuzaki and Yasuda (2000) reported that the rate of electrochemical reaction of hydrogen is about two times greater than that of carbon monoxide. They experimentally showed that the rate of electrochemical oxidation of  $H_2$  was between 1.9 and 3.1 times higher than that of CO, depending on the operating temperature. For an operating temperature of  $1000^{\circ}C$ , this ratio was between 2.3 and 3.1 and for  $800^{\circ}C$  between 1.9 and 2.3. They concluded that the rate of the water-gas shift reaction was much faster than the CO direct oxidation rate. The mechanism of the CO electrochemical oxidation is not clear yet and to determine the validity of these two approaches, more experimental investigations of carbon monoxide reactions should be carried out, and this is an open field of research. However, since the preferred path of oxidation for carbon monoxide in the presence of steam is the water-gas shift reaction (Petruzzi et al., 2003), in this work, the first approach was employed, which means the electrochemical reactions expressed in Equations 13-15 were considered.

The methane reforming reaction is highly endothermic, and the carbon monoxide water-gas shift reaction is exothermic. The combination of both reactions (as takes place in the SOFC) is endothermic (Fuel Cell Handbook, 2004), and the required heat should be supplied to the system.

In early modeling works, this heat was supplied by the hot gas turbine exhaust streams (Harvey and Richter, 1994a). But in recent models, this heat is usually provided by the heat released in the significantly exothermic electrochemical reactions within the SOFC (Calise et al., 2006a). It has been shown that the heat generated in the electrochemical reactions is greater than the heat required for the steam reforming reaction, and excess heat should be removed from the fuel cell by exhaust streams. Ahmed and Forger (2000) reported that, under typical operating conditions, the rate of heat generation in the electrochemical reactions was about twice that of the thermal energy consumption in the steam reforming reaction.

#### 4.3.2.1.3 Mathematical formulation to determine SOFC exhaust composition

The outlet composition of the fuel and air streams depends on the amount of fuel consumed in the SOFC. As noted earlier, the fuel cannot be completely consumed in the fuel cell. In order to take into account this phenomenon, a parameter called the fuel utilization factor is defined as the amount of hydrogen spent within the fuel cell divided by the amount of available hydrogen:

$$U_f = \frac{[H_{2,react}]}{[H_{2,available}]} \quad (19)$$

where the brackets refer to the concentration of each species per molar flow rate of the anode stream. The fuel utilization factor is a user-defined constant in the present model and was set to 85%. The range of fuel utilization factor used in the literature is between 80% (Riensch et al., 1998a; Calise et al., 2006a; Cunnell et al., 2002) and 85% (Harvey and Richter, 1994b; Calise et al., 2007; Möller et al., 2004; Stiller et al., 2005; Chan et al., 2003b; Riensch et al., 2000; Lobachyov and Richter, 1996; Sucipta et al., 2007). The available hydrogen consists of the inlet hydrogen and the hydrogen generated in the methane reforming and water-gas shift reactions. Equations 10 and 11 indicate that for every mole of  $CH_4$  reacting in the methane reforming reaction, three moles of  $H_2$  are generated, and for every mole of  $CO$  reacting in the water-gas shift reaction, one mole of  $H_2$  is generated. Therefore, Equation 19 can be rewritten as Equation 20:

$$U_f = \frac{[H_{2,react}]}{([H_{2,in}] + 3[CH_{4,react}] + [CO_{react}])} \quad (20)$$

where the subscript “in” represents the concentration of species at the anode inlet stream, and the subscript “react” refers to the moles reacting within the fuel channels. The fuel utilization factor is specified by the user and indicates the amount of  $H_2$  reacting within the SOFC, and thus the extent of the electrochemical reaction. The amount of hydrogen reacting within the SOFC stack can be obtained by rearranging Equation 20:

$$[H_{2,react}] = ([H_{2,in}] + 3[CH_{4,react}] + [CO_{react}])U_f \quad (21)$$

In Equation 21, in order to determine the reacting hydrogen in the SOFC, the reacting methane and carbon monoxide should be found. In this model, it was assumed that the  $CH_4$  reforming and water-gas shift reactions reach chemical equilibrium. These assumptions are commonly used in the SOFC modeling (for example Calise et al., 2006 a; Achenbach, 1994; Palsson et al., 2000; Campanari, 2001; Massardo and Lubelli, 2000; Chan et al., 2002a; Sucipta et al., 2007; Costamagna et al., 2001; Freeh et al., 2004). Some references reported that the rate of the steam reforming reaction is low; however, in the presence of a catalyst the reaction rate is sufficient to provide enough hydrogen for the electrochemical reaction, and the assumption of the chemical equilibrium of the reaction is valid (Fuel Cell Handbook, 2004). Achenbach and Riensche (1994) reported that the methane reforming conversion rate predicted for the reaction at  $1000^\circ C$  and for a  $CH_4$  partial pressure of 0.17 bar is 81 folds greater than the molar flux necessary to sustain a current density of  $3000 \text{ A/m}^2$  in the SOFC. This ratio at  $900^\circ C$  and  $700^\circ C$  is 42 and 7.4, respectively (Achenbach and Riensche, 1994). This fast reaction rate should be considered in the SOFC design because it can cause a local subcooling, which may in turn cause an internal thermal stress, in the order of tens of MPa (Yakabe et al., 2001) and mechanical failure of the stack (Ackmann, De Haart, Lehnert, and Thom, 2000).

Similarly, the rate of the water-gas shift reaction is high, and most studies in the open literature assumed that this reaction was in chemical equilibrium. However, some studies contradicted this assumption (such as Young, 2007; Calise et al., 2008; Bustamante et al., 2004; Graven and Long, 1954). For instance, Bustamante et al. (2004) stated that thermodynamic equilibrium of the water-gas shift reaction favours low temperatures because of the exothermic nature of the reaction (also Kikuchi and Eguchi, 2004; Fuel Cell Handbook, 2004). At high temperatures, as in the case of the SOFC, the rate of this reaction may be too low to reach chemical equilibrium (Young, 2007). Also, Kikuchi and Eguchi (2004) stated that in their experimental work,

depending on the catalyst material, the shift reaction reached equilibrium at a temperature between 250°C and 600°C. On the other hand, Ahmed and Forger (2000) reported that due to the consumption of hydrogen in the electrochemical reaction within the cells, the reactions can even proceed beyond the equilibrium condition. Moreover, the high concentration of steam in the mixture helps to force the reactions to the equilibrium condition (Fuel Cell Handbook, 2004).

By using these assumptions, the equilibrium constant of the water-gas shift reaction can be used to find the concentration of reacting CO. For the general case of a reaction of gaseous reactants in the equilibrium condition, namely Equation 22, the equilibrium constant is defined as Equation 23 (Campanari, 2001; Massardo and Lubelli, 2000; Chan et al., 2002a):



$$K = \frac{[C]^c \times [D]^d}{[A]^a \times [B]^b} \quad (23)$$

where a, b, c, and d represent the stoichiometric coefficients of the reactants and products. The water-gas shift reaction's equilibrium constant can be written based on the reaction presented in Equation 11:

$$K_{CO} = \frac{[H_{2,out}] \times [CO_{2,out}]}{[CO_{in}] \times [H_2O_{in}]} \quad (24)$$

where  $K_{CO}$  refers to the equilibrium constant of the water-gas shift reaction at the given temperature. It has been shown that the equilibrium constant depends on the reaction temperature (Ahmed and Foger, 2000; Achenbach, 1994; Calise et al., 2006a; Dicks et al., 2000; Massardo and Lubelli, 2000; Chan et al., 2002a), in this case the SOFC operating temperature. Calise et al. (2006a) proposed the following equation for the equilibrium constant of the reaction:

$$K_{CO} = e^{(4594/T - 4.35)} \quad (25)$$

Several other more complicated correlations for the equilibrium constant of the water-gas shift reaction have been proposed in the literature, such as Dicks et al. (2000), Ahmed and Foger (2000), Achenbach (1994), Ackmann et al. (2000), Massardo and Lubelli (2000), and Chan et al. (2002a). For this work, the following approximation was derived by running a parametric study varying the temperature in a chemical reactor model in Aspen Plus<sup>®</sup> (Suther et al., 2010a).

$$K_{CO} = 8 \times 10^{11} \times T^{-3.9017} \quad (26)$$

where T is temperature (K) at which the reaction takes place. By substituting Equation 26 into Equation 24, Equation 27 can be obtained.

$$8 \times 10^{11} \times T^{-3.9017} = \frac{[H_{2,out}] \times [CO_{2,out}]}{[CO_{in}] \times [H_2O_{in}]} \quad (27)$$

In Equation 27, the outlet concentration of H<sub>2</sub> and CO<sub>2</sub> can be expressed as a function of the concentration of inlet streams and reactant species. The reactant species include spent and created components. For instance, in the case of carbon dioxide, for one mole of carbon monoxide, one mole of CO<sub>2</sub> is produced.

$$[H_{2,out}] = [H_{2,in}] - [H_{2,react}] + 3[CH_{4,react}] + [CO_{react}] \quad (28)$$

$$[CO_{2,out}] = [CO_{2,in}] + [CO_{react}] \quad (29)$$

Equations 21, 27, 28, and 29 are a system of non-linear equations, with four equations and five unknowns. In these equations, all terms with subscript “in”,  $U_f$ , and T are knowns, and terms with subscript “out” and “react” are unknowns. In order to solve this system of non-linear equations, one more equation was required. This extra equation could be obtained by assuming that the methane reforming reaction continues until all the inlet methane moles were consumed. This assumption was used in other works, such as Van herle et al. (2004), Calise et al. (2006a), and Tanaka et al. (2000). In other words, for the purpose of this model, it could be assumed that the equilibrium state of the CH<sub>4</sub> reforming reaction was reached when all the CH<sub>4</sub> entering the anode reacted in the reforming reaction, and the reaction was driven to completion. Kikuchi and Eguchi (2004), based on their experiments, reported that in the steam reforming reaction, the equilibrium methane conversion reached 100% at temperatures higher than 750°C. Also, the availability of steam due to the high steam-to-carbon ratio (higher than 2), as will be shown in Subsection 4.4.1, can help to force the reaction to completion (Fuel Cell Handbook, 2004). The following two equations (Equations 30 and 31) equally represent this assumption.

$$[CH_{4,in}] = [CH_{4,react}] \quad (30)$$

$$[CH_{4,out}] = 0 \quad (31)$$

This assumption was very close to what happened in reality because the consumption of hydrogen in the electrochemical reaction can force the methane reforming reaction to completion (Ahmed and Forger, 2000). Even those works that did not consider this assumption found that

the concentration of methane in the outlet stream was very low (less than 1%) (Calise et al., 2006a; Larminie and Dicks, 2003; Chan et al., 2003a).

At this step, there is a system of five non-linear equations and five unknowns. By substituting  $[H_{2,out}]$  from Equation 28,  $[CO_{2,out}]$  from Equation 29,  $[H_{2,react}]$  from Equation 21, and  $[CH_{4,react}]$  from Equation 30 into Equation 27, the system of equations can be reduced to a second order equation with the amount of CO reacting within the fuel cell stack as the only unknown. Solving this equation,  $[CO_{react}]$  could be calculated. Then,  $[H_{2,react}]$  could be estimated using Equation 21. However, the electrochemical reaction requires oxygen in the cathode as well as hydrogen in the anode. In this step, the model ran a check to verify if there was enough oxygen in the catholyte stream to complete the electrochemical reaction of hydrogen. In order to perform this check, first the number of moles of  $O_2$  required to complete the electrochemical reaction of hydrogen was estimated:

$$\dot{n}_{O_2,required} = \frac{[H_{2,react}] \times \dot{n}_{anolyte}}{2} \quad (32)$$

where  $\dot{n}_{anolyte}$  is the total number of moles in the anolyte stream. It should be noted that for every two hydrogen moles, one mole of oxygen is required in the hydrogen electrochemical oxidation. If the number of oxygen moles in the catholyte stream is lower than  $\dot{n}_{O_2,required}$ , the concentration of hydrogen that can react with existing oxygen can be calculated by the following equation:

$$[H_{2,react}] = \frac{2 \dot{n}_{O_2,available}}{\dot{n}_{anolyte}} \quad (33)$$

where  $\dot{n}_{O_2,available}$  is the number of existing oxygen moles in the catholyte stream. With this new value for the concentration of reacting hydrogen, the new concentration of reacting CO can be estimated by Equation 21. Having the inlet concentration of all components and calculating the amount of  $H_2$ ,  $CH_4$ , and CO reacting within the fuel cell, the outlet concentration of species in the anode and cathode streams can be estimated based on the equations in Table 26. Also, the current generated by the SOFC stack for each mole of reacting hydrogen can be calculated by Equation 34 (Calise et al., 2006b).

$$I = 2 \dot{n}_{H_{2,react}} F = 2 [H_{2,react}] \dot{n}_{anolyte} F \quad (34)$$

where  $F$  is Faraday's constant ( $96,485 \times 10^3$  C/kmole).

**Table 26: Composition of the SOFC outlet streams**

Parameter	Value in anode stream	Value in cathode stream
$[H_2O_{out}]$	$[H_2O_{in}] + [H_{2,react}] - [CO_{react}] - [CH_{4,react}]$	$[H_2O_{in}]$
$[CO_{out}]$	$[CO_{in}] + [CH_{4,react}] - [CO_{react}]$	$[CO_{in}]$
$[CO_{2,out}]$	$[CO_{2,in}] + [CO_{react}]$	$[CO_{2,in}]$
$[CH_{4,out}]$	$[CH_{4,in}] - [CH_{4,react}] = 0$	-
$[H_{2,out}]$	$[H_{2,in}] - [H_{2,react}] + [CO_{react}] + 3 [CH_{4,react}]$	-
$[N_{2,out}]$	$[N_{2,in}]$	$[N_{2,in}]$
$[O_{2,out}]$	-	$[O_{2,in}] - [H_{2,react}]/2$

It should be noted that only oxygen from catholyte stream participates in the reactions and other components in the cathode inlet are treated as inert gases by the SOFC model (Chan et al., 2002b).

#### 4.3.2.2 Estimation of SOFC output power

##### 4.3.2.2.1 Reversible open circuit potential difference

The next step was to calculate output electricity from the SOFC. As noted, in an SOFC, the chemical potential energy of the fuel is directly converted to electrical energy. There are several approaches to estimate potential energy of the fuel, such as entropy, exergy, calorific value, Helmholtz free energy, and Gibbs free energy. For each specific application, one of these approaches is more useful. In the case of fuel cells, the Gibbs free energy is the most helpful approach to evaluate and express the fuel energy. The Gibbs free energy is the system ability to do non-mechanical work. In other words, the Gibbs free energy is the available energy to do work, when the work done by changes in pressure and volume are neglected. Since in fuel cells, the energy is converted only by electrochemical reactions, and there is no power production by changes in pressure and volume, the Gibbs free energy is the most suitable parameter to express fuel chemical energy. Using this concept, the reversible voltage for the hydrogen electrochemical



reaction can be expressed in Equation 35 (Singhal and Kendall, 2003; Calise et al., 2006a; Larminie and Dicks, 2003; Noren and Hoffman, 2005). This equation is called the Nernst equation after the German chemist Walther Hermann Nernst (1864 – 1941), and since very early modeling works (such as Harvey and Richter, 1994a, 1994b) , this equation was used to estimate the reversible voltage of the SOFC.

$$E_{\text{rev}} = \frac{\Delta \bar{g}}{-2F} + \frac{R_u T}{2F} \ln \left[ \frac{P_{\text{H}_2}/P_{\text{ref}} \left[ P_{\text{O}_2}/P_{\text{ref}} \right]^{0.5}}{P_{\text{H}_2\text{O}}/P_{\text{ref}}} \right] \quad (35)$$

where  $E_{\text{rev}}$  represents the reversible voltage (V),  $\Delta \bar{g}$  is the Gibbs energy change (J/kmole) of the  $\text{H}_2$  electrochemical reaction,  $R_u$  is the universal gas constant (8,314.6 J/kmole K),  $T$  is the SOFC operating temperature (K),  $P_i$  is the partial pressures (Pa) of the reactants and products, and  $P_{\text{ref}}$  is the reference pressure (101,325 Pa). It can be seen in the equation that reversible voltage of the SOFC depends on changes in the Gibbs free energy, the operating temperature of the fuel cell, and partial pressure of hydrogen, oxygen, and steam. The other components of the anolyte and catholyte streams only affect this voltage by affecting partial pressure of the reactants. It should be noted that the increase in the operating temperature of the SOFC reduces the reversible voltage of the SOFC. This is due to a considerable decrease in the Gibbs free energy with the increase in operating temperature of the SOFC (Calise et al., 2006a). For the hydrogen electrochemical reaction, the magnitude of the Gibbs free energy decreases from 237 kJ/mole at 25°C to 177 kJ/mole at 1000°C (Larminie and Dicks, 2003). However, the actual voltage of the SOFC increases with the temperature increase because of the effects of overpotentials (Calise et al., 2006a), which will be explained later and can be seen in Figure 25. This equation shows that in order to have a reasonable output voltage, the partial pressure of hydrogen and oxygen should be sufficiently high, and the partial pressure of steam should be reasonably low. That is why the fuel and air utilization factors in the SOFC cannot be 100%. The Gibbs free energy change can be computed by the following equation (Vielstich, Gasteiger, and Lamm, 2003):

$$\Delta \bar{g} = (-247.4 + 0.0541 T) \quad (36)$$

The partial pressures of H<sub>2</sub>, O<sub>2</sub>, and H<sub>2</sub>O used in Equation 35 are taken as average values of the inlet and outlet partial pressures and are estimated based on the average number of moles of each species in the inlet and outlet streams:

$$P_{H_2} = \frac{\dot{n}_{H_2,in}/\dot{n}_{anolyte,in} + \dot{n}_{H_2,out}/\dot{n}_{anolyte,out}}{2} P_{anolyte} \quad (37)$$

$$P_{O_2} = \frac{\dot{n}_{O_2,in}/\dot{n}_{catholyte,in} + \dot{n}_{O_2,out}/\dot{n}_{catholyte,out}}{2} P_{catholyte} \quad (38)$$

$$P_{H_2O} = \frac{\dot{n}_{H_2O,in}/\dot{n}_{anolyte,in} + \dot{n}_{H_2O,out}/\dot{n}_{anolyte,out}}{2} P_{anolyte} \quad (39)$$

where  $P_{anolyte}$  and  $P_{catholyte}$  refer to the anolyte and catholyte stream pressures [Pa],  $\dot{n}_{H_2,in}$ ,  $\dot{n}_{O_2,in}$ , and  $\dot{n}_{H_2O,in}$  refer to the molar flow rate of the corresponding species before the reactions, and  $\dot{n}_{H_2,out}$ ,  $\dot{n}_{O_2,out}$ , and  $\dot{n}_{H_2O,out}$  refer to the molar flow rates after the reactions. It should be noted that the inlet or outlet partial pressure of the streams can be considered in the calculations; however, as explained in Subsection 3.3.1 and shown in Figure 9, the average values can provide the most accurate results for a 0-D model. Of course, finding the pressure profile along the fuel cell stack is the most accurate option; however, for a 0-D model this type of calculation is not feasible.

#### 4.3.2.2.2 Actual potential difference

The open circuit potential difference of an SOFC is usually very close to the reversible voltage given by the Nernst equation, Equation 35 (Costamagna et al., 2004). However, due to several losses, which are also called polarizations or overpotentials, the actual voltage of fuel cells is lower than the Nernst potential. Main voltage losses are referred to as activation, ohmic, and concentration losses and losses due to the internal current and fuel crossover. The dominant overpotential depends on the fuel cell type.

The activation loss is the potential needed to overcome the energy barrier of the electrochemical reactions. This loss is not considerable in the SOFCs. The resistance against immigration of ions

across the electrolyte and electrons through the electrodes and interconnects as well as the contact resistance over the interface of materials is referred to as the ohmic loss. This loss is the dominant overpotential in SOFCs, at least for tubular SOFCs, and causes linear reduction in the fuel cell voltage. The concentration loss is caused by reduction of the local concentration of fuel in the anode and oxidant in the cathode as the fuel and air are spent as well as increase in the concentration of reaction products in the anode. This loss is important when the fuel cell operates at a high current density. In order to find the actual operating voltage of an SOFC, all these losses should be deducted from the open circuit voltage (Equation 40). The actual operating voltage is used to compute the output power of the SOFC.

$$E_{\text{act}} = E_{\text{rev}} - E_{\text{activ}} - E_{\text{ohm}} - E_{\text{conc}} \quad (40)$$

where  $E_{\text{act}}$  represents the actual output voltage,  $E_{\text{activ}}$ ,  $E_{\text{ohm}}$ , and  $E_{\text{conc}}$  refer to the activation, ohmic, and concentration losses, respectively. These irreversibilities will be discussed in the following subsections.

#### 4.3.2.2.3 Losses due to internal current and fuel crossover

An ideal electrolyte should only transfer ionic charges between electrodes and block direct transformation of electrons and the flow of fuel and oxygen between electrodes. However, an actual electrolyte cannot perform these tasks perfectly, and always there are some electron conduction through the electrolyte and some fuel crossover. Internal current is the amount of electrons that are conducted through the electrolyte. Both these losses are similar in nature and essentially equivalent. These losses are not usually very important, especially for high temperature fuel cells. The fuel crossover and internal current loss can be taken into account by adding an equivalent internal current density to the operating current density for calculating the overpotentials, (Larminie and Dicks, 2003; Freeh et al., 2004) as shown in Equation 41.

$$i_{\text{act}} = i_{\text{op}} + i_{\text{I}} \quad (41)$$

where  $i_{\text{act}}$  is the actual current density ( $\text{A}/\text{m}^2$ ),  $i_{\text{op}}$  is the desired operating current density ( $\text{A}/\text{m}^2$ ), and  $i_{\text{I}}$  is the internal current density ( $\text{A}/\text{m}^2$ ). In this model, the actual current density was a user-defined constant (Kuchonthara et al., 2003a) and considered to be equal to  $3200 \text{ A}/\text{m}^2$  (Calise et al., 2006a). The current density used in the literature is in the range of 2500 to  $4000 \text{ A}/\text{m}^2$

(Achenbach, 1994; Calise et al., 2006a; Van herle et al., 2004; Massardo and Lubelli, 2000; Cunel et al., 2002; Chan et al., 2002b; Riensche et al., 2000; Suci et al., 2007; Magistri et al., 2005). Also, the internal current density was considered to be 20 A/m<sup>2</sup> (Freeh et al., 2004).

#### 4.3.2.2.4 Activation losses

In any chemical reaction, the bonds between atoms or molecules should be first broken and then reformed. The energy required to break these bonds is called the activation energy and is provided in the form of the kinetic energy of the reacting molecules. The kinetic energy of molecules can be increased by increasing their temperature. In early models, this overpotential was commonly neglected because of the lower activation loss at high operating temperature of early SOFCs and very high magnitude of ohmic loss of the fuel cell in comparison to activation loss. However, in modern SOFCs, especially low temperature planar cells, none of these conditions is valid anymore because of lower than 800°C operating temperature and lower ohmic loss as a result of the thinner electrolyte (Noren and Hoffman, 2005). The activation losses in fuel cells can be calculated by either the Tafel equation (Kuchonthara et al., 2003a; Freeh et al., 2004) or the Butler-Vollmer equation (Singhal and Kendall, 2003; Noren and Hoffman, 2005). These two equations are different representations based on the same experimental observations. As can be seen from Equations 42 and 43, for the current density equal to zero, the Tafel equation results in activation loss equal to  $\frac{R_u T}{2\alpha F}$ , whereas Butler-Vollmer gives zero activation loss for zero current density. This indicates that the Butler-Vollmer equation is more accurate than the Tafel equation (Calise et al., 2006a; Chan et al., 2002a). The Tafel equation is usually used when the activation losses are high, and the second term in the Butler-Vollmer equation can be neglected, reducing it to the Tafel equation. The Tafel equation is usually valid if  $i/i_0 > 4$  (Noren and Hoffman, 2005). It should be noted that some authors, such as Hussain, Dincer, and Li (2004), proposed other equations with different forms but the same nature for estimation of activation losses.

$$E_{\text{activ}} = \frac{R_u T}{2\alpha F} \ln\left(\frac{i}{i_0}\right) \quad \text{Tafel equation} \quad (42)$$

$$i = i_0 \left[ e^{\left(\beta_1 \frac{FE_{\text{activ}}}{R_u T}\right)} - e^{\left(-\beta_2 \frac{FE_{\text{activ}}}{R_u T}\right)} \right] \quad \text{Butler-Vollmer equation} \quad (43)$$

where  $i$  and  $i_0$  represent the current density and exchange current density ( $A/m^2$ ), respectively, and  $\alpha$ ,  $\beta_1$ , and  $\beta_2$  represent the charge transfer coefficients and are functions of the electron transfer process in the interface of the electrode and electrolyte in the cell (Noren and Hoffman, 2005). The charge transfer coefficients are in the range of 0.0-1.0 (Larminie and Dicks, 2003). These equations can be applied to both electrodes. The exchange current density can be defined as the maximum current density, for which the rate of the electrochemical reactions and their reverse reactions are the same, so there is no actual output current in the fuel cell at the open-circuit condition across the electrode-electrolyte interface (Noren and Hoffman, 2005). It is important to try to increase this current density because it means that the surface of the electrode is more active (Larminie and Dicks, 2003). The exchange current density strongly depends on cell materials and construction as well as operating temperature of the fuel cell and reactant and product partial pressures (Noren and Hoffman, 2005). It should be noted that the effect of temperature on the exchange current density outweighs the direct effect of the temperature on the activation losses. In reality, in most cases, increasing the temperature decreases the activation overpotential. For some fuel cells, such as hydrogen fuelled fuel cells, the activation overpotential for the anode is much smaller than that for the cathode (Larminie and Dicks, 2003). However, for other fuel cells, the activation overpotential of both electrodes should be taken into account. It should be noted that for high temperature and pressure fuel cells, these losses are less important in comparison to other overpotentials. However, this statement may not be true for some SOFCs, especially planar electrode-supported SOFCs. The activation overpotential can be reduced (which means a higher exchange current density) by increasing the operating temperature and pressure of the fuel cell, a more effective catalyst, electrodes with higher roughness, and higher concentrations of the reactants (Larminie and Dicks, 2003).

In this model, it was assumed that each reaction is a one-step, single-electron transfer process (Noren and Hoffman, 2005), which means the possibility of intermediate reactions in the electrochemical reactions was overlooked. This assumption results in the following form of the Butler-Volmer equation (Singhal and Kendall, 2003; Calise et al., 2006a; Van herle et al., 2003; Noren and Hoffman, 2005; Bove et al., 2005; Chan et al., 2002a):

$$i = i_0 \left[ e^{\left( \beta \frac{FE_{\text{activ}}}{R_u T} \right)} - e^{\left( (\beta-1) \frac{FE_{\text{activ}}}{R_u T} \right)} \right] \quad (44)$$

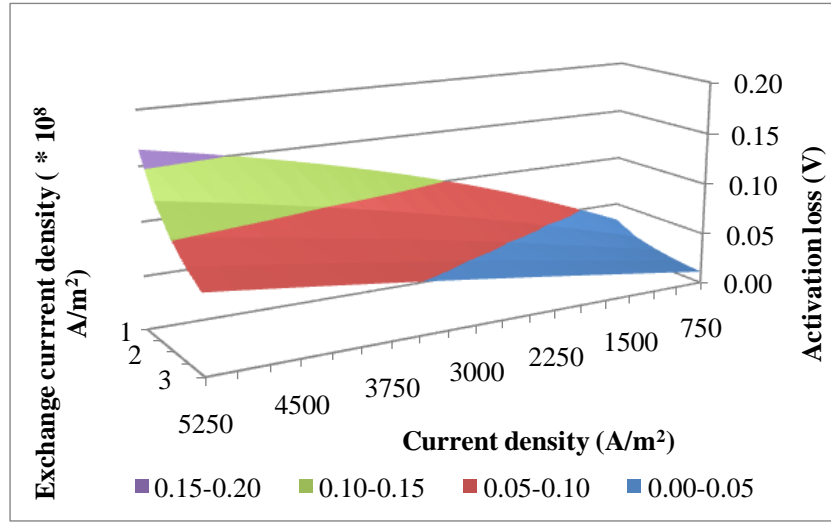
The exchange current density of the anode and cathode can be estimated by Equations 45 and 46 (Calise et al., 2006a, 2008; Costamagna et al., 2004; Bove et al., 2005):

$$i_{0,\text{anode}} = \gamma_{\text{anode}} \left( \frac{P_{\text{H}_2}}{P_{\text{ref}}} \right) \left( \frac{P_{\text{H}_2\text{O}}}{P_{\text{ref}}} \right) e^{\left( \frac{\varepsilon_{\text{activ},\text{anode}}}{R_u T} \right)} \quad (45)$$

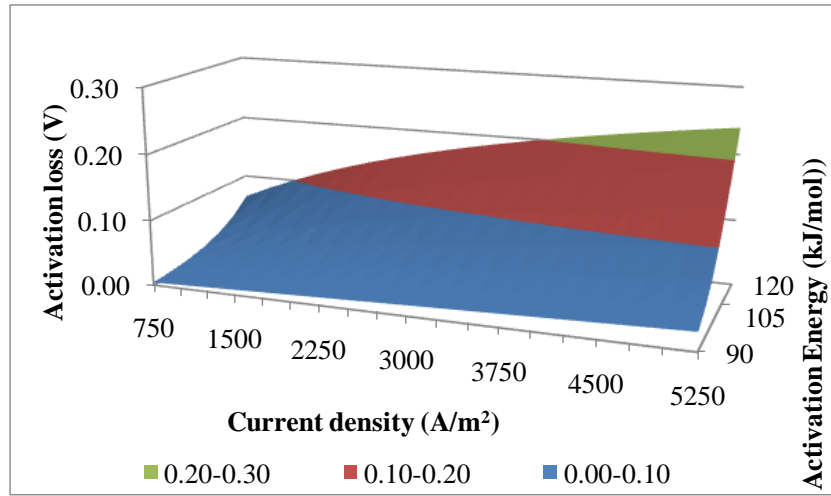
$$i_{0,\text{cathode}} = \gamma_{\text{cathode}} \left( \frac{P_{\text{H}_2}}{P_{\text{ref}}} \right)^{0.25} e^{\left( \frac{\varepsilon_{\text{activ},\text{cathode}}}{R_u T} \right)} \quad (46)$$

where  $\gamma$  is a pre-exponential factor ( $\text{A/m}^2$ ) and  $\varepsilon_{\text{activ},\text{anode}}$  and  $\varepsilon_{\text{activ},\text{cathode}}$  are the anode and cathode activation energies (kJ/mole), respectively. In the model, the exchange current densities were first calculated, and then the secant method was used to solve the non-linear Butler-Volmer equation to find the activation losses.

The major parameters that should be defined by the user for activation losses are the exchange current density constants ( $\gamma_{\text{anode}}$  and  $\gamma_{\text{cathode}}$ ), activation energies ( $\varepsilon_{\text{activ},\text{anode}}$  and  $\varepsilon_{\text{activ},\text{cathode}}$ ), and charge transfer coefficients ( $\beta_{\text{anode}}$  and  $\beta_{\text{cathode}}$ ). Figures 19 and 20 illustrate the variation of the activation loss versus these three constants in 3-D curves and their 2-D representation, respectively. In this work, whenever possible, both 3-D and 2-D curves are presented, 3-D for better understanding of the variation of parameters and 2-D for better readability of them. It should be noted that the raw data for some of these curves as well as 2-D graphs were provided by Suther et al. (2010a), for which the current author was a collaborator. Since both the anode and cathode activation losses were estimated by the same equations, the effects of the input parameters on the losses are the same, and only the results for the anode activation loss are presented. As expected, and Figures 19a and 19b show, the activation loss steadily increases with the current density. Also, the activation loss increases with a decrease in the exchange current density (Figure 19a) and the charge transfer coefficient (Figure 19c). On the other hand, the increase in the activation energy causes an increase in the activation loss (Figure 19b).



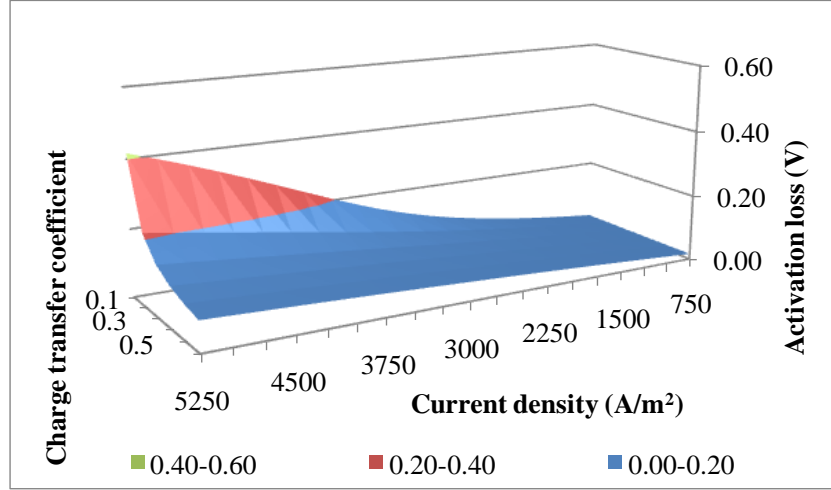
(a)



(b)

Figure 19: Dependency of the activation loss on the constants in Equations 44 and 45 (3-D curves)

a) the exchange current density b) the activation energy



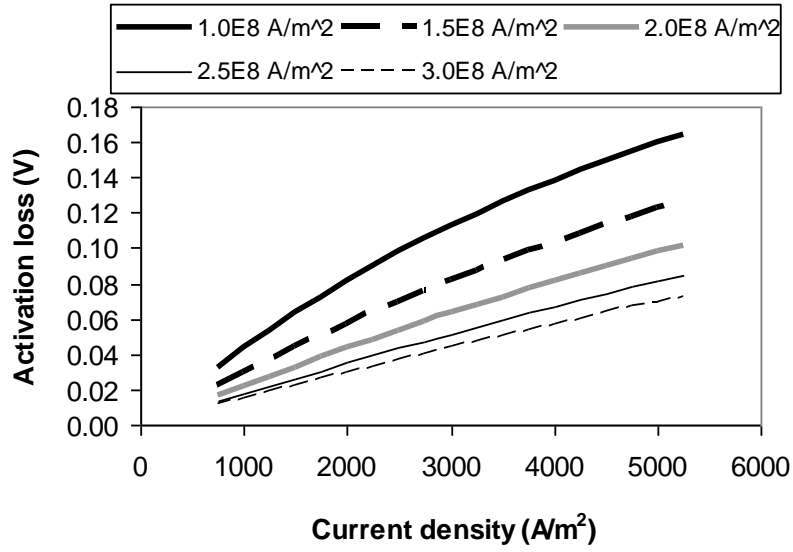
(c)

**Figure 19: Dependency of the activation loss on the constants in Equations 44 and 45 (3-D curves)**

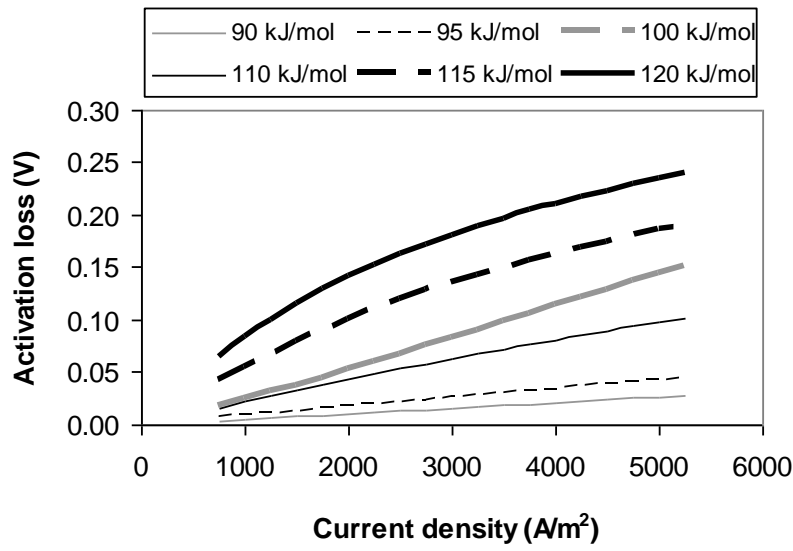
**a) the exchange current density b) the activation energy c) the charge transfer coefficient**

Calise et al. (2006b) suggested that the activation energies were equal to 110 kJ/mole for both the anode and cathode electrodes, while Costamagna et al. (2001) proposed values of 100 and 120 kJ/mole for the anode and cathode, respectively. The range of the activation energies used in the literature is 100-116 kJ/mole for the anode and 110-160 kJ/mole for the cathode (Achenbach, 1994; Van herle et al., 2003). In this work, the activation energies were equal to 100 and 120 kJ/mole for the anode and cathode electrodes, respectively (Calise et al., 2006a). In this model, the exchange current density constants were considered to be  $2.13 \times 10^8$  and  $1.49 \times 10^8$  A/m<sup>2</sup> for the anode and cathode, respectively (Calise et al., 2006a). Theoretically, the charge transfer coefficient is in the range of 0–1, and it was reported, based on the experimental works, to be approximately 0.5 (Hoogers, 2002; Noren and Hoffman, 2005). It has been suggested that when fitting the model results to the available experimental data, the anode charge transfer coefficient is taken equal to 0.5, and then the cathode value is manipulated in the range of 0.3–0.6 (Larminie and Dicks, 2003; Noren and Hoffman, 2005). In this work, the values of  $\beta$  for both the anode and cathode were considered to be 0.5 (Calise et al., 2006a; Larminie and Dicks, 2003; Chan et al., 2002a; Noren and Hoffman, 2005).



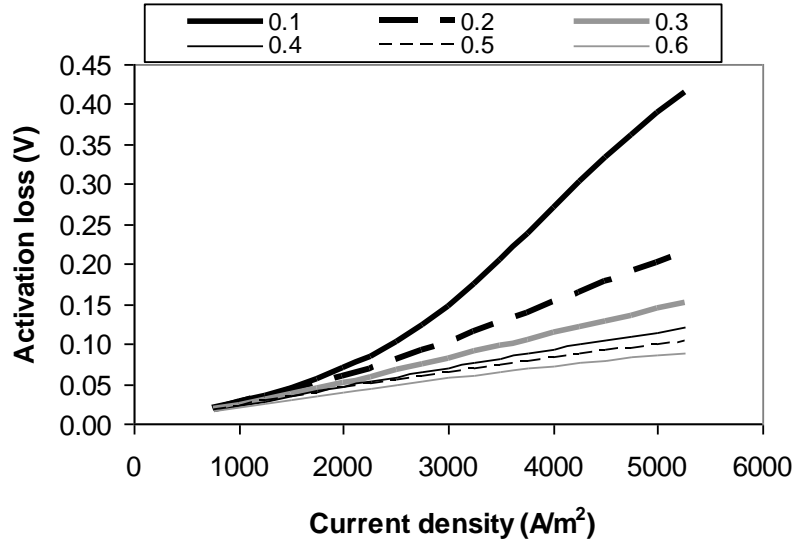


(a)



(b)

**Figure 20: Dependency of activation loss on the constants in Equations 44 and 45 (2-D curves)**  
the exchange current density b) the activation energy



(c)

**Figure 20: Dependency of activation loss on the constants in Equations 44 and 45 (2-D curves)**

a) the exchange current density b) the activation energy c) the charge transfer coefficient (Suther et al., 2010a)

#### 4.3.2.2.5 Ohmic losses

The ohmic losses account not only for the electrical resistance of electrodes and interconnects, and the contact resistance over the interface of materials, but also for the electrolyte resistance to the flow of ions. The ohmic losses were important for all types of fuel cells, particularly the SOFC, and can be reduced by using electrodes and interconnects with high conductivity and a thinner electrolyte. Various approaches have been used to estimate ohmic losses. For instance, some models kept resistances separate and modeled them individually (Gopalan and DiGiuseppe, 2003; Suwanwarangkul et al. 2005). Also, some authors, such as Lazzaretto et al. (2004), calculated the ohmic resistance through the electrolyte, found the voltage drop due to this resistance, and then assumed this voltage drop to be a fixed fraction of the total ohmic loss of the fuel cell.

Generally, this overpotential is proportional to the current and the resistance (Larminie and Dicks, 2003; Kuchonthara et al., 2003a; Freeh, Pratt, and Brouwer, 2004):

$$E_{ohm} = I_{act} R_{ohm} \quad (47)$$

where  $E_{ohm}$  represents the ohmic losses (V),  $I_{act}$  is actual current (A), and  $R_{ohm}$  the resistance ( $\Omega$ ).  $R_{ohm}$  depends on the geometry and material property of the cell. In order to make Equation 47 consistent with the other equations, it should be expressed as a function of the current density (Equation 48). This requires introduction of area-specific resistance ( $r$ ), which is the resistance of  $1 \text{ cm}^2$  of the cell (Larminie and Dicks, 2003).

$$E_{ohm} = i_{act} r_{ohm} \quad (48)$$

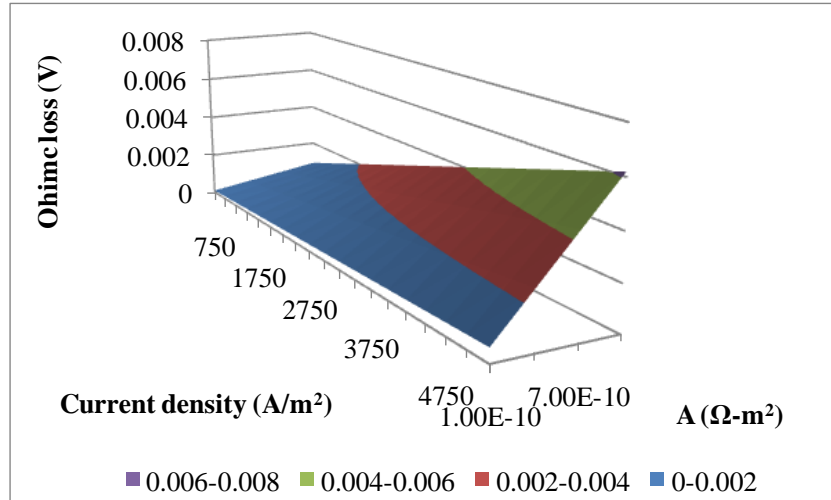
where  $i_{act}$  refers to the actual current density ( $\text{A/m}^2$ ) and  $r_{ohm}$  refers to the area-specific resistance ( $\Omega\text{m}^2$ ). The area-specific resistance depends on material properties of the electrodes, electrolyte, and interconnects as well as operating temperature and can be estimated by the empirical correlation given in Equation 49 (Massardo and Lubelli, 2000; Freeh et al., 2004).

$$r = \sum_i A_i e^{(B_i/T)} \quad (49)$$

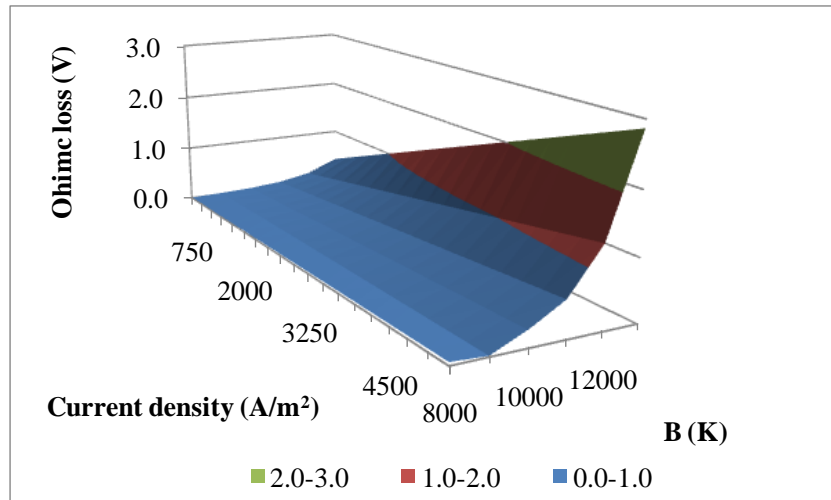
where  $i$  refers to the cell component (the anode, cathode, electrolyte, and interconnects),  $A_i$  ( $\Omega\text{m}^2$ ) and  $B_i$  (K) are dimensional constants and vary for different materials. In this model, the constants  $A$  and  $B$  for all components were added up and represented by a single value, as shown in Equation 50 (Li, 2006; Calise et al., 2006a; Chan et al., 2002a), assuming these overall values eliminated the need for the specific dimensions of the fuel cell.

$$r = A e^{(B/T)} \quad (50)$$

Figures 21 and 22 demonstrate the dependency of the SOFC total ohmic loss on constants  $A$  and  $B$  in 3-D and 2-D curves, respectively. As the figures show, an increase in both constants causes an increase in the ohmic loss. Also, obviously, ohmic loss increases with an increase in the current density. In this model, the constants  $A$  and  $B$  were considered to be equal to  $2.1 \times 10^{-10} \Omega\text{m}^2$  and 10,000 K, respectively (Chan et al., 2002a).

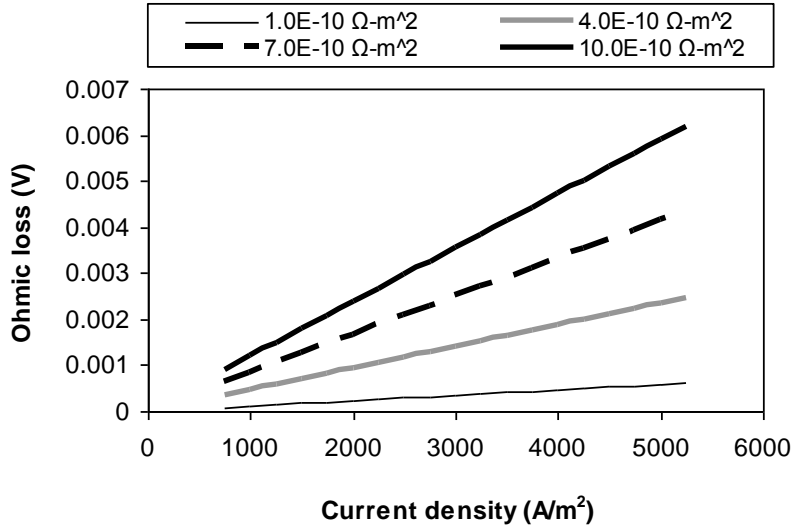


(a)

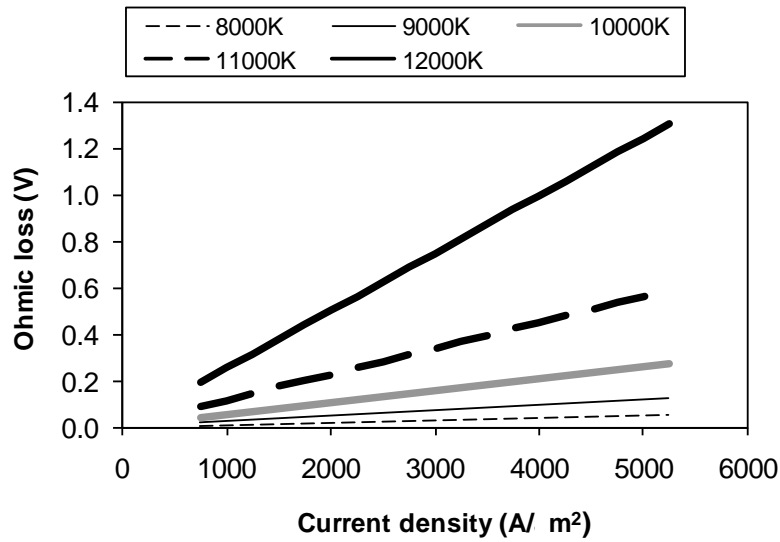


(b)

**Figure 21: Dependency of the total ohmic loss on the constants in Equations 48 and 50 (3-D curves) a)  $A$  and b)  $B$**



(a)



(b)

Figure 22: Dependency of the total ohmic loss on the constants in Equations 48 and 50 (2-D curves) a) A and b) B (Suther et al., 2010a)

#### 4.3.2.2.6 Concentration losses

Concentration losses are due to limitation of transportation of reactants from bulk flow to the reaction sites in the anode and cathode, and transportation of reaction products from the reaction

site to the exhaust stream (Noren and Hoffman, 2005; Singhal and Kendall, 2003). As fuel and air participate in the reactions within the fuel cell and are consumed by these reactions, the concentration of reacting species and as a result their partial pressure are reduced (Larminie and Dicks, 2003). The reduction in the concentration and partial pressure of the reactants leads to a reduction in the voltage of the fuel cell. This voltage loss is known as the concentration or the mass transport loss and depends on the rate of hydrogen consumption (and thus fuel cell current) and the hydrogen supply characteristics.

There is no general analytical formulation to calculate concentration overpotential in fuel cells (Kim, Lee, Srinivasan, and Chamberlin, 1995). However, many models in the literature made use of the adjusted Nernst equation to roughly estimate this loss (Equation 51) (Kuchonthara et al., 2003a; Freeh et al., 2004).

$$E_{\text{conc}} = \frac{R_u T}{n_e F} \ln \left( \frac{P_2}{P_1} \right) \quad (51)$$

where  $P_1$  represent the pressure for the limiting current density ( $i_L$ ),  $P_2$  is pressure at the actual current density  $i_{\text{act}}$ , and  $n_e$  is number of electrons transferred in the electrochemical reaction (which is equal to 2 for the hydrogen electrochemical reaction). This approach has some weaknesses, especially when the fuel and oxidant are a mixture of different gases. It also does not take into account production and removal of reaction products (Singhal and Kendall, 2003; Larminie and Dicks, 2003). At the limiting current density all inlet fuel is consumed in the fuel cell. It is the maximum possible current density because it is not possible to increase the fuel supply to the reaction sites beyond this point, and there is not enough ion flow to/from the electrodes to supply the reactions. It can be assumed that at the limiting current density, the local concentration of reactants will drop to zero. By assumption of a linear relationship between the pressure drop and current density, the pressure  $P_2$  of any actual current density  $i_{\text{act}}$  can be estimated by the following equation (Larminie and Dicks, 2003):

$$P_2 = P_1 \left( 1 - \frac{i_{\text{act}}}{i_L} \right) \quad (52)$$

where  $i_L$  is the limiting current density ( $\text{A/m}^2$ ). Substituting Equation 52 in Equation 51, the voltage drop due to the concentration loss for a fuel cell with hydrogen electrochemical oxidation can be calculated from Equation 53 (Calise et al., 2006a; Kuchonthara et al., 2003a; Larminie and Dicks, 2003; Freeh et al., 2004).

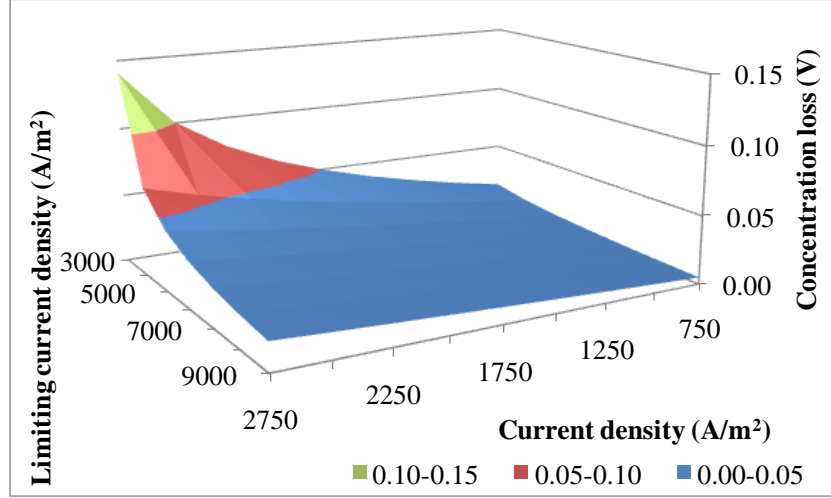
$$E_{\text{conc}} = \frac{R_u T}{2F} \ln \left( 1 - \frac{i_{\text{act}}}{i_L} \right) \quad (53)$$

The influence of pressure on the concentration loss was taken into account using a pressure adjusted limiting current density. For the operating pressure of the fuel cell anode, the limiting current density can be adjusted as follows (Freeh et al., 2004):

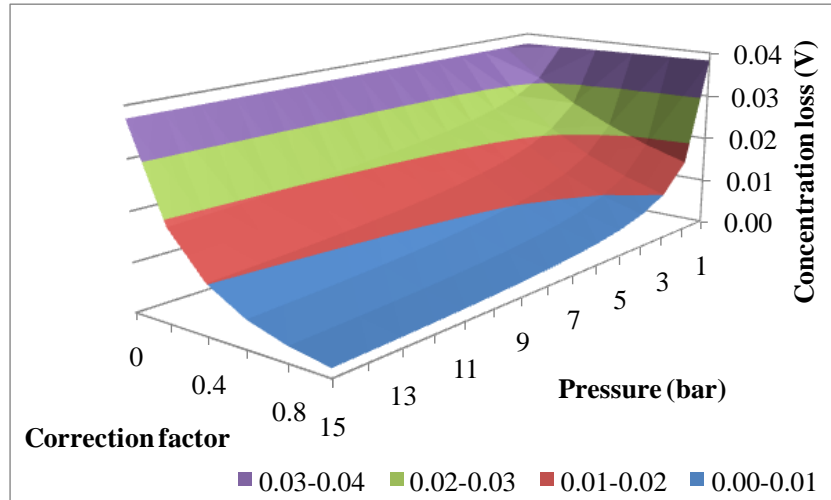
$$i_{L,\text{adj}} = i_L \left( \frac{P_{\text{anolyte,in}}}{P_{\text{ref}}} \right)^{C_{\text{corr}}} \quad (54)$$

where  $i_{L,\text{adj}}$  is pressure adjusted limiting current density, and  $C_{\text{corr}}$  is the limiting current density correction factor.

The dependency of the concentration loss of the SOFC on the limiting current density versus current density is shown in Figures 23a and 24a. As the figures show, the concentration loss increases with increase in current density and decrease in limiting current density. Also, Figure 23b and 24b illustrate the effects of the limiting current density correction factor on the SOFC concentration loss over a pressure range of 1–15 bar, at a constant operating current density of 3,200 A/m<sup>2</sup>. Figure 23b indicates that by increasing the SOFC operating pressure, the concentration loss can be reduced. Similarly, a higher correction factor results in a lower concentration loss. Figure 24b shows that when the correction factor is equal to zero, the concentration loss is not affected by fuel cell operating pressure. In the model, the limiting current density was equal to 6,500 A/m<sup>2</sup> (Singhal and Kendall, 2003), and the limiting current density correction factor was equal to 0.35 (Freeh et al., 2004).



(a)



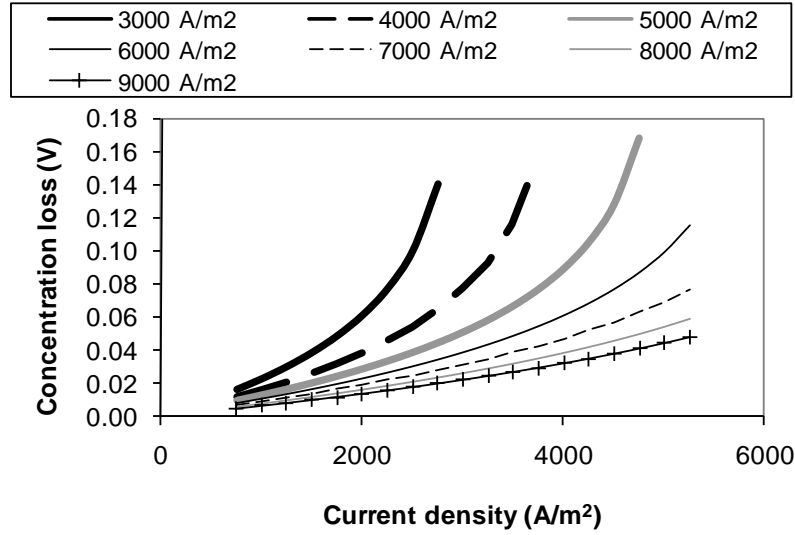
(b)

**Figure 23: Dependency of concentration loss on the constants in Equations 53 and 54 (3-D curves) a) limiting current density b) correction factor**

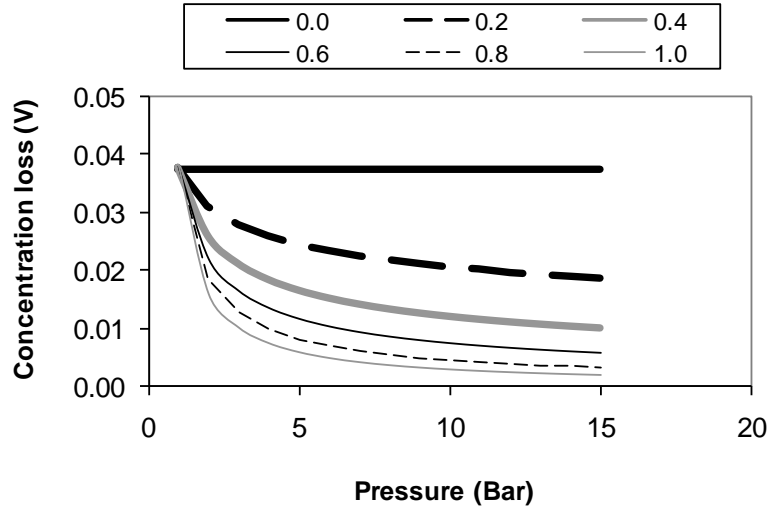
Now, according to Equation 40, the actual voltage of the SOFC can be estimated by deducting all losses from the cell reversible voltage. Figure 25a and 25b illustrate the reversible and actual voltage of the SOFC, respectively, as a function of the current density and operating temperature of the SOFC. As can be seen from Figure 25a, the reversible voltage of the SOFC reduces with operating temperature increase; however, the actual voltage trend is reversed and is increased at higher temperatures. As explained in Subsection 4.3.2.2.1, this is due to the greater reduction in



the fuel cell's overpotentials in comparison to the reduction in the reversible voltage. Also, as expected, while the SOFC reversible voltage is independent of current density, the SOFC actual voltage reduces with increase in current density.

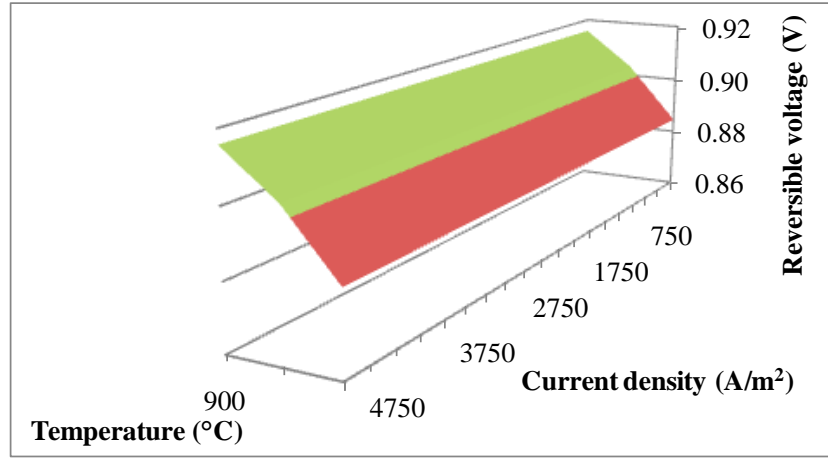


(a)

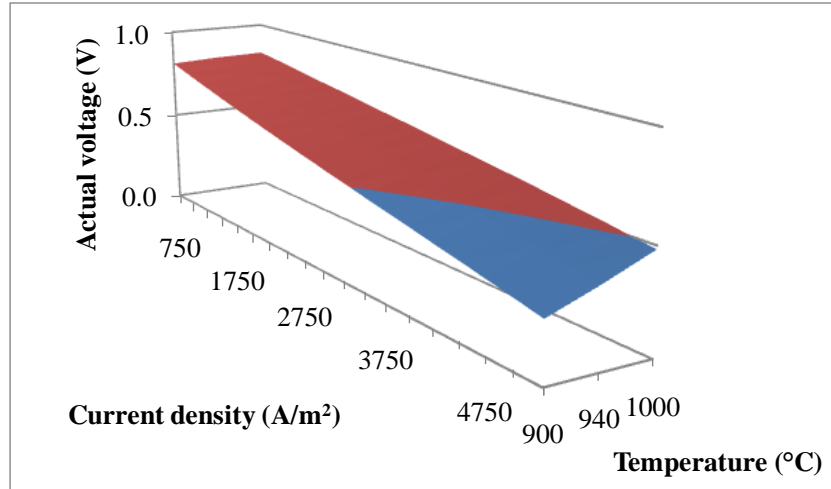


(b)

**Figure 24: Dependency of concentration loss on the constants in Equations 53 and 54 (2-D curves) a) limiting current density b) correction factor (Suther et al., 2010a)**



(a)



(b)

**Figure 25: Reversible voltage (a) and actual voltage (b) of the SOFC as functions of the current density and operating temperature**

#### 4.3.2.3 Output power of the SOFC

Having the cell current from Equation 34 and the cell voltage from Equation 40, the output power of the SOFC stack can be estimated from Equation 55 (Colpan et al., 2008).

$$\dot{W}_{\text{net,SOFC}} = E_{\text{act}} \times I \quad (55)$$

Substituting I from Equation 34, the following equation can be obtained for the output power of the SOFC (Calise et al., 2006a):

$$W_{\text{net,SOFC}} = E_{\text{act}} 2 \dot{n}_{\text{H}_2, \text{react}} F \quad (56)$$

Similarly, the power density can be estimated by Equation 55 only by replacing current by current density. Figure 26 illustrates the power density of the SOFC versus its current density for various operating temperatures.

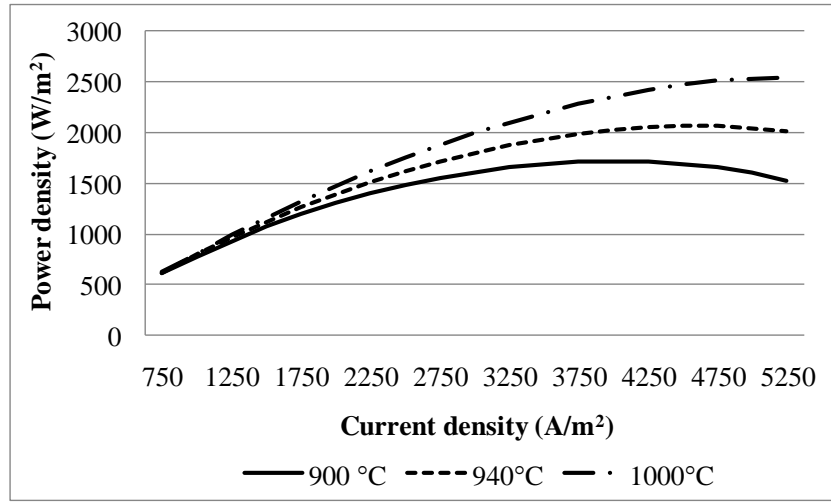


Figure 26: SOFC power density versus current density for various operating temperatures (°C)

#### 4.3.2.4 Calculation of the heat output from the stack and outlet temperature

To calculate the heat output from the stack, first the maximum available energy in the SOFC should be estimated. The maximum available energy is equal to the isothermal enthalpy difference between the inlet and outlet streams and can be computed based on the rate of energy at inlet to the SOFC ( $\dot{E}_{\text{in}}$ ) and the rate of energy exiting the SOFC ( $\dot{E}_{\text{out}}$ ).

$$\begin{aligned} \dot{E}_{\text{available}} = \dot{E}_{\text{in}} - \dot{E}_{\text{out}} = & \dot{n}_{\text{anolyte, in}} \times \rho_{\text{anolyte, in}} \times h_{\text{anolyte, in}} + \dot{n}_{\text{catholyte, in}} \times \rho_{\text{catholyte, in}} \times \\ & h_{\text{catholyte, in}} - \dot{n}_{\text{anolyte, out}} \times \rho_{\text{anolyte, out}} \times h_{\text{anolyte, out}} - \dot{n}_{\text{catholyte, out}} \times \rho_{\text{catholyte, out}} \times \\ & h_{\text{catholyte, out}} \end{aligned} \quad (57)$$

where  $\dot{E}_{\text{available}}$ ,  $\dot{E}_{\text{in}}$ ,  $\dot{E}_{\text{out}}$  are available, inlet, and outlet energy rate (J/s), respectively;  $\dot{n}_{\text{anolyte,in}}$  and  $\dot{n}_{\text{anolyte,out}}$  represent the anode inlet and outlet molar flow rates (kmole/s), respectively;  $\dot{n}_{\text{catholyte,in}}$  and  $\dot{n}_{\text{catholyte,out}}$  represent the cathode inlet and outlet molar flow rates (kmole/s), respectively;  $h$  represents the specific enthalpy of the streams (kJ/kg); and  $\rho$  represents the molecular weights (kg/kmole). It should be noted that thermodynamic properties of outlet streams were calculated by Aspen Plus<sup>®</sup>.

The outlet temperature of the anolyte and catholyte streams are usually higher than that of inlet streams because some of the heat generated in the reactions is consumed to heat the streams. The temperature increase of between 60°C (Calise et al., 2007) and 100°C (Riensch, 1998a; Achenbach, 1994) in the SOFC stack has been reported in the literature. However, in some models, the SOFC outlet stream temperature was considered to be equal to the operating temperature of the SOFC (such as Costamagna et al. (2001)). In order to account for the temperature increase of the outlet streams in the SOFC due to the generated heat, it was assumed that a certain fraction ( $X$ ) of the power generated by the SOFC was consumed to increase the temperature of these streams.

$$\dot{Q}_{\text{streams}} = X \times \dot{W}_{\text{net,SOFC}} \quad (58)$$

where  $\dot{Q}_{\text{streams}}$  is the heat transferred to the anode and cathode outlet streams,  $X$  is stream heat factor, and  $\dot{W}_{\text{net,SOFC}}$  is the SOFC net output power. For this work, the stream heat factor was considered to be equal to 0.01, which means basically the assumption of the outlet stream temperature equal to the inlet stream temperature could be applied to the model (similar to Costamagna et al. (2001)). The output heat from the SOFC stack then could be found by performing an energy balance of the stack:

$$\dot{Q}_{\text{SOFC}} = \dot{E}_{\text{available}} - \dot{W}_{\text{net,SOFC}} - \dot{Q}_{\text{streams}} \quad (59)$$

### 4.3.3 Model constants and parameters

The summary of the constants, parameters, and operating conditions of the SOFC that were used in this model to solve the above equations and were already explained in corresponding subsections are presented in Table 27. These constants are based on values found in the

literature, as well as the results from the validation of this model. The Fortran user-defined model received all the inputs from the overall model in Aspen Plus<sup>®</sup> as arrays of data; therefore, these inputs can be easily adjusted in Aspen Plus<sup>®</sup>. In the same fashion, the results of calculations in the SOFC Fortran model were transferred to the overall model in Aspen Plus<sup>®</sup> to be used in the simulation of the hybrid cycle. Sensitivity analyses were carried out in Suther et al. (2010a) to investigate the influence of the model constants and parameters on the model outputs. The results of those analyses were used to tune the model output parameters to fit to the available experimental data from Siemens Westinghouse tubular SOFC (Singhal and Kendall, 2003).

The SOFC operating temperature and pressure depend on the fuel cell type and application, and should be sufficiently high for reasonable electrolyte conductivity, but within the operating conditions of the cell structure (Harvey and Richter, 1994b). Various values have been proposed in the literature for the operating temperature of the SOFC; for example, for the planar SOFC the operating temperature is between 800°C and 900°C (Rienschke et al., 1998a; Achenbach, 1994; Möller et al., 2004; Stiller et al., 2005; Van herle et al., 2004; Magistri et al., 2005) and for the tubular SOFC, between 850°C and 1000°C (Stiller et al., 2005; Chan et al., 2003a; Rienschke et al., 2000; Lobachyov and Richter, 1996; Kuchonthara et al., 2003a; Kakac et al., 2007). For the operating pressure, the range has been between 3 bar and 5 bar (Palsson et al., 2000; Stiller et al., 2005; Massardo and Lubelli, 2000; Cunnel et al., 2002; Rienschke et al., 2000; Sucipta et al., 2007; Veyo et al., 2002a).

The developed model was capable of calculating the composition of the exhaust streams, the output work, and heat released as well as several electrochemical properties as listed in Table 28.

**Table 27: SOFC model constants**

Parameter	Used value	Range in literature	Units	Reference
<b>Actual current density, <math>i_{act}</math> (Equation 41)</b>	3,200	2500 - 4000	A/m <sup>2</sup>	Massardo and Lubelli, 2000; Cunnell et al., 2002, Riensche et al., 2000; Sucipta et al., 2007; Magistri et al., 2005
<b>Internal current density</b>	20	20	A/m <sup>2</sup>	Freeh et al., 2004
<b>Pre-exponential factor <math>\gamma_{anode}</math> (Equation 45)</b>	$2.13 \times 10^8$	$2.0 \times 10^8$	A/m <sup>2</sup>	Calise et al., 2006a
<b>Pre-exponential factor <math>\gamma_{cathode}</math> (Equation 46)</b>	$1.49 \times 10^8$	$1.5 \times 10^8$	A/m <sup>2</sup>	Calise et al., 2006a
<b>Activation energy (anode), <math>\epsilon_{activ,anode}</math> (Equation 45)</b>	100	100 - 116	kJ/mole	Calise et al., 2006a; Van herle et al., 2003
<b>Activation energy (cathode), <math>\epsilon_{activ,cathode}</math> (Equation 46)</b>	120	110 - 158	kJ/mole	Calise et al., 2006a; Van herle et al., 2003
<b>Charge transfer coefficient (anode), <math>\beta_{anode}</math> (Equation 44)</b>	0.5	0.5	-	Noren and Hoffman, 2005
<b>Charge transfer coefficient (cathode), <math>\beta_{cathode}</math> (Equation 44)</b>	0.5	0.5	-	Noren and Hoffman, 2005
<b>Constant A (Equation 50)</b>	$2.1 \times 10^{-10}$	$2.0 \times 10^{-10}$	$\Omega m^2$	Chan et al., 2002a
<b>Constant B (Equation 50)</b>	10,000	9,000	K	Chan et al., 2002a
<b>Limiting current density, <math>i_L</math> (Equation 54)</b>	6,500	6,500	A/m <sup>2</sup>	Singhal and Kendall, 2003
<b>Limiting current density correction factor, <math>C_{corr}</math> (Equation 54)</b>	0.35	0.35	-	Freeh et al., 2004
<b>SOFC fuel utilization factor</b>	85	80 - 85	%	Möller et al., 2004; Stiller et al., 2005; Chan et al., 2003b; Riensche et al., 2000; Sucipta et al., 2007
<b>SOFC operating temperature</b>	1000	850 - 1000	°C	Stiller et al., 2005; Riensche et al., 2000; Lobachyov and Richter, 1996; Kuchonthara et al., 2003a; Kakac et al., 2007
<b>SOFC operating pressure</b>	3	3 - 5	bar	Palsson et al., 2000; Stiller et al., 2005; Cunnell et al., 2002; Sucipta et al., 2007; Veyo et al., 2002a

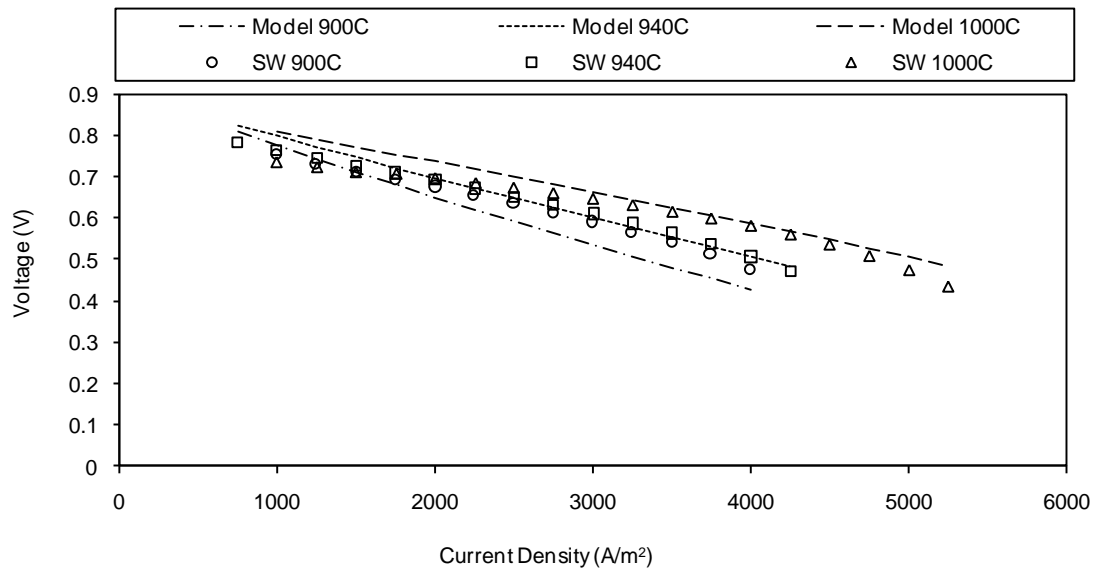
**Table 28: Output electrochemical properties of the model**

Parameter	Unit
Nernst voltage, $E_{rev}$	V
Actual operating voltage, $E_{act}$	V
Overall activation loss, $E_{activ}$	V
Ohmic loss, $E_{Ohm}$	V
Exchange current density (anode), $i_{0,anode}$	A/m <sup>2</sup>
Exchange current density (cathode), $i_{0,cathode}$	A/m <sup>2</sup>
Activation loss (anode and cathode)	V
Pressure adjusted limiting current density, $i_{L,adj}$	A/m <sup>2</sup>
Generated power, W	W
Generated heat, Q	W

#### 4.3.4 Validation

The mathematical model developed in the previous subsections along with the parameters and constants were implemented in a Fortran code, which was used as a user-defined model in Aspen Plus<sup>®</sup>. The next step was to validate the model by comparing its results with the available experimental data. These experimental results are not usually readily available and as reported by Young (2007), in some areas they have been outstripped by modeling works. The most common objective of any experimental and modeling work on fuel cells is to accurately characterize the relationship between voltage and current density of the stack (Noren and Hoffman, 2005). The experimental polarization curves reported by Singhal and Kendall (2003) were used for this purpose. The experimental SOFC unit was a 1.5 m active length tubular SOFC and fed with streams composed of 89% H<sub>2</sub>–11% H<sub>2</sub>O and 21% O<sub>2</sub>–79% N<sub>2</sub> (air) as the fuel and oxidant, respectively. In the experiments, for investigating the temperature dependency of the SOFC, four times the stoichiometric amount of air, and for the pressure dependency six times the stoichiometric amount of air were used. In order to compare experimental and simulation results, voltage-current density curves were used. These curves are commonly used in the literature to describe the electrochemical performance of fuel cells. Figures 27a and 27b illustrate the current density versus output voltage at various operating temperatures and pressures for the experimental measurements and simulation outputs. It should be noted that only a qualitative

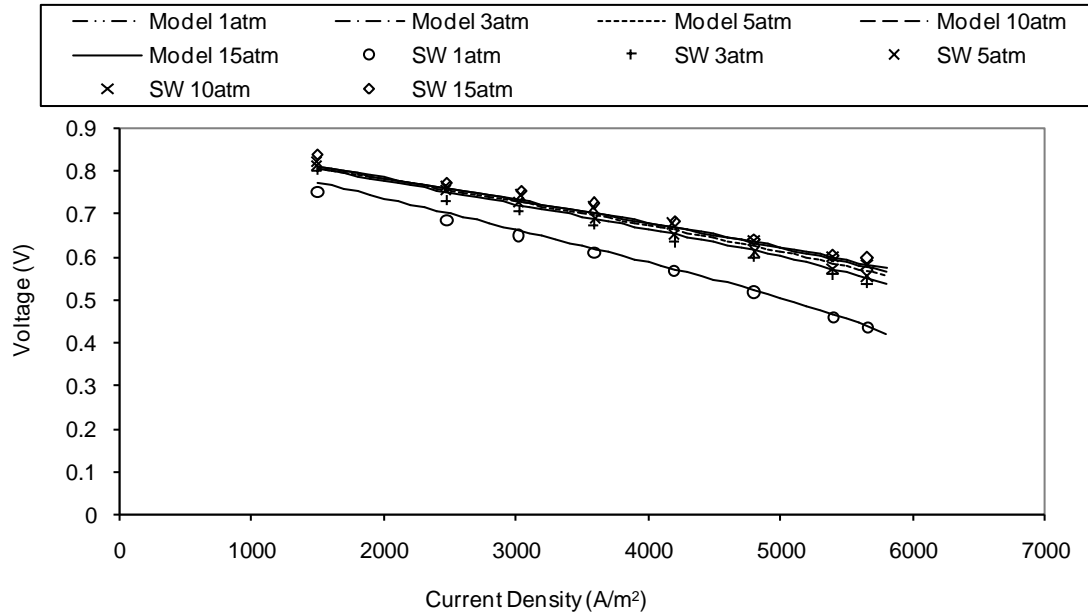
comparison of the simulation and experimental results was carried out. Figure 27a shows the temperature dependency of the model and experimental cell at atmospheric pressure for three temperatures 900°C, 940°C, and 1000°C. There is an acceptable qualitative agreement between simulation results and experimental data especially at medium and high values of the current density. The experimental voltage data are generally lower than those of the simulated results at high temperatures and low current densities. It should be noted that in the typical operation of a tubular SOFC, the current density lies in the range of 3000-3500 A/m<sup>2</sup>. In Figure 27b, the voltage-current density dependency on pressure is illustrated at a temperature of 1000°C for five pressures 1, 3, 5, 10, and 15 bar. There is a good qualitative match between the experimental and simulated results for the entire pressure range. Due to the lack of detail experimental data, the uncertainty analysis cannot be conducted on these graphs. At conditions other than those covered by Figure 27, it is not certain how well the results of the SOFC model would match the performance data of an actual fuel cell due to the lack of available experimental data.



(a)

**Figure 27: The model validation using current density versus voltage curves: a) dependency on operating temperature**





(b)

**Figure 27: The model validation using current density versus voltage curves: a) dependency on operating temperature b) dependency on operating pressure (Suther et al., 2010a)**

#### 4.4 Hybrid Cycle Model

The SOFC Fortran model, developed based on the description presented in the previous subsections, was integrated into a hybrid SOFC-GT cycle model in Aspen Plus<sup>®</sup>. During the execution of the hybrid cycle model, when the SOFC stack was encountered, the SOFC model was called. For the execution of the SOFC stack as a stand-alone model, the flow rates of the fuel and air, the composition of the fuel, and the operating temperature and pressure of the SOFC must be specified by the user. When the model was executed within the hybrid cycle model, the flow rates and composition of the streams entering the SOFC were fed to the SOFC model based on the calculation of the hybrid model configuration and operating parameters in Aspen Plus<sup>®</sup>. The user also needed to input several thermodynamic and electrochemical parameters and constants to complete the calculations of the SOFC model. The hybrid cycle model required thermodynamic models for the compressors, gas turbine, fuel reformer, combustor, material stream mixers and splitters, and heat exchangers. Built-in models of Aspen Plus<sup>®</sup> were used to model these components.

The hybrid SOFC-GT model was developed considering the following general assumptions and considerations:

- The inlet fuel to the cycle was a mixture of gases, which consisted of any combination of  $\text{CH}_4$ ,  $\text{H}_2$ ,  $\text{H}_2\text{O}$ ,  $\text{CO}$ ,  $\text{CO}_2$ ,  $\text{O}_2$ , and  $\text{N}_2$ , which means the inlet fuel was sulfur free and no desulfurization equipment was required. The inlet fuel was delivered to the system at ambient temperature and pressure.
- The air supplied to the fuel cell could be comprised of any combination of  $\text{O}_2$ ,  $\text{N}_2$ ,  $\text{CO}_2$ , and  $\text{H}_2\text{O}$ . For this study, the composition of air was 21%  $\text{O}_2$  and 79%  $\text{N}_2$ .
- Chemical components behaved as ideal gases at the operating temperature and pressure of the cycle (similar to Jiang et al., 2008; Sucipta et al., 2008a).
- No pressure losses occurred within the equipment (similar to Cunnell et al., 2002; Calise et al., 2006b; Palsson et al., 2000). It should be noted that in order to consider pressure losses, some preliminary information about system physical configuration and its dimensions is required. However, in this work the objective was to develop a thermodynamic model of the system. Therefore, the pressure drop of the components was out of the scope of this work.
- The fuel reformer considered methane steam reforming and water-gas shift reactions at chemical equilibrium.
- The fuel reformer and SOFC were designed such that the heat produced by the SOFC could be utilized in the fuel reformer.
- There were no heat losses in the equipment (similar to Costamagna et al., 2001; Jiang et al., 2008; Calise et al., 2006b; Magistri et al., 2005; Stiller et al., 2005).
- The mechanical losses of turbomachinery and DC/AC convertor losses were neglected.

#### 4.4.1 System configurations

The basic configuration of the hybrid SOFC-GT cycle investigated in this research is shown in Figure 28. This figure shows the model components in the Aspen Plus<sup>®</sup> model; however, the actual system configuration depends on the system's operation mode, i.e. with or without anode exhaust recirculation, which will be explained later in this subsection. The equipment models encircled by the dashed line represent the SOFC stack and its internal components. Figure 29 illustrates a schematic diagram of an actual SOFC module (Siemens, 2010). The model components encircled by the dashed line in Figure 28 can be compared with Figure 29 to find how each component in the model corresponds to the equipment in the real system. This comparison shows that the model configuration and the real system resemble each other, and this is one of the distinguishing points of this work and most other modeling works in the literature.

In the SOFC-GT cycle model, the inlet fuel to the system is first compressed from standard temperature and pressure (STP) to system pressure (at F-COMP), and its temperature is increased at FHX by heat recovered from the GT exhaust. It should be noted that in real systems, natural gas is normally delivered to the system at high pressure and ambient temperature. Some models in the literature, such as Massardo and Lubelli (2000), considered these conditions. Assuming that the inlet natural gas is at ambient pressure and temperature, two major differences between the model and the real system can result: some work must be consumed to pressurize the stream and as a result the temperature of the stream significantly increases. However, this assumption, the inlet fuel at ambient temperature and pressure, is common in the literature and is consistent with many modeling works on the natural gas fuelled power generation systems (Harvey and Richter, 1994b; Bolland and Stadaas, 1993). In order to provide required water for the fuel reforming reactions, and to prevent coking in the reformer and SOFC stack, in the cycle with anode recirculation, the fuel is mixed with the recycled part of the anode off-gas stream in a mixer (AN-MIXER). The actual configuration of the cycle with anode recirculation is shown in Figure 30. The mixture of fuel and anode exhaust recirculation, containing enough steam for the fuel reforming process, is then fed to the fuel pre-reformer (REFORMER).

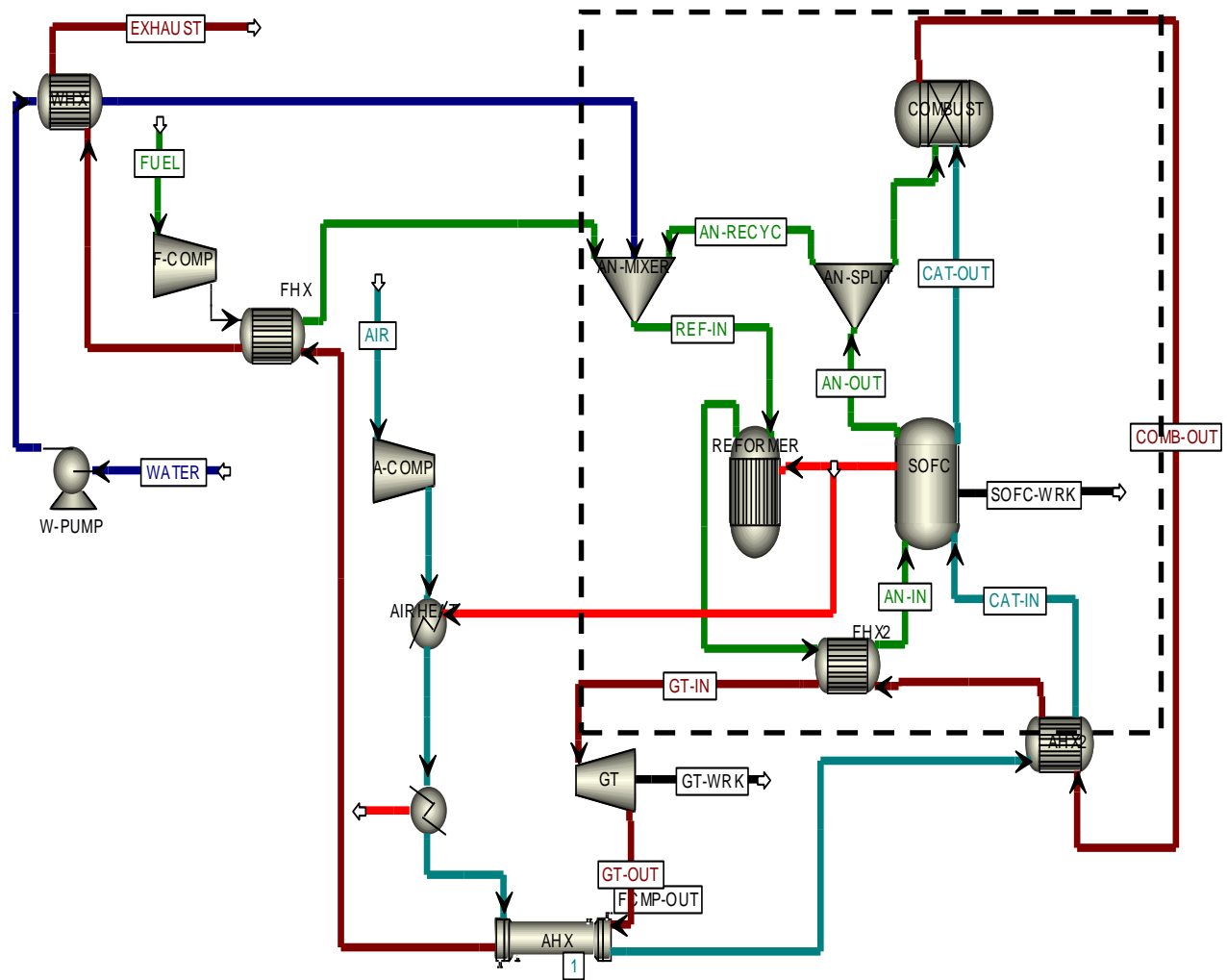
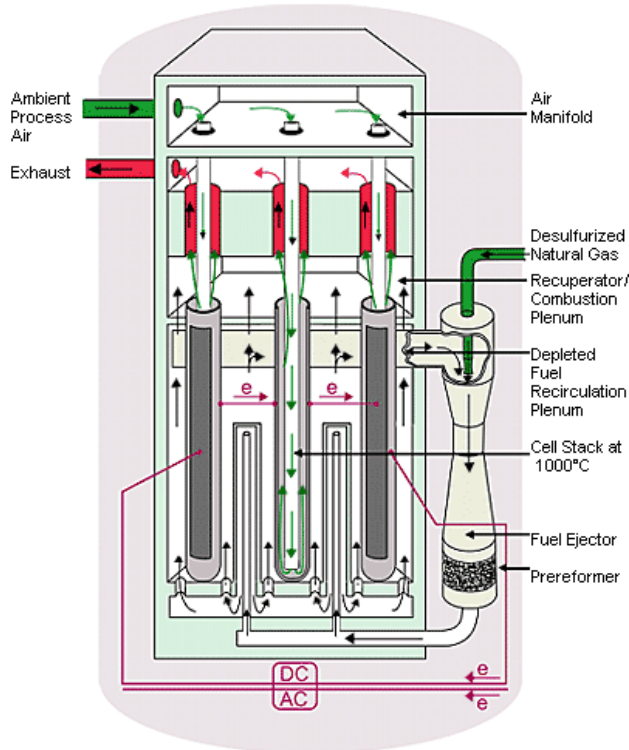


Figure 28: Hybrid SOFC-GT cycle configuration



**Figure 29: A schematic diagram of an actual SOFC module (Siemens, 2010)**

The fuel reforming reactions are endothermic (see Subsections 4.3.2.1.1 and 4.3.2.1.2). On the other hand, there is excess heat generated in the SOFC. In an actual SOFC stack, since the fuel reformer and SOFC stack are physically close, required heat for the reformer can be provided by the SOFC. In the simulation, the excess heat released by the SOFC stack is first exchanged with the reformer and then with the incoming air (at AIR HE) and finally discharged to the environment. The reformer outlet is heated to SOFC operating temperature at FHX2, if its temperature is not high enough, before it is fed to the SOFC anode at AN-IN.

The inlet air, entering the system at STP, is compressed at A-COMP and heated at AIR HE and AHX by the excess heat extracted from the SOFC and the gas turbine exhaust, respectively. If the temperature at the AHX outlet is lower than the SOFC operating temperature, the air is heated by the high energy COMB-OUT stream at AHX2 before being fed to the SOFC cathode at CAT-IN. It should be noted that although the simultaneous reforming and electrochemical reactions are significantly exothermic, the fuel and air inlet streams to the SOFC stack require preheating to avoid a large temperature gradient in the cells (Calise et al., 2006a).

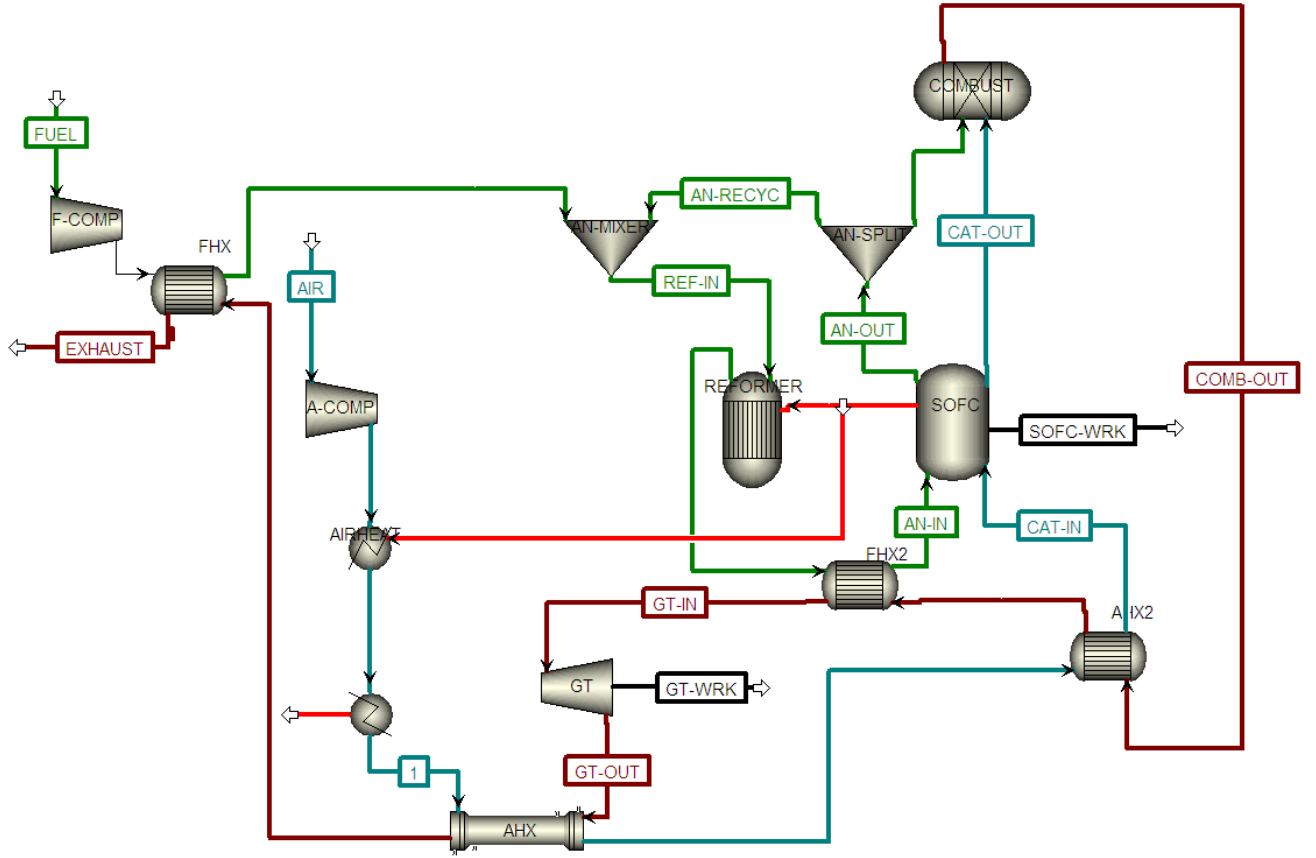


**Figure 30: Actual implemented configuration of the hybrid SOFC-GT cycle model with anode recirculation**

The fuel and air, entering the SOFC at the anode and cathode, respectively, participate in the electrochemical and reforming reactions producing electrical work and releasing heat. The anode off-gas is split into two streams at AN-SPLIT. Since anode exhaust contains a high percentage of steam, part of this stream is recycled to mix with the fuel. It is shown that the amount of steam generated in the electrochemical reaction of hydrogen is twice as much as is required for the reforming process (Achenbach, 1994). The user-defined steam-to-carbon ratio determines anode recirculation flow rate to provide steam for the fuel reforming reactions. The anode exhaust recirculation flow rate depends on the desired steam-to-carbon ratio, molar flow rate of carbon contents in the inlet fuel, and molar flow rate of steam in the anode exhaust stream and is calculated by the following equation:

$$\text{Recirculation ratio} = \text{SCR} \times \frac{\dot{n}_{\text{C},\text{fuel}}}{\dot{n}_{\text{H}_2\text{O},\text{anode-out}}} \quad (60)$$

where SCR is the steam-to-carbon ratio,  $\dot{n}_{C,fuel}$  is the molar flow rate of carbon entering the reformer as fuel, and  $\dot{n}_{H_2O,anode-out}$  is the molar flow rate of steam in the anode exhaust stream. Van herle et al. (2004) showed that at the operating temperature of 800°C, the SCR equal to 0.37 is theoretically sufficient to avoid carbon formation, and at the ratio of 1.3, theoretically, there is no carbon formation at any temperature. They used SCR=0.5 for their model. However, various steam-to-carbon ratios were used in the literature, mostly higher than 2 (Achenbach, 1994; Hengyong and Stimming, 2004), to avoid carbon formation and to force the reactions to completion (Fuel Cell Handbook, 2004) (with very few exceptions, such as Tanaka et al. (2000) with SCR=1.2), for example: 2 (Calise et al., 2006a, 2007), 2.32 (Harvey and Richter, 1994b), 2.5 (Riensch et al., 1998a; Achenbach, 1994; Palsson et al., 2000; Stiller et al., 2005; Sucipta et al., 2007), and even higher than 3 (Tanaka et al., 2000). For this work, this user-defined constant was considered to be equal to 2. It should be noted that in real systems in order to generate the recirculation flow and to overcome the effect of pressure drop in the system, an additional device, such as an ejector or blower, is required. However, since in this model pressure drop was not considered, such equipment was not required.

The rest of the anode exhaust stream (unrecycled part of AN-OUT) is burnt with the cathode exhaust stream (CAT-OUT) at the GT combustor. The combustor outlet, after passing through AHX2 and FHX2, enters the gas turbine. The turbine inlet temperature (TIT) is a critical parameter in GT operation. The TIT should not exceed a certain limit because of the material's thermal stress limitation. For current small scale gas turbines (< 2 MW), the TIT is usually limited to 1100°C (Tanaka et al., 2000; Chan et al., 2003a). This temperature for the 4.5 MW Mercury advanced gas turbine is 1150°C (Lundberg et al., 2003). However, depending on the GT technology, different values have been suggested and used in the literature, such as 1260°C (Harvey and Richter, 1994b) and even as high as 1300°C (Tanaka et al., 2000). For this model, with a futuristic approach, TIT was considered to be 1400°C but for analyses in the later chapters, it was reduced to 1200°C. In the model, in order to achieve the user-defined TIT, the air-to-fuel ratio of the system was automatically adjusted for constant fuel molar flow rate (similar to Palsson et al. (2000)). Finally, in the cycle, the GT exhaust is used to heat the inlet fuel in AHX and FHX.

As previously noted, the model can simulate two cycle configurations, with anode off-gas recirculation and with heat recovery steam generator (HRSG) to provide steam for the reforming reaction. Thus far, the cycle with anode off-gas recirculation has been explained. By enabling or disabling the anode exhaust recirculation feature, both cycles can be studied. If the anode recycling is disabled; steam provided by the HRSG (WHX) is mixed with the fuel to meet the required the SCR of the fuel reforming reactions (as shown in Figure 31).

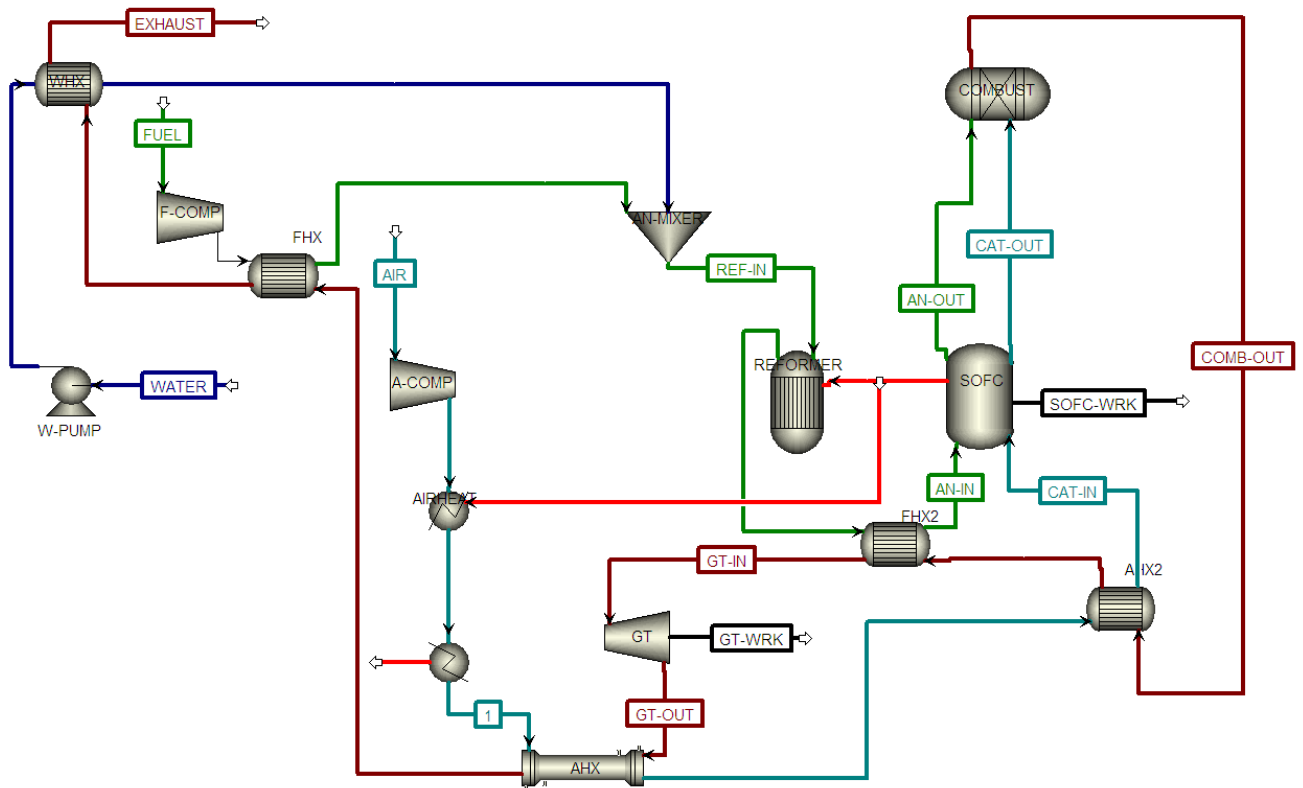


**Figure 31: Actual implemented configuration of the hybrid SOFC-GT cycle model without anode recirculation**

In this case, the HRSG covers the entire steam requirement of the reformer. Otherwise no steam is generated in the HRSG. Similar to the anode exhaust recirculation flow rate, the HRSG flow rate is dependent on the molar flow rate of carbon at the inlet fuel and the user-defined SCR and can be estimated by the following equation:



$$\dot{n}_{\text{H}_2\text{O,HRSG}} = \text{SCR} \times \dot{n}_{\text{C,fuel}} \quad (61)$$

where  $\dot{n}_{\text{H}_2\text{O,HRSG}}$  is the molar flow rate of the water inlet to the heat recovery steam generator. For the calculation of both anode recirculation ratio and the molar flow rate of HRSG inlet water, the steam-to-carbon ratio is a user-defined input.

#### 4.4.2 Input and output parameters

The hybrid SOFC-GT cycle model required several user-specified inputs, which are presented in Table 29. These inputs are directly related to the hybrid cycle performance, and the constants and inputs for the SOFC modeling can be found in Table 27.

It should be noted that some models in the literature used the polytropic efficiencies for the calculation of turbomachinery (such as Harvey and Richter, 1994b; Palsson et al., 2000; Massardo and Lubelli, 2000; Lobachyov and Richter, 1996) while others used the isentropic or adiabatic efficiencies (such as Stiller et al., 2005; Sucipta et al., 2007; Möller et al., 2004; Granovskii et al., 2007a). In this work, like many others in the literature, the isentropic compression model was employed for this purpose. Both isentropic and polytropic efficiencies are used to relate the system's actual work (changes in enthalpy) to the system's isentropic work. Here the system's work refers to the work the system can generate in a turbine or the work the system requires in a compressor. The difference between these two efficiencies is how they treat the isentropic process. In the definition of the isentropic efficiency, the isentropic process is simply defined between the inlet and outlet pressure of the system, while for polytropic efficiency, the process is divided into infinitesimal small processes and the isentropic process is defined for each step. It should be noted that the polytropic efficiency is smaller than the isentropic efficiency, and its calculation is more complicated. The polytropic efficiency is more applicable to actual turbomachinery design. Since in this work, the objective is to develop a thermodynamic model of the cycles, the isentropic efficiency is more suitable (Cunneel et al., 2002). Also, the combustor model was modeled using the built-in Gibbs reactor unit in Aspen Plus<sup>®</sup>. This block minimizes the Gibbs free energy of the inlet streams at equilibrium conditions to determine the outlet streams' compositions (Aspentech, 2010).

**Table 29: Hybrid SOFC-GT model constants**

Parameter	Used value	Range in literature	Units	Reference
SOFC operating temperature	1000	850 - 1000	°C	Stiller et al., 2005; Chan et al., 2003a; Riensche et al., 2000; Lobachyov and Richter, 1996; Kuchonthara et al., 2003a; Kakac et al., 2007
SOFC operating pressure	3	3 - 5	bar	Palsson et al., 2000; Stiller et al., 2005; Massardo and Lubelli, 2000; Cunnell et al., 2002; Riensche et al., 2000; Suciata et al., 2007; Veyo et al., 2002a
SOFC fuel utilization factor	85	80 - 85	%	Harvey and Richter, 1994b; Calise et al., 2007; Möller et al., 2004; Stiller et al., 2005; Chan et al., 2003b; Riensche et al., 2000; Lobachyov and Richter, 1996; Suciata et al., 2007
Inlet fuel temperature	25	Ambient temperature	°C	Harvey and Richter, 1994b; Bolland and Stadaas, 1993
Inlet fuel pressure	1	1	bar	Harvey and Richter, 1994b; Bolland and Stadaas, 1993
Inlet fuel molar flow rate	1	-	kmole /h	-
Inlet air temperature	25	Ambient temperature	°C	-
Inlet air pressure	1	Ambient pressure	bar	-
Inlet air composition	21% O <sub>2</sub> - 79% N <sub>2</sub>	-	-	-
System pressure	3	3 - 5	bar	Palsson et al., 2000; Stiller et al., 2005; Massardo and Lubelli, 2000; Cunnell et al., 2002; Riensche et al., 2000; Suciata et al., 2007; Veyo et al., 2002a
Compressor isentropic efficiency	85	81 - 85	%	Möller et al., 2004; Granovskii et al., 2007a
Pump isentropic efficiency	85	81 - 85	%	Möller et al., 2004; Granovskii et al., 2007a
GT isentropic efficiency	85	84 - 93	%	Möller et al., 2004; Granovskii et al., 2007a
Heat exchanger temperature difference (pinch point)	10	10, 30, 50	°C	Harvey and Richter, 1994b; Palsson et al., 2000; Möller et al., 2004; Stiller et al., 2005; Massardo and Lubelli, 2000
Steam-to-carbon ratio	2	2, 2.3, 2.5	kmole H <sub>2</sub> O / kmole C	Calise et al., 2006a, 2007; Riensche, 1998a, 1998b; Harvey and Richter, 1994b; Stiller et al., 2005
Turbine inlet temperature	1400	1250, 1260, 1300	°C	Calise et al., 2007; Harvey and Richter, 1994b; Van herle et al., 2003

In addition, the built-in equilibrium reactor model was used to model the pre-reformer. In this component's model, the outlet streams' composition is calculated based on the reactions specified by the user and optionally the extent of the reactions.

The hybrid model performance parameters are defined as follows. The net output power of the cycle is equal to the sum of the power generated in the SOFC and GT deducted by the power consumed in the air and fuel compressors and water pump (for the cycle without anode recirculation):

$$\dot{W}_{\text{net}} = \dot{W}_{\text{SOFC}} + \dot{W}_{\text{GT}} - (\dot{W}_{\text{COMP-FUEL}} + \dot{W}_{\text{COMP-AIR}} + \dot{W}_{\text{WPUMP}}) \quad (62)$$

Although output power is an important parameter in a power generation system, it does not indicate any information about the size of equipment and the system as a whole. Therefore, specific work is defined as the output power of the system divided by the inlet air mass flow rate. The specific work can be considered as a representative of the system physical size.

The cycle net efficiency based on the LHV and HHV can be estimated by the following equations, respectively:

$$\eta_{\text{net}} = \frac{\dot{W}_{\text{net}}}{\dot{m}_f \times \text{LHV}} \quad (63)$$

$$\eta_{\text{net}} = \frac{\dot{W}_{\text{net}}}{\dot{m}_f \times \text{HHV}} \quad (64)$$

where  $\dot{m}_f$  is the flow rate of fuel. Also, the air-to-fuel ratio and the SOFC-to-GT power ratio are defined by Equations 65 and 66, respectively:

$$\text{AF} = \frac{\dot{n}_{\text{AIR}}}{\dot{n}_{\text{FUEL}}} \quad (65)$$

$$\psi = \frac{\dot{W}_{\text{SOFC}}}{\dot{W}_{\text{GT}}} \quad (66)$$

where AF refers to the air-to-fuel ratio,  $\dot{n}$  to the molar flow rate of streams, and  $\psi$  to the SOFC-to-GT power ratio. The SOFC-to-total output power ratio is typically around  $2/3$  (Pálsson et al., 2000).

The developed hybrid SOFC-GT model was used to perform several analyses, which will be presented in the following chapters.

## 4.5 Conclusion and future work

In this chapter, a steady-state 0-D macro-level thermodynamic model of the SOFC system was developed in Aspen Plus<sup>®</sup>. It was shown that the developed model can successfully capture the dependency of the SOFC performance on its operating pressure and temperature when the model results were compared with experimental data. Then, the SOFC model was used to create the model of the hybrid SOFC-GT cycle. This model will be used for various analyses in the following chapters.

The following recommendations can improve the SOFC-GT cycle model:

1. As noted in Subsection 4.3.2.1.2, in this model only the hydrogen electrochemical reaction was considered. However, the direct electrochemical reaction of carbon monoxide in the SOFC is well accepted in the SOFC community and is supported by experimental works, though its contribution to the total electricity generation in the stack is not clearly known. As a next step, this reaction should be added to the model. The comparison of the results of the modeling in two cases can provide a significant insight to the system internal operation.
2. As noted in Subsection 4.1, although the 0-D model used in this work is deemed sufficient for the purpose of this research, this approach cannot provide any information about variation of parameters within cells. Particularly, it cannot capture internal peak-temperatures of the cells. Developing a 1-D or higher dimensional model with the same assumptions that takes into account stack geometry and material characteristics, and comparing the results of the different modeling approaches can be a significant contribution to the field, since this type of analysis is lacking in the literature.
3. In order to account for the SOFC heat transfer, a sensitivity analysis should be performed to find a proper value for  $X$  (stream heat factor) introduced in Subsection 4.3.2.4. However, eventually it is more beneficial to include a heat transfer model to take into account the stack characteristics, such as its geometry, material properties, and design.

4. In order to make the SOFC model capable of accepting higher hydrocarbons, a pre-reformer can be included to reform these heavy hydrocarbons and convert them to methane and carbon monoxide:



5. As noted in Subsections 4.3.1 and 4.4, in this model pressure drops within the cycle were neglected because in order to realistically consider pressure losses, some preliminary information about system's physical configurations and its dimensions is required. In this work, the objective was to develop a thermodynamic model of the system. Therefore, the pressure drop of the components is out of the scope of this work. However, for the modified models, the equipment pressure drops should be considered. Table 30 shows some samples of the pressure drop ranges in different components in the literature.

**Table 30: Pressure drops in the system equipment**

Equipment	Pressure drop range	Unit	Reference
Inlet air duct	0.01	bar	Harvey and Richter (1994b), Bolland and Stadaas (1993)
Air filter	0.01	bar	Harvey and Richter (1994b), Bolland and Stadaas (1993)
Shell-and-tube heat exchangers	0.03	bar	Harvey and Richter (1994b), Palsson et al. (2000), Möller et al. (2004), Stiller et al. (2005), Massardo and Lubelli (2000)
	2 - 4	%	
Plate heat exchangers	0.07- 0.1	bar	Harvey and Richter (1994b), Palsson et al. (2000), Möller et al. (2004), Stiller et al. (2005), Massardo and Lubelli (2000)
	2 - 4	%	
SOFC (anode and cathode)	0.01- 0.1	bar	Harvey and Richter (1994b), Palsson et al. (2000), Riensche et al. (1998a), Möller et al. (2004), Stiller et al. (2005), Massardo and Lubelli (2000)
	2	%	
Pre-reformer	2	%	Stiller et al. (2005)
Combustion chamber	2 - 5	%	Harvey and Richter (1994b), Palsson et al. (2000), Stiller et al. (2005), Massardo and Lubelli (2000)
HRSG	0.03	bar	Harvey and Richter (1994b), Massardo and Lubelli (2000), Kuchonthara et al. (2003a)
	2 - 3	%	

6. When the pressure drop of the equipment is considered, the output pressure of the air and fuel compressors and water pump should be adjusted accordingly. Also, in the cycle with

anode recirculation, a device is required to compensate pressure drop of the stream and allow recirculation of the anode off-gas. For this purpose, usually an ejector is used, which also operates as the mixer and pre-reformer.

7. In modern gas turbines, turbine blade cooling technologies are utilized to make the system capable of operating with a higher TIT, which can increase the efficiency and output power of the gas turbine. For this purpose, usually compressor high pressure air is used in most modern gas turbines (Harvey and Richter, 1994b; Bolland and Stadaas, 1993). However, in some systems, the superheated steam generated in the HRSG is used for blade cooling (Harvey and Richter, 1994b). This technology should be added to this model, when high values of TIT are used.
8. The heat losses from equipment can be considered in the model to increase its accuracy. Heat losses of 1% for turbines (Harvey and Richter, 1994b) and 2% for HRSG (Lobachyov and Richter, 1996) have been used in the literature.
9. Some other components can be added to the model to increase the similarity of the model to a real world industrial system, such as an AC/DC inverter and electric generator with efficiency between 93%-95% (Möller et al., 2004; Tanaka et al., 2000). Furthermore, addition of some detailed information of the components can increase the accuracy of the model results. For instance, some models in the literature used mechanical efficiency between 99.5% and 99.7% (Möller et al., 2004; Massardo and Lubelli, 2000) for turbomachinery models.

## **CHAPTER FIVE**

### **Performance of Methane Fuelled Hybrid SOFC-GT Cycle**

In the first part of this chapter, all important properties, such as temperature; pressure; mass, specific volume, and molar flow rates; and composition of all major streams in the methane fuelled hybrid SOFC-GT cycle are investigated for two configurations: cycle with and without anode recirculation. In addition, operational conditions, like output power, specific work, efficiency, and heat duty of all equipment, such as SOFC stack, GT, fuel reformer, compressors, heat exchangers, and pump are evaluated. This analysis can help in better understanding of the hybrid SOFC-GT cycle inner workings.

In the second part of this chapter, the effects of design and operational parameters on the performance of the system are evaluated through a parametric analysis. In order to perform this analysis, the system performance is evaluated by monitoring parameters such as the specific work of the SOFC, GT, and system as a whole; SOFC-to-GT work ratio; and cycle efficiency, while varying system operating parameters such as the SOFC operating temperature, fuel utilization factor, current density; system operating pressure; TIT; and isentropic efficiency of the GT and air compressor.

#### **5.1 Variation of operational parameters throughout the cycle in the methane fuelled hybrid SOFC-GT system**

In this subsection, the model described in Chapter 4 was applied to observe the performance parameters of the hybrid SOFC-GT cycle with two configurations, with and without anode recirculation, when the system was fuelled by methane. Pure methane was chosen as the fuel to facilitate understanding of the processes. In Chapter 6, the effects of more realistic fuels on the

performance of the cycle will be investigated. The SOFC and hybrid system constants presented in Tables 27 and 29 were used for this analysis, except for the TIT which was equal to 1200°C. In order to monitor the performance of the system, stream parameters such as temperature, pressure, flow rate (mass, volume, and molar), and composition of flows were considered. For the equipment, their characteristics, such as power, specific work, efficiency, and heat duty were investigated.

To explain the inner working of the system, the air and fuel flows are followed and all major processes are investigated (Tables 31 and 32). Figure 32, similar to Figure 28, illustrates the configuration of the cycle under investigation. In this figure, the streams are numbered to facilitate explanation. Discussion is first presented for the cycle with anode recirculation. Then, major differences for the cycle without anode recirculation are explained. Tables 33 and 34 show the power, specific work, and efficiency of mechanical systems, i.e. gas turbine and compressors, for cycles with and without anode recirculation, respectively. Also, the heat duty of various heat exchangers can be seen in Table 35 for both configurations.

In order to explain the system with anode recirculation, the fuel flow is followed first. Fixed amount of fuel (1 kmole/h), stream 6, enters the cycle at STP and is pressurized at the fuel compressor to 3 bar. The mass flow rate, temperature, and pressure of the inlet fuel before entering the compressor are 16 kg/h, 25°C, and 1 bar, respectively. Also, the lower and higher heating values of the fuel are 50,030 and 55,515 kJ/kg, respectively. The power required for this compression is equal to 1 kW at 85% isentropic efficiency, and the temperature of the stream at the outlet of the fuel compressor is 121°C. The stream 7 is heated at the heat exchanger (FHX), and its temperature increases to 345°C. The heat duty of this heat exchanger is 2.9 kW.

The stream 8 then mixes with the recycled part of the anode exhaust (stream 14) before entering the reformer. Since the anode exhaust contains a high concentration of steam, part of this stream can be recycled to mix with the fuel and provide required steam for methane reforming and the water-gas shift reactions. The mass flow rate of the anode exhaust recirculation is 86 kg/h, and its temperature is 1000°C. Stream 14 contains 2.1 kmole/h of steam. Since in this configuration all required steam comes from anode recirculation, the flow rate of external water at streams 22, 23, and 24 is zero. The mass flow rate of stream 9, which is equal to the flow rate of the SOFC anode inlet, is 102 kg/h, and its temperature is 813°C.





kg/h, and the molar flow rate of steam increases from 1.5 to 3.7 kmole/h. Similarly, the molar flow rate of carbon dioxide increases from 0.3 to 1.3 kmole/h. In the meantime, the molar flow rate of hydrogen and carbon monoxide decreases from 3.1 to 0.8 kmole/h and from 1.9 to 1.0 kmole/h, respectively. The SOFC anode exhaust is then divided into two streams. One part is recycled to the reformer to provide required steam for the reactions; the other part is fed to the combustor. As noted, the concentration of  $H_2$  and CO at the anode exhaust is considerable. Therefore, in stream 13 there is some unused hydrogen and carbon monoxide (0.4 kmole/h for each of  $H_2$  and CO), which can be combusted to increase temperature of the stream before it is fed to the gas turbine. In fact, the LHV of the flow before and after the SOFC are 12,627 and 3,074 kJ/kg, respectively.

The inlet air enters the system (stream 1) at STP with the mass flow rate of 656 kg/h. The air pressure is increased to 3 bar at the compressor by consuming 20.8 kW power at the isentropic efficiency of 85%. Then, the air is heated by the heat transferred from the reformer (unused heat from the SOFC) in AIR HEAT. All of this heat (21 kW) is used to increase the temperature of air from 153°C after the compressor to 283°C, and there is nothing left to be discharged to the atmosphere. Furthermore, the air stream temperature needs to be increased to the operating temperature of the SOFC. Therefore, it is further heated in AHX and AHX2 by the GT discharge stream and the outlet of the combustor, respectively. The air stream temperature rises to 913°C and 1000°C at streams 3 and 4, respectively. The heat duties of AHX and AHX2 are 111 and 16 kW, respectively. The air stream is then fed to the SOFC at the cathode inlet. Some of oxygen in the air flow participates in the SOFC reactions (1.6 kmole/h); therefore, the molar flow rate of air reduces from 19.6 to 18 kmole/h. The cathode exhaust is then fed to the combustor, where it mixes with the anode exhaust stream. This mixture is combusted in the combustor, and the temperature of combustion products increases to 1275°C. It is assumed that all  $H_2$  and CO are burnt, and the combustor outlet only consists of  $H_2O$ ,  $CO_2$ ,  $O_2$ , and  $N_2$ . The mass flow rate of the combustor outlet stream is 581 kg/h.

**Table 31: Properties of streams in the hybrid SOFC-GT system with anode recirculation fuelled by methane**

	1	2	3	4	5	6	7	8	9	10	11	12	13	14	15	16	17	18	19	20	21
Temperature(°C)	25	283	913	1000	1000	25	121	345	813	1000	1000	1000	1000	1000	1275	1200	1200	923	355	339	339
Pressure (bar)	1	3	3	3	3	1	3	3	3	3	3	3	3	3	3	3	3	1	1	1	1
Molar flow (kmole/h)	19.6	19.6	19.6	19.6	18.0	1.0	1.0	1.0	4.8	6.8	6.8	6.8	3.0	3.8	20.6	20.6	20.6	20.6	20.6	20.6	20.6
Mass flow (kg/h)	565	565	565	565	514	16	16	16	102	102	102	154	68	86	581	581	581	581	581	581	581
Volume flow (m <sup>3</sup> /h)	485	302	645	692	635	25	11	17	145	240	241	241	106	135	884	841	841	2049	1076	1048	1048
Molar flow (kmole/h)	H <sub>2</sub> O	0.0	0.0	0.0	0.0	0.0	0.0	0.0	0.0	2.1	1.5	1.5	3.7	1.6	2.1	2.0	2.0	2.0	2.0	2.0	2.0
	CO	0.0	0.0	0.0	0.0	0.0	0.0	0.0	0.0	0.6	1.9	1.9	1.0	0.4	0.6	0.0	0.0	0.0	0.0	0.0	0.0
	CO <sub>2</sub>	0.0	0.0	0.0	0.0	0.0	0.0	0.0	0.0	0.7	0.3	0.3	1.3	0.6	0.7	1.0	1.0	1.0	1.0	1.0	1.0
	CH <sub>4</sub>	0.0	0.0	0.0	0.0	0.0	1.0	1.0	1.0	1.0	0.0	0.0	0.0	0.0	0.0	0.0	0.0	0.0	0.0	0.0	0.0
	H <sub>2</sub>	0.0	0.0	0.0	0.0	0.0	0.0	0.0	0.0	0.5	3.1	3.1	0.8	0.4	0.5	0.0	0.0	0.0	0.0	0.0	0.0
	N <sub>2</sub>	15.5	15.5	15.5	15.5	15.5	0.0	0.0	0.0	0.0	0.0	0.0	0.0	0.0	0.0	15.5	15.5	15.5	15.5	15.5	15.5
	O <sub>2</sub>	4.1	4.1	4.1	4.1	2.5	0.0	0.0	0.0	0.0	0.0	0.0	0.0	0.0	0.0	2.1	2.1	2.1	2.1	2.1	2.1

**Table 32: Properties of streams in the hybrid SOFC-GT system without anode recirculation**

	1	2	3	4	5	6	7	8	9	10	11	12	15	16	17	18	19	20	21	22	23	24
Temperature(°C)	25	153	915	1000	1000	25	121	278	273	717	1000	1000	1314	1246	1200	925	288	280	151	25	25	270
Pressure (bar)	1	3	3	3	3	1	3	3	3	3	3	3	3	3	3	1	1	1	1	1	3	3
Molar flow (kmole/h)	25.3	25.3	25.3	25.3	24.0	1.0	1.0	1.0	3.1	4.7	4.7	5.1	28.4	28.4	28.4	28.4	28.4	28.4	28.4	2.1	2.1	2.1
Mass flow (kg/h)	731	731	731	731	688	16	16	16	54	54	54	98	785	785	785	785	785	785	785	38	38	38
Volume flow (m <sup>3</sup> /h)	628	300	836	895	847	25	11	15	47	129	166	180	1252	1199	1162	2836	1328	1309	1004	0	0	31
Molar flow (kmole/h)	H <sub>2</sub> O	0.0	0.0	0.0	0.0	0.0	0.0	0.0	0.0	2.1	1.0	1.0	3.4	4.1	4.1	4.1	4.1	4.1	4.1	2.1	2.1	2.1
	CO	0.0	0.0	0.0	0.0	0.0	0.0	0.0	0.0	0.0	0.5	0.5	0.6	0.0	0.0	0.0	0.0	0.0	0.0	0.0	0.0	0.0
	CO <sub>2</sub>	0.0	0.0	0.0	0.0	0.0	0.0	0.0	0.0	0.0	0.3	0.3	0.4	1.0	1.0	1.0	1.0	1.0	1.0	0.0	0.0	0.0
	CH <sub>4</sub>	0.0	0.0	0.0	0.0	0.0	1.0	1.0	1.0	1.0	0.2	0.2	0.0	0.0	0.0	0.0	0.0	0.0	0.0	0.0	0.0	0.0
	H <sub>2</sub>	0.0	0.0	0.0	0.0	0.0	0.0	0.0	0.0	0.0	2.7	2.7	0.7	0.0	0.0	0.0	0.0	0.0	0.0	0.0	0.0	0.0
	N <sub>2</sub>	20.0	20.0	20.0	20.0	20.0	0.0	0.0	0.0	0.0	0.0	0.0	20.0	20.0	20.0	20.0	20.0	20.0	20.0	0.0	0.0	0.0
	O <sub>2</sub>	5.3	5.3	5.3	5.3	4.0	0.0	0.0	0.0	0.0	0.0	0.0	3.3	3.3	3.3	3.3	3.3	3.3	3.3	0.0	0.0	0.0

The combustor exhaust is used to increase the air temperature at AHX2 and if necessary the reformat at FHX2, which is not needed in this case, before being fed to the GT. For this analysis, the turbine inlet temperature (TIT) is fixed at 1200°C. The output power generated in the GT is 57.9 kW at the isentropic efficiency of 85%. The flow exits the GT at a temperature of 923°C and pressure of 1 bar. This stream heats the air stream at AHX and fuel at FHX, and its temperature reduces to 355°C and 339°C, respectively. Eventually the exhaust is discharged to the atmosphere at a temperature of 339°C.

The net output power of the cycle can be estimated by deducting the power consumed at the air and fuel compressors from the power generated at the SOFC and GT. In this case, the net output power is 166.3 kW at a total efficiency of 74.6%. The cycle's net specific work is 1059 kJ/kg<sub>air</sub>. The specific work of other equipment is presented in Table 33.

Table 32 shows the streams' information for the cycle without anode recirculation. Since most of the processes in both configurations are similar, only main differences between the two cycles are highlighted.

**Table 33: Power, specific work, and efficiency of mechanical systems in the hybrid SOFC-GT system with anode recirculation**

Equipment	Power (kW)	Specific work (kJ/kg <sub>air</sub> )	Efficiency (%)
Air compressor	20.5	130.4	85
Fuel compressor	1.0	6.4	85
Water pump	-	-	-
SOFC	129.9	827.1	58.2
GT	57.9	369.0	85
Total/net	166.3	1059.4	74.6

In the cycle without anode recirculation, the anode recirculation flow rate is zero, and that is why in Table 33 streams 13 and 14 are removed from Table 32 and streams 22, 23, and 24 are added. Instead, all required steam for the methane reforming and water-gas shift reaction are provided by the external water resource. For this purpose, 38 kg/h of water enters the system and is

pressurized in the water pump by consuming 0.002 kW power. Then, the water is boiled at WHX by the GT exhaust stream, and its temperature increases to 270°C before mixing with the fuel. The heat duty of this heat exchanger is 32 kW. As Tables 31 and 32 show, the water molar flow rate of both inlet water in the cycle without anode recirculation and the anode exhaust recycled stream in the cycle with anode recirculation is equal to 2.1 kmole/h. The reason is that, with the SCR equal to 2.1, for 1 kmole/h of the inlet fuel (for both configurations), 2.1 kmole/h of steam is required, regardless of where the source of the water is.

Using external water or anode recirculation to provide required steam causes considerable differences between two configurations. For instance, comparison of the GT output power in Tables 33 and 34 shows that the output power of the GT in the configuration without anode recirculation is higher than that in the configuration with anode recirculation (80 kW vs. 58 kW, respectively). The reason is when the SOFC exhaust is partially recycled before entering the GT, the actual mass flow rate of the GT (stream 17) reduces from 785 kg/h in the cycle without anode recirculation to 581 kg/h in the cycle with anode recirculation. Therefore, there is less power generated in the GT.

**Table 34: Power, specific work, and efficiency of mechanical systems in the hybrid SOFC-GT system without anode recirculation**

Equipment	Power (kW)	Specific work (kJ/kg <sub>air</sub> )	Efficiency (%)
Air compressor	26.5	130.4	85.0
Fuel compressor	1.0	5.0	85.0
Water pump	0.002	0.01	85.0
SOFC	112.1	551.9	50.3
GT	80.1	394.5	85.0
Total/net	164.7	811.0	73.9

On the other hand, the output power of the SOFC in the configuration with anode recirculation is higher than that in the configuration without anode recirculation (130 kW vs. 112 kW, respectively). When the anode exhaust is recycled, the overall net fuel utilization factor is higher even though the fuel utilization efficiency of the fuel cell is constant. The reason is that some of

the unused fuel in the recycled anode exhaust stream is consumed in the fuel cell. This can be seen in the molar flow rate of  $H_2$  in the anode outlet stream that enters the combustion chamber, where the  $H_2$  concentration in the system with anode recirculation is lower than that in the system without anode recirculation (0.4 kmole/h vs. 0.7 kmole/h, respectively). This means more hydrogen is consumed in the SOFC in the cycle with anode recirculation, which in turn confirms that the net fuel utilization factor of the SOFC is higher in the configuration with anode recirculation. This is also the reason for the higher efficiency of the SOFC in the cycle with anode recirculation in comparison to the cycle without anode recirculation (58.2% vs. 50.3%, respectively).

In addition, the total output power of the system in the configuration with anode recirculation is 166 kW, which is very close to the total output power of the configuration without anode recirculation at 165 kW. This is because of the fact that output power reduction in the GT, due to the anode exhaust recirculation, is mostly compensated by power increase in the SOFC.

Although the physical configuration of the cycle in two systems is identical, the actual configuration (the components that actually take part in the processes) is different. For instance, Table 35 shows that the heat duty of FHX2 for the cycles with and without anode recirculation is 0 and 14 kW, respectively. On the other hand, the heat duty of AIR HEAT is 21 kW and 0, respectively. The reason for this behaviour is that in the cycle with anode recirculation, the anode recycled stream mixes with the fuel, and thus temperature of the reformer inlet (stream 9) increases to 813°C. This temperature for the cycle without anode recirculation is 273°C. Therefore, for the cycle without anode recirculation, all the heat that is transferred from the SOFC to the reformer is consumed and nothing remains for AIR HEAT. On the other hand, even with all heat transfer from the SOFC, the temperature of the reformer outlet (stream 10) is 717°C, which is lower than the SOFC operating temperature. Thus, this stream should be further heated in FHX2, so that its temperature is increased to 1000°C. In contrast, in the cycle with anode recirculation, due to the high temperature of the reformer inlet, part of the heat transferred from the SOFC is enough to increase the temperature of the reformer outlet to 1000°C and the remaining heat (21 kW) is transferred to AIR HEAT. Also, there is no need for heating in FHX2, so the heat duty of this heat exchanger is zero.

Another difference of the two configurations is in their exhaust stream temperature. This temperature for the cycle with and without anode recirculation is 339°C and 151°C, respectively. The reason is that in the cycle without anode recirculation, the exhaust stream is used to generate steam in WHX. This means in the cycle without anode recirculation, the sensible waste energy in the exhaust stream is lower.

**Table 35: Heat duty of heat exchangers in the hybrid SOFC-GT system (both configurations)**

Heat exchanger	Cycle with anode recirculation (kW)	Cycle without anode recirculation (kW)
<b>Air Heat</b>	21	0
<b>AHX</b>	111	171
<b>AHX2</b>	16	20
<b>SOFC</b>	100	65
<b>Reformer</b>	79	65
<b>FHX</b>	2.9	2
<b>FHX2</b>	0	14
<b>WHX</b>	0	32

The comparison of Tables 31 and 32 shows that the air mass flow rate of the cycle in the configuration without anode recirculation is higher than that in the cycle with anode recirculation (731 vs. 565 kg/h, respectively). In order to explain this behaviour, first, the control strategy of the model should be reemphasized. In this model, to keep the TIT constant, the fuel molar flow rate is maintained at 1 kmole/h, and accordingly the air flow rate is manipulated. That means when the energy content of the anode outlet stream changes, the available heat for combustion in the GT combustor also changes. Therefore, in order to keep the TIT constant, the air-to-fuel ratio and as a consequence, the air flow rate has to be adjusted. In this cycle, the LHV, mass flow rate, and energy content of the combustor inlet stream for the cycle with anode recirculation are 3,074 kJ/kg, 67.5 kg/h, and 57.6 kW, respectively, and for the cycle without anode recirculation are 3,378 kJ/kg, 97.6 kg/h, and 91.6 kW, respectively. Due to this much higher energy content of the combustor inlet stream in the cycle without anode recirculation, to keep the TIT at 1200°C, the air-to-fuel ratio of this configuration should be higher than that of the other one (25.3 for the

configuration without anode recirculation vs. 19.6 for the other configuration), which causes a higher inlet air mass flow rate.

The comparison of specific work of the SOFC, GT, and cycle as a whole for two configurations (Tables 33 and 34) shows that the SOFC and cycle total specific work are higher in the configuration with anode recirculation. It should be noted that in order to investigate specific work, both the output power and air mass flow rate should be considered. For example, although the net output power of the system as a whole for both configurations is almost equal (about 165 kW), due to the higher air mass flow rate of the cycle without anode recirculation (731 vs. 565 kg/h, respectively), the net specific work is lower in the configuration without anode recirculation (811 vs. 1059 kJ/kg<sub>air</sub>, respectively).

The efficiencies of the cycles are presented in Tables 33 and 34. Since efficiency depends on output power and energy content of consumed fuel to generate this power, these two parameters should be considered to investigate the efficiency. However, in this system since both the LHV of the inlet fuel and fuel mass flow rate for both configurations are equal, energy content of the inlet fuel is the same for both configurations. Thus, the efficiency is only influenced by output power of the cycle. That is why the efficiency of the cycle as a whole is almost equal for both configurations (around 74%).

## **5.2 Parametric analysis of methane fuelled hybrid SOFC-GT cycle**

In this subsection, the parametric analysis of the hybrid SOFC-GT cycle to investigate the effects of various design and operating parameters on the cycle's performance is presented based on the previously explained model, when the system is fuelled with methane. In this analysis, all model constants were according to Tables 27 and 29, except for the parameters under investigation that varied within a range to perform sensitivity analyses.

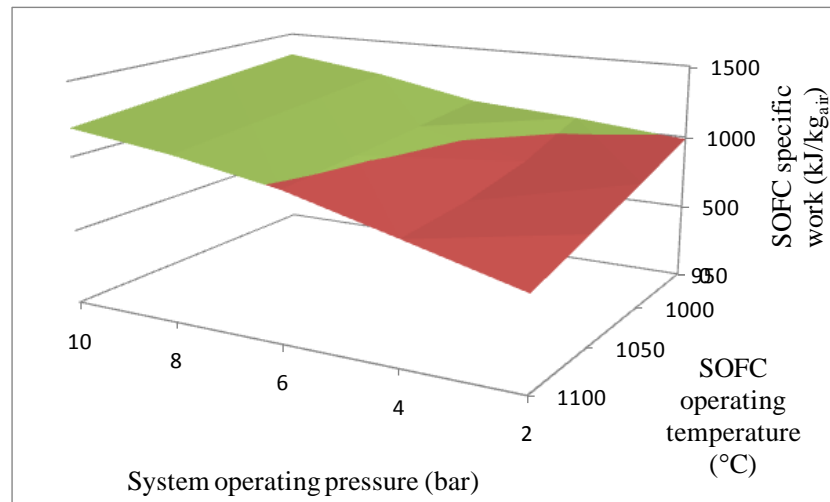
The SOFC operating temperature, fuel utilization factor, current density; system operating pressure; TIT; and isentropic efficiency of the GT and air compressor were investigated as the system operating and design parameters. The system performance was monitored by recording and evaluating the following parameters: specific work of the SOFC, GT, and system as a whole; SOFC-to-GT work ratio; and cycle efficiency (based on the LHV). The results presented in this



subsection are for the cycle without anode recirculation to keep the length of text in a reasonable range. However, as shown in Suther et al. (2010a), the trend of changes in the most of the operating parameters are similar in both configurations, though their quantity can be significantly different.

### 5.2.1 Impacts of system operating pressure and SOFC operating temperature

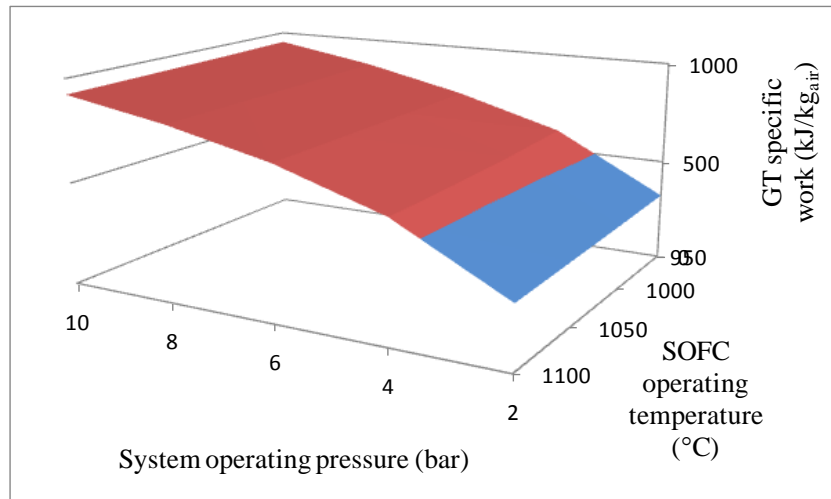
Figures 33a to 33d, 34, and 35 show the variation of the system performance parameters while the system pressure is varied between 2 and 10 bar, and the SOFC operating temperature is varied between 950°C and 1100°C.



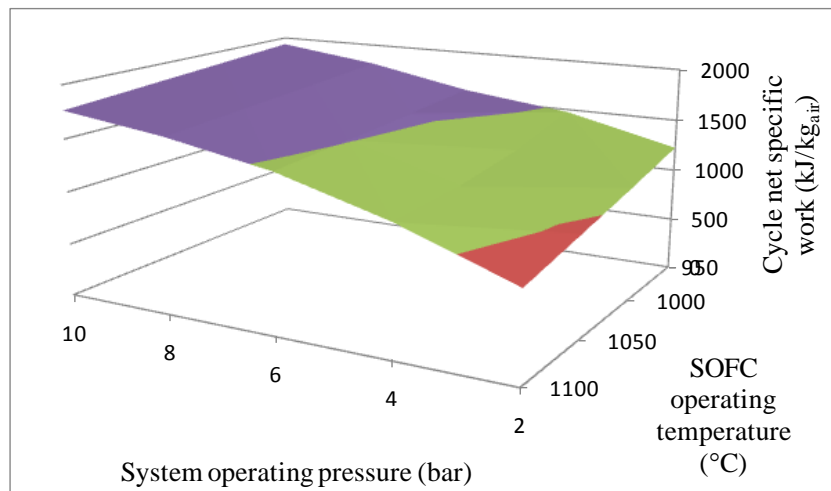
(a)

**Figure 33: Influence of system operating pressure and SOFC operating temperature on specific works**

**a) SOFC specific work**



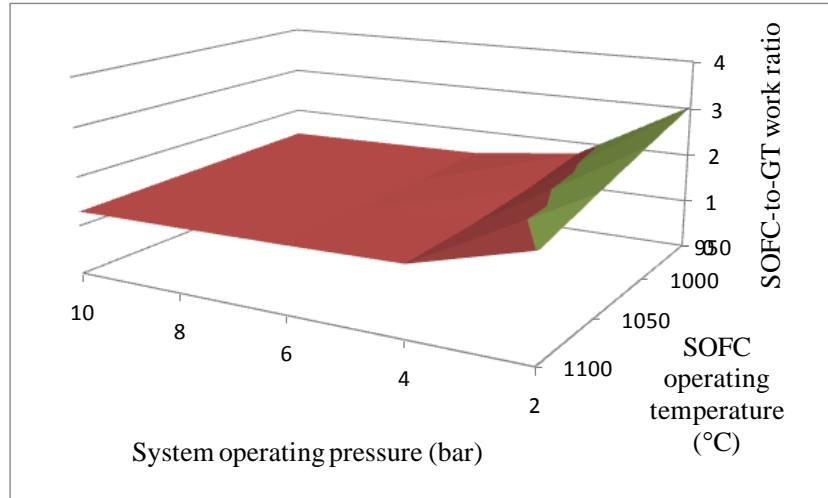
(b)



(c)

**Figure 33: Influence of system operating pressure and SOFC operating temperature on specific works**

**b) GT specific work c) cycle net specific work**



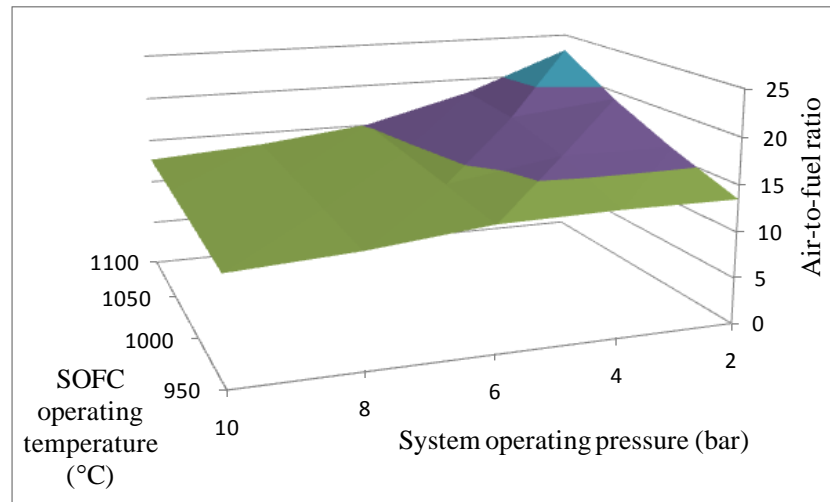
(d)

**Figure 33: Influence of system operating pressure and SOFC operating temperature on specific works a) SOFC specific work b) GT specific work c) cycle net specific work d) SOFC-to-GT work ratio**

As Figures 33a to 33d illustrate, the increase in the system operating pressure improves the performance of both the SOFC and GT and, as a result, the whole cycle by increasing their specific works. This improvement is more significant for the GT at an operating pressure lower than 4 bar. The effect of this improvement in the GT output can be seen in the SOFC-to-GT work ratio, where the ratio is increased remarkably at low pressures. This sharp increase in the specific work at low pressures followed by flattening out at high pressure in the GT is similar to conventional stand-alone gas turbines (El-Wakil, 2002, page 321). Improvement in the SOFC specific work is also expected, as can be seen in Figure 27b, where for a constant current density, an increase in operating pressure results in a higher output voltage, due to increased Nernst potential and decreased polarization. Increasing the pressure of the system can also reduce system size and capital cost due to smaller gas channels. The positive impact of the higher SOFC operating pressure on the system performance has been experimentally proven up to 15 bar (Bevc, 1997).

Figures 33a to 33c show that the specific work of the SOFC and cycle as a whole reduces with increase in the SOFC operating temperature, whereas the specific work of the GT is almost unaffected by this temperature. In order to explain this behaviour, the air-to-fuel ratio should be investigated (Figure 34). As Figure 34 shows, the air-to-fuel ratio increases with increase in the

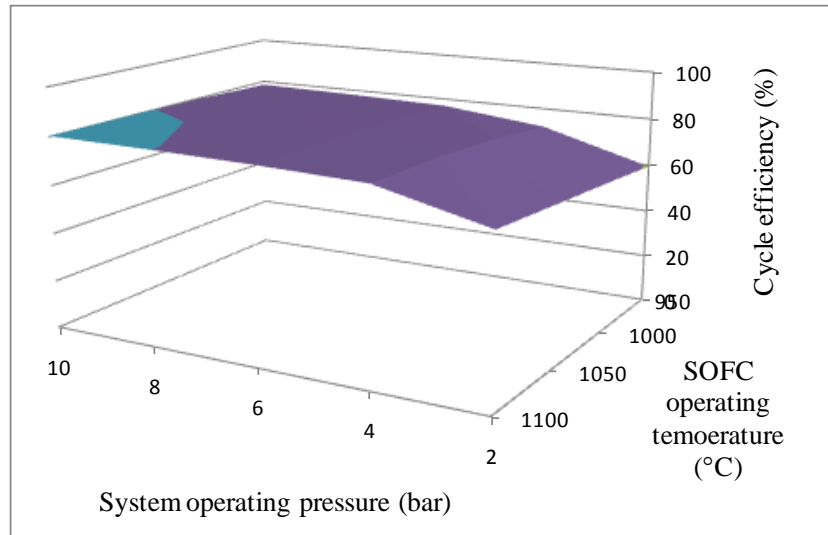
SOFC operating temperature because a higher air flow rate is required in the combustor for a given TIT. This higher air mass flow rate reduces the SOFC specific work. However, the GT output power is directly proportional to the mass flow rate of combustion products from the combustor. Therefore, increase in GT output power cancels out the increase of the air mass flow rate, and so the specific work of the GT is virtually unaffected by the SOFC operating temperature.



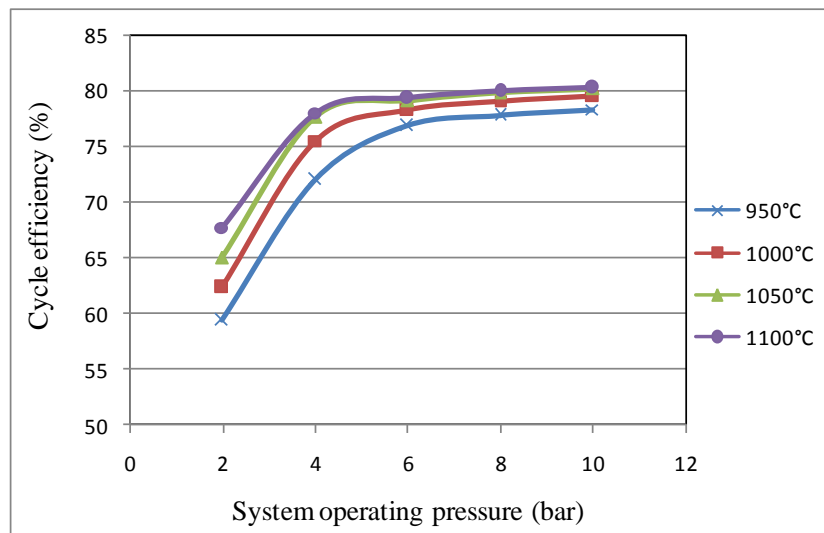
**Figure 34: Influence of system operating pressure and SOFC operating temperature on air-to-fuel ratio**

Figure 35 shows the impacts of variation of the system operating pressure and the SOFC operating temperature on the cycle total efficiency. Due to the importance of this graph and for better illustration, both 3D and 2D graphs are presented. As Figure 35a indicates, increase in both SOFC operating temperature and system operating pressure are beneficial for the efficiency of the cycle. Figure 35b, on the other hand, shows that for a constant temperature, the change in the efficiency is flattened out at high pressures after sharp increase at low pressures. This trend is in agreement with the results presented by Winkler and Lorenz (2002) and Yi et al. (2004). Also, as shown in Figure 12, there is similarity between these results and the results of the modeling presented by Chan et al. (2002a). However, due to the different control strategies used in this work and in Palsson et al. (2000), there is significant discrepancy between results of these two modeling works in terms of the effects of operating pressure of the system on the cycle

performance (compare Figures 11 and 35b). More discussion on this issue can be found in Subsection 3.4.3.



(a)



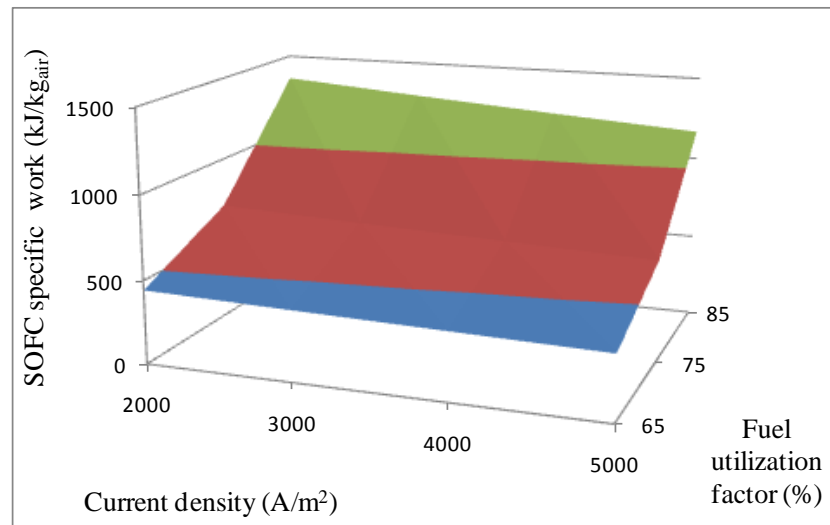
(b)

**Figure 35: Influence of system operating pressure and SOFC operating temperature on cycle total efficiency (based on LHV) a) 3D graph b) 2D graph**

### 5.2.2 Impacts of current density and fuel utilization factor

Figures 36a to 36d and 37 show the variation of the system performance parameters while the SOFC fuel utilization factor is varied between 65% and 80% and the SOFC current density is varied between 2000 and 5000 A/m<sup>2</sup>. The current density of a fuel cell is the magnitude of current drawn from the cell divided by the conductor area. It is important to evaluate this parameter because due to the limited size of a fuel cell, the current density is an indication of cell's total current.

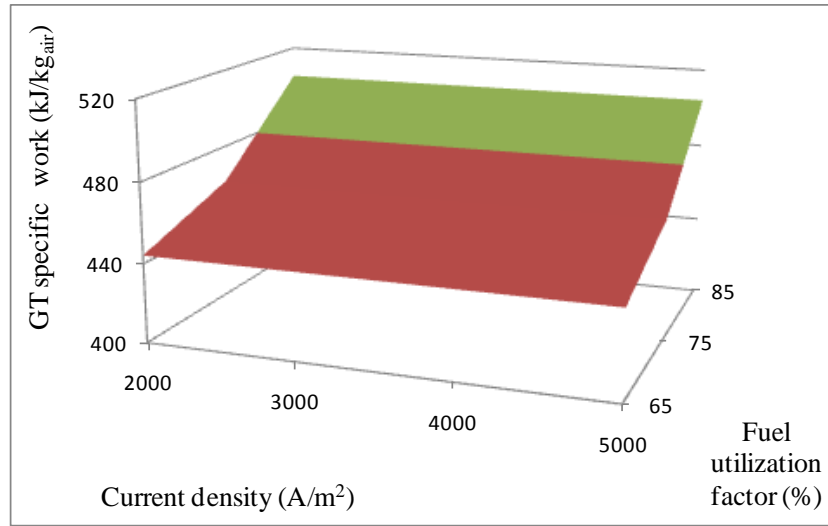
As Figures 36a and 36b illustrate, increasing current density has a negative influence on both the specific work of the SOFC and the cycle as a whole. This can stem from increase in the SOFC overpotentials with increase in the current density. However, the GT specific work remains unaffected by current density. The effect of reduction in the SOFC specific work and the constant GT specific work can be seen on the SOFC-to-GT work ratio (Figure 36d).



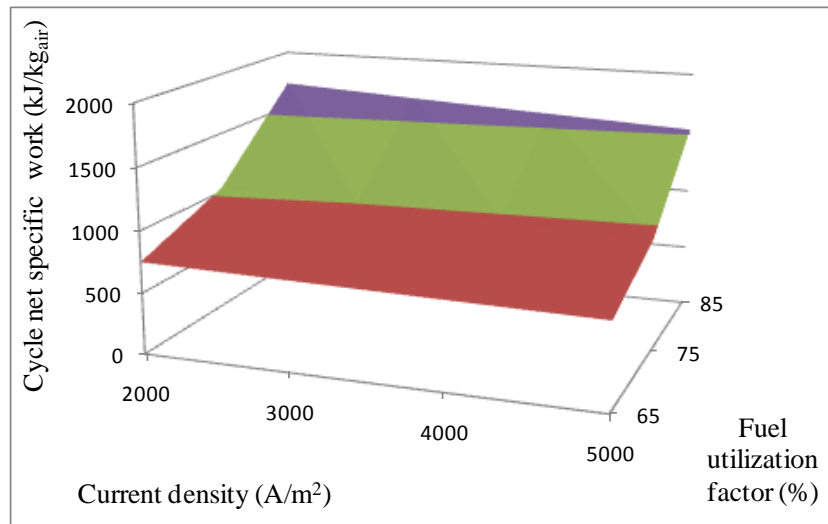
(a)

**Figure 36: Influence of current density and fuel utilization factor on specific works**

**a) SOFC specific work**



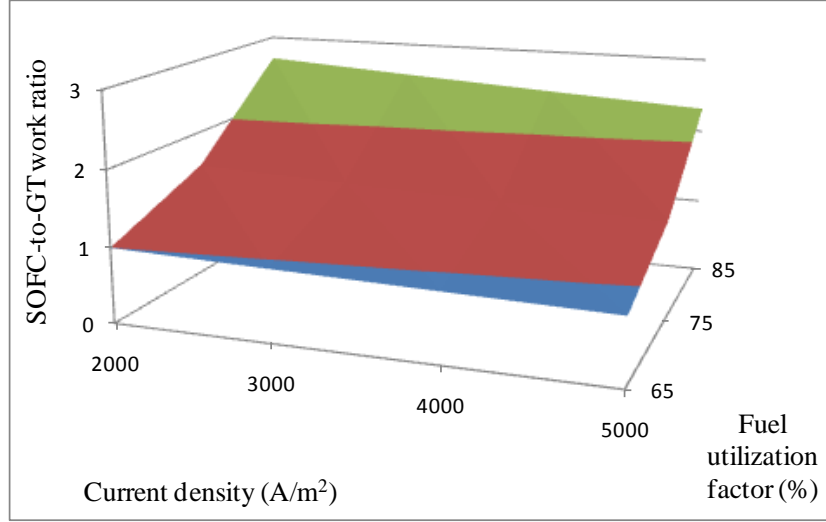
(b)



(c)

**Figure 36: Influence of current density and fuel utilization factor on specific works**

**b) GT specific work c) cycle net specific work**



(d)

**Figure 36: Influence of current density and fuel utilization factor on specific works**

a) SOFC specific work b) GT specific work c) cycle net specific work d) SOFC-to-GT work ratio

Figure 37 shows the influence of the current density and fuel utilization factor on the cycle total efficiency. Increase in current density has a significant negative impact on the cycle efficiency, while the impact of fuel utilization factor is less remarkable. In fact, the direction, positive or negative, and significance of the fuel utilization factor impact on the efficiency of the cycle depends on the isentropic efficiency of the GT (Figure 38).



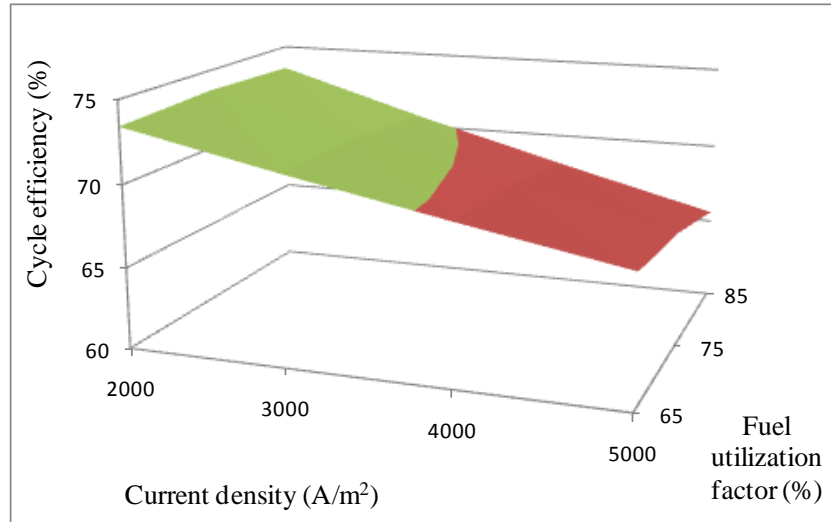


**Figure 37: Influence of current density and fuel utilization factor on cycle efficiency**

Figure 38 illustrates the variation of the cycle efficiency when the fuel utilization factor varies between 65% and 85% and the GT isentropic efficiency, between 60% and 90%. As can be seen in the figure, depending on the GT isentropic efficiency, the effect of the fuel utilization factor on the cycle efficiency can be positive or negative. In order to explain this graph, it should be noted that the fuel utilization factor is the parameter that indicates what percentage of the fuel energy is consumed in the SOFC and thus in the GT. The lower fuel utilization factor means that more fuel energy is consumed in the GT. At lower GT isentropic efficiency, since the efficiency of energy conversion in the GT is lower than that of the SOFC, increasing the fuel utilization factor increases the cycle efficiency. At high GT efficiency, however, the impact of increasing the fuel utilization factor is not favourable because more power is generated in the device that has lower efficiency, i.e. the SOFC. These results support the findings reported by Calise et al. (2006b). They reported that in an SOFC-GT cycle with no anode recirculation, increasing the fuel utilization factor slightly improved the cycle efficiency, when the isentropic efficiency of the GT was 80%.

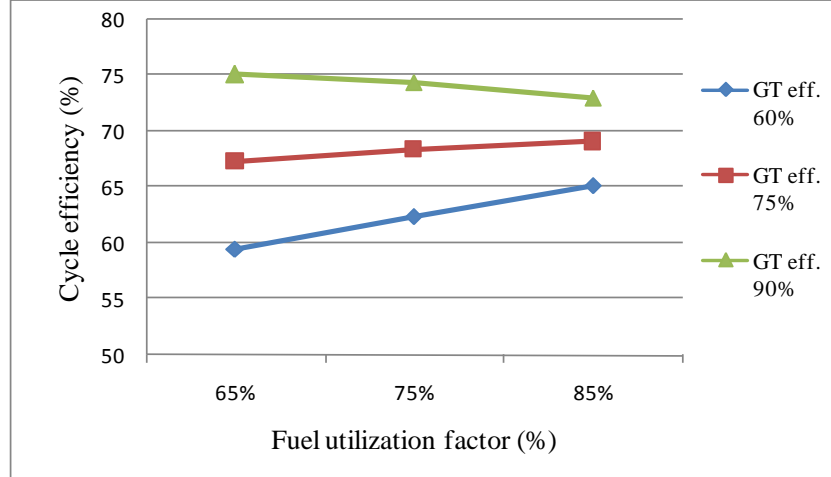


**Figure 38: Influence of current density and GT isentropic efficiency on cycle efficiency**

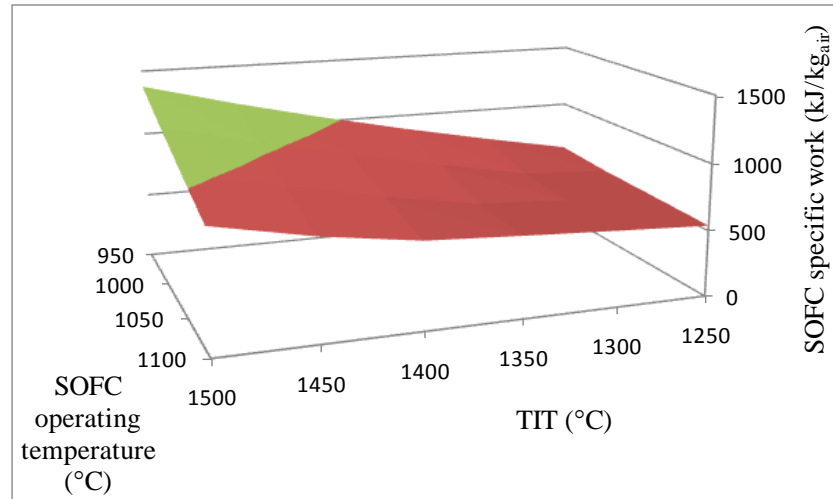
### 5.2.3 Impacts of TIT and SOFC operating temperature

Figures 39a to 39d illustrate the influences of the TIT and SOFC operating temperature on the performance of the SOFC-GT cycle. An increase in the TIT can improve the specific work of the SOFC, GT, and cycle as a whole. However, the effect on the efficiency of the cycle is not favourable (Figure 40). A higher TIT requires more energy per unit flow in the combustor, which can be achieved with a lower air-to-fuel ratio.

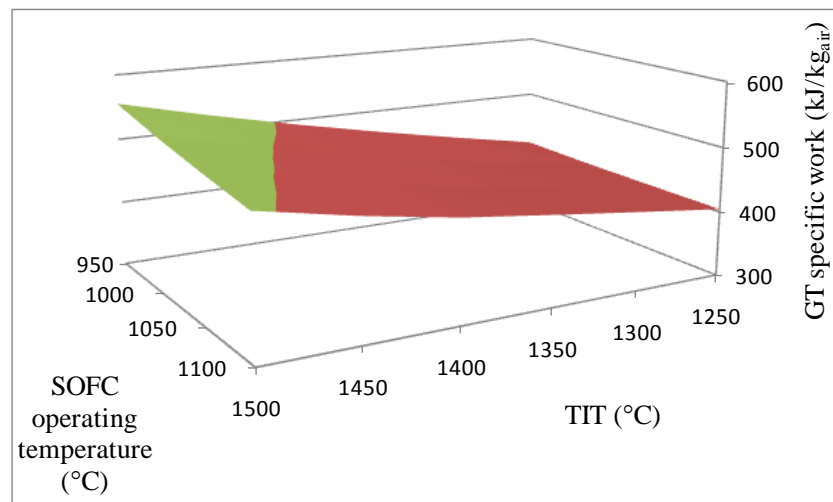
### 5.2.4 Impacts of isentropic efficiency of GT and isentropic efficiency of air compressor

Figures 41a to 41d and 42 show the effect of the turbine and air compressor isentropic efficiencies on the specific work of the SOFC and GT, the net specific work of the cycle, and the cycle efficiency. The effects are studied for the entire range from 50% to 100% for both turbine and air compressor isentropic efficiencies. As expected, while the specific work of the SOFC remains unchanged, the specific work of the GT is significantly improved with an increase in the isentropic efficiency of the GT. This effect can be observed in Figure 41d where the SOFC-to-GT work ratio reduces with increase in the GT efficiency. On the other hand, increasing the air compressor isentropic efficiency reduces work required by the compressor; therefore, an increase in both GT and compressor efficiencies has a positive impact on the cycle net specific work, the

efficiency of the GT having a more significant effect (Figure 41c). Similar behaviour can be seen for the cycle efficiency in Figure 42.



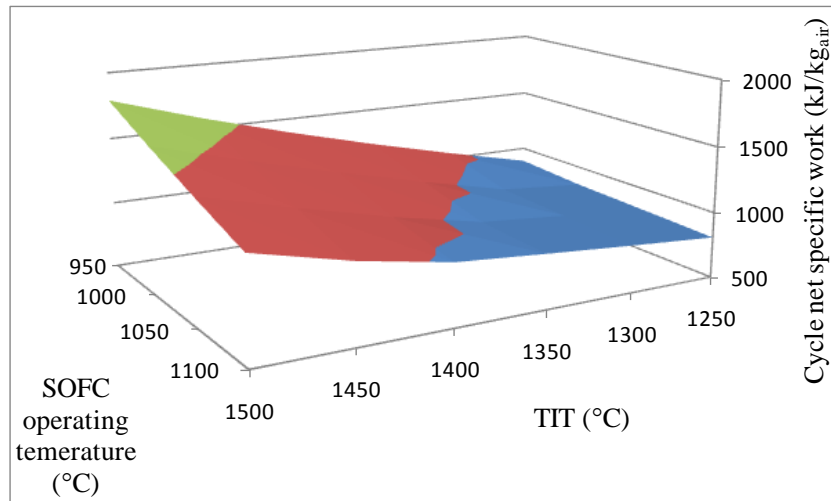
(a)



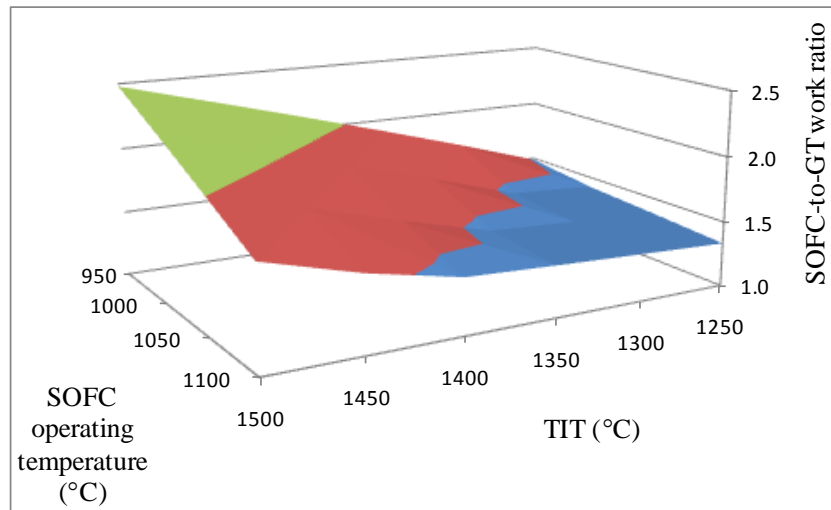
(b)

**Figure 39: Influence of TIT and SOFC operating temperature on specific works**

**a) SOFC specific work b) GT specific work**



(c)



(d)

**Figure 39: Influence of TIT and SOFC operating temperature on specific works**

**a) SOFC specific work b) GT specific work c) cycle net specific work d) SOFC-to-GT work ratio**

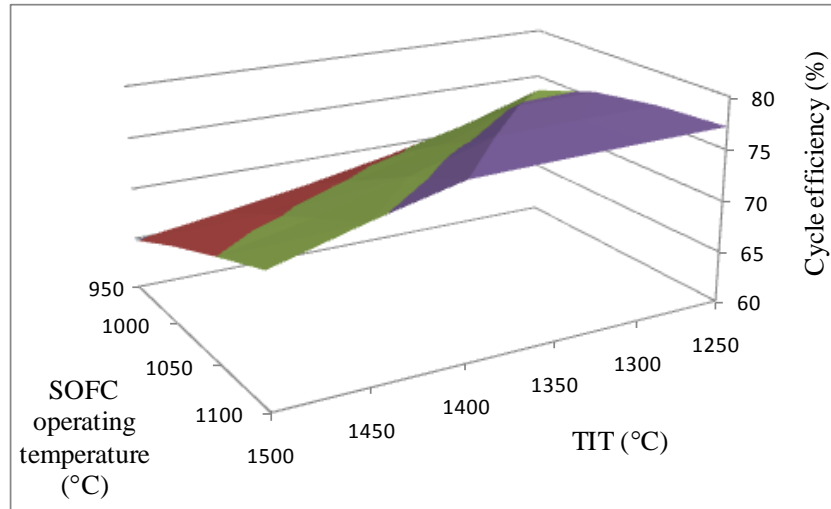
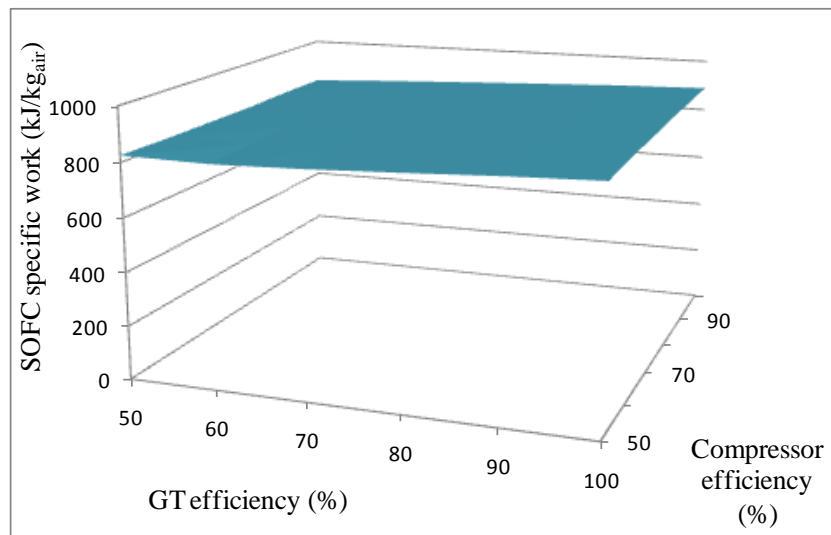


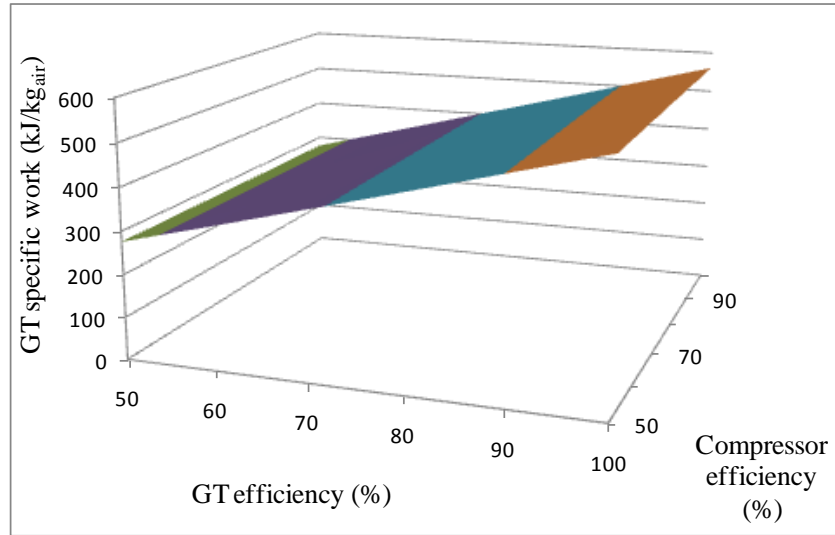
**Figure 40: Influence of TIT and SOFC operating temperature on cycle efficiency**



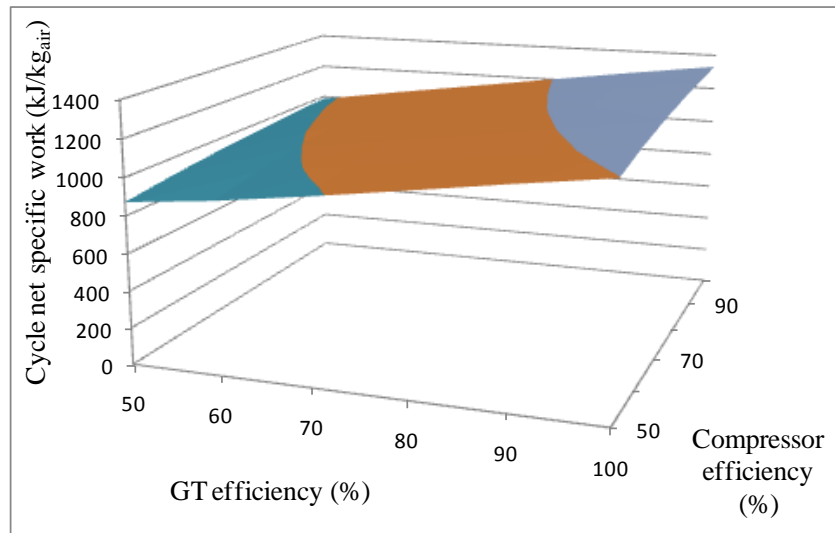
(a)

**Figure 41: Influence of isentropic efficiency of GT and air compressor on specific works**

a) SOFC specific work

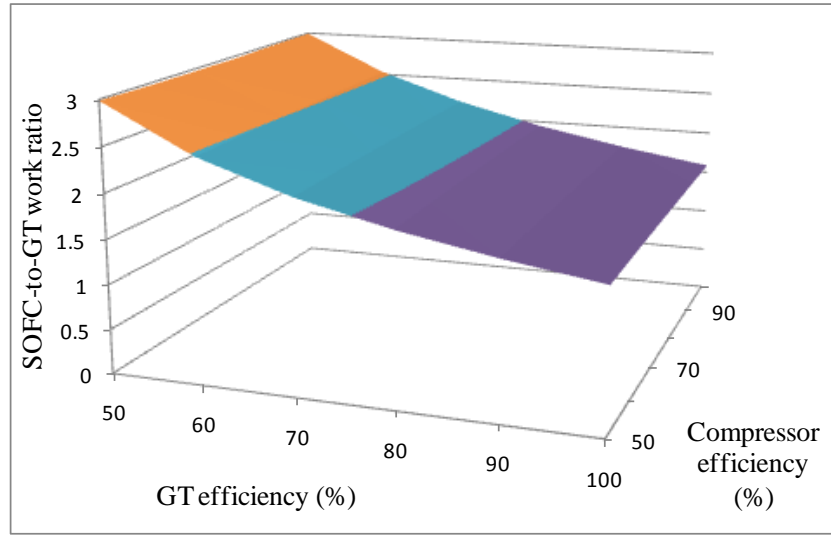


(b)



(c)

**Figure 41: Influence of isentropic efficiency of GT and air compressor on specific works**  
**b) GT specific work c) cycle net specific work**



(d)

**Figure 41: Influence of isentropic efficiency of GT and air compressor on specific works**

a) SOFC specific work b) GT specific work c) cycle net specific work d) SOFC-to-GT work ratio

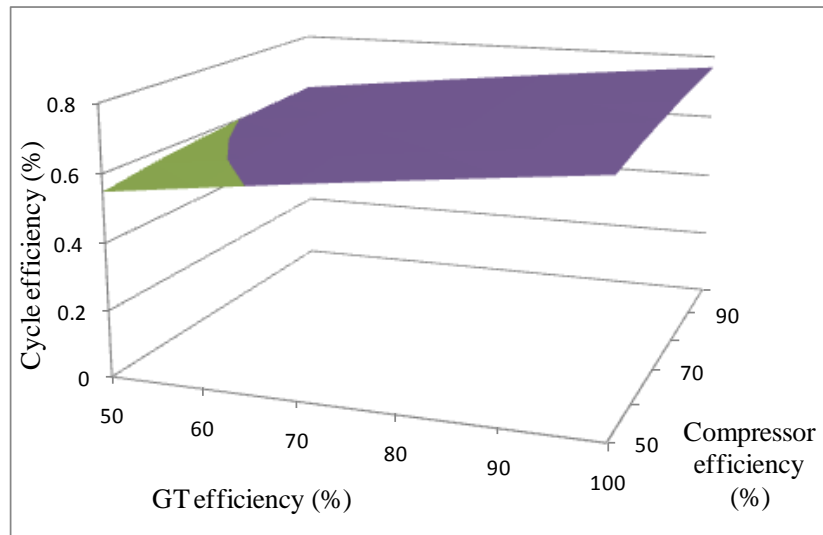


**Figure 42: Influence of isentropic efficiency of GT and air compressor on cycle efficiency**

### 5.3 Conclusion and future work

At the beginning of this chapter, the results of the simulation of the methane fuelled hybrid SOFC-GT cycle were employed to explain the variation of the stream properties throughout the

cycle. Moreover, the operating conditions of the equipment were presented. This analysis can be very helpful to understand cycle internal working. In addition, the comparison of the characteristics of the system when it was operated with two different schemes to provide required steam for the cycle (with anode recirculation and with an external source of water) provided some interesting insight to the system operation. For instance, it was shown that although the physical configuration of the cycle in two systems is the same, the actual configuration (the equipment actually taking part in the process) can be different.

In the second part of the chapter, sensitivity analyses were performed to investigate the influence of operating and design parameters on the performance of the methane fuelled hybrid SOFC-GT cycle. The following conclusions could be drawn from these analyses:

- The system operating pressure remarkably improves the system performance by increasing both cycle net specific work and its efficiency.
- Increasing the SOFC operating temperature increases the efficiency of the cycle, but decreases the system net specific work.
- Both the cycle net specific work and its efficiency were negatively influenced by the SOFC current density.
- Increasing the fuel utilization factor has a positive impact on the cycle net specific work. But its influence on the cycle efficiency depends on the GT isentropic efficiency.
- Increasing the TIT has a positive impact on the cycle net specific work and negative impact on the cycle efficiency.
- Finally, increasing the GT and air compressor isentropic efficiencies improves both the net specific work and cycle efficiency.

For future work, these analyses can be repeated with an improved model, based on the comments presented in the Subsection 4.5. It would be very interesting to compare these results with those of the improved model.



## **CHAPTER SIX**

### **Effects of Inlet Fuel Type and Composition on Hybrid SOFC-GT Cycle Performance**

Recently, utilization of alternative fuels such as biomass and syngas has gained special interest due to their significant environmental benefits, especially in terms of GHG emission reduction potentials (particularly if their life cycle is considered), and/or their renewable nature. For instance, production and consumption of biogas can result in very low net GHG emissions. On the other hand, due to the abundant supply of coal throughout the world, if the environmental impact of syngas can be reduced, it is an attractive source of energy derived from fossil fuels.

Although these fuels are ideal choices, there are some problems associated with their applications. These problems should be addressed before their widespread applications in hybrid SOFC systems can be secured. One of these problems is variation of inlet fuel composition to the hybrid power generation system.

Unlike natural gas, biogas and syngas are produced by processing other fuels; therefore, their characteristics vary by different parameters in the process. The first parameter that influences the composition and quality of these fuels is the type of biomass or coal that is processed. When the input biomass or coal is changed, the outlet fuel composition also changes. The other parameters are the fuel production process and process control parameters. For example, both biomass and coal syngas are conventionally produced by a gasification process. In this process, fuel composition heavily depends on the gasifying agent, namely, steam, air, or oxygen. The fuel usually contains methane ( $\text{CH}_4$ ), hydrogen ( $\text{H}_2$ ), carbon dioxide ( $\text{CO}_2$ ), water ( $\text{H}_2\text{O}$ ), nitrogen ( $\text{N}_2$ ), carbon monoxide ( $\text{CO}$ ), and minor amounts of other compounds, though the concentration of each component depends on the aforementioned parameters. For example, in the air and steam-blown gasification processes, the produced fuel contains a high concentration of nitrogen

and steam, respectively. In the oxygen-blown gasification process, CO and/or CO<sub>2</sub> can be found high in concentration (Sucipta, Kimijima, Song, and Suzuki, 2008b; Na, Park, Kim, Lee, and Kim, 2003; Van Der Drift, Van Doorn, and Vermeulen, 2001). Thus, the composition of biogas and syngas can be altered with variation of different parameters. Therefore, in order to have a proper utilization of these fuels in hybrid SOFC cycles, it is very important to investigate the effects of variation in fuel composition on the system's overall performance.

This chapter starts with the analysis of the syngas fuelled hybrid SOFC-GT cycle, including thermodynamic properties of all major streams in the cycle and operational conditions of all main equipment. Then, the system performance is evaluated when it is fuelled by natural gas, biogas, gasified biomass, and other fuels with different compositions. Finally, the sensitivity analysis of the impact of hydrogen, carbon dioxide, carbon monoxide, and nitrogen in the fuel on the performance of the hybrid SOFC-GT cycle are presented.

## **6.1 Variation of operating parameters of syngas fuelled hybrid SOFC-GT cycle**

In this subsection, similar to Subsection 5.1, in order to understand the inner working of the syngas fuelled SOFC-GT cycle, all important thermodynamic properties, such as temperature, pressure, flow rates, and composition of all major streams are evaluated in the cycle's model for two configurations, with and without anode off-gas recirculation. Also, output power, specific work, efficiency, and heat duty of all system equipment are investigated. All model constants and the system operating conditions are similar to those introduced in Tables 27 and 29, except for the TIT which is equal to 1200°C. The composition of syngas used in this work is listed in Table 36 (Kee, Zhu, Sukeshini, and Jackson, 2008).

In order to explain the operation of the system, a similar approach is used as in Subsection 5.1 by following the air and fuel flows and investigating all major processes based on Figure 32. Discussion is first presented for the cycle with anode recirculation. Then, major differences for the cycle without anode recirculation are explained. Table 37 shows the selected thermodynamic properties of the cycle with anode recirculation.

**Table 36: Molar composition of a syngas used in this analysis (Kee et al., 2008)**

Fuel type		Syngas (dry coal feed)
Composition (%)	CH <sub>4</sub>	1.4%
	H <sub>2</sub>	30.0%
	CO <sub>2</sub>	1.6%
	CO	60.3%
	H <sub>2</sub> O	2.0%
	N <sub>2</sub>	4.7%

**Table 37: Properties of streams in the hybrid SOFC-GT system with anode recirculation fuelled with syngas**

		1	2	3	4	5	6	7	8	9	10	11
Temperature(°C)		25	172	907	1000	1000	25	152	219	311	1000	1000
Pressure (bar)		1	3	3	3	3	1	3	3	3	3	3
Molar flow (kmole/h)		16.0	16.0	16.0	16.0	15.8	1.0	1.0	1.0	1.1	1.1	1.1
Mass flow (kg/h)		462	462	462	462	457	20	20	20	23	23	23
Volumetric flow (m <sup>3</sup> /h)		397	198	524	566	559	25	12	14	18	40	40
LHV (kJ/kg)		0	0	0	0	0	12,658	12,658	12,658	11,913	12,039	12,039
Mass flow (kg/h)	H <sub>2</sub> O	0.0	0.0	0.0	0.0	0.0	0.4	0.4	0.4	0.9	0.7	0.7
	CO	0.0	0.0	0.0	0.0	0.0	16.9	16.9	16.9	18.5	18.9	18.9
	CO <sub>2</sub>	0.0	0.0	0.0	0.0	0.0	0.7	0.7	0.7	1.2	1.2	1.2
	CH <sub>4</sub>	0.0	0.0	0.0	0.0	0.0	0.2	0.2	0.2	0.2	0.0	0.0
	H <sub>2</sub>	0.0	0.0	0.0	0.0	0.0	0.6	0.6	0.6	0.6	0.7	0.7
	N <sub>2</sub>	354.5	354.5	354.5	354.5	354.5	1.3	1.3	1.3	1.5	1.5	1.5
	O <sub>2</sub>	107.6	107.6	107.6	107.6	102.1	0.0	0.0	0.0	0.0	0.0	0.0

**Table 37: Properties of streams in the hybrid SOFC-GT system with anode recirculation fuelled with syngas (cont.)**

		12	13	14	15	16	17	18	19	21
<b>Temperature(°C)</b>		1000	1285	1000	1285	1200	1200	917	229	225
<b>Pressure (bar)</b>		3	3	3	3	3	3	1	1	1
<b>Molar flow (kmole/h)</b>		0.1	16.6	0.1	16.6	16.6	16.6	16.6	16.6	16.6
<b>Mass flow (kg/h)</b>		3	482	3	482	482	482	482	482	482
<b>Volumetric flow (m<sup>3</sup>/h)</b>		4	716	4	716	677	677	1640	692	686
<b>LHV (kJ/kg)</b>		6,622	0	6,622	0	0	0	0	0	0
<b>Mass flow (kg/h)</b>	<b>H<sub>2</sub>O</b>	5.4	4.9	0.5	6.3	6.3	6.3	6.3	6.3	6.3
	<b>CO</b>	16.6	15.0	1.6	0.0	0.0	0.0	0.0	0.0	0.0
	<b>CO<sub>2</sub></b>	4.8	4.4	0.5	27.9	27.9	27.9	27.9	27.9	27.9
	<b>CH<sub>4</sub></b>	0.0	0.0	0.0	0.0	0.0	0.0	0.0	0.0	0.0
	<b>H<sub>2</sub></b>	0.2	0.2	0.0	0.0	0.0	0.0	0.0	0.0	0.0
	<b>N<sub>2</sub></b>	1.5	1.3	0.1	355.8	355.8	355.8	355.8	355.8	355.8
	<b>O<sub>2</sub></b>	0.0	0.0	0.0	92.3	92.3	92.3	92.3	92.3	92.3

Syngas with the flow rate of 1 kmole/h (20 kg/h) and the lower and higher heating values of 12,658 and 13,376 kJ/kg, respectively, enters the cycle at STP, 25°C and 1 bar (stream 6), and is pressurized to 3 bar and 152°C at stream 7. The fuel compressor consumes 1 kW at 85% isentropic efficiency. The temperature of stream 7 increases to 219°C by 0.6 kW heat transfer at FHX. The streams 8 and 14 are then mixed to form stream 9 with a high concentration of steam (0.5 kg/h) required for the methane reforming and water-gas shift reaction. The mass flow rate and temperature of streams 14 and 9 are 3 kg/h at 1000°C, and 23 kg/h at 311°C, respectively. The electrochemical reactions in the SOFC generate 14.2 kW power and 10.5 kW excess heat, which is transferred to the reformer from which 8 kW is consumed for methane reforming in the reformer, and the rest is used to heat the air flow at AIR HEAT. The efficiency of power generation in the SOFC is 20.1% (based on LHV), which is much lower than the SOFC efficiency, when the cycle was fuelled with methane (at the efficiency of 58.2%). The reason for this low efficiency can be explained based on the low concentration of hydrogen in the SOFC inlet (2.1 kmole/h for methane fuelled cycle vs. 0.9 kmole/h for syngas fuelled cycle), since only H<sub>2</sub> can be consumed in the SOFC. Because of the electrochemical reaction in the anode and formation of water, the mass flow rate of the anode increases to 28 kg/h, and the mass flow rate

of steam increases from 0.5 to 5.4 kg/h. In the meantime, the mass flow rate of hydrogen and carbon monoxide decreases from 0.7 to 0.2 kg/h and from 18.9 to 16.6 kg/h, respectively, whereas the mass flow rate of carbon dioxide increases from 1.2 to 4.8 kg/h. The LHV of the flow before and after the SOFC are 12,039 and 6,622 kJ/kg, respectively. Comparing these LHVs with the same values for the cycle fuelled with methane (12,627 and 3,074 kJ/kg, respectively) shows that although the LHV of the inlet streams to the SOFC are very close, the LHV of outlet streams are very different. The reason can be the high concentration of CO in the inlet stream to the SOFC in the cycle fuelled with syngas in comparison to that in the cycle fuelled with methane (18.9 vs. 1.9 kg/h). It should be noted that in this model, CO cannot be electrochemically oxidized in the SOFC, rather it participates in the water-gas shift reaction to generate  $H_2$ . The SOFC anode exhaust is then divided into two streams: one is recycled to the reformer (stream 14) and the other is fed to the combustor (stream 13). The mass flow rates of  $H_2$  and CO in stream 13 are 0.2 and 15 kg/h, respectively, which can be combusted to increase the temperature of the stream before it is fed to the gas turbine (stream 15).

On the other hand, the inlet air enters the system (stream 1) at STP with the mass flow rate of 462 kg/h. The air pressure is increased to 3 bar at the air compressor (A-COMP) by consuming 16.7 kW of power at the isentropic efficiency of 85%. Then, the air is heated by the heat transferred from the reformer (unused heat from the SOFC) in AIR HEAT. All of this heat (2.5 kW) is used to increase the temperature of the air from 153°C after the compressor to 172°C, and there is no heat left to discharge to the atmosphere. The air stream temperature is further increased in AHX and AHX2 by the GT discharge stream and the combustor exhaust, respectively, and its temperature rises to 907°C and 1000°C at streams 3 and 4, respectively. The heat duties of AHX and AHX2 are 104 and 14 kW, respectively.

The air stream is then fed to the SOFC at the cathode inlet. 5.5 kg/h of oxygen in the air flow participates in the SOFC reactions; therefore, the molar flow rate of the air reduces from 16 to 15.8 kmole/h. The cathode exhaust is then fed to the combustor, where it mixes with the anode exhaust stream. This mixture is combusted in the combustor, so the temperature of combustion products increases to 1285°C. It is assumed that all  $H_2$  and CO are burnt, and the combustor exhaust only consists of  $H_2O$ ,  $CO_2$ ,  $O_2$ , and  $N_2$ . The mass flow rate of the stream 15 is 482 kg/h.

The combustor exhaust is used to increase air temperature to 1000°C at AHX2, and if necessary reformat at FHX2, although not in this case, before being fed to the GT. The TIT is fixed at the user-defined value of 1200°C by adjusting the air-to-fuel ratio. The GT generates 46.5 kW at an isentropic efficiency of 85%. The combustion products leave the GT at a temperature of 917°C and pressure of 1 bar (stream 18). This stream heats the air at AHX and the fuel at FHX, and its temperature reduces to 229°C and 225°C, respectively. Eventually the exhaust is discharged to the atmosphere at a temperature of 225°C.

The net output power of the cycle is 42.9 kW at an efficiency of 60.7%, which is much lower than that in the cycle fuelled by methane (74.6%). The specific work of the other equipment is presented in Table 38. Also, the heat duty of various heat exchangers can be seen in Table 39 for both configurations.

**Table 38: Power, specific work, and efficiency of mechanical systems in the hybrid SOFC-GT system with anode recirculation**

Equipment	Power (kW)	Specific work (kJ/kg <sub>air</sub> )	Efficiency (%)
Air compressor	16.7	130.4	85
Fuel compressor	1.0	8.1	85
Water pump	-	-	-
SOFC	14.2	110.4	20.1
GT	46.5	362.1	85
Total/net	42.9	334.1	60.7

**Table 39: Heat duties of heat exchangers in the hybrid SOFC-GT system (both configurations)**

Heat exchanger	Heat duty in cycle with anode recirculation (kW)	Heat duty in cycle without anode recirculation (kW)
Air Heat	2.5	1.6
AHX	104.5	107.8
AHX2	14.1	14.6
SOFC	10.5	9.8
Reformer	8.0	8.2
FHX	0.6	0.5
FHX2	0.0	0.0
WHX	0.0	0.4

Table 40 shows the stream information for the cycle without anode recirculation. Since most of the processes in both configurations are similar, only main differences between two cycles are highlighted. In this table, streams 13 and 14 are removed from Table 37, and streams 22, 23, and 24 are added. In this configuration, 0.5 kg/h of the external water steam is pressurized in the water pump and then is boiled at WHX by the GT exhaust before being mixed with the fuel at a temperature of 209°C.

One of the differences in the operation of the two cycles is the lower sensible waste energy in the exhaust stream in the cycle without anode recirculation. The exhaust stream temperature for cycles with and without anode recirculation is 225°C and 209°C, respectively. The reason is that in the cycle without anode recirculation, the exhaust stream is used to generate steam in WHX. However, the efficiency of the cycle as a whole is almost equal for both configurations (around 61%). This can be because of the higher concentration of steam in the exhaust stream of the cycle without anode recirculation (6.8 vs. 6.3 kg/h, respectively), which means a higher latent waste energy in the exhaust stream of this cycle.

Also, the air mass flow rate of the cycle in the configuration without anode recirculation is higher than that in the cycle with anode recirculation (473 vs. 462 kg/h, respectively). This can be explained based on the fact that the LHV, mass flow rate, and energy content of the combustor inlet stream for the cycle with anode recirculation are 6,622 kJ/kg, 25.7 kg/h, and 47.3 kW, respectively, and for the cycle without anode recirculation are 6,708 kJ/kg, 25.9 kg/h, and 48.3 kW, respectively. The higher energy content of the combustor inlet in the cycle without anode recirculation requires a higher air-to-fuel ratio to keep the TIT at 1200°C (16.4 for the configuration without anode recirculation vs. 16.0 for the other configuration).

**Table 40: Properties of streams in the hybrid SOFC-GT system without anode recirculation**

	1	2	3	4	5	6	7	8	9	10	11
Temperature(°C)	25	165	907	1000	1000	25	152	213	213	1000	1000
Pressure (bar)	1	3	3	3	3	1	3	3	3	3	3
Molar flow (kmole/h)	16.4	16.4	16.4	16.4	16.2	1.0	1.0	1.0	1.0	1.1	1.1
Mass flow (kg/h)	473	473	473	473	468	20	20	20	21	21	21
Volumetric flow (m <sup>3</sup> /h)	406	199	537	579	573	25	12	13	14	37	37
LHV (kJ/kg)	0	0	0	0	0	12,658	12,658	12,658	12,333	12,459	12,459
Mass flow (kg/h)	H <sub>2</sub> O	0.0	0.0	0.0	0.0	0.0	0.4	0.4	0.4	0.9	0.5
	CO	0.0	0.0	0.0	0.0	0.0	16.9	16.9	16.9	16.9	17.1
	CO <sub>2</sub>	0.0	0.0	0.0	0.0	0.0	0.7	0.7	0.7	0.7	1.0
	CH <sub>4</sub>	0.0	0.0	0.0	0.0	0.0	0.2	0.2	0.2	0.2	0.0
	H <sub>2</sub>	0.0	0.0	0.0	0.0	0.0	0.6	0.6	0.6	0.6	0.7
	N <sub>2</sub>	363.0	363.0	363.0	363.0	363.0	1.3	1.3	1.3	1.3	1.3
	O <sub>2</sub>	110.2	110.2	110.2	110.2	104.9	0.0	0.0	0.0	0.0	0.0

**Table 40: Properties of streams in the hybrid SOFC-GT system without anode recirculation (cont.)**

	12	15	16	17	18	19	20	21	22	23	24
Temperature(°C)	1000	1284	1199	1199	917	223	219	216	25	25	209
Pressure (bar)	3	3	3	3	1	1	1	1	1	3	3
Molar flow (kmole/h)	1.1	17.0	17.0	17.0	17.0	17.0	17.0	17.0	0.03	0.03	0.03
Mass flow (kg/h)	26	494	494	494	494	494	494	494	0.5	0.5	0.5
Volumetric flow (m <sup>3</sup> /h)	37	733	693	693	1680	700	695	691	~0	~0	~0
LHV (kJ/kg)	6,708	0	0	0	0	0	0	0	-	-	-
Mass flow (kg/h)	H <sub>2</sub> O	5.3	6.8	6.8	6.8	6.8	6.8	6.8	0.5	0.5	0.5
	CO	15.2	0.0	0.0	0.0	0.0	0.0	0.0	0.0	0.0	0.0
	CO <sub>2</sub>	3.9	27.9	27.9	27.9	27.9	27.9	27.9	0.0	0.0	0.0
	CH <sub>4</sub>	0.0	0.0	0.0	0.0	0.0	0.0	0.0	0.0	0.0	0.0
	H <sub>2</sub>	0.2	0.0	0.0	0.0	0.0	0.0	0.0	0.0	0.0	0.0
	N <sub>2</sub>	1.3	364.3	364.3	364.3	364.3	364.3	364.3	0.0	0.0	0.0
	O <sub>2</sub>	0.0	94.9	94.9	94.9	94.9	94.9	94.9	0.0	0.0	0.0



Table 41 shows the output power, specific work, and efficiency of the mechanical systems in the hybrid SOFC-GT system without anode recirculation. Comparing the performance of the equipment in the cycles with and without anode recirculation, shown in Tables 38 and 41, respectively, indicates some differences. First, the output power in the GT in the configuration without anode recirculation is slightly higher than that in the configuration with anode recirculation (47.6 vs. 46.5 kW, respectively) due to the recycling of part of the SOFC exhaust stream. This also can be seen in small reduction in the mass flow rate of GT (stream 17), from 494 kg/h in the cycle without anode recirculation to 482 kg/h in the cycle with anode recirculation. This difference in the GT output in the cycle fuelled with syngas is much lower than that in the cycle fuelled with methane (Tables 33 and 34). The reason is that in this case, less steam is required for fuel reforming due to the much lower percentage of methane in the fuel (0.5 kmole/h in the cycle fuelled with syngas vs. 2.1 kmole/h in the cycle fuelled with methane).

**Table 41: Power, specific work, and efficiency of mechanical systems in the hybrid SOFC-GT system without anode recirculation**

Equipment	Power (kW)	Specific work (kJ/kg <sub>air</sub> )	Efficiency (%)
Air compressor	17.1	130.4	85
Fuel compressor	1.0	7.9	85
Water pump	~ 0.0	~ 0.0	85
SOFC	13.7	103.9	19.3
GT	47.6	362.2	85
Total/net	43.1	327.8	61.0

However, the output power of the SOFC in the configuration with anode recirculation is higher than that in the configuration without anode recirculation (14.2 vs. 13.7 kW, respectively) because of the higher overall net fuel utilization factor of the former. This also can be observed in the mass flow rate of H<sub>2</sub> in the anode outlet stream that enters the combustion chamber, where the H<sub>2</sub> concentration in the system with anode recirculation is lower than that in the system without anode recirculation (0.078 vs. 0.083 kmole/h, respectively). This is also the reason for

higher efficiency of the SOFC in the cycle with anode recirculation in comparison to the cycle without anode recirculation (20.1% vs. 19.3%, respectively).

In addition, the total output power of the system for the configuration with anode recirculation is 42.9 kW, which is very close to the total output power of the configuration without anode recirculation at 43.1 kW, because of the opposite effect of the output power reduction in the GT, due to the anode exhaust recirculation, and the output power increase in the SOFC.

Furthermore, the cycle net specific work in the configuration with anode recirculation is higher than those in the cycle without anode recirculation because although the output power of the system as whole for both configurations is almost equal (about 43 kW), due to the higher air mass flow rate of the cycle without anode recirculation (473 vs. 462 kg/h, respectively), its specific work is lower (327.8 vs. 334.1 kJ/kg<sub>air</sub>, respectively).

In this subsection, the performance of the hybrid SOFC-GT cycle was investigated by a detailed analysis of its operational parameters. The next subsection compares the performance of the SOFC-GT cycle when fuelled with various gaseous fuels, especially manufactured fuels.

## **6.2 Performance of hybrid SOFC-GT cycle fuelled with various fuels**

As noted in Subsection 3.2, the high operating temperature of SOFCs allows internal reforming of natural gas, syngas from coal and biomass, and various biofuels, which facilitate their utilization in the system. In this subsection, the SOFC-GT model explained in the previous chapters was fuelled with various fuels to capture the variation in the performance of the cycle. As can be seen in Table 25, in most published papers in the open literature, methane or natural gas has been used as fuel for hybrid SOFC system models. However, there are limited numerical studies that investigated utilization of non-conventional fuels. Lobachyov and Richter (1996), in one of the earliest numerical works in the field, developed a model that incorporated a coal gasification process into a hybrid SOFC-GT cycle. Similarly, Kivisaari et al. (2004) conducted a feasibility study to integrate an MCFC or SOFC to a coal gasification plant in a CHP plant. Kuchonthara et al. (2005) modeled the integrated power generation cycle combining thermochemical recuperation, brown coal gasification, and an SOFC. Rao et al. (2005) compared an integrated gasification SOFC and an integrated gasification combined cycle (IGCC) in their

thermoeconomic analysis. Van herle et al. (2003) conducted an energy balance analysis on an existing biogas production unit integrated into an SOFC cycle in a small CHP system. Sucipta et al. (2007) further investigated the gasification system integrated to an SOFC-MGT cycle by adding and comparing different biomass gasification processes, namely, air, oxygen, and steam-blown. Using the same model, Sucipta et al. (2008a) studied the efficiency and temperature distributions in cases where natural gas, the normal fuel of the hybrid system, was mixed or completely replaced by biofuel. They investigated effects of composition changes on the performance of the SOFC-MGT hybrid system. They found that the efficiencies of the SOFC module and of the hybrid system noticeably decreased when natural gas was completely replaced by biofuel but the SOFC-MGT hybrid system could still be operated with reasonable performance. A more detailed review of these papers can be found in Subsection 3.4.9.

In this subsection, it was shown that the results of a limited number of studies on utilization of non-conventional fuels have been published in the open literature. However, further studies are required in this area to investigate all aspects of the issue for different configurations and assumptions. This subsection focuses on how fuels with different compositions can affect the performance of the hybrid SOFC-GT system. In this subsection, in order to monitor the performance of the system, parameters such as SOFC and system thermal efficiency; net and specific work of the SOFC, GT, and cycle as a whole; air-to-fuel ratio; and air and fuel mass flow rate are investigated. The results of simulation for different types of fuel, namely, pure methane, natural gas, coal syngas, different types of biomass syngas, and farm and sewage biogas are presented.

Table 42 shows the cycle operating conditions when it is fuelled by pure methane, natural gas, farm biogas, and two types of sewage biogas. Similarly, Table 43 shows the same information for dry coal syngas, dry biomass syngas, biofuel, and different types of gasified biomass.

**Table 42: Performance of the hybrid SOFC-GT system fuelled by methane, natural gas, and farm and sewage biogas**

Fuel type		Pure methane		Natural gas (Palsson et al., 2000)		Farm biogas (Van herle et al., 2003)		Sewage biogas (Van herle et al., 2003)		Sewage biogas (Van herle et al., 2004)	
Cycle config.		W *	W/O**	W	W/O	W	W/O	W	WO	W	W/O
Composition (%)	CH <sub>4</sub>	100.0		97.4		63.0		61.5		62.6	
	H <sub>2</sub>	0.0		0.0		0.0		0.0		0.0	
	CO <sub>2</sub>	0.0		1.6		36.0		38.3		34.8	
	CO	0.0		0.0		0.0		0.0		0.0	
	H <sub>2</sub> O	0.0		0.0		0.0		0.0		1.8	
	N <sub>2</sub>	0.0		1.0		1.0		0.2		0.8	
Overall efficiency (LHV, %)		74.6	73.9	74.6	73.7	74.4	75.1	74.4	74.6	74.3	74.6
SOFC efficiency (LHV, %)		58.2	50.3	58.1	49.9	53.8	48.5	53.4	48.0	53.9	48.4
Total work (kW)		166	164	161	160	104	105	102	102	104	104
SOFC work (kW)		130	112	126	108	75	68	73	66	75	68
GT work (kW)		58	80	57	79	46	57	46	56	45	56
SOFC-to-GT work ratio		2.2	1.4	2.2	1.4	1.6	1.2	1.6	1.2	1.7	1.2
Air-to-fuel ratio (molar)		19.6	25.4	19.2	24.9	15.3	17.9	15.3	17.5	15.0	17.5
Air mass flow rate (kg/h)		565	731	554	718	442	517	440	506	434	504
Total specific work (kJ/kg <sub>air</sub> )		1,059	811	1,053	801	850	734	834	729	861	743
SOFC specific work (kJ/kg <sub>air</sub> )		827	552	820	543	615	474	598	468	624	483
GT specific work (kJ/kg <sub>air</sub> )		369	394	369	394	374	397	374	398	375	398
Fuel LHV (kJ/kg)		50,030		47,065		19,277		18,433		19,394	
Fuel mass flow rate (kg/h)		16.0		16.6		26.2		26.8		25.9	
Fuel energy content (kW)		222		217		140		137		140	

\* W: Cycle with anode recirculation

\*\* W/O: Cycle without anode recirculation

**Table 43: Performance of hybrid SOFC-GT system fuelled by coal and biomass syngas, biofuel, and gasified biomass**

Fuel type		Syngas (dry coal feed) (Kee et al., 2008)		Syngas (dry biomass) (Kee et al., 2008)		Biofuel (Sucipta et al., 2008a)		Gasified biomass, H <sub>2</sub> O-blown (Sucipta et al., 2007)		Gasified biomass, Air-blown (Sucipta et al., 2007)	
Cycle config.		W*	W/O**	W	W/O	W	W/O	W	W/O	W	W/O
Composition (%)	CH <sub>4</sub>	1.4		4.7		13.0		10.0		5.0	
	H <sub>2</sub>	30.0		20.0		45.0		50.0		10.0	
	CO <sub>2</sub>	1.6		12.9		15.0		20.0		10.0	
	CO	60.3		15.3		25.0		15.0		10.0	
	H <sub>2</sub> O	2.0		0.0		0.0		0.0		0.0	
	N <sub>2</sub>	4.7		47.1		2.0		5.0		65.0	
Overall efficiency (LHV, %)		60.7	61	62.9	61.6	65.9	67.3	65.7	66.9	59.8	58.6
SOFC efficiency (LHV, %)		20.1	19.3	32.5	30.8	41.5	38.6	42.3	40.1	31.5	30.3
Total work (kW)		43	43	23	22	52	53	44	45	15	15
SOFC work (kW)		14	14	12	11	33	30	29	27	8	8
GT work (kW)		46	48	18	18	31	36	26	29	12	12
SOFC-to-GT work ratio		0.3	0.3	0.7	0.6	1.1	0.8	1.1	0.9	0.7	0.7
Air-to-fuel ratio (molar)		16.0	16.4	5.5	5.4	10.4	11.9	8.5	9.4	3.3	3.1
Air mass flow rate (kg/h)		462	473	158	155	301	343	244	273	94	90
Total specific work (kJ/kg <sub>air</sub> )		334	328	516	514	622	556	656	598	586	604
SOFC specific work (kJ/kg <sub>air</sub> )		110	104	267	258	392	319	423	358	308	312
GT specific work (kJ/kg <sub>air</sub> )		632	362	404	411	373	378	379	384	447	464
Fuel LHV (kJ/kg)		12,658		5,321		16,548		14,317		3,506	
Fuel mass flow rate (kg/h)		20.1		24.3		17.2		17.0		26.4	
Fuel energy content (kW)		71		36		79		68		26	

\* W: Cycle with anode recirculation

\*\* W/O: Cycle without anode recirculation

Tables 42 and 43 illustrate that different fuel compositions vary significantly. For instance, hydrogen concentration can be as low as 0% or as high as 50% and the concentration of carbon monoxide can be between 0% and 60%. Even for the same type of feed stock, such as biomass, gasification technology and gasifying agent can alter fuel composition significantly. For example, nitrogen concentration can be as low as 5% in steam-blown and as high as 65% in air-blown gasified biomass fuels. The range of the lower heating value for the fuels is between 3,506 and 50,030 kJ/kg. Table 44 shows the range of fuel component concentrations for various fuels.

**Table 44: Range of variation of fuel composition and cycle operational parameters**

		Minimum		Maximum	
Cycle configuration		W	W/O	W	W/O
Composition (%)	CH <sub>4</sub>	1.4		100.0	
	H <sub>2</sub>	0.0		50.0	
	CO <sub>2</sub>	1.6		38.3	
	CO	0.0		60.3	
	H <sub>2</sub> O	0.0		2.0	
	N <sub>2</sub>	0.0		65.0	
Overall efficiency (LHV, %)		59.8	58.6	74.6	75.1
SOFC efficiency (LHV, %)		20.1	19.3	58.2	50.3
Total work (kW)		15	15	166	164
SOFC work (kW)		8	8	130	112
GT work (kW)		12	12	58	80
SOFC-to-GT work ratio		0.3	0.3	2.2	1.4
Air-to-fuel ratio (molar)		3.3	3.1	19.6	25.4
Air mass flow rate (kg/h)		94	90	565	731
Total specific work (kJ/kg <sub>air</sub> )		334	328	1,059	811
SOFC specific work (kJ/kg <sub>air</sub> )		110	104	827	552
GT specific work (kJ/kg <sub>air</sub> )		369	362	632	464
Fuel LHV (kJ/kg)		1,843		50,030	
Fuel mass flow rate (kg/h)		16.0		26.8	
Fuel energy content (kW)		222		26	

Also, Tables 42 and 43 show that the operational parameters of the cycle can vary widely based on different fuel compositions. For instance, the range of the cycle efficiency for cycles with and without anode exhaust recirculation is 59.8% to 74.6% and 58.6% to 75.1%, respectively. This range for the SOFC efficiency is 20.1% to 58.2% and 19.3% to 50.3%, respectively. Table 44 also shows the range of variation of operational parameters for two configurations.

Tables 42 and 43 show that system output is greatly influenced by the type of the inlet fuel. For instance, the overall efficiency of the hybrid system can be decreased from 74.6% and 73.7%, for the configurations with and without anode recirculation, respectively, to 59.8% and 58.6%, when natural gas fuel was replaced by air-blown gasified biomass. These results are in agreement with Sucipta et al. (2007). Also, the total specific work decreases from 1,053 and 801 kJ/kg<sub>air</sub> in the configurations with and without anode recirculation, respectively, to 656 and 598 kJ/kg<sub>air</sub>, if natural gas is replaced by steam-blown gasified biomass. Similarly, the air-to-fuel ratio in the configurations with and without anode recirculation can reduce from 15.3 and 17.9 to 5.5 and 5.4, respectively, if farm biogas is replaced by syngas from dry gasified biomass.

Investigating Tables 42 and 43 reveals a few patterns, some of which will be explained in the following part. Generally, the overall efficiency of the cycle for two configurations is close. However, the efficiency of the SOFC in two configurations is different, and the efficiency of the SOFC with anode recirculation is always greater than that in the other configuration. Furthermore, the output power of the SOFC in the configuration with anode recirculation is higher than that in the configuration without anode recirculation. The output power of the GT in the configuration without anode recirculation is also higher than that in the case with anode recirculation. Also, the specific work of the cycle with anode recirculation is always higher than that of the other cycle, which can result in the lower capital cost of the system. However, it should be noted that difference between specific works of two configurations depends on the inlet fuel type.

Considering the variation of the cycle operating parameters in Tables 42 and 43 as well as the range of their changes in Table 44, the importance of inlet fuel composition is obvious. The results show that all important parameters of the cycle including the SOFC and system thermal efficiencies; as well as the net and specific work of the SOFC, GT, and cycle as a whole are influenced by the variation in fuel composition. The results confirm that the inlet fuel variation

and its effects on the cycle performance should be considered in the design of hybrid SOFC-GT plants.

### **6.3 Effects of fuel composition on performance of hybrid SOFC-GT cycle**

One of the advantages of hybrid SOFC cycles in comparison to other fuel cell systems is their fuel flexibility. Different fuels with a wide range of properties and composition have been adopted for hybrid SOFC system modeling in the open literature. However, the analysis of the effects of variation in the fuel composition on the performance of the SOFC-GT cycle is scarce in the literature. In one study, Van herle et al. (2003) evaluated efficiencies of an SOFC (electrical efficiency) and CHP system (total efficiency) in a biogas production plant integrated with an SOFC in a CHP plant as a function of the CO<sub>2</sub> fraction in the biogas feed in a range of 20% to 65%.

In a more comprehensive study, in 2008, Sucipta et al. (2008) published their research on a biomass fuelled hybrid SOFC-MGT cycle. They evaluated the effects of biomass fuel chemical species composition, namely, H<sub>2</sub>, CO, CO<sub>2</sub>, H<sub>2</sub>O, and N<sub>2</sub> on the system performance parameters. In order to evaluate system performance, they considered voltage, electric current, power, efficiency, distributions of temperature in the SOFC, and distributions of mole fractions of participating chemical species in the internal reformer. They found that change of H<sub>2</sub>O and H<sub>2</sub> concentration in the fuel from 0% to 50% slightly reduced the efficiency of the hybrid system. Changes in the hybrid system performance and in all studied parameters were similar between the two cases. Changes of N<sub>2</sub> concentration resulted in a slight decrease of efficiency both for the SOFC module and for the hybrid system. On the other hand, an increase of the CO concentration produced similar effects as that of CO<sub>2</sub> concentration and resulted in a decrease of the efficiency of both the SOFC module and hybrid system significantly.

In this section, the model described in Chapter 4 is applied to observe the effects of fuel composition on the performance of the hybrid SOFC-GT cycle with two configurations: with and without anode recirculation. In order to monitor the performance of the system, parameters such as SOFC and system thermal efficiencies; net and specific work of SOFC, GT, and cycle; air-to-fuel ratio; air and fuel mass flow rate, and so on are investigated. In order to perform the analysis, the reference case is introduced when the hybrid SOFC-GT system is fuelled by pure



methane. Then, discussion of the cases where methane is partially replaced by  $H_2$ ,  $CO_2$ ,  $CO$ , and  $N_2$ , the chemical species that can be found in fuels, is developed.

### 6.3.1 Reference Case

In this case, when the cycle is fuelled with pure methane, the overall efficiencies of the hybrid cycle for the configurations with and without anode recirculation are 74.6% and 73.9%, respectively. The corresponding efficiencies for the SOFC are 58.2% and 50.3%, respectively. On the other hand, since the molar flow rate of the fuel is fixed for all cases, the fuel mass flow rate for both configurations is 16 kg/h with an LHV of 50.03 MJ/kg. However, the air mass flow rate and air-to-fuel ratio for the system with anode recirculation are lower than those in the other configuration (19.6 vs. 25.3 kg/h, and 19.6 vs. 25.3, respectively). Specific works for the SOFC and GT in the system with anode recirculation are 827 and 369 kJ/kg<sub>air</sub>, respectively. These specific works for the system without anode recirculation are 551 and 394 kJ/kg<sub>air</sub>, respectively. These values can be observed from Figures 43 to 54 at 0% hydrogen concentration.

To evaluate the effects of fuel composition on the cycle performance, sensitivity analyses are performed on the model when the fuel is a mixture of  $CH_4$  with each of the following:  $H_2$ ,  $CO_2$ ,  $CO$ , and  $N_2$ , with different percentages. In this analysis, 5% of methane has been replaced by other species at each step in the corresponding range for each case.

### 6.3.2 Effect of hydrogen concentration in inlet fuel on cycle performance

Hydrogen and methane are two main components of fuels, and their concentration can vary considerably, especially in manufactured fuels. Table 45 shows the concentration of methane and hydrogen in some fuels. As this table points out, the concentration of hydrogen can vary from 0% to greater than 50%. This range for methane is from around 1% to more than 97%.

Figures 43 to 54 show the performance of the hybrid SOFC-GT system when methane is partially replaced by  $H_2$  with an increment of 5% at each step from 0% to 95%.

**Table 45: Variation of methane and hydrogen concentration in some fuels**

<b>Fuel type</b>	<b>CH<sub>4</sub> (%)</b>	<b>H<sub>2</sub> (%)</b>
<b>Natural gas</b> (Palsson et al., 2000)	97.4	0.0
<b>Farm biogas</b> (Van herle et al., 2003)	63.0	0.0
<b>Sewage biogas</b> (Van herle et al., 2003, 2004)	61.5-62.6	0.0
<b>Syngas</b> (Kee et al., 2008)	1.4	30.0
<b>Syngas (dry biomass)</b> (Kee et al., 2008)	4.7	20.0
<b>Biofuel</b> (Sucipta et al., 2008a)	13.0	45.0
<b>Gasified biomass, H<sub>2</sub>O-blown</b> (Sucipta et al., 2007)	10.0	50.0
<b>Gasified biomass, Air-blown</b> (Sucipta et al., 2007)	5.0	10.0

### 6.3.2.1 Hydrogen concentration at various streams

Figure 43 illustrates the molar flow rate of hydrogen in a few streams in the cycle, namely the inlet fuel, SOFC anode inlet (reformer outlet), anode outlet, and combustor inlet in the cycle with anode recirculation with respect to the concentration of  $H_2$  in the inlet fuel. Exactly the same pattern can be seen for the cycle without anode recirculation. The only difference is that since there is no anode exhaust recirculation, the anode outlet stream directly enters the combustor.

The first point that can be noticed in Figure 43 is that, probably unexpectedly, with an increase in hydrogen concentration in the inlet fuel, the molar flow rate of hydrogen in the anode inlet stream decreases. This variation of hydrogen molar flow rate can be explained by revisiting reactions in Equations 1 and 2. These reactions show that for one mole of  $CH_4$  reacting in the cycle, four moles of  $H_2$  can be produced (three moles from methane reforming and one mole from the water-gas shift reaction). Accordingly, the molar flow rate of hydrogen in the anode outlet and combustor inlet streams decreases. Figure 43 also points out that the concentration of  $H_2$  in the inlet fuel and anode inlet converges. The reason is that as the concentration of methane in the fuel decreases, there is less methane to be reformed in the reformer; therefore, the

composition of the anode inlet stream and inlet fuel converges. Similar pattern can be seen for hydrogen concentration in the anode outlet and combustor inlet streams.

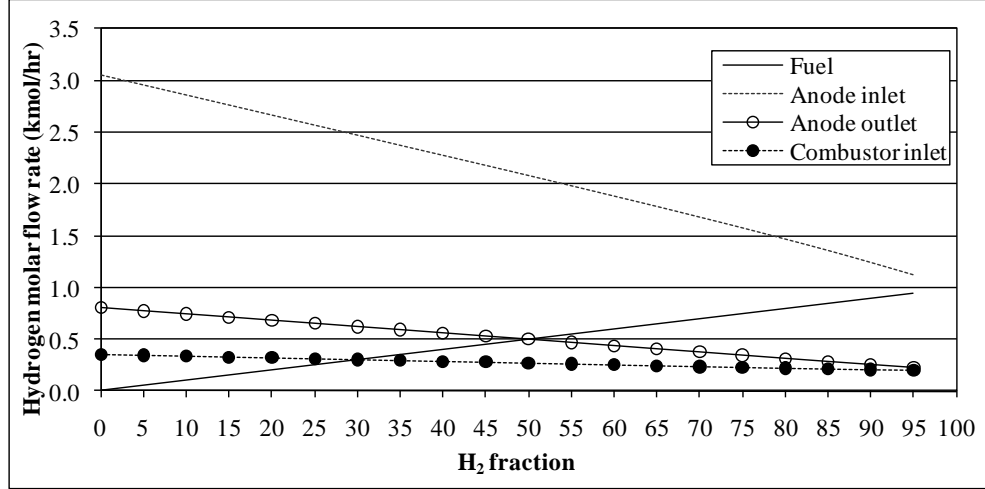
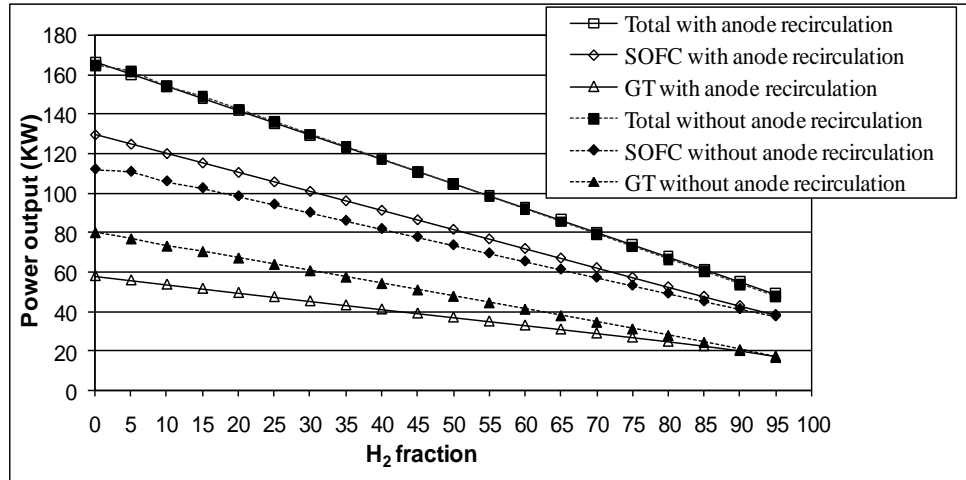


Figure 43: Hydrogen molar flow rate in the inlet fuel, anode inlet (reformer outlet), anode outlet, and combustor inlet streams for the cycle with anode recirculation versus H<sub>2</sub> concentration in the inlet fuel

### 6.3.2.2 Output power

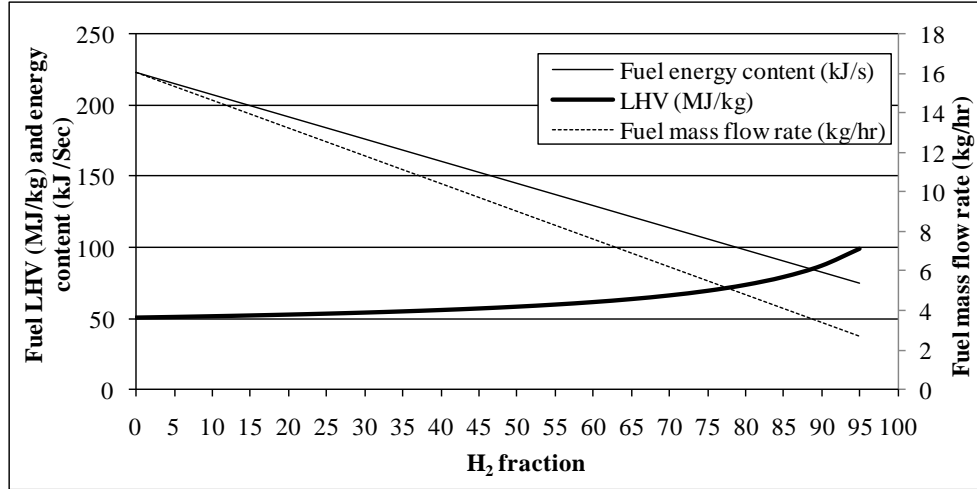
Since the objective of a hybrid SOFC-GT cycle is to generate electricity, the output power of the system is the most important parameter to evaluate. Figure 44 shows the output power of the SOFC, GT, and system as a whole versus the concentration of H<sub>2</sub> in the fuel for two configurations.



**Figure 44: Output power of GT, SOFC, and whole system for different configurations versus H<sub>2</sub> concentration in the inlet fuel**

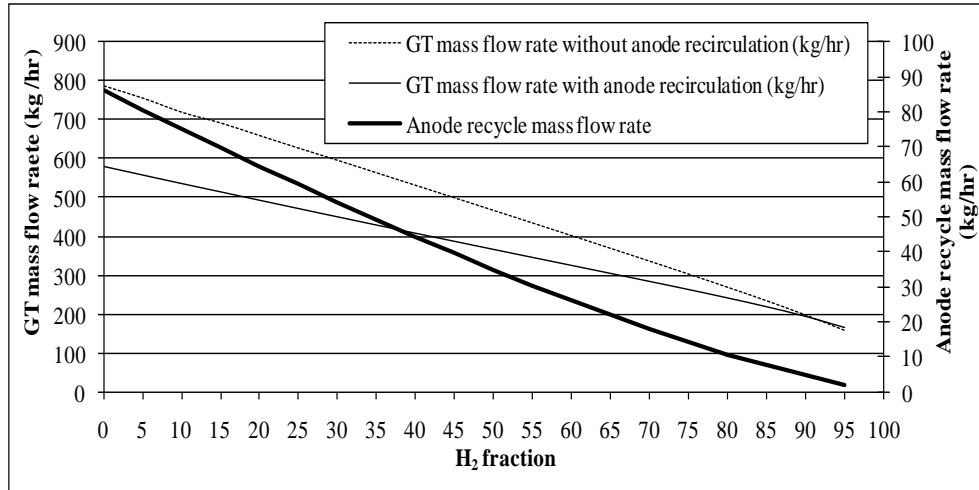
Figure 44 illustrates that the output power decreases with an increase in the H<sub>2</sub> concentration in all cases under investigation. The reason can be explained based on Figure 45, where the changes of the input fuel's LHV, mass flow rate, and energy content versus H<sub>2</sub> concentration in the inlet fuel for both configurations are shown. These graphs are identical for both configurations because, in the model, the fuel molar flow rate is kept constant. Therefore, the fuel flow rate is an independent variable in the model and is equal for both configurations.

Figure 45 shows that with increase in H<sub>2</sub> concentration, the LHV of the fuel gradually increases. This is due to the much higher LHV of hydrogen compared to methane (120 MJ/kg for H<sub>2</sub> vs. 50 MJ/kg for CH<sub>4</sub>). On the other hand, for a constant molar fuel flow rate of 1 kmole/h, the fuel mass flow rate decreases because of the higher atomic weight of CH<sub>4</sub> in comparison to H<sub>2</sub> (16 for CH<sub>4</sub> vs. 2 for H<sub>2</sub>). However, the rate of increase in the fuel's LHV is lower than the rate of reduction in the fuel mass flow rate. As a result, the energy content of the fuel reduces. As an example, when the methane concentration is reduced from 90% to 50%, the LHV increases by 6.8 MJ/kg, and the fuel mass flow rate decreases by 5.6 kg/h. These two effects cause the fuel energy content to decrease by 62.4 kJ/s. Thus, the input energy of the fuel and, as a result, the output power of the cycle reduces as the CH<sub>4</sub> concentration of the fuel decreases. Moreover, the reduction in the GT and SOFC efficiencies (as shown in Figure 51 in Subsection 6.3.2.4) further reduces the output power of both configurations.



**Figure 45: Inlet fuel's LHV, mass flow rate, and energy content versus H<sub>2</sub> concentration**

Moreover, Figure 44 indicates that the output power for the gas turbine in the configuration with anode recirculation is lower than that of the configuration without anode recirculation. This can be explained based on the fact that when the SOFC exhaust is partially recycled before going through the GT, the actual mass flow rate of the GT reduces. Thus, there is less power generated in the GT. Figure 46 shows the GT mass flow rate for both configurations and, as explained, the mass flow rate through the GT in the configuration with anode recirculation is lower than that of the configuration without anode recirculation.



**Figure 46: GT mass flow rate for both configurations and the anode recirculation mass flow rate in the cycle with anode recirculation with respect to H<sub>2</sub> concentration in the fuel**

Figure 46 also shows that the curves for the GT mass flow rate for two configurations converge with an increase of H<sub>2</sub> concentration. This is because when the CH<sub>4</sub> concentration of the inlet fuel reduces, there is less fuel that requires reforming, so the amount of steam required for reforming is reduced, as shown in Figure 47. Accordingly, this means a lower flow rate of anode recirculation is required (Figure 46, curve for the anode recirculation mass flow rate). The impact of this issue can be seen in Figure 44, where the curves for the GT output power of two configurations converge with the increase in hydrogen concentration in the fuel.

Figure 47 illustrates the molar and mass flow rates of required steam for reforming reactions in the cycle. These curves are equal for both configurations because of the constant and similar fuel molar flow rate for both cycles. However, the method to provide this steam is different in two configurations. In the cycle with anode recirculation, this steam is provided by anode off-gas recirculation, and the steam content in the recycled stream should be equal to the required steam. But in the cycle without anode recirculation, the flow rate of required steam should be equal to the external water stream's flow rate.

In summary, when more methane is replaced by hydrogen, the difference between the two configurations decreases. As a consequence, when methane is completely replaced by hydrogen, the performance of the two configurations should be exactly the same.

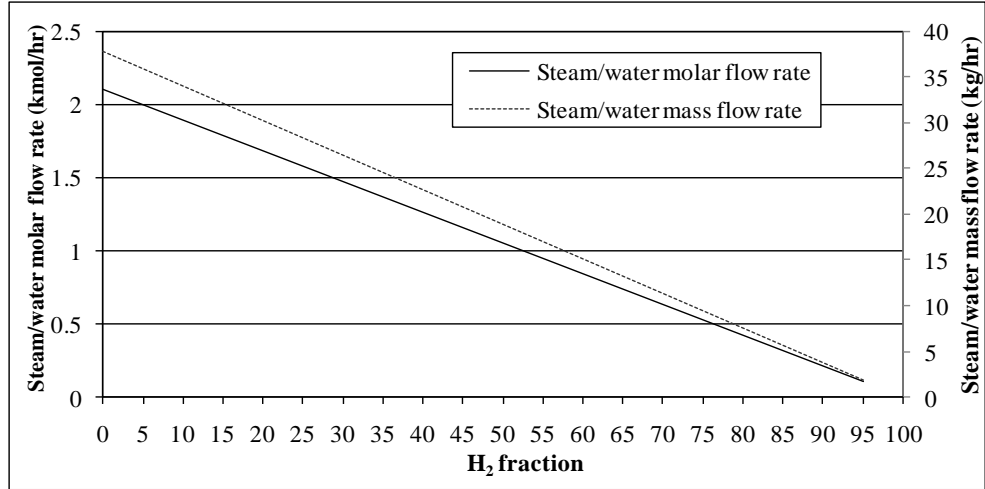


**Figure 47: Steam molar and mass flow rate required for fuel reforming process for both configurations**

Figure 44 also shows that the output power of the SOFC in the configuration with anode recirculation is higher than that in the configuration without anode recirculation. This can be explained based on the fact that the overall net fuel utilization factor of the fuel cell in the configuration with anode recirculation is higher, even though the fuel utilization efficiency of the fuel cell is constant. This is because some unused fuel in the recycled anode exhaust is consumed in the fuel cell in the cycle with anode recirculation. This can be verified in Figure 48. The figure shows the molar flow rate of H<sub>2</sub> in the anode exhaust that enters the combustion chamber versus the H<sub>2</sub> concentration in the inlet fuel. As Figure 48 illustrates, the H<sub>2</sub> concentration in the system with anode recirculation is lower than that in the system without anode recirculation, which indicates that in the cycle with anode recirculation, more fuel is consumed in the SOFC, which in turn, confirms that the net fuel utilization factor in the SOFC is higher in this configuration.

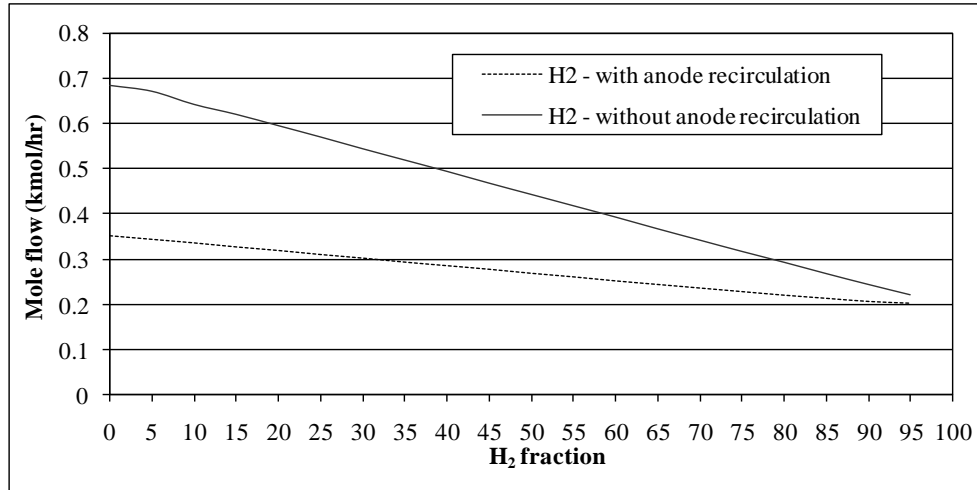


**Figure 48: Molar flow rate of H<sub>2</sub> in anode exhaust**

In addition, Figure 44 shows that the total output powers of the system for both configurations are very close. This is as a result of compensation of the output power reduction in the GT, due to anode exhaust recirculation, by power increase in the SOFC, due to the higher SOFC fuel utilization factor.

### 6.3.2.3 Specific work

Figure 49 shows how specific works of the GT, SOFC, and system as a whole vary with respect to H<sub>2</sub> concentration in the inlet fuel for two configurations.



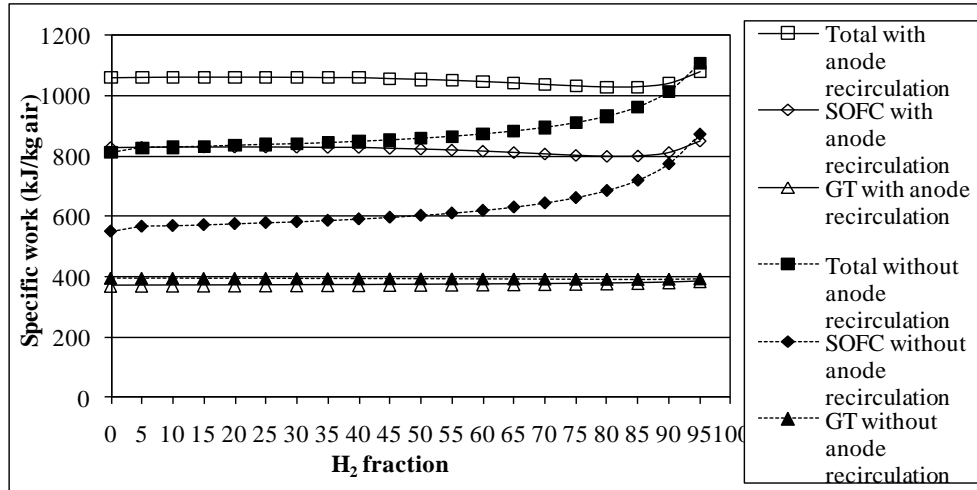


**Figure 49: GT, SOFC, and system specific works versus H<sub>2</sub> concentration in the inlet fuel**

To understand the trend in these graphs, both the output power and air mass flow rate should be investigated. Figure 50 shows the inlet air mass flow rate and air-to-fuel ratio versus H<sub>2</sub> concentration in the fuel for the system with and without anode recirculation. As noted earlier, in the model, the TIT is kept constant by manipulating the air-to-fuel ratio. That means to keep the TIT constant, for lower fuel energy content of the combustor inlet (as shown in Figure 45), the air-to-fuel ratio should be reduced. That is why in Figure 50, the inlet air mass flow rate and the air-to-fuel ratio reduce in both configurations. Also Figure 50 indicates that both the air-to-fuel ratio and inlet fresh air mass flow rate are lower in the cycle with anode recirculation. The higher net fuel utilization factor in the cycle with anode recirculation is the reason for this trend, as explained in subsection 6.3.2.2, which means there is less fuel to be burned in the combustion chamber to increase the TIT.

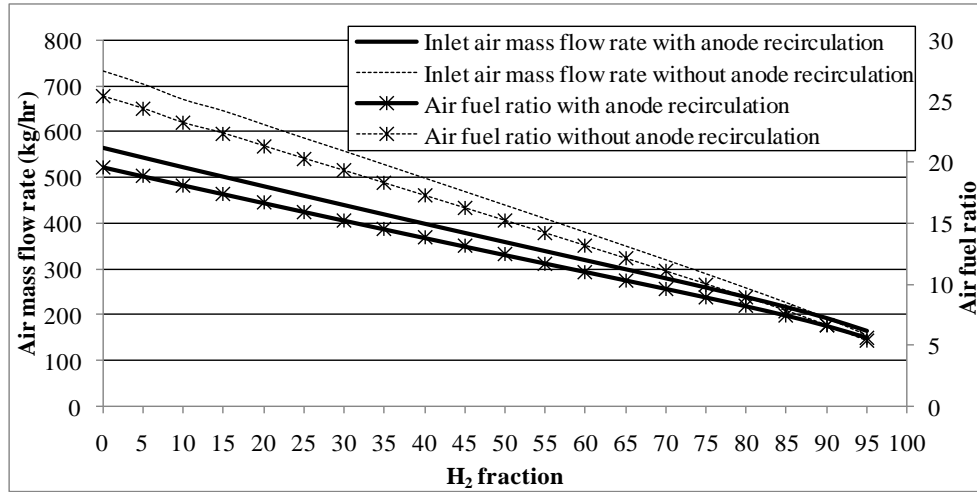


**Figure 50: Inlet air mass flow rate and air-to-fuel ratio versus H<sub>2</sub> concentration for different configurations**

In order to justify the variations in Figure 49, the reduction rate of both the output power and inlet air mass rate in Figures 44 and 50, respectively, should be investigated. Table 46 shows the rate of variations of the inlet air mass flow rate in Figure 50, the output power in Figure 44, and the specific work in Figure 49 for different components. In the cycle with anode recirculation, the inlet air mass flow rate is reduced by 71.2%, while the GT, SOFC, and total output power are reduced by 70%, 70.4%, and 70.6%, respectively. As the results show, the reduction rate for both the output power and the air mass flow rate are very close in this case. This is the reason for almost constant specific works and the nearly horizontal line for their curves in the system with anode recirculation.

For the cycle without anode recirculation, a similar pattern can be recognized for the GT. However, the reduction rate of 66.6% and 71% for the SOFC and total output power, respectively, are lower than 78.8% reduction rate of the air mass flow rate. Thus, in the cycle without anode recirculation, the SOFC specific work increases from 550 to 871 kJ/kg, and the total specific work increases from 810 to 1110 kJ/kg, when the H<sub>2</sub> concentration of the fuel is increased from 0% to 95%.

**Table 46: Rate of variation of the inlet air mass flow rate and output power and specific work of different components**

	Variation rate in cycle with anode recirculation (%)	Variation rate in cycle without anode recirculation (%)
Air mass flow rate	-71.2	-78.8
GT output power	-70.0	-78.9
SOFC output power	-70.4	-66.6
Total output power	-70.6	-71.0
GT specific work	4	-0.5
SOFC specific work	2.7	57.9
Total specific work	1.9	36.8

#### 6.3.2.4 Efficiency

Figure 51 represents the efficiency of the SOFC and cycle for both configurations versus  $H_2$  concentration in the fuel. Since efficiency depends on the output power (Figure 44) and the energy content of the consumed fuel to generate this power (Figure 45), these two parameters should be considered to investigate Figure 51.

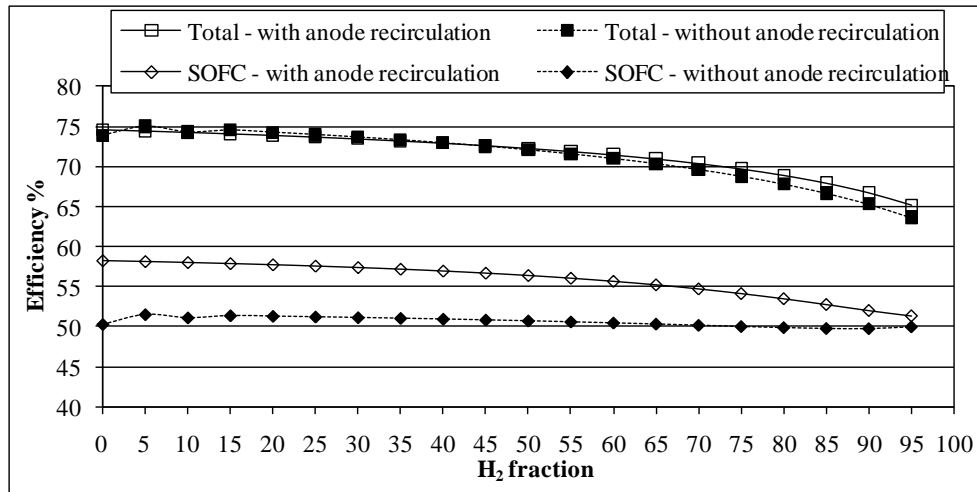


**Figure 51: Efficiency of the SOFC, GT, and cycle for both configurations versus  $H_2$  concentration**

Another table similar to Table 46 can help to explain the trends in Figure 51. As Table 47 shows, for the SOFC in the cycle without anode recirculation, the reduction rate of the inlet fuel energy content and SOFC output power are very close; thus, the graph for the SOFC efficiency is almost horizontal. But for the other cases (the SOFC in the cycle with anode recirculation and whole cycle for both configurations), the reduction rate of the output power is higher than the reduction rate of the inlet fuel energy content. Therefore, the efficiency for these cases decreases by the increase in  $H_2$  concentration in the inlet fuel. The trend of the results illustrated in Figure 51 shows good agreement with the results presented by Sucipta et al. (2008b).

**Table 47: Rate of variation of the inlet fuel energy content, output power, and efficiencies of different components**

	Variation rate in cycle with anode recirculation (%)	Variation rate in cycle without anode recirculation (%)
<b>Inlet fuel energy content</b>	-66.38	-66.38
<b>SOFC output power</b>	-70.38	-66.58
<b>Total output power</b>	-70.61	-71.05
<b>SOFC efficiency</b>	-11.91	-0.60
<b>Total efficiency</b>	-12.58	-13.89

#### 6.3.2.5 SOFC-to-GT work ratio

As Figure 52 illustrates, the SOFC-to-GT work ratio for the cycle with anode recirculation is higher than that in the other configuration. The reason stems from the higher output power of the SOFC and lower output power of the GT in this configuration in comparison to the cycle without anode recirculation.

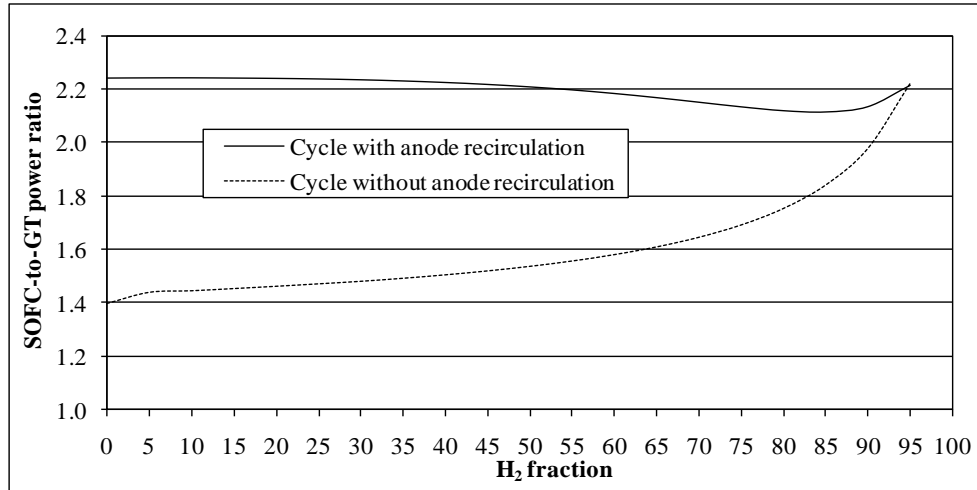


**Figure 52: SOFC-to-GT work ratio for two configurations**

#### 6.3.2.6 Temperature of exhaust stream

Cycle exhaust temperature is an important parameter because it indicates the amount of unused energy that is wasted to the environment. Figures 53 and 54 show the temperature in the GT, AHX, FHX, and WHX outlets for the configurations with and without anode recirculation, respectively. It should be noted that the WHX outlet temperature is actually the cycle exhaust temperature for the cycle without anode recirculation. But for the cycle with anode recirculation, since there is no external water and WHX is not in service, the temperature of the cycle exhaust is equal to the temperature of the FHX outlet. That is the reason for removing the FHX outlet temperature from Figure 53.

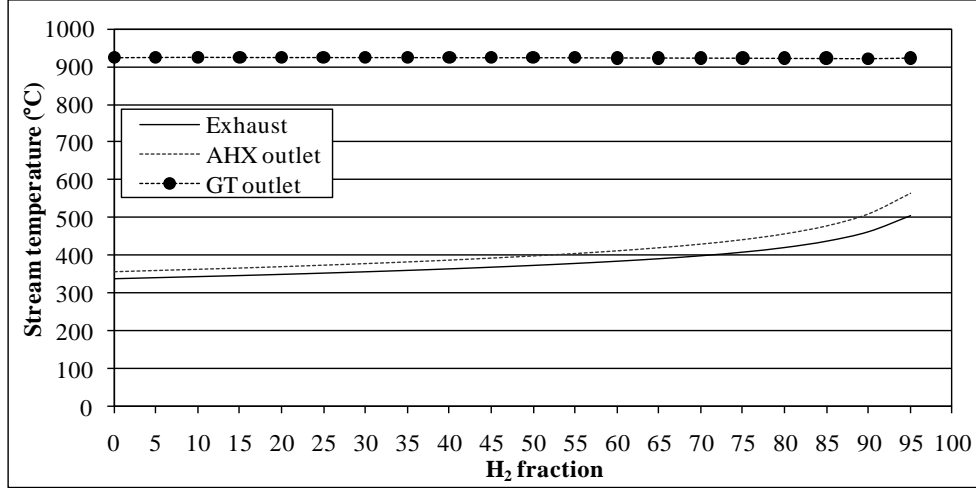


**Figure 53: Temperature of several outlet streams at the cycle with anode recirculation**

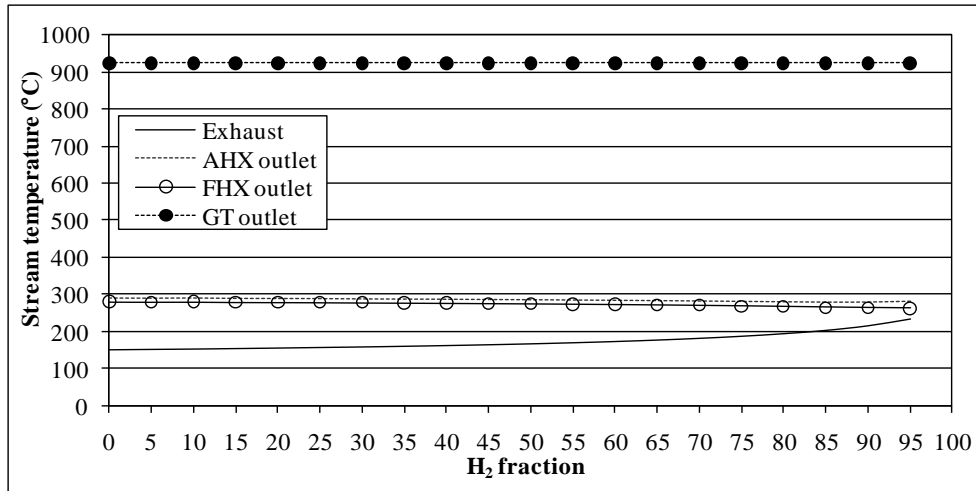


**Figure 54: Temperature of several outlet streams at the cycle without anode recirculation**

The comparison of Figures 53 and 54 shows that the exhaust temperature of the cycle without anode recirculation is much lower than that of the cycle with anode recirculation (151°C vs. 339°C for pure methane). This can be explained based on the fact that in the cycle without anode recirculation, the FHX outlet stream is further used to generate steam at WHX, which reduces the exhaust temperature and wasted heat in this configuration.

Moreover, in both configurations, the exhaust temperature increases with a decrease in the methane concentration in the inlet fuel. However, the rate of temperature increase in the cycle

with anode recirculation is much higher. It should be noted that the GT outlet temperature is constant for both configurations at approximately 924°C (Figures 53 and 54, the GT outlet temperature curve). Therefore, to evaluate the variation of the exhaust temperature, only heat exchangers AHX, FHX, and WHX need to be considered. In the cycle with anode recirculation, the AHX and FHX outlet temperatures increase due to the reduction in the air (Figure 50) and fuel mass flow rate (Figure 45), which means less energy is required to increase the air and fuel temperature. But in the cycle without anode recirculation, the AHX and FHX outlet temperatures are almost constant because of the higher air flow rate (Figure 50) in this configuration. However, the exhaust temperature increases in the cycle without anode recirculation because of a decrease in the external water mass flow rate (Figure 47). Therefore, the sensible waste energy in the cycle with anode recirculation is higher than that in the cycle without anode recirculation. It should be noted that the latent waste energy of the cycle without anode recirculation is higher than that of the cycle with anode recirculation because of the external water added to the system for the reforming process.

### 6.3.3 Effect of carbon dioxide concentration in inlet fuel on cycle performance

Table 48 shows the concentrations of methane and carbon dioxide in some fuel sources. As this table points out, the concentration of carbon dioxide can vary from around 2% to almost 40%.

**Table 48: Variation of methane and carbon dioxide concentration in some fuels**

<b>Fuel type</b>	<b>CH<sub>4</sub> (%)</b>	<b>CO<sub>2</sub> (%)</b>
<b>Natural gas</b> (Palsson et al., 2000)	97.4	1.6
<b>Farm biogas</b> (Van herle et al., 2003)	63.0	36.0
<b>Sewage biogas</b> (Van herle et al., 2003, 2004)	61.5-62.6	34.8-38.3
<b>Syngas</b> (Kee et al., 2008)	1.4	1.6
<b>Syngas (dry biomass)</b> (Kee et al., 2008)	4.7	12.9
<b>Biofuel</b> (Sucipta et al., 2008a)	13.0	15.0
<b>Gasified biomass, H<sub>2</sub>O-blown</b> (Sucipta et al., 2007)	10.0	20.0
<b>Gasified biomass, Air-blown</b> (Sucipta et al., 2007)	5.0	10.0

As this table indicates, the concentrations of methane and carbon dioxide can vary widely in the inlet fuel, which means their effects can be profound. Similar to the case of hydrogen, Figures 55 to 63 illustrate the hybrid SOFC-GT cycle performance when methane is partially replaced by CO<sub>2</sub> with an increment of 5% at each step.

### 6.3.3.1 Output power

In Figure 55, variation of output power of the SOFC, GT, and whole system for different concentrations of CO<sub>2</sub> in the fuel for two configurations is shown.

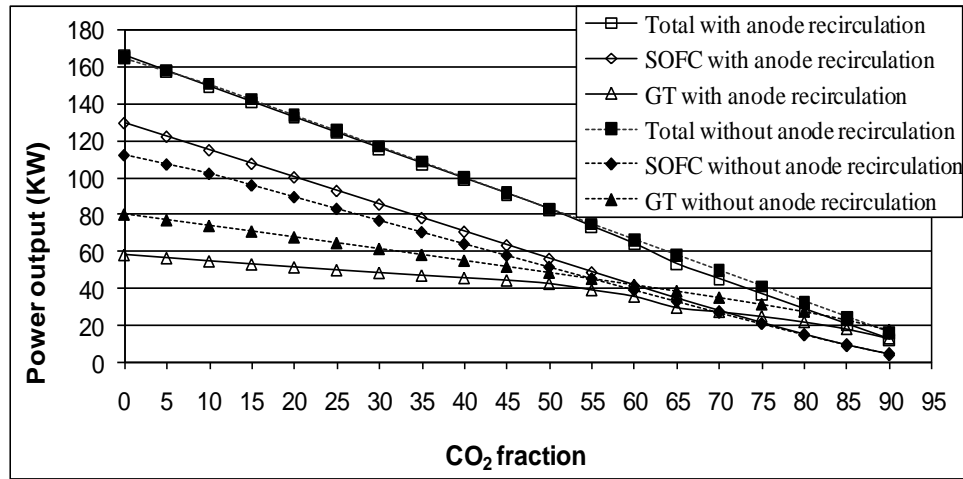
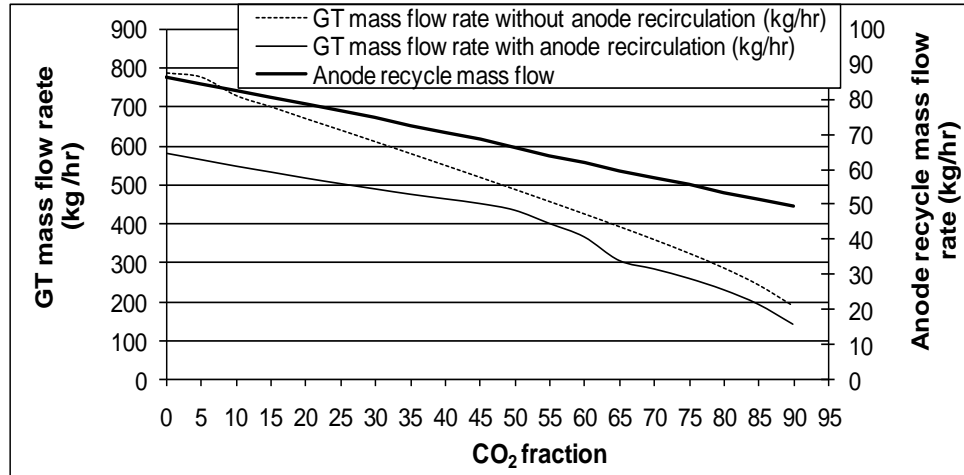


Figure 55: Output power of the GT, SOFC, and whole cycle for different configurations versus the CO<sub>2</sub> concentration in the fuel

Similar to the case of hydrogen, the output power of the GT in the configuration without anode recirculation is higher than that in the configuration with anode recirculation. As Figure 56 shows, this is because of the higher GT mass flow rate of the cycle without anode recirculation.





**Figure 56: GT mass flow rate for different configurations and anode recycle mass flow rate in cycle with anode recirculation versus CO<sub>2</sub> concentration in fuel**

The main difference between Figures 44 and 55 is that in Figure 44, the SOFC output power is always higher than that of the GT for both configurations. In Figure 55, however, for the lower concentrations of CO<sub>2</sub>, the SOFC output power is higher. Then, in some points (55% of CO<sub>2</sub> for the cycle without anode recirculation and 70% of CO<sub>2</sub> for the cycle with anode recirculation) the GT output power overtakes the SOFC output power.

In addition, in Figure 55, the output power for all cases is close to zero when there is a very high concentration of CO<sub>2</sub>. The reason for these behaviours is that, unlike H<sub>2</sub>, CO<sub>2</sub> has no energy content, and with a very high concentration of CO<sub>2</sub>, the energy content of the inlet fuel is reduced dramatically.

Figure 56 shows the GT mass flow rate for both configurations versus the concentration of CO<sub>2</sub> in the inlet fuel. In Figure 56, similar to Figure 46, the difference of the GT mass flow rate for the two configurations reduces; therefore, the GT output powers of the two configurations converge with an increase in the CO<sub>2</sub> concentration of the fuel in Figure 55. Furthermore, in Figure 56, the curve for the GT mass flow rate in the cycle with anode recirculation experiences an increase in reduction rate after CO<sub>2</sub> reaches a level of 55%. The reason for this will be explained later on. This GT mass flow rate reduction causes a lower output power of the GT, which in turn results in a lower SOFC-GT output power. This can be seen in Figure 55, where

the total output power in the configuration without anode recirculation is slightly higher than that in the other configuration, especially for a  $\text{CO}_2$  concentration of more than 60%.

Moreover, Figure 55 shows that the output power of the SOFC in the configuration with anode recirculation is higher than that of the configuration without anode recirculation. Again, this is because of the higher net fuel utilization factor in the configuration with anode recirculation. Figure 57 shows the molar flow rate of  $\text{H}_2$  and  $\text{CO}$  in the anode exhaust stream that enters the combustion chamber. As the graphs illustrate, the  $\text{H}_2$  molar flow rate in the system with anode recirculation is lower than that in the system without anode recirculation. But the  $\text{CO}$  molar flow rate in the configuration with anode recirculation overtakes the other configuration at a  $\text{CO}_2$  level of 55%. However, overall, more fuel is consumed in the SOFC in the cycle with anode recirculation, which requires a higher net fuel utilization factor in the SOFC. Also, the  $\text{CO}$  molar flow rate starts to reduce at a  $\text{CO}_2$  level of 65% for both configurations. The reason will be explained later on.

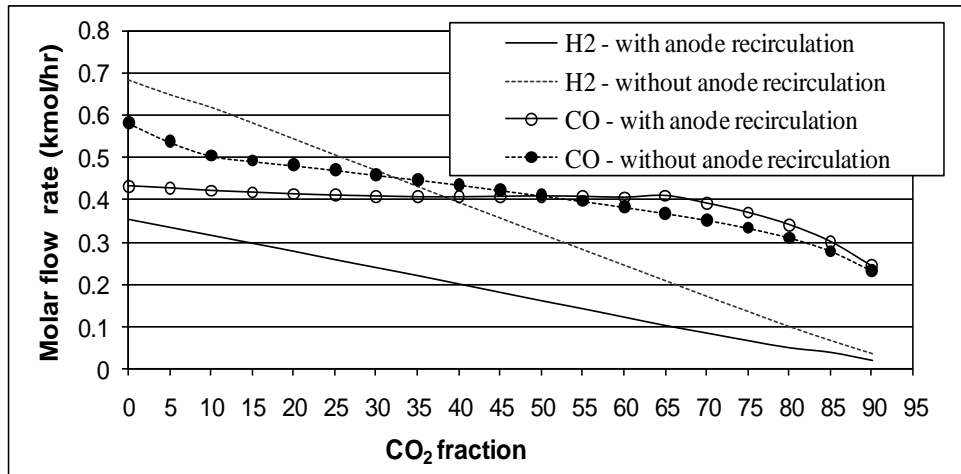


**Figure 57: Molar flow rate of  $\text{H}_2$  and  $\text{CO}$  in anode exhaust**

Figure 55 also shows that in all cases the output power reduces with an increase in the  $\text{CO}_2$  concentration. This can be explained by the inlet fuel energy content variation in Figure 58. The figure shows the variation of the input fuel's LHV, mass flow rate, and energy content with respect to the  $\text{CO}_2$  concentration in the inlet fuel for both configurations.

Although in Figure 58 the variation of the inlet fuel mass flow rate and LHV are entirely different from those in Figure 45, the fuel energy content follows the same pattern. The graphs illustrate that when the  $\text{CO}_2$  concentration is increased, the LHV of the fuel is decreased. The reason is that in this case methane (with 50 MJ/kg LHV) is replaced by  $\text{CO}_2$  with no energy content. On the other hand, for constant fuel molar flow rate, the fuel mass flow rate is increased due to higher atomic weight of  $\text{CO}_2$  in comparison to that for  $\text{CH}_4$  (16 for  $\text{CH}_4$  vs. 44 for  $\text{CO}_2$ ). Figure 58 points out that the rate of increase in the fuel mass flow rate is lower than the rate of reduction in the inlet fuel's LHV. As a consequence, the input energy of the fuel reduces as the  $\text{CH}_4$  concentration of the fuel is reduced, which in turn causes lower output power from the GT, SOFC, and cycle as a whole (Figure 55).

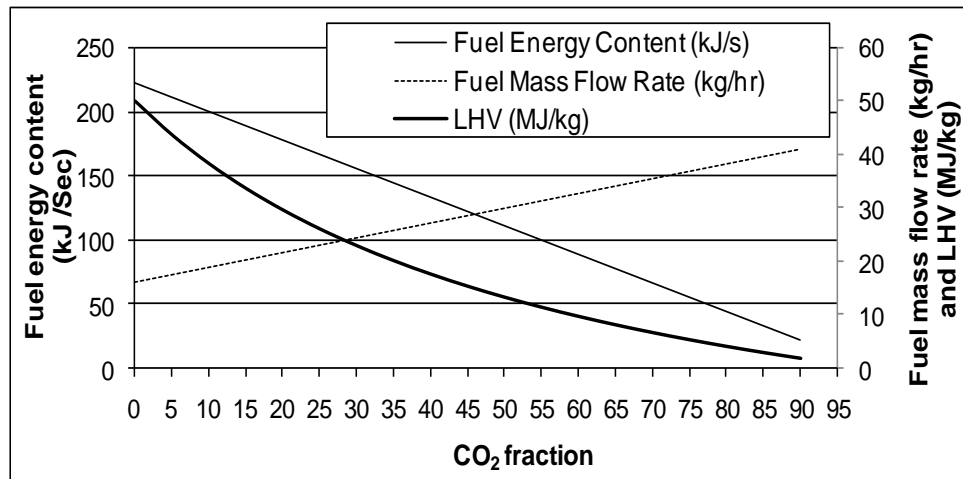


**Figure 58: Input fuel's LHV, mass flow rate, and energy content with respect to  $\text{CO}_2$  concentration**

Furthermore, comparing Figures 58 and 45 indicates that the rate of the inlet fuel energy content reduction for the mixture of  $\text{CO}_2$  and  $\text{CH}_4$  is higher than that for the mixture of  $\text{H}_2$  and  $\text{CH}_4$  (2.23 kJ/h reduction for 1% reduction in  $\text{CO}_2$  concentration vs. 1.56 kJ/h reduction for 1% reduction in  $\text{H}_2$  concentration). This is the reason for a higher output power reduction rate (in both configurations) for the mixture of  $\text{CO}_2$  and  $\text{CH}_4$  with a rate of 1.7 kW reduction for 1% reduction in  $\text{CO}_2$  concentration (Figure 55) in comparison to that for the mixture of  $\text{H}_2$  and  $\text{CH}_4$  with a rate of 1.3 kW reduction for 1% reduction in  $\text{H}_2$  concentration (Figure 44).

### 6.3.3.2 Specific Work

Figure 59 shows the variation of the specific work of the GT, SOFC, and whole cycle for different configurations with respect to the variation of  $\text{CO}_2$  concentration in the inlet fuel.

In this figure, the GT specific work is almost constant, similar to Figure 49. However, the SOFC and whole cycle specific works follow different patterns. They both reduce with the increase in the  $\text{CO}_2$  concentration. Moreover, there is a shift at a  $\text{CO}_2$  level of 65% in the cycle with anode recirculation.

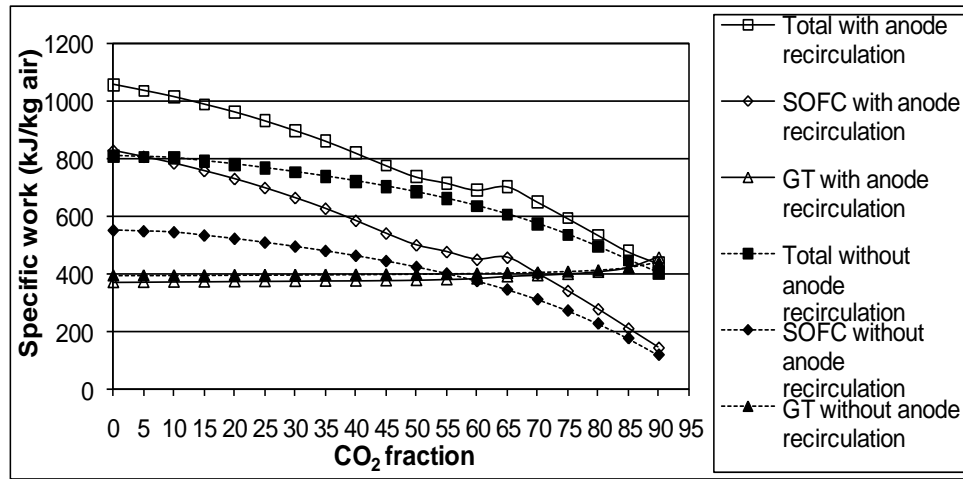


**Figure 59: Specific work of GT, SOFC and whole cycle for different configurations versus  $\text{CO}_2$  concentration**

Again, in order to investigate these graphs, both the output power and air mass flow rate should be considered. Figure 60 shows the inlet air mass flow rate and air-to-fuel ratio for different configurations versus the  $\text{CO}_2$  concentration in the inlet fuel. As previously explained for Figure 50, in order to keep the TIT constant, for less fuel energy content (Figure 58), the air-to-fuel ratio should be reduced. Also, the rate of reduction of these parameters in Figure 60 is higher than that in Figure 50. This is because of the higher rate of the inlet fuel energy content reduction in the mixture of  $\text{CO}_2$  and  $\text{CH}_4$  in comparison to that in the mixture of  $\text{H}_2$  and  $\text{CH}_4$  (Figures 45 and 58).

Similar to Figure 50, both the air-to-fuel ratio and inlet fresh air mass flow rate in Figure 60 are lower in the cycle with anode recirculation, and the curves converge.

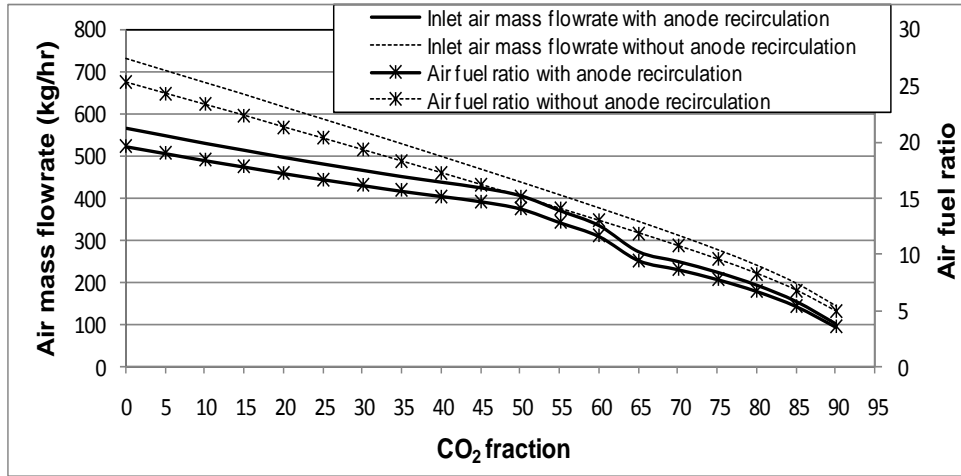


**Figure 60: Inlet air mass flow rate and air-to-fuel ratio for different configurations versus CO<sub>2</sub> concentration**

Another important feature of Figure 60 is a shift in the graphs for the configuration with anode recirculation. The main reason for this shift is temperature reduction in the fuel reformer. When CO<sub>2</sub> concentration exceeds 45%, the reformer temperature gradually declines, as shown in Figure 61. Therefore, there is no heat to be recovered in the air heater (AIRHE) and to be discharged to the atmosphere in the heat exchanger after that. Instead, the reformate should be heated at the heat exchanger FHX2 to increase the temperature to 1000°C, before entering the SOFC module. Thus, although the physical configuration of the cycle is unchanged, the real cycle configuration (the equipment that is actually involved in processes) has been altered. As a result of all these events, the inner working of the cycle is changed, and that is the reason for the shift in Figures 59 and 60 among others for the cycle with anode recirculation.

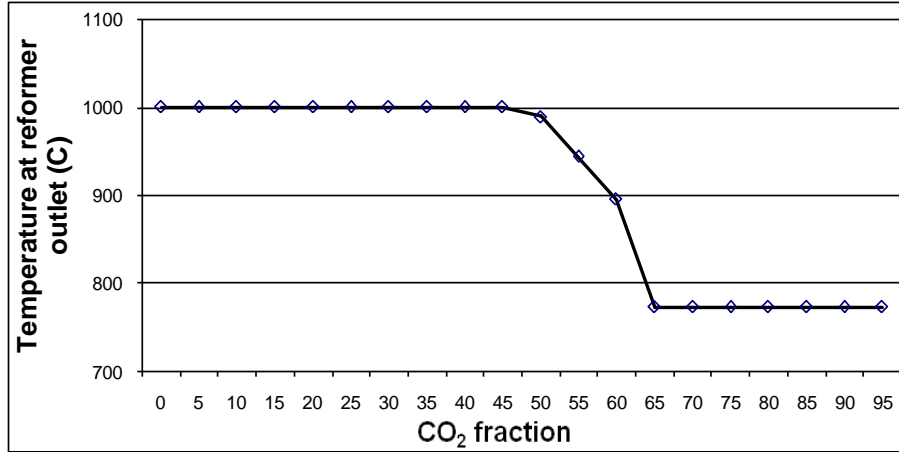


**Figure 61: Reformat temperature for the cycle with anode recirculation versus CO<sub>2</sub> concentration in fuel**

In Figure 59, the reason for the reduction in the specific work of the SOFC module and SOFC-GT cycle is that the reduction rate of their output work (Figure 55) is higher than the reduction rate of the air mass flow rate (Figure 60).

### 6.3.3.3 Efficiency

Figure 62 shows the efficiency of the SOFC and GT modules and SOFC-GT cycle for different configurations versus CO<sub>2</sub> concentration in the fuel. The variation in this figure should be investigated in conjunction with the output power (Figure 55) and the energy content of the consumed fuel (Figure 58).

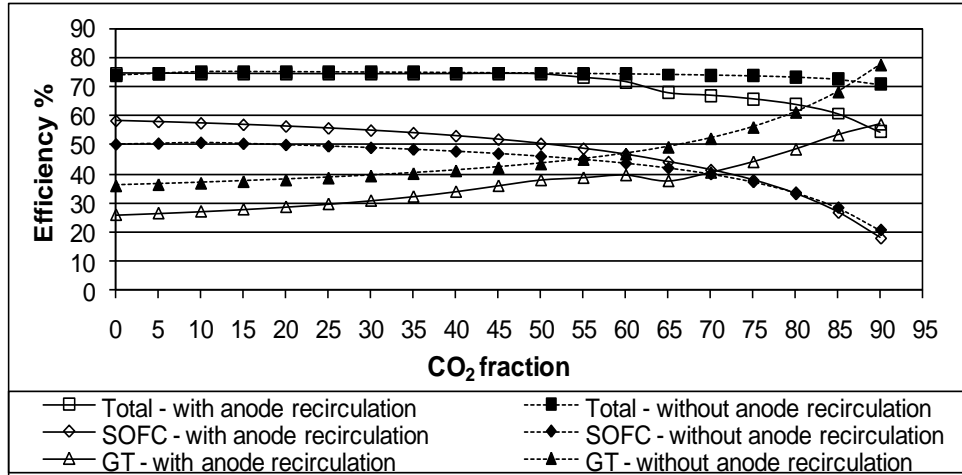


**Figure 62: Efficiency of SOFC, GT, and whole cycle for different configurations versus CO<sub>2</sub> concentration in fuel**

Figure 62 illustrates that for both configurations, the SOFC efficiency decreases and the GT efficiency increases. The SOFC-GT efficiency for the cycle without anode recirculation is almost constant, which means the reduction of the SOFC output power is compensated by the increase in the GT output power. However, in the configuration with anode recirculation, there is a shift in the GT and SOFC efficiencies. The reason for this shift was previously explained in Subsection 6.3.3.2. The trends in Figure 62, especially for the SOFC efficiency, are in good agreement with the results of Sucipta et al. (2008b).

#### 6.3.3.4 SOFC-to-GT output work ratio

Figure 63 shows the ratio of the work generated in the SOFC to the work generated in the GT. The figure indicates that less power is generated in the SOFC and more power is generated in the GT when the concentration of carbon dioxide increases in the inlet fuel.

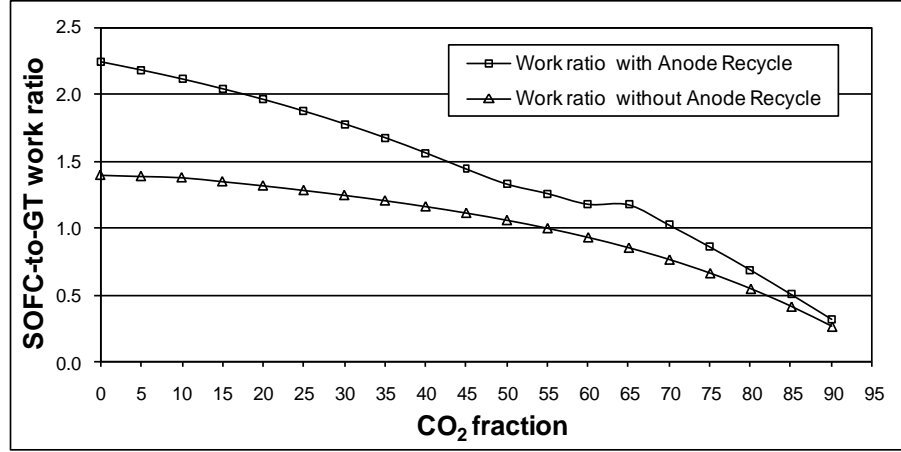


Figure 63: SOFC-to-GT output work ratio for two configurations versus CO<sub>2</sub> concentration in the fuel

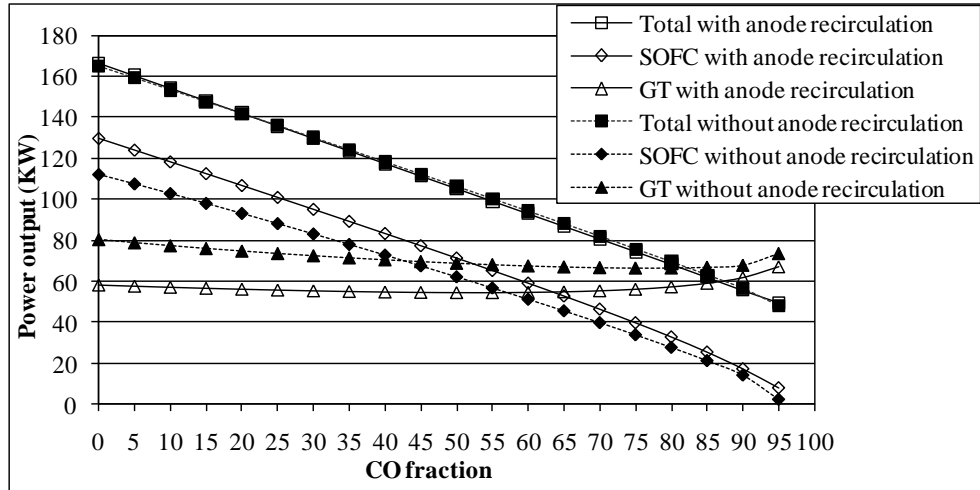
### 6.3.4 Effect of carbon monoxide concentration in inlet fuel on cycle performance

Figures 64 to 73 show the performance of the hybrid SOFC-GT system when methane is partially replaced by CO with the increment of 5% at each step in the range of 0% to 95%.

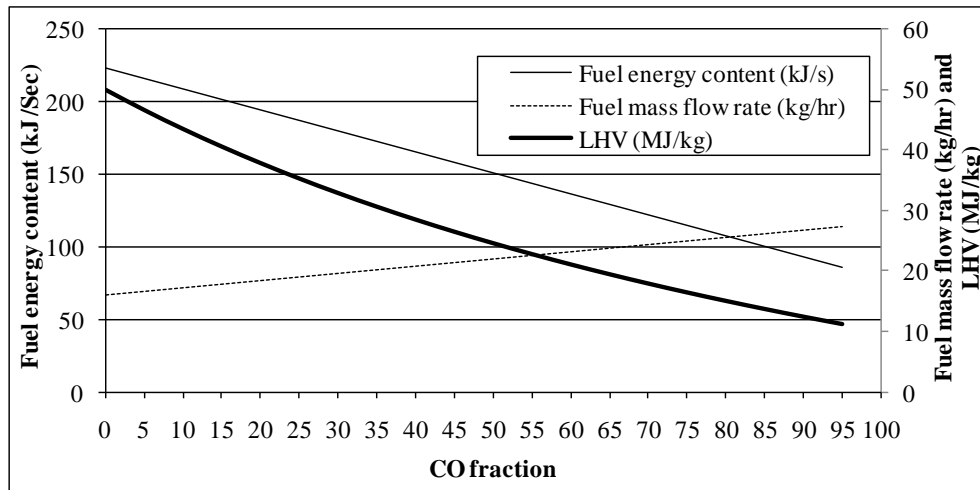
#### 6.3.4.1 Output power

Figure 64 shows the output power of the SOFC, GT, and system as a whole for different percentages of CO in the fuel for two configurations, with and without anode recirculation. Figure 64 shows that the total output power of the system reduces with an increase in CO concentration. The reason can be explained based on Figure 65. Figure 65 shows the variation of the inlet fuel's LHV, mass flow rate, and energy content with respect to CO concentration in the inlet fuel for both configurations.





**Figure 64: Output power of SOFC, GT, and system as a whole for different configurations versus CO concentration in fuel**



**Figure 65: Inlet fuel's LHV, mass flow rate, and energy content with respect to CO concentration in inlet fuel**

Figure 65 illustrates that when CO concentration is increased, the LHV of the fuel decreases significantly because of the much lower LHV of carbon monoxide in comparison to that of methane (11 MJ/kg for CO vs. 50 MJ/kg for  $\text{CH}_4$ ). On the other hand, for a constant fuel molar flow rate of the fuel, the fuel mass flow rate is increased due to the lower atomic weight of  $\text{CH}_4$  in comparison to CO (16 for  $\text{CH}_4$  vs. 28 for CO). Figure 65 points out that the rate of decrease in the fuel's LHV is higher than the rate of increase in the fuel mass flow rate. As a result, energy

content of the fuel reduces. For instance, if the methane concentration of the fuel is reduced from 90% to 50%, the LHV will be decreased by 18.8 MJ/kg, and the fuel mass flow rate will be increased by 4.8 kg/h. These two effects will cause fuel energy content to reduce by 57.7 kJ/s. Therefore, the input energy of the fuel and as a result the total output power of the cycle reduces as  $\text{CH}_4$  concentration of the fuel decreases. Moreover, the reduction in the system efficiency, as shown in Subsection 6.3.4.3 in Figure 73, further reduces the output power.

In Figure 64, the variation of the GT output power follows a completely different pattern in comparison to the previous cases. The GT output power slightly decreases with an increase in CO concentration for both configurations. It reaches a minimum at a CO level of 55% for the cycle with anode recirculation and 75% for the cycle without anode recirculation. Then, the GT output power increases. In order to explain these curves, it should be noted that since the TIT and the GT efficiency are maintained constant, the output power of the gas turbine only depends on the mass flow rate of the stream that passes through it. Figure 66 shows the mass flow rate of the GT inlet for two configurations.

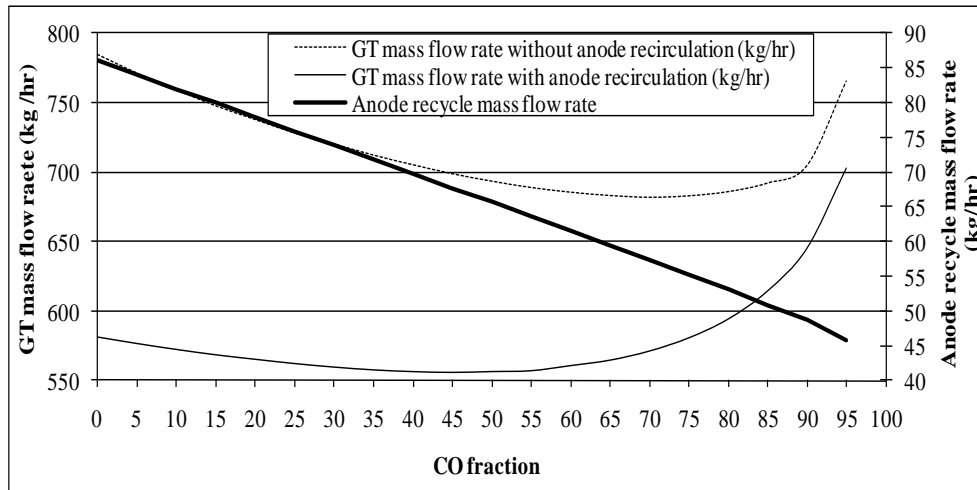


**Figure 66: GT mass flow rate for both configurations and anode recycle mass flow rate in cycle with anode recirculation versus CO concentration**

Figure 66 points out that the GT mass flow rate for both configurations follows exactly the same pattern as the GT output power. This variation of the GT mass flow rate can be explained by

revisiting reactions in Equations 1 and 2. These reactions show that for one mole of  $\text{CH}_4$  reacting in the cycle, four moles of  $\text{H}_2$  can be produced, whereas for one mole of  $\text{CO}$ , only one mole of  $\text{H}_2$  can be produced. On the other hand, the electrochemical reaction of the SOFC only consumes hydrogen. Therefore, as carbon monoxide replaces methane, less hydrogen is available for the reaction in the SOFC.

Figures 67 and 68 illustrate the concentrations of  $\text{H}_2$  and  $\text{CO}$  in the anode inlet and the anode outlet, respectively. Figure 67 shows that at the reformer outlet (anode inlet) the concentration of  $\text{CO}$  increases gradually in contrast to the concentration of  $\text{H}_2$ , which decreases sharply. Regarding the fact that the fuel utilization factor of the SOFC is fixed to 85%, this reduction in concentration of hydrogen in the anode inlet can explain the reason for the decrease in the output power of the SOFC. A similar pattern can be observed for carbon monoxide and hydrogen concentration in the anode outlet stream (the part that is not recycled in the cycle with anode recirculation) in Figure 68.

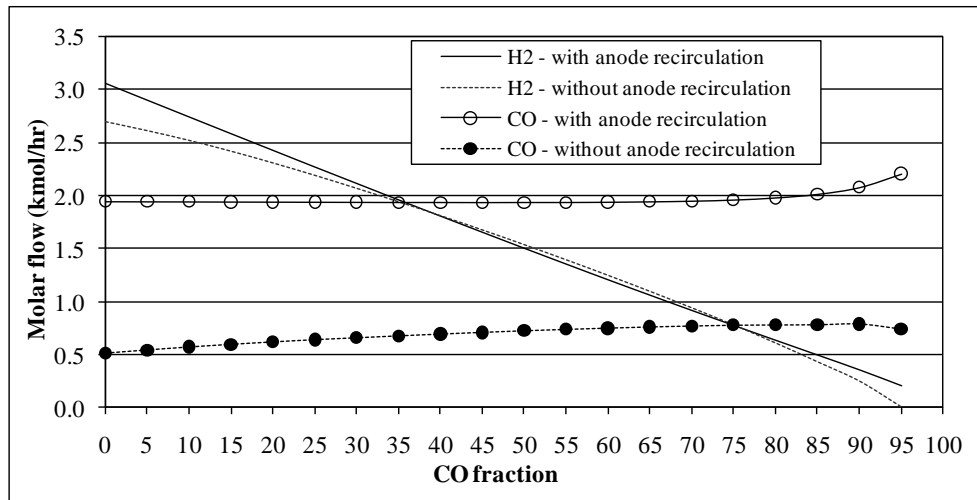


**Figure 67: Molar flow rate of  $\text{H}_2$  and  $\text{CO}$  in anode inlet for both configurations with respect to  $\text{CO}$  concentration**

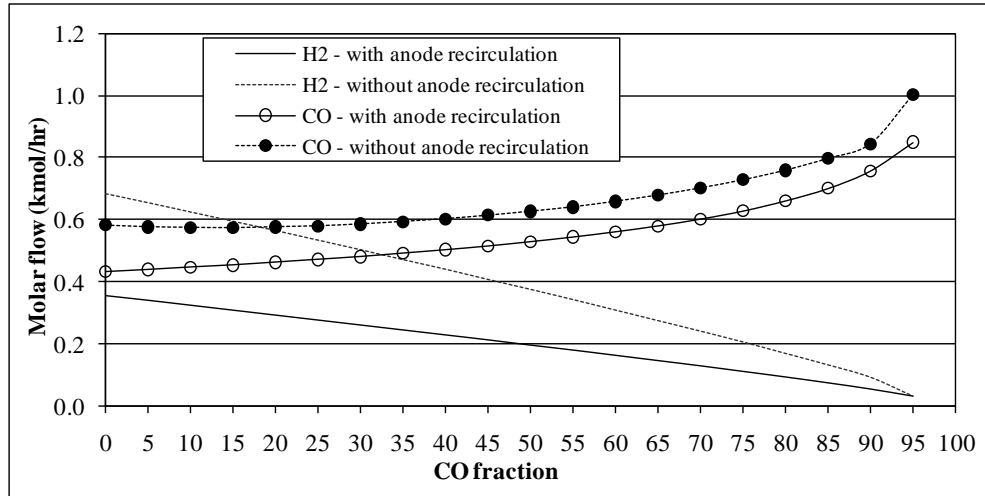


**Figure 68: Molar flow rate of H<sub>2</sub> and CO in anode outlet for both configurations with respect to CO concentration**

The effect of these variations in the composition of the streams on the LHV, mass flow rate, and energy content of the anode inlet and outlet streams can be seen in Figures 69 and 70. As Figure 69 illustrates, both the LHV and mass flow rate of the anode inlet stream decrease for both configurations. Therefore, the energy content of the flow reduces. The combination of the reduction in energy content and concentration of hydrogen in the anode inlet stream results in the reduction of the output power from the SOFC.

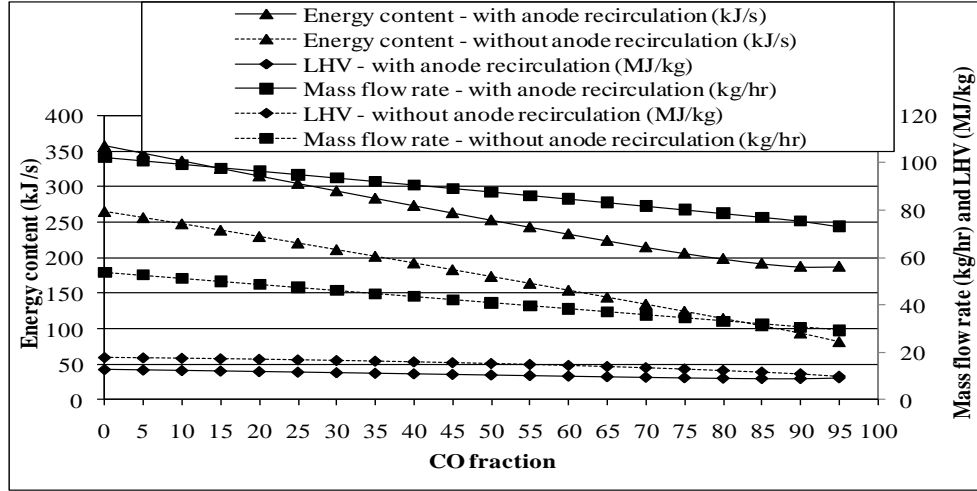


Figure 69: LHV, mass flow rate, and energy content of anode inlet stream for both configurations with respect to fuel CO concentration

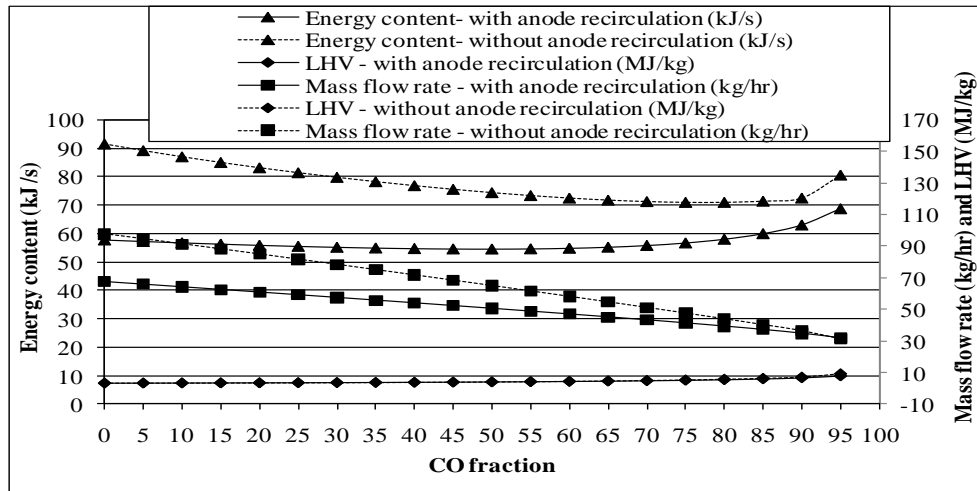
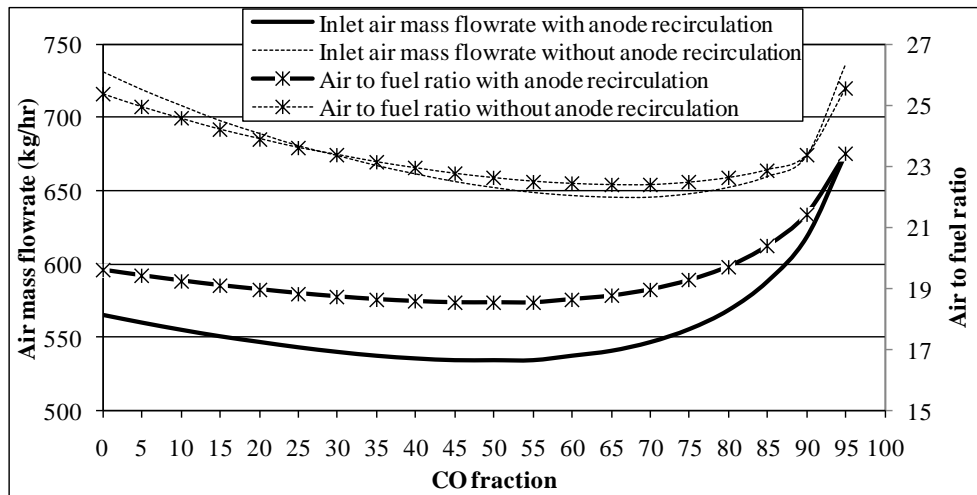


Figure 70: LHV, mass flow rate, and energy content of anode outlet stream for both configurations

On the other hand, Figure 70 shows that in the anode output stream, while the LHV of the stream increases, the mass flow rate decreases for both configurations. Initially, the rate of mass flow reduction is higher than the rate of increase in the LHV. As a result, the energy content of the anode outlet gradually decreases until it reaches a minimum. This minimum occurs at a CO level of 55% for the cycle with anode recirculation and 75% for the cycle without anode recirculation.

Then, the effect of the increase in the LHV overtakes the effect of the decrease in the mass flow rate, so the energy content of the stream increases. This pattern is similar to the trend that has already been observed for the mass flow rate of the GT and its output power (Figures 66 and 64, respectively). A similar trend can be seen in Figure 71 for variation of the air-to-fuel ratio and inlet air mass flow rate versus CO concentration in the inlet fuel. The reason is that, when the energy content of the anode outlet and as a result the available heat for combustion in the GT combustor changes, in order to keep the TIT constant, the air-to-fuel ratio and as a consequence the air flow rate has to be adjusted.



**Figure 71: Inlet air mass flow rate and air-to-fuel ratio for both configurations versus CO concentration in inlet fuel**

Now, since the general trends in Figure 64 have been explained, the already presented figures can be revisited to evaluate other properties of the curves. Figure 66 shows that the difference of the GT mass flow rate for two configurations reduces and the curves get closer with the increase of CO concentration in the inlet fuel. This is due to the fact that for processing of  $\text{CH}_4$ , both the methane reforming and water-gas shift reactions are required. But for carbon monoxide processing, the water-gas shift reaction is the only required reaction. As a result, for methane processing more steam is required, which in turn requires more anode recirculation. This can be observed in the curve for anode recycle mass flow rate (Figure 66). The curve shows that with

decrease in methane concentration in the inlet fuel, the mass flow rate of the anode recirculation stream decreases.

The effect of this pattern can be seen in Figure 64, where the curves for the GT output power of two configurations get closer with an increase in carbon monoxide concentration in the fuel. However, since even with 100% carbon monoxide some steam is still required for the water-gas shift reaction, the anode mass flow rate does not approach zero at the end of the curve in Figure 66. Therefore, in all other curves, properties of the system for two configurations get closer with the increase in the CO concentration in the inlet fuel but they do not completely converge. Generally, when more  $\text{CH}_4$  is replaced by CO, the difference between the two configurations decreases.

#### 6.3.4.2 Specific Work

Figure 72 shows how specific work of SOFC, GT, and system as a whole for different configurations vary with respect to CO concentration in the inlet fuel.

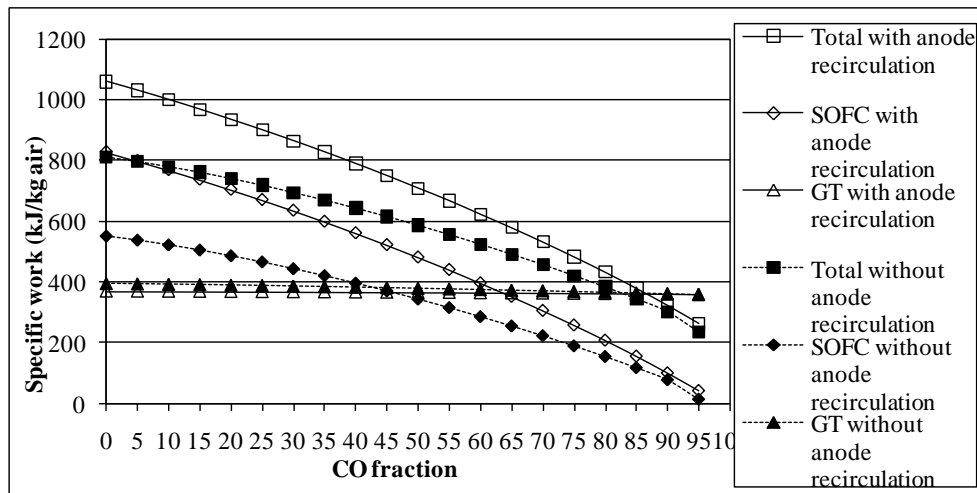


Figure 72: Specific work of SOFC, GT, and system as a whole for two configurations versus CO concentration in fuel

In order to investigate the curves in Figure 72, both output power (Figure 64) and air mass flow rate (Figure 71) should be considered. As Figure 71 shows, both air-to-fuel ratio and inlet fresh air mass flow rate are lower in the cycle with anode recirculation. This is because of the higher SOFC net fuel utilization factor in the cycle with anode recirculation, which means there is less fuel to be combusted in the combustion chamber to increase the TIT. This can be seen in Figure 70, where the energy content of the anode outlet in the configuration with anode recirculation is much lower than that in the configuration without anode recirculation.

Figure 72 points out that the total and SOFC specific works sharply reduce when the concentration of CO increases. Figure 71 shows that the inlet air mass flow rate first decreases and then increases; however, the rate of decrease in output power is much higher. Therefore, the specific work of the SOFC and cycle as a whole reduces continuously. Also, since the variation of the GT output power and the air mass flow rate follow the same pattern, the specific work of the GT is almost constant.

In addition, the total and SOFC specific works of the configuration with anode recirculation are higher than those in the other configuration. This can be explained based on the fact that the inlet air mass flow rate of the cycle with anode recirculation is lower than that in the cycle without anode recirculation (Figure 71). On the other hand, the total output power is almost equal for both configurations (Figure 64), and the SOFC output power in the configuration with anode recirculation is higher (Figure 64). The combination of these effects results in the higher specific work of the SOFC and the cycle as a whole in the configuration with anode recirculation. But for the GT, the output power of the cycle without anode recirculation is higher (Figure 64), and the difference between the output powers of the two configurations is very close to the difference between the air mass flow rate of the two configurations. As a result, the specific output power of the GT for two configurations is very close.

#### **6.3.4.3 Efficiency**

Figure 73 shows the efficiency of the SOFC, GT, and cycle for both configurations versus CO concentration in the fuel. Since efficiency depends on the output power (Figure 64) and the



energy content of the consumed fuel to generate this power (Figure 65), these two parameters should be considered to investigate Figure 73.

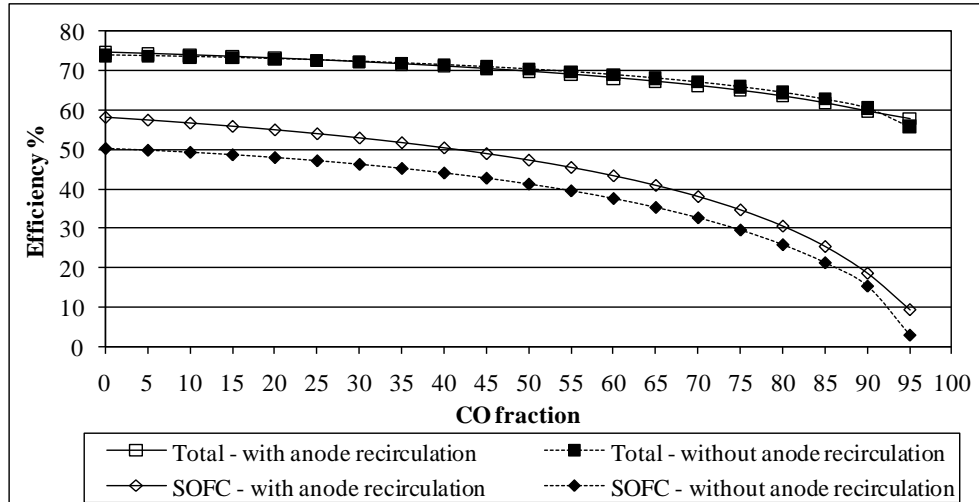


**Figure 73: Efficiency of SOFC and cycle as a whole for both configurations versus CO concentration**

Figures 64 and 65 illustrate that the output power of the SOFC and cycle as a whole as well as the energy content of the fuel reduce when  $\text{CH}_4$  is replaced by CO. But since the rate of reduction in the output power is greater than the rate of reduction in the inlet fuel energy content, the efficiencies of both the cycle and the SOFC decrease. The trend of the variation in the SOFC and whole cycle efficiencies in Figure 73 is in good agreement with the results presented by Sucipta et al. (2008b).

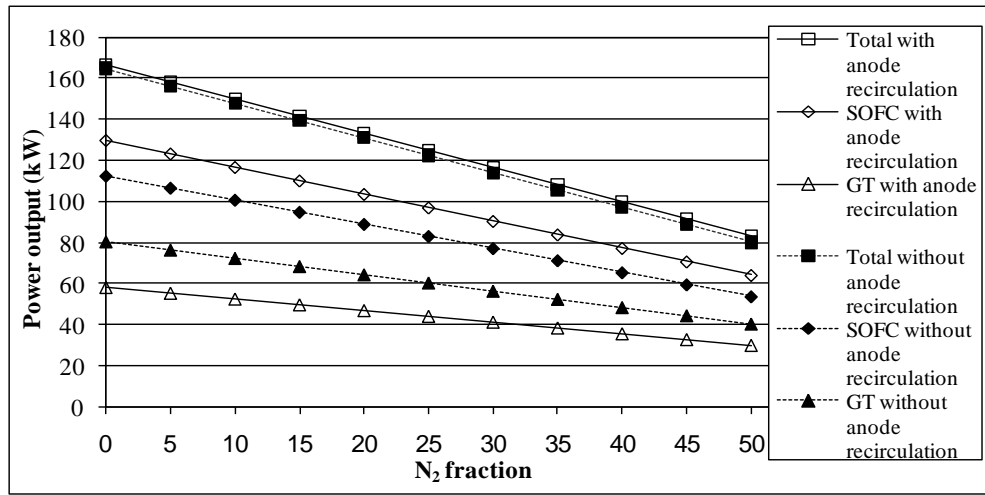
### 6.3.5 Effect of nitrogen concentration in inlet fuel on cycle performance

The concentration of nitrogen can vary substantially in manufactured fuels, especially in fuels produced by the gasification process. In this process, fuel composition depends on the gasifying agent (steam, air, or oxygen). Due to the high concentration of nitrogen in air, depending on the gasifying agent, the concentration of nitrogen in produced fuels can vary greatly, from around 5% in steam and oxygen blown gasification to more than 50% in air blown systems.

Figures 74 to 80 show the performance of the hybrid SOFC-GT system when methane was partially replaced by  $N_2$  with the increment of 5% at each step.

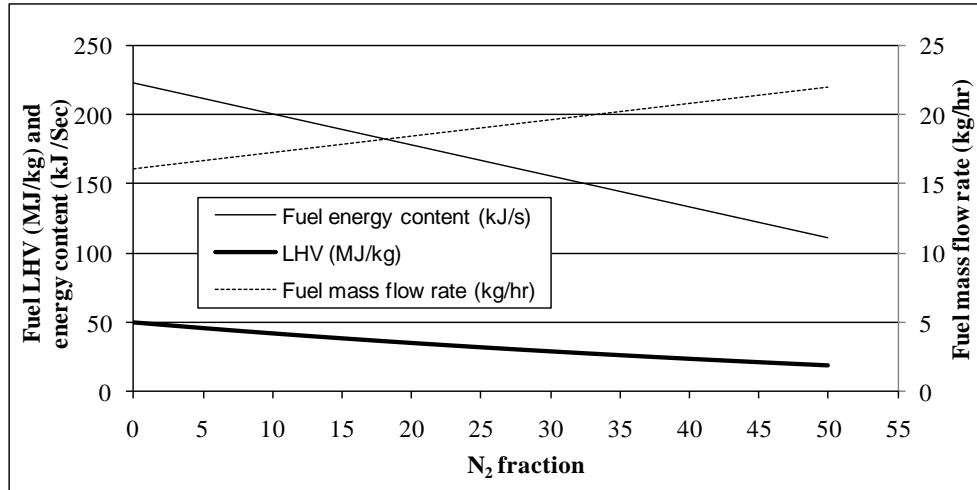
### 6.3.5.1 Output power

Figure 74 shows the output power of the SOFC, GT, and the system as a whole for different percentages of  $N_2$  in the fuel for both configurations.



**Figure 74: Output power of SOFC, GT, and system as a whole for different configurations versus  $N_2$  concentration in fuel**

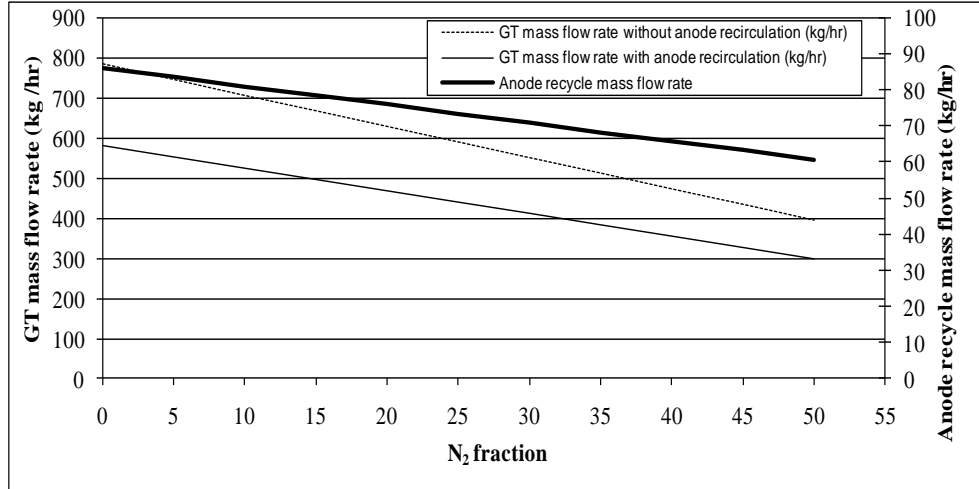
Figure 74 shows that output powers for all cases reduce with an increase in  $N_2$  concentration. The reason can be explained based on Figure 75, which shows the variation of the input fuel's LHV, mass flow rate, and energy content with respect to  $N_2$  concentration in the inlet fuel for both configurations.



**Figure 75: Inlet fuel's LHV, mass flow rate, and energy content with respect to N<sub>2</sub> concentration in inlet fuel**

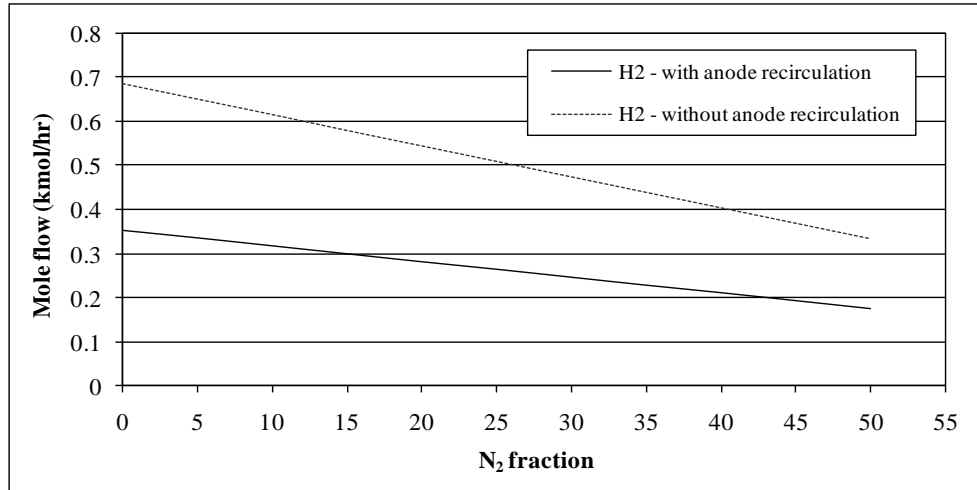
Figure 75 illustrates that when N<sub>2</sub> concentration is increased, the LHV of the fuel decreases significantly. The reason is that methane (with 50 MJ/kg LHV) is replaced by N<sub>2</sub> with no energy content. On the other hand, for a constant fuel molar flow rate (1 kmole/h), the fuel mass flow rate is increased due to the lower atomic weight of CH<sub>4</sub> in comparison to that of N<sub>2</sub> (16 for CH<sub>4</sub> vs. 28 for N<sub>2</sub>). Figure 75 points out that the rate of decrease in the fuel's LHV is higher than the rate of increase in the fuel mass flow rate. As a result, the energy content of the fuel reduces. For instance, if the methane concentration of the fuel is reduced from 90% to 50%, the LHV will be decreased by 23.7 MJ/kg (from 41.9 to 18.2 MJ/kg), and fuel mass flow rate will be increased by 4.8 kg/h (from 17.2 to 22.0 kg/h). These two effects will cause the fuel energy content to reduce by 89.2 kJ/s (from 200.7 to 111.5 kJ/s). Therefore, the input energy of the fuel and as a result the SOFC, GT, and total output powers of the cycle reduce as the CH<sub>4</sub> concentration of the fuel decreases.

Figure 74 also shows that the output power of the GT in the configuration without anode recirculation is also higher than the case with anode recirculation due to the lower actual mass flow rate of the GT as a result of the anode exhaust recirculation. Figure 76 shows the GT mass flow rate for both configurations. It can be seen that the mass flow rate through the GT in the configuration without anode recirculation is higher than that of the configuration with anode recirculation.



**Figure 76: GT mass flow rate for both configurations and anode recycle mass flow rate in cycle with anode recirculation versus N<sub>2</sub> concentration**

Figure 74 shows that output power of the SOFC in the configuration with anode recirculation is higher than that of the configuration without anode recirculation due to the higher SOFC net fuel utilization factor of the former. Figure 77 shows the molar flow rate of H<sub>2</sub> in the anode outlet that enters the combustion chamber. As the curves illustrate, the H<sub>2</sub> concentration in the system with anode recirculation is lower than that in the system without anode recirculation. This means more hydrogen is consumed in the SOFC in the cycle with anode recirculation, which in turn confirms that the net fuel utilization factor in the SOFC is higher in this configuration.



**Figure 77: Molar flow rate of H<sub>2</sub> in the anode outlet for both configurations with respect to N<sub>2</sub> concentration**

In addition, Figure 74 shows that the total output power of the system for both configurations is very close. This is because the output power reduction in the GT, due to the anode exhaust recirculation, is partially compensated by the power increase in the SOFC.

### 6.3.5.2 Specific Work

Figure 78 shows the specific work of the SOFC, GT, and system as a whole for different configurations with respect to N<sub>2</sub> concentration in the inlet fuel. In order to investigate Figure 78, both the output power and air mass flow rate should be considered. Figure 79 shows the inlet air mass flow rate and air-to-fuel ratio for different configurations versus N<sub>2</sub> concentration in the fuel. As Figure 79 shows, both the air-to-fuel ratio and inlet fresh air mass flow rate are lower in the cycle with anode recirculation.

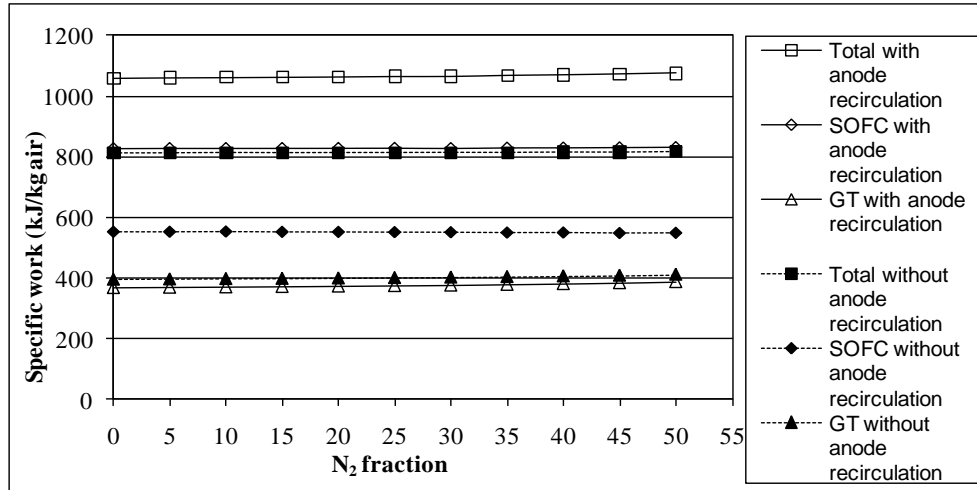


**Figure 78: Specific work of SOFC, GT, and the system as a whole for two configurations versus N<sub>2</sub> concentration in fuel**

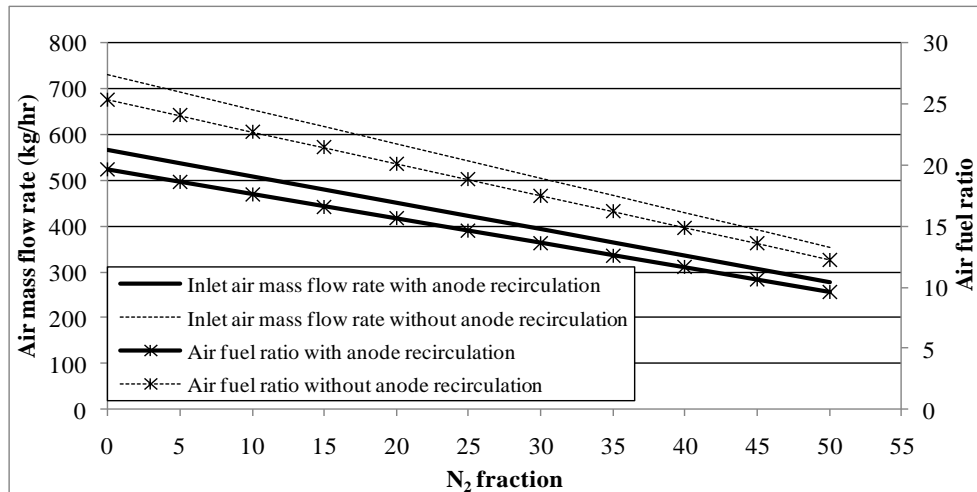


**Figure 79: Inlet air mass flow rate and air-to-fuel ratio for both configurations versus N<sub>2</sub> concentration**

Figure 78 points out that the SOFC, GT, and total specific work are almost constant when the concentration of N<sub>2</sub> increases. The reason is that the rate of reduction in the SOFC output power (Figure 74) is very close to the rate of reduction in the air mass flow rate (Figure 79).

### 6.3.5.3 Efficiency

Figure 80 shows the efficiency of the SOFC and cycle as a whole for both configurations versus  $N_2$  concentration in the fuel.

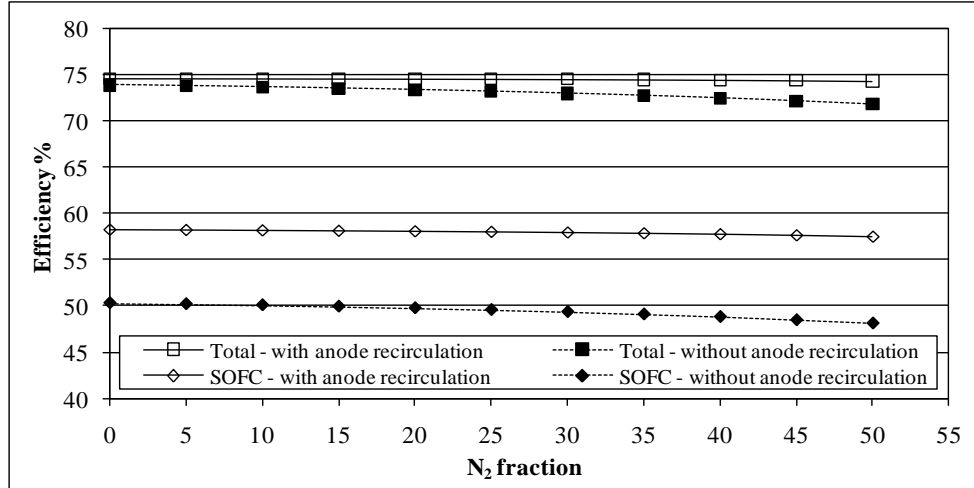


Figure 80: Efficiency of SOFC and cycle as a whole for both configurations versus  $N_2$  concentration

Figures 74 and 75 illustrate that the output power of the SOFC and cycle as a whole as well as the energy content of the fuel reduce when  $CH_4$  is partially replaced by  $N_2$ . Since the rate of reduction in the output power is very close to the rate of reduction in the inlet fuel energy content, the efficiencies of the cycle with anode recirculation are constant and the efficiencies of the cycle without anode recirculation slightly reduce.

## 6.4 Conclusions and future work

In this chapter, the model described in the previous sections was applied to investigate the effects of the inlet fuel type and composition on the performance of the hybrid SOFC-GT cycle. This type of analysis is vital for the real world application of the hybrid SOFC-GT system due to the fact that the manufactured fuels' composition, especially biogas and syngas, depends on the type of material that is processed, the fuel production process, and process control parameters.

In the first part of the chapter, the detailed information of the operation of the syngas fuelled SOFC-GT cycle was presented. This analysis can be very helpful in understanding cycle internal working and can provide some interesting insights to the system operation.

In the second part of the chapter, the results of the simulation for different types of the inlet fuel showed that system outputs and operational parameters were greatly influenced by changes in the fuel type. Therefore, the possibility of variation of the inlet fuel type should be considered, and its impacts should be investigated before utilization of biogas, gasified biomass, and syngas as fuel in hybrid SOFC-GT cycles.

Finally, in the third part of the chapter, the sensitivity analyses of the impacts of the concentration of the different components, namely, hydrogen, carbon dioxide, carbon monoxide, and nitrogen, in the inlet fuel on the performance of the hybrid SOFC-GT cycle were performed. The simulation results were presented with respect to a reference case, when the system was fuelled by pure methane. Then, the performance of the hybrid SOFC-GT system when methane was partially replaced by each component within a corresponding range of concentration with an increment of 5% at each step was investigated.

The results showed that the output power of the SOFC, GT, and cycle as a whole decreased sharply when methane was replaced with other species in all cases, except for the GT output power for CO. The specific work and efficiency of the SOFC, GT, and cycle as a whole could be increased, decreased, or remain unaffected when methane was replaced with other species, depending on each individual case. Also, in all cases, the differences of the cycle with two configurations, with and without anode recirculation, were presented. All these changes were justified by investigating the system's operational parameters. This study confirmed the importance of fuel composition impacts on the SOFC-GT cycle performance.

The following recommendations can extend and add to the results presented in this chapter in the future:

- 1- The ultimate objective of this work is to provide 3-D mapping of the effect of the concentration of various species in the inlet fuel on the hybrid cycle performance. In these analyses, for each three species, such as CH<sub>4</sub>, H<sub>2</sub>, and CO<sub>2</sub>, 3-D graphs should be prepared for none-methane species concentration as axes x and y, and axis z for the



performance parameter of the cycle. In these diagrams, the concentration of methane will be equal to the balance of the other two species.

- 2- Similar to the future work of Chapter 5, it will be interesting to repeat these analyses with the improved model based on the comments from Chapter 4, and to evaluate the impacts of the assumptions of this study on the results.
- 3- As noted in Subsection 4.3.2.1.2, in this model hydrogen is the only electrochemically active species. However, for high concentrations of CO and other species in the inlet fuel, the validity of neglecting CO electrochemical oxidation is not certain, and there are no experimental or numerical data available in the literature to evaluate this assumption. This is particularly important for the analysis in Subsection 6.3.4, and the results of this subsection should be revisited after adjusting the model by including the CO electrochemical reaction.
- 4- It can be interesting to run the model based on the assumption of either a fixed inlet fuel mass flow rate or a fixed inlet air mass flow rate as a control parameter of the model and compare the results with those of the present work.

## **CHAPTER SEVEN**

### **Performance Analysis of Micro Gas Turbines Fuelled by Blends of Biodiesel and Petroleum-Based Diesel: Experimental and Modeling Approach**

Micro gas turbines (MGT) are an alternative to conventional power generation in many applications. In addition, biodiesel is a renewable alternative for petroleum-based diesel. The objective of the first part of this work is to experimentally evaluate the performance of a 100 kW micro gas turbine fuelled by the blends of biodiesel and petroleum-based diesel. The concentration of biodiesel in the fuel was 10%, 20%, and 30% (mass-based). The engine performance was modified by mounting various sensors to monitor and record system performance parameters, such as shaft rotational speeds, pressures, temperatures, and flow rates at various locations as well as output power, ambient conditions, and exhaust stream composition. The results indicated that some parameters, such as system electrical efficiency, compressor rotational speed, compressor pressure ratio, and exhaust stream temperature, were slightly influenced by changes in the fuel composition. Some parameters were affected significantly, such as the mass and volumetric flow rate of the fuel. Also, the changes in turbine inlet temperature strongly depended on the output power.

In the second part of this work, a steady-state model of a micro gas turbine was developed to evaluate the performance of the system, when fuelled by the blends of biodiesel and petrodiesel. In order to validate the developed model, the results of the modelling work were compared against the experimental data obtained in the first part of this chapter. The results indicated that most parameters were influenced, to some degree, by changes in the fuel composition.

The results of this chapter point out that although most MGTs can be potentially operated using a high concentration of biodiesel blends, before this fuel switching can be implemented, the system operational parameters should be evaluated by the system modeling to predict possible negative impacts of biodiesel in the inlet fuel on the engine performance.

## **7.1 Introduction**

Micro gas turbines are gas turbines with the power generation capacity of lower than 1 MW. There is no universally accepted output power range for MGTs, and various references reported different ranges, such as between 30 to 350 kW (Aras and Balli, 2008) or 25 to 1000 kW (U.S. Department of Energy, 2000). However, a power range of 10 to several hundred kilowatts seems reasonably wide enough to cover all MGTs. Due to their compact size and relatively low capital costs, MGTs are suitable for some applications, such as distributed and residential power generation, peak shaving, uninterrupted generation, back-up power, mechanical drive, premium power, remote power, and combined heat and power (CHP) or combined cooling, heat, and power (CCHP). Micro turbine development started in the 1940s for automotive and transportation applications. Later, their applications shifted toward distributed, mobile, and military electric power generation.

The most common configuration of MGTs consists of a compressor, turbine, and generator connected by a single shaft and a combustor, where almost all types of liquid and gaseous fuels can be combusted (Aras and Balli, 2008). They are usually equipped with a regenerator (recuperator) to recover thermal energy from the turbine exhaust stream and increase inlet air temperature to the combustor, which results in lower fuel consumption and significantly higher efficiency. The regenerator can be rotating or stationary (parallel ducts). The rotating regenerators are usually more compact and efficient. They can be made of metal or ceramics. The rotating regenerators can suffer from leakage between hot and cold gas streams. The sealing problem can be intensified by deformation caused by the temperature gradient between the hot and cold faces in the metallic disks. The ceramic disk expansion is almost negligible, so the sealing is simpler. The rotating regenerators can be driven by applying torque either at the rim or the centre (Chiang, Hong, and Lee, 2007). It should be noted that some companies have developed dual-shaft systems and cycles with no heat recovery system. Chiang et al. (2007)

compared the specifications and configurations of some of the commercially available micro turbines. The electrical efficiency of between 23% to 33% for the system with a regenerator and around 15% without a regenerator has been reported (Chiang et al., 2007).

To improve the performance of micro gas turbines and/or reduce their environmental impacts, several approaches have been proposed, such as utilization of micro turbines in CCHP plants (Popovic, 2002), hybrid solid oxide fuel cell and MGT cycles (Song et al., 2005), and biodiesel fuelled MGTs (Chiang, Chiang, and Li, 2009).

Biofuels, such as biodiesel, are environmentally friendly alternatives for conventional fossil fuels. They can be derived from renewable resources, such as vegetable oils or animal fat. Their advantages can be enumerated as: very low emissions (especially when the life cycle emissions are taken into account, though some specific emission sources, such as  $\text{NO}_x$ , may increase), easy to use in conventional engines, nontoxic, biodegradable, improved lubricity, and free of sulfur and aromatics (Chiang et al., 2009). However, biodiesel's volumetric and mass heating value is lower than that of petroleum-based diesel, and it suffers from poor cold flow performance, due to higher viscosity and density, which may cause some problems in the fuel injection system (Karra, Veltman, and Kong, 2008). Also, it has been reported that the  $\text{NO}_x$  emission increases in biodiesel fuelled engines (Senatore, Cardone, Rocco, and Prati, 2000; Li, 2010). Biodiesel can be used alone or can be blended with petroleum diesel at any level to form a biodiesel blend. The "B" factor is an internationally accepted system, which refers to the mass-based percentage of biodiesel in the biodiesel blend. For instance, B30 refers to a blend with 30% biodiesel and 70% petroleum-based diesel, and B100 refers to a pure biodiesel. A biodiesel blend, particularly with a low concentration of biodiesel ( $< \text{B}20$ ), can be easily used in conventional engines with little or no modifications (Chiang et al., 2009). Some properties of petroleum-based diesel and biodiesel are compared in Table 49.

The objective of this part is to present the performance of a micro gas turbine, when it is fuelled by blends of biodiesel and petroleum-based diesel with different concentrations.

**Table 49: Properties of typical diesel and biodiesel fuels (Borbely and Kreider, 2001)**

Fuel property		Diesel	Biodiesel
Fuel standard		ASTM D975	ASTM D6751
Lower heating value (kJ/m <sup>3</sup> )		~35,944×10 <sup>3</sup>	~32,914×10 <sup>3</sup>
Kinematic viscosity (m <sup>2</sup> /s@40°C)		1.3×10 <sup>-6</sup> to 4.1×10 <sup>-6</sup>	4.0×10 <sup>-6</sup> to 6.0×10 <sup>-6</sup>
Density (kg/m <sup>3</sup> @15°C)		849	879
Boiling point (°C)		180 to 340	315 to 350
Flash point (°C)		60 to 80	100 to 170
Cloud point (°C)		-15 to 5	-3 to 12
Pour point (°C)		-35 to -15	-15 to 10
Cetane number		40 to 55	48 to 65
Composition	Carbon (wt%)	87	77
	Hydrogen (wt%)	13	12
	Oxygen (wt%)	0	11
	Sulfur (wt%)	max 0.05	0.0 to 0.0024

## 7.2 Description of micro gas turbine set

A dual-shaft 100 kW Teledyne RGT-3600 micro gas turbine generator set, shown in Figure 81, was used to conduct the experimental part of this work. In this system, as Figure 82 shows, the inlet air is pressurized in the centrifugal compressor and discharges through the diffuser and is directed to the regenerator. The temperature of high pressure air increases as it passes the regenerator disks, and then enters the combustor. In the combustion chamber, biodiesel blend fuel is burned and the high temperature and pressure products expand first through the compressor turbine and then through the power turbine. The turbine outlet stream passes through the hot portion of the regenerator disks before it is discharged to the exhaust pipe.



**Figure 81: Regenerative micro turbine generator set**

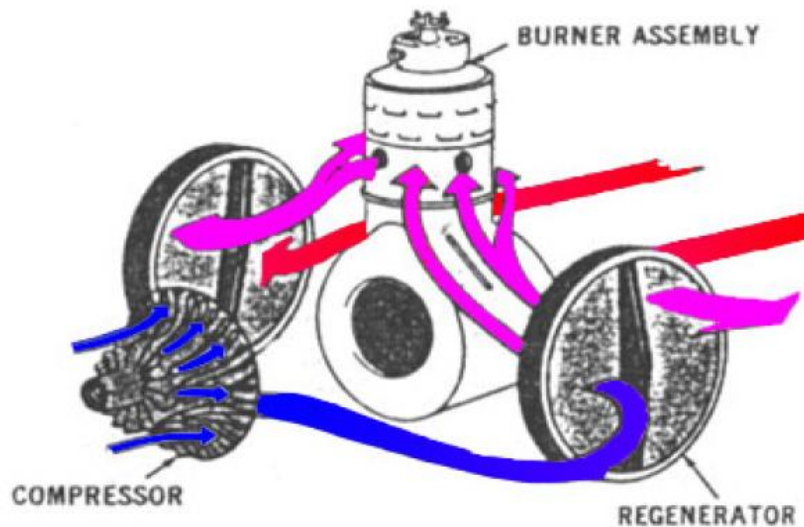


**Figure 82: Flow pattern for twin rotating disk regenerator micro gas turbine (Chiang et al., 2009)**

The compressor assembly consists of a radial flow compressor with a single-stage, cast-aluminum impeller at the front end of the common shaft (Figure 83a) and a single-stage, axial flow turbine at the other end (Figure 83b), which drive the compressor. The compressor also includes a vane type diffuser (Figure 83c). The combustor is a can-type and mounted on the top

of the machine and is equipped with a single fuel nozzle and igniter (Figure 83d). The regenerator subsystem is composed of two ceramic matrix disks at the sides of the engine (Figure 83e). The disks are rim-driven with rotational speed of about 14.5 rpm. Finally, the power turbine has a variable nozzle guide vane and is connected to the generator (Figure 83f) by a common shaft. The system also includes a reduction and accessory drive gearbox, fuel management system, and start-up equipment.

The micro turbine manual control system and start-up sequence were explained in Chiang et al. (2007). In order to control the system, the turbine inlet temperature, the speed of compressor and power turbines, variable power turbine nozzle guide vane schedule, lubricant and exhaust gas temperature are monitored. Figure 84 illustrates the schematic of the system components and material streams. The system design specifications are presented in Table 50.

The MGT set testing facility (Figure 85a) includes a Teledyne RGT-3600 micro gas turbine generator set (Figure 81), a three-phase AC 100 kW generator (Figure 83f), a load bank to simulate the load (Figure 85b), and instruments to measure engine critical parameters as well as a computer-based data acquisition system to record the measured parameters at a sampling rate of 1 Hz per channel.



a



b



c



d



e



f

**Figure 83: Major components of the micro gas turbine: a) compressor b) compressor turbine c) compressor diffuser d) combustion chamber e) ceramic regenerator disk f) generator**



### 7.3 Instrumentation

In order to measure and record the required parameters, including temperature, pressure, flow rate, and rotational speed at different locations in the cycle, the MGT was equipped with various sensors and instruments. The measured parameters in the test engine are as follows: compressor shaft rotational speed ( $N_1$ , Figure 86a); power turbine shaft rotational speed ( $N_2$ , Figure 86b); generator shaft rotational speed ( $NOS$ , Figure 86b); compressor outlet pressure ( $P_3$ , Figure 86c); combustor outlet stream temperature (turbine inlet temperature,  $T_4$ , Figure 86d); exhaust stream temperature ( $T_7$ , Figure 86e); fuel volumetric flow rate ( $W_f$ , Figure 86f); compressor inlet air mass flow rate ( $W_a$ , Figure 86g and 86h); output power; ambient temperature, pressure, and relative humidity ( $T_0$ ,  $P_0$ , and  $RH_0$ , Figure 86i and 86j); and exhaust stream composition (Figure 86k). The exhaust stream gas analyzer was HORIBA MEXA-584L and was capable of measuring carbon monoxide, carbon dioxide, hydrocarbons, and nitrogen oxides. Table 51 presents the sensor specifications and location for these parameters.

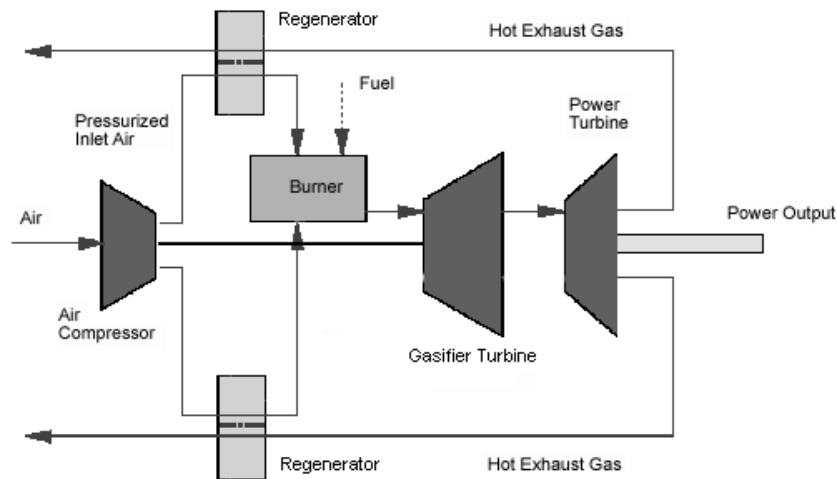
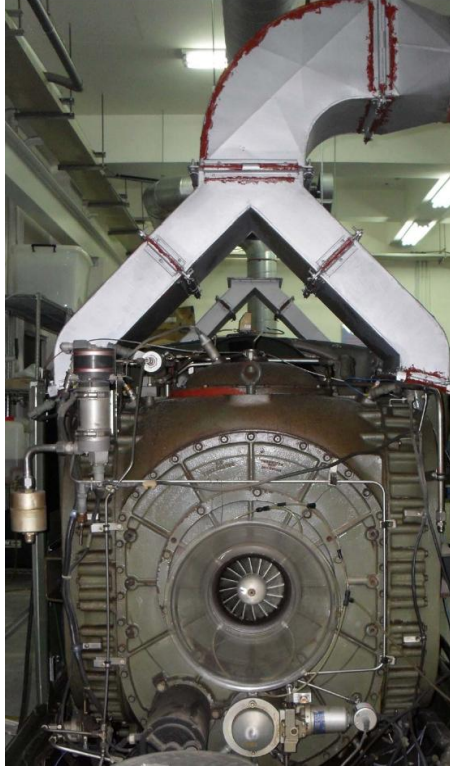


Figure 84: Schematic of the micro gas turbine components and material streams (Chiang et al., 2007)

**Table 50: Micro gas turbine (RGT-3600) measured specifications**

<b>Parameters</b>	<b>Measured data</b>
<b>Max compressor speed (rpm)</b>	38,000
<b>Power turbine speed (rpm)</b>	26,100
<b>Generator speed (rpm)</b>	3,000
<b>Regenerator speed (rpm)</b>	14.5
<b>Max power (kW)</b>	100
<b>Max fuel consumption (L/min)</b>	1.3
<b>Max air flow rate (kg/sec)</b>	2.0
<b>Max combustor exit temperature (°C)</b>	1035
<b>Max exhaust stream temperature (°C)</b>	330
<b>Max compressor pressure ratio</b>	4.1
<b>Compressor isentropic efficiency (%)</b>	80
<b>Turbine isentropic efficiency (%)</b>	88
<b>Regenerator effectiveness (%)</b>	89
<b>Engine weight (kg)</b>	816



a



b

**Figure 85: a) The micro gas turbine set testing facility b) The load bank**



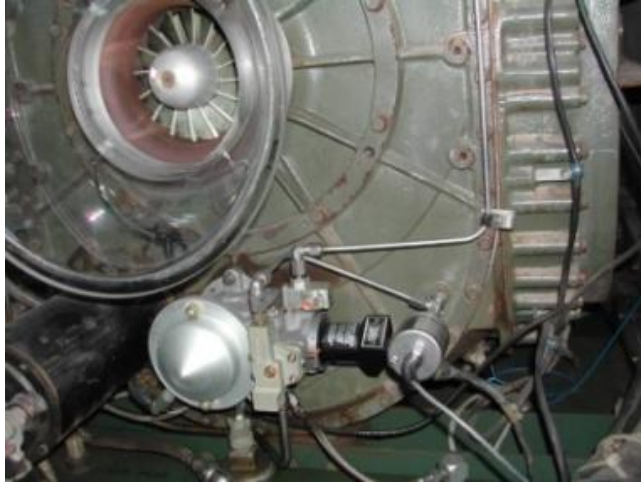
a



b

**Figure 86: Measuring instrument locations (Li, 2010):**

**a) compressor shaft rotational speed (N1) b) accessory gear shaft speed (NAC)**



c



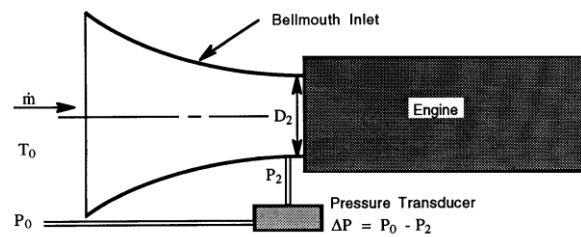
d



e



f



g

Figure 86: Measuring instrument locations (Li, 2010): (cont.)

c) compressor outlet pressure ( $P_3$ ) d) combustor outlet stream temperature ( $T_4$ ) e) exhaust stream temperature ( $T_7$ ) f) fuel volumetric flow rate ( $W_f$ ) g) compressor inlet air mass flow rate ( $W_a$ )



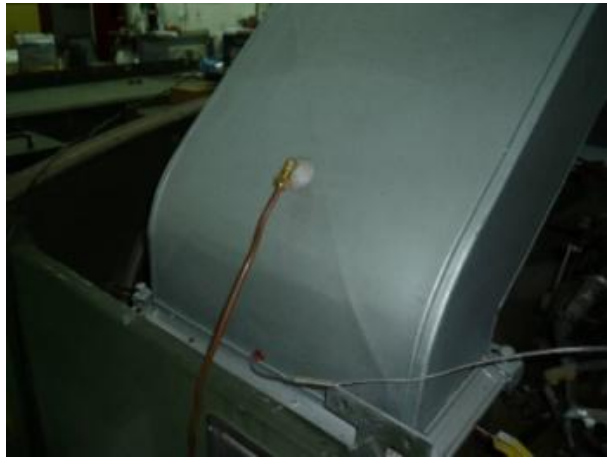
h



i



j



k

**Figure 86: Measuring instrument locations (Li, 2010): (cont.)**

a) compressor shaft rotational speed ( $N_1$ ) b) accessory gear shaft speed ( $NAC$ ) c) compressor outlet pressure ( $P_3$ ) d) combustor outlet stream temperature ( $T_4$ ) e) exhaust stream temperature ( $T_7$ ) f) fuel volumetric flow rate ( $W_f$ ) g and h) compressor inlet air mass flow rate ( $W_a$ ) i) ambient pressure ( $P_0$ ) j) ambient temperature and relative humidity ( $T_0$  and  $RH_0$ ) k) exhaust stream composition

**Table 51: Instrument specifications (Chiang et al., 2009)**

Sensor	Location	Detect property	Accuracy	Range	Note
Remote optical sensor	Compressor inlet	Compressor shaft speed (N1)	$\pm 0.1\%$	0 to 50,000 rpm	
Remote optical sensor	Accessory gear	Accessory gear shaft speed (NAC)	$\pm 0.1\%$	0 to 10,000 rpm	To calculate power turbine (N2) and generator (NOS) shaft speed
Pressure transducer	Compressor discharge chamber	Compressor discharge static pressure (P3)	$\pm 0.13$ psig	0 to 100 psig	
Flow meter	Combustion chamber fuel inlet	Fuel volumetric flow rate ( $W_f$ )	$\pm 10$ c.c./min	0.1 to 2 L/min	
K type thermocouple	Combustion chamber exit	Combustor exit temperature (T4)	$\pm 1\%$	0 to 1250°C	4 probes average
K type thermocouple	Exhaust duct	Regenerator outlet temperature (T7)	$\pm 1\%$	0 to 400°C	2 probes average
Pressure transducer	Bellmouth throat	Compressor inlet static pressure (P2)	$\pm 20$ Pa	0 to 10000 Pa	To calculate inlet air mass flow rate ( $W_a$ )
Barometer	Generator side	Ambient pressure (P0)	$\pm 30$ Pa	800 to 1,060 kPa	
Humidity and temperature transducer	Generator side	Ambient humidity and temperature (RH0, T0)	$\pm 0.3^\circ\text{C}$ (T0) $\pm 1.5\%$ (RH0)	-40 to 180°C (T0) 0 to 100% (RH0)	

## 7.4 Recorded data

Diagrams in Figures 87 and 88 illustrate some sample measurements from the test set, when the engine is fuelled by B10 (Chiang, 1995). The data for the analysis in this chapter was provided by Chiang (1995) and Li (2010), and the author of this thesis joined the research team from June 26, 2010 to August 22, 2010 at National Tsing Hua University in Taiwan. Figure 87 shows the



compressor, power turbine, and generator shaft rotational speeds (N1, N2, and NOS, respectively); air mass flow rate; and compressor outlet pressure (P3) of the system in idle condition and with output power of 25, 47, 69, 89, and 98 kW. Similarly, Figure 88 shows the turbine inlet temperature (T4), exhaust stream temperature (T7), compressor inlet air mass flow rate, and ambient temperature (T0).

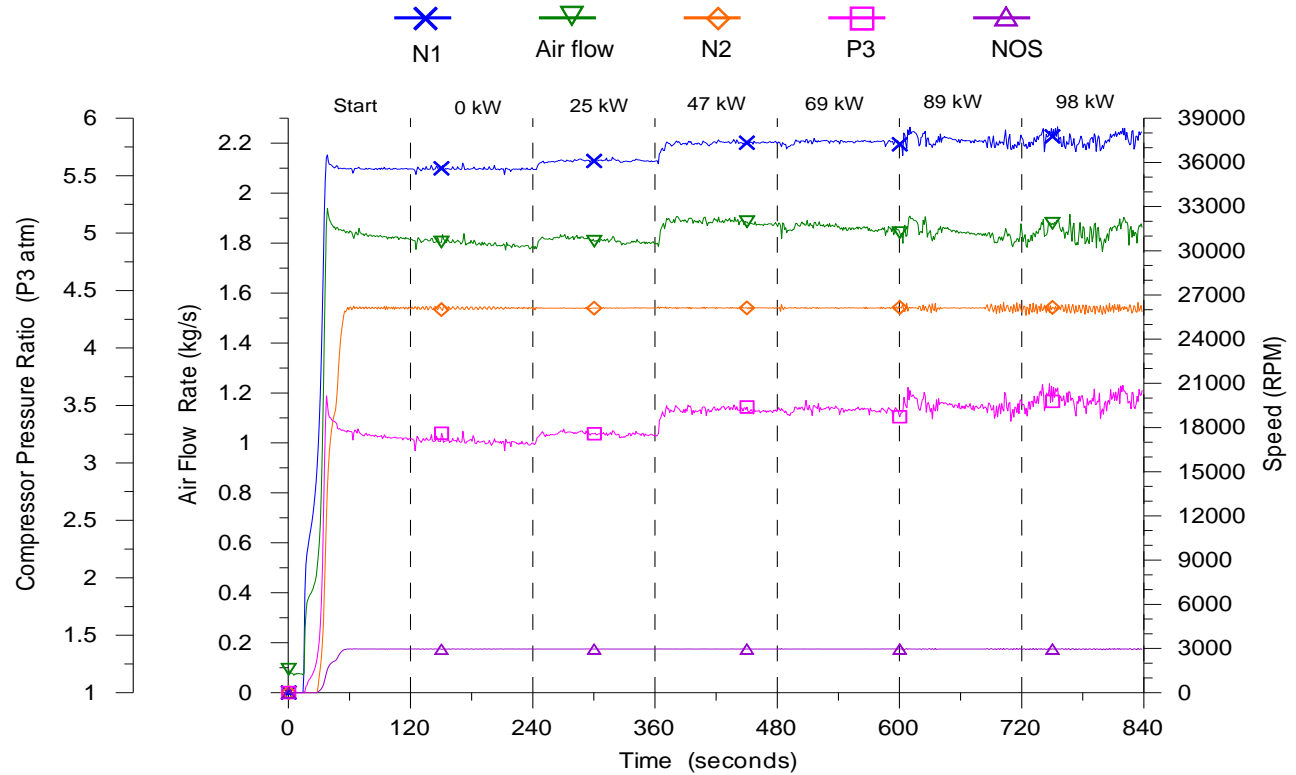


**Figure 87: Compressor, power turbine, and generator shaft rotational speeds; air mass flow rate; and compressor outlet pressure for various output powers when the system was fuelled by B10 (Chiang, 1995)**

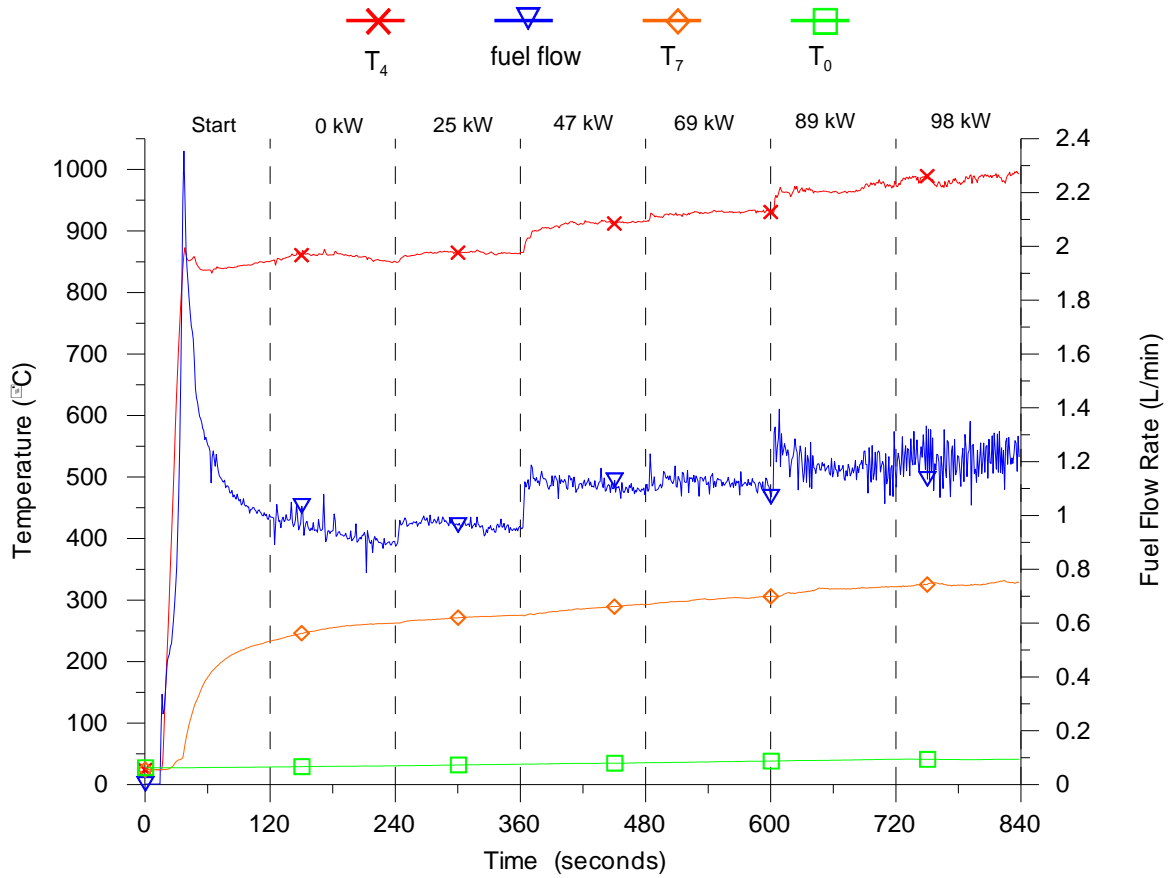


**Figure 88: Turbine inlet temperature, exhaust stream temperature, compressor inlet air mass flow rate, and ambient temperature for various output powers when the system was fuelled by B10 (Chiang, 1995)**

In order to conduct the experiments, the MGT was fuelled by three biodiesel blends: B10, B20, and B30. For each fuel, the external load was varied from idle to full load (0, 25, 48, 69, 89, and 98 kW). The biodiesel was manufactured by the Taiwan NJC Corporation. The characteristics of the biodiesel were according to the ASTM D6751 standard (Table 49). The summary of experimental results, including fuel and air flow rate, pressure ratio, turbine inlet temperature, exhaust temperature, electrical efficiency, and ambient conditions, is shown in Table 52.



**Table 52: The summary of experimental results from the micro gas turbine system (Chiang, 1995; Li, 2010)**

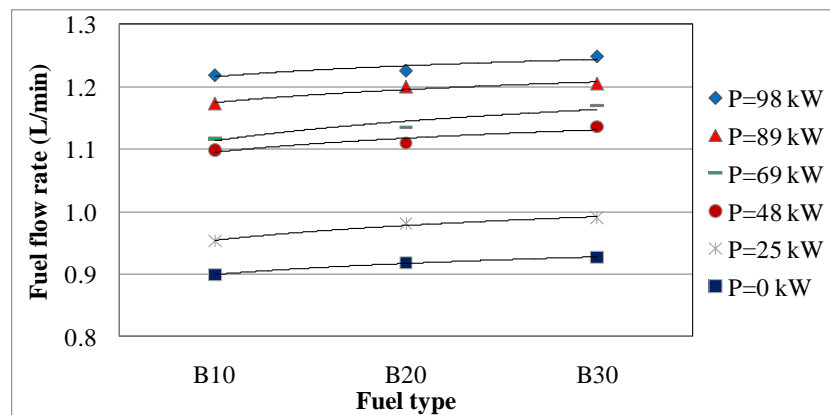
Power (kW)	Fuel type	Fuel volumetric flow rate (L/min)	Air mass flow rate (kg/s)	Pressure ratio	Turbine inlet temperature (°C)	Exhaust temperature (°C)	Thermal efficiency (%)	Ambient temperature (°C)	Ambient pressure (kPa)
<b>0</b>	B10	0.899	1.789	3.172	851.5	252.9	0.000	30.3	99.956
	B20	0.918	1.782	3.169	850.6	251.7	0.000	30.6	100.101
	B30	0.927	1.797	3.204	853.4	254.2	0.000	32.6	100.393
<b>25</b>	B10	0.953	1.802	3.245	863.6	270.4	4.205	32.8	99.955
	B20	0.981	1.806	3.256	870.4	271.6	4.124	32.3	100.096
	B30	0.990	1.821	3.275	869.9	271.7	4.122	31.8	100.386
<b>48</b>	B10	1.098	1.876	3.453	914.3	284.9	7.006	35.1	99.939
	B20	1.110	1.867	3.434	918.8	286.6	6.998	35.1	100.077
	B30	1.136	1.902	3.489	916.6	285.7	6.899	32.6	100.377
<b>69</b>	B10	1.117	1.853	3.457	932.4	301.3	9.906	38.0	99.923
	B20	1.135	1.856	3.467	934.1	303.3	9.833	38.0	100.059
	B30	1.170	1.900	3.522	930.7	299.3	9.631	32.1	100.362
<b>89</b>	B10	1.173	1.826	3.478	970.8	316.3	12.162	40.9	99.906
	B20	1.200	1.853	3.517	967.3	318.4	12.001	39.7	100.040
	B30	1.205	1.873	3.525	956.7	313.1	12.063	34.2	100.337
<b>98</b>	B10	1.219	1.848	3.554	988.5	325.7	12.891	41.0	99.879
	B20	1.226	1.841	3.529	993.7	326.1	12.935	41.9	100.016
	B30	1.249	1.905	3.624	966.3	324.5	12.811	36.2	100.315

## 7.5 Discussion of experimental results

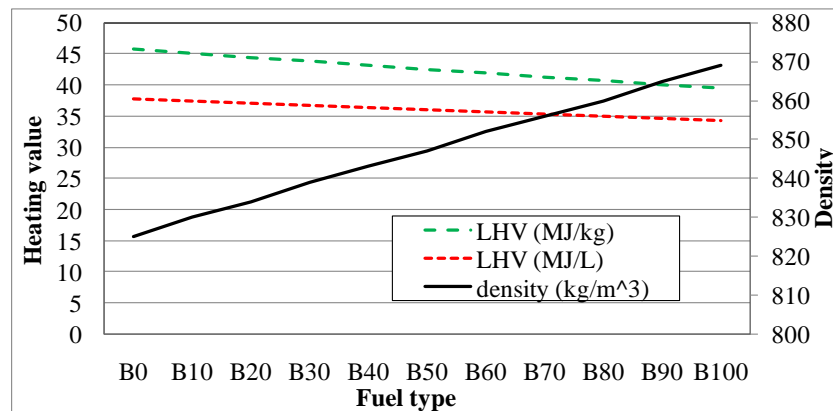
Figures 89 to 95 show how the performance parameters of the MGT are influenced by the fuel type. In these diagrams, for constant output power, the parameter variations are investigated for three fuels; B10, B20, and B30.

Figure 89a shows the variation of the fuel flow rate and Figure 90 illustrates the uncertainty of the fuel flow rate measurement at the output power of 89 kW. Figure 89a indicates that the fuel volumetric flow rate increases with a higher percentage of biodiesel in the fuel. In order to

investigate this diagram, the variations of the fuel density and its heating value should be considered. As mentioned in the introduction, Figure 89b illustrates that mass and volumetric LHV of the fuel (from measurement) reduce and density increases with the increase of the concentration of biodiesel in the fuel blend (based on the data from Chiang (1995)). The effect of variation of these two parameters on the inlet fuel energy content can be seen in Figure 89c, where the graph shows that the energy content of inlet fuel slightly increases with the increase in the biodiesel content of the fuel. Since the heating value of the fuel decreases, the fuel mass and volumetric flow rates should increase.

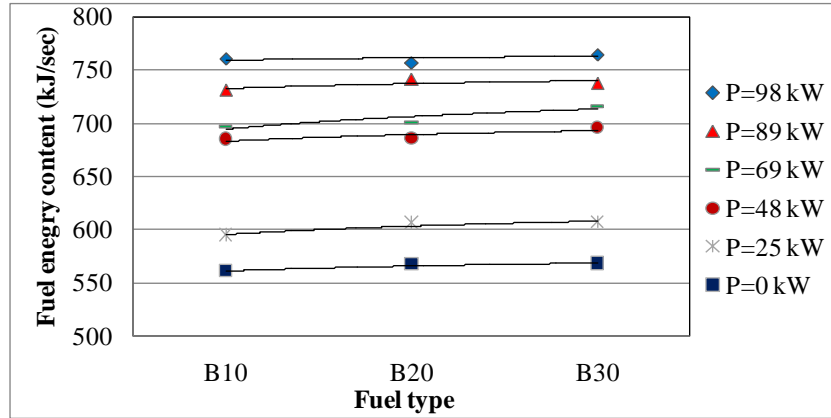


(a)



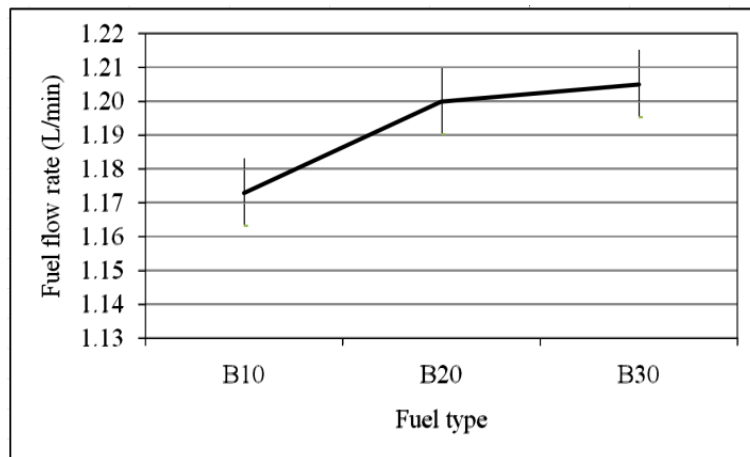
(b)

**Figure 89: Diagrams to investigate the variation of the inlet fuel flow rate a) the inlet fuel volumetric flow rate b) the fuel lower heating value and density vs. the biodiesel content of fuel blend**



(c)

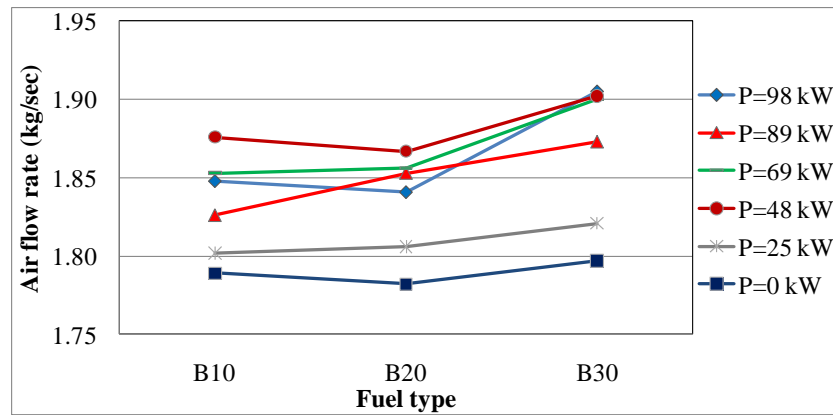
**Figure 89: Diagrams to investigate the variation of the inlet fuel flow rate a) the inlet fuel volumetric flow rate b) the fuel lower heating value and density vs. the biodiesel content of fuel blend c) the energy content of inlet fuel**



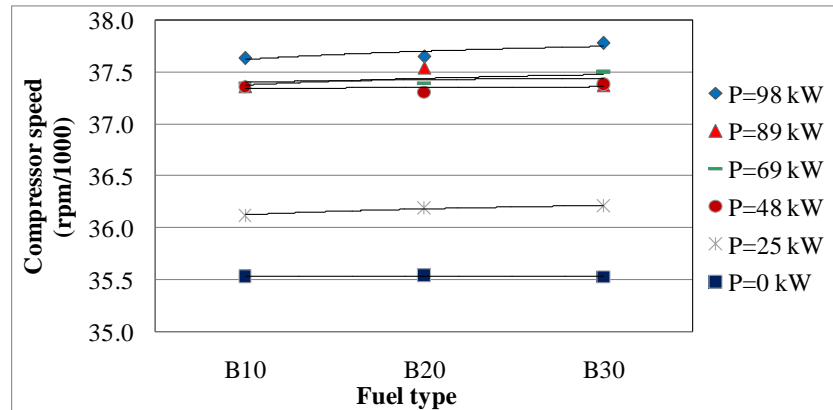
**Figure 90: Uncertainty of fuel flow rate measurement at the output power of 89 kW**

Figure 91a shows changes in the air mass flow rate versus fuel type for constant output power in the system. The lack of an understandable pattern in the figure can be explained based on the fact that if the compressor rotational speed remains constant, the air volumetric flow rate will be constant. In the MGT under investigation, as shown in Figure 91b, the change in rotational speed of the compressor for a particular load is negligible. Therefore, the air volumetric flow rate is essentially constant and thus the air mass flow rate strongly depends on the air density, which in

turn depends on the ambient conditions. Since the variation in the ambient pressure is negligible, as shown in Figure 91c, the air mass flow rate is only affected by the ambient temperature. Figure 91d shows the variation of ambient temperature during the recording of the data. For the majority of the recordings, Figures 91a and 91d are in agreement, which means when the ambient temperature increases, the air mass flow rate reduces. Figures 92a to 92c illustrate the uncertainty of the measurements in Figures 91a to 91d at the output power of 89 kW. Due to the lack of the data for the instrument for the air flow rate measurement, a similar graph could not be prepared for this parameter.

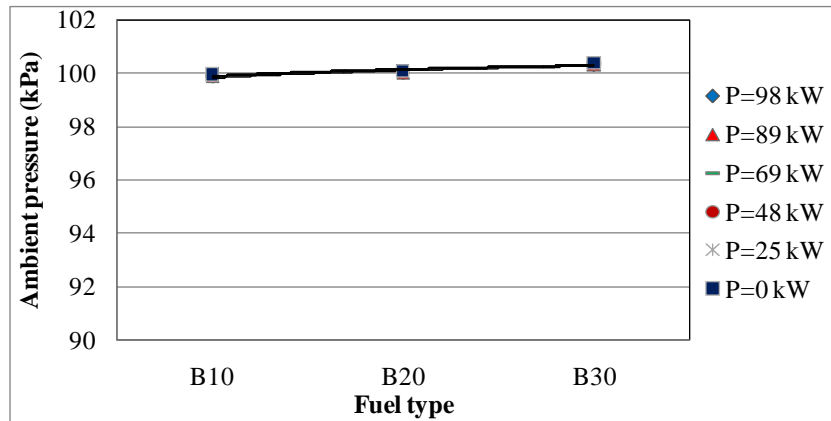


(a)

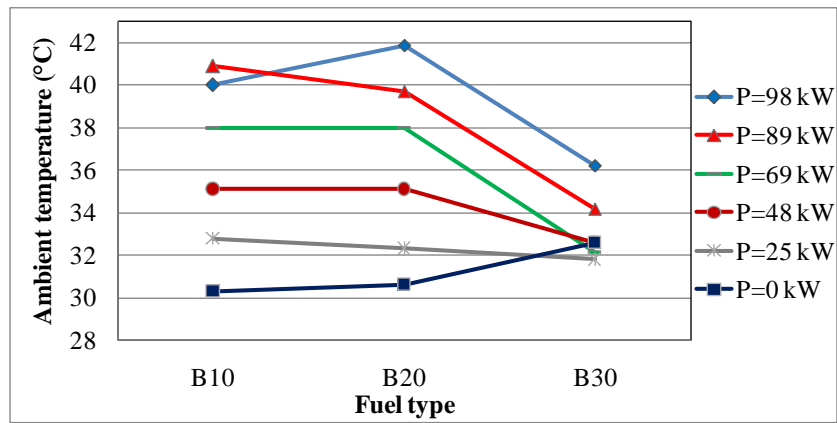


(b)

**Figure 91: Diagrams to investigate the variation of the inlet air flow rate: a) the air mass flow rate b) the compressor rotational speed**

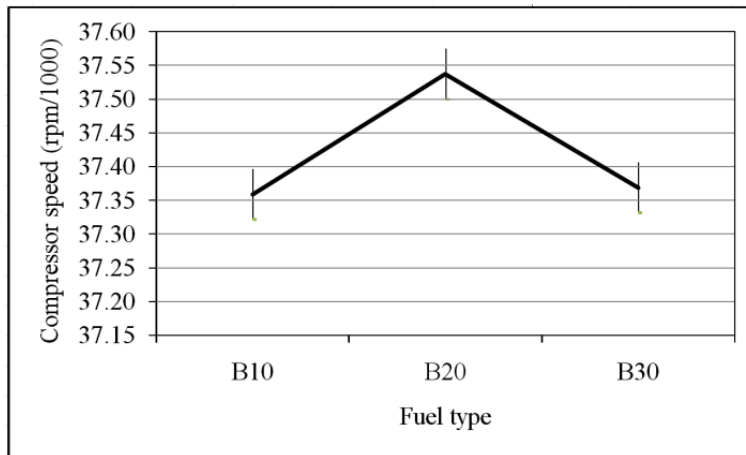


(c)

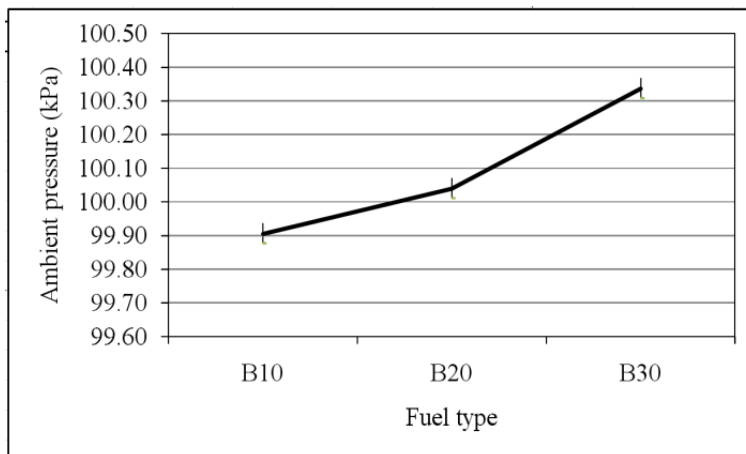


(d)

Figure 91: Diagrams to investigate the variation of the inlet air flow rate: a) the air mass flow rate b) the compressor rotational speed c) the ambient pressure d) the ambient temperature

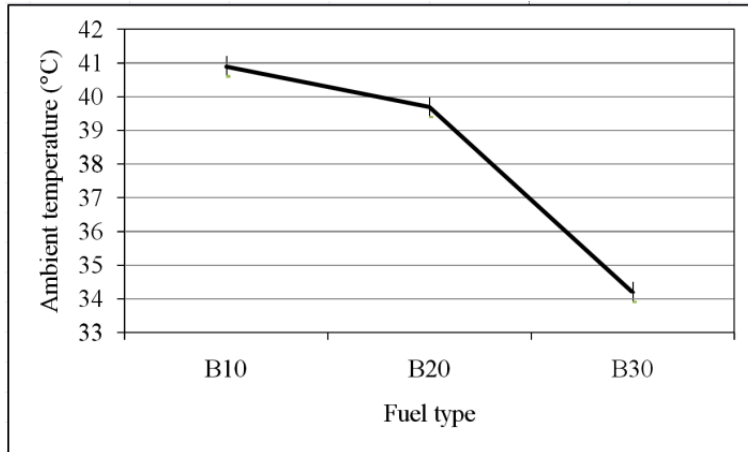


(a)



(b)

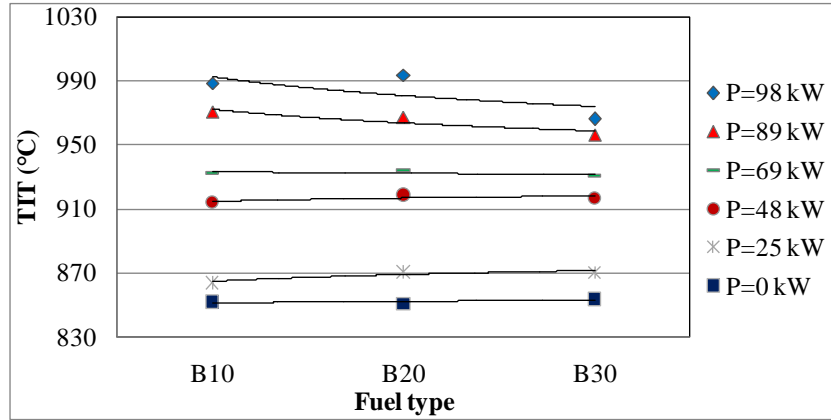
**Figure 92: Uncertainty of measurements at the output power of 89 kW: a) the compressor rotational speed b) the ambient pressure**



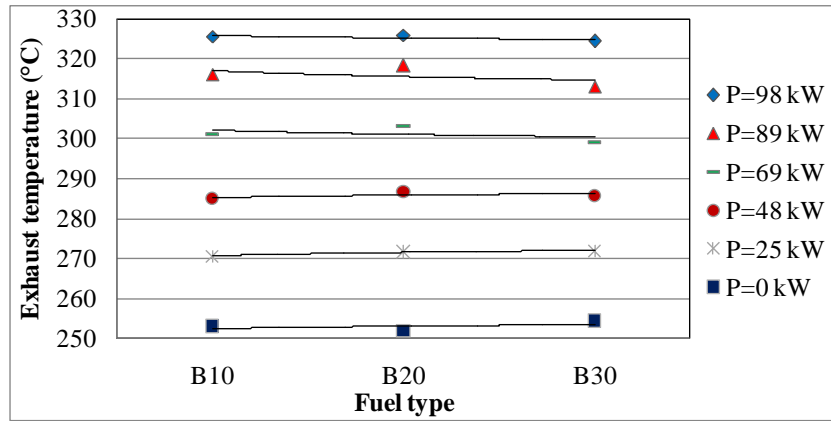
(c)

**Figure 92: Uncertainty of measurements at the output power of 89 kW: a) the compressor rotational speed b) the ambient pressure c) the ambient temperature**

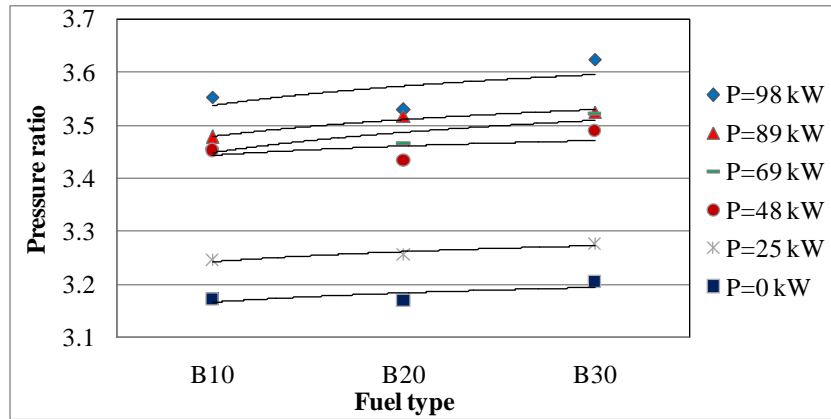
Figures 93a to 93c show the turbine inlet temperature (TIT), exhaust temperature, and the compressor pressure ratio of the MGT. Figures 94a to 94c illustrate the uncertainty of the measurements in Figures 93a to 93c at the output power of 89 kW. Figures 94a and 94b signify that the variation of the TIT and exhaust temperature and the uncertainty of the instruments are in the same order; therefore, the variation of these parameters, if any, cannot be detected by these instruments. Figure 93c indicates that a higher concentration of biodiesel results in an increase in the compressor pressure ratio. Obviously, all these three parameters decrease at lower output powers (partial loads).



(a)



(b)



(c)

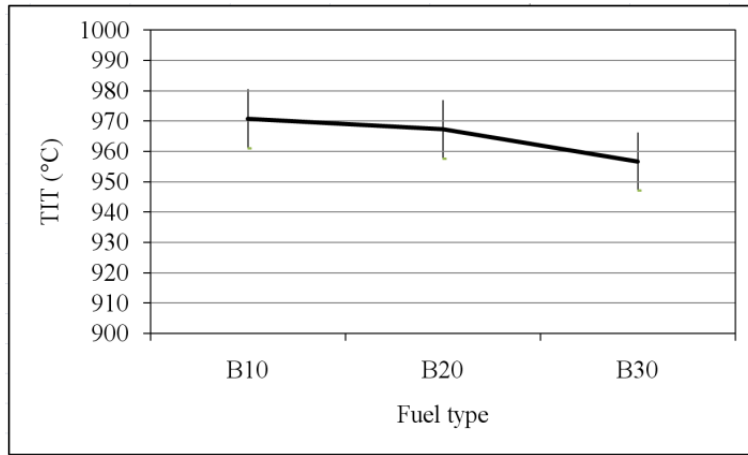
Figure 93: The variation of the MGT performance parameters when the system is fuelled by B10, B20, and B30 a) turbine inlet temperature b) exhaust temperature c) compressor pressure ratio



Figure 95 shows that the electrical efficiency of the system is almost constant when the concentration of biodiesel increases in the fuel. Also, the efficiency of the cycle reduces with reduction in the output power due to lower efficiency of the components at partial loads. The efficiency of the system was estimated by using following equation:

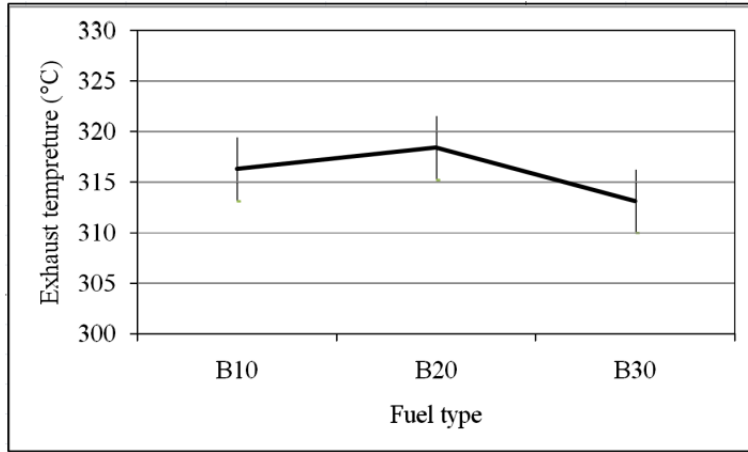
$$\eta = \frac{\dot{W}}{\dot{m}_f \times \text{LHV}} = \frac{\dot{W}}{\rho \times \dot{V}_f \times \text{LHV}} \quad (67)$$

where  $\eta$  represents the efficiency of the system (%),  $\dot{W}$  represents output power (kW),  $\dot{m}_f$  (kg/s),  $\rho$  (kg/m<sup>3</sup>), and LHV (IJ/kg) represent fuel mass flow rate, density, and lower heating value, respectively.

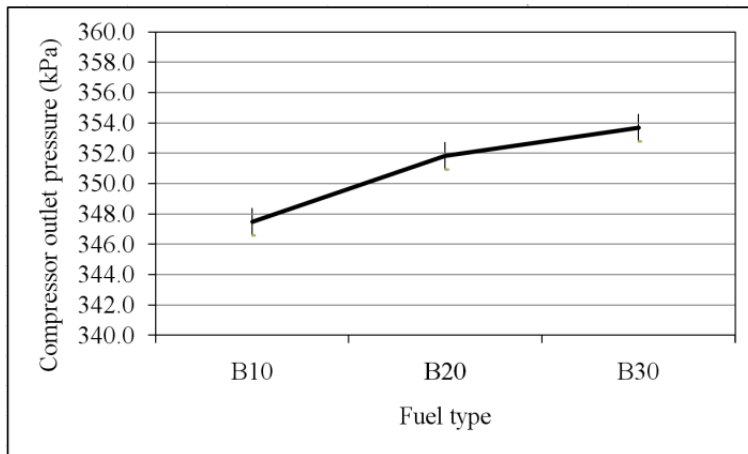


(a)

**Figure 94: Uncertainty of measurements at the output power of 89 kW: a) turbine inlet temperature**



(b)



(c)

**Figure 94: Uncertainty of measurements at the output power of 89 kW: a) turbine inlet temperature b) exhaust temperature c) compressor pressure ratio**

The efficiency of the system at an output power of 89 kW (fuelled with B10) can be estimated by using the data provided in Table 52 and LHV from Figure 89b:

$$\eta = \frac{\dot{W}}{\rho \times \dot{V}_f \times \text{LHV}} = \frac{89 \text{ kW}}{830 \left[ \frac{\text{kg}}{\text{m}^3} \right] \times 1.173 \left[ \frac{\text{L}}{\text{min}} \right] \times \frac{1}{60,000} \times \left[ \frac{\text{m}^3}{\text{s}} / \frac{\text{L}}{\text{min}} \right] \times 45,108 \left[ \frac{\text{kJ}}{\text{kg}} \right]} \times 100 = 12.16\% \quad (68)$$

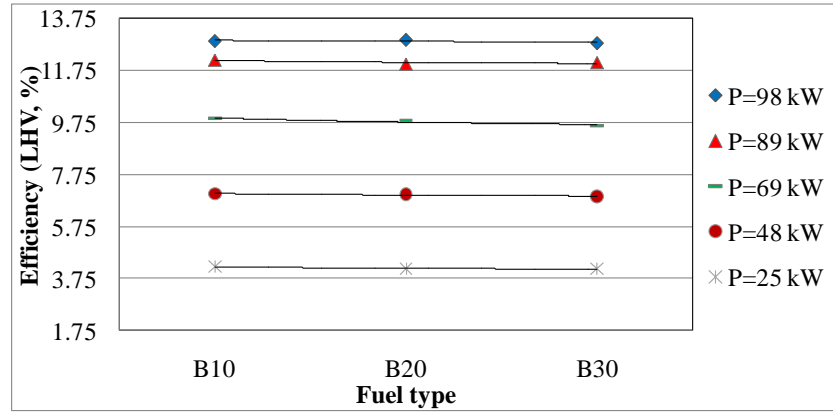


**Figure 95: MGT electrical efficiency vs. fuel type for constant output powers**

The results of these experiments will be used to develop and validate the model of the regenerative micro gas turbine in the following subsections.

## 7.6 Modeling of micro gas turbine

The objective of this section is to present the results of the modeling of the micro gas turbine, when it is fuelled by blends of biodiesel and petroleum-based diesel with different concentrations. In the following subsections, first the modeling approach will be explained. Then the model will be validated against experimental data. Finally, the modeling results will be presented.

### 7.6.1 Modeling approach

The proposed model was intended for the steady-state simulation of the MGT fuelled with biodiesel and was developed in Aspen Plus<sup>®</sup>. For this study, a macro level model was developed based on the built-in models of the compressor, gas turbine, combustor, material stream mixer and splitter, and heat exchanger in Aspen Plus<sup>®</sup>.

The basic configuration of the MGT cycle investigated in this subsection is shown in Figure 96. In the model, the inlet air (AIR-IN), entering the system at ambient conditions, is compressed at AIR-COMP to the system operating pressure. The compressor pressure ratio in this case is 3.5.

Then the high pressure inlet air is divided into two streams. The majority (about 96%) goes to the power generation cycle, and approximately 4% is used for turbine blade cooling. The air stream then is heated at REGEN by recovering heat from the exhaust stream. On the other hand, the inlet fuel to the system is first pumped from the specified conditions to the system pressure (at FUELPUMP) and mixed with high pressure inlet air before being fed to the combustor. The combustion products are passed through the turbine to generate power. The waste heat in the gas turbine exhaust stream is recovered at REGEN before being discharged to the atmosphere.

The model requires some constants, and equipment operating parameters should be defined. These parameters and constants are listed in Table 53. It should be noted that for all output power levels, it was assumed that the operational characteristics of the system components, such as isentropic and mechanical efficiencies, were constant, regardless of the input fuel.

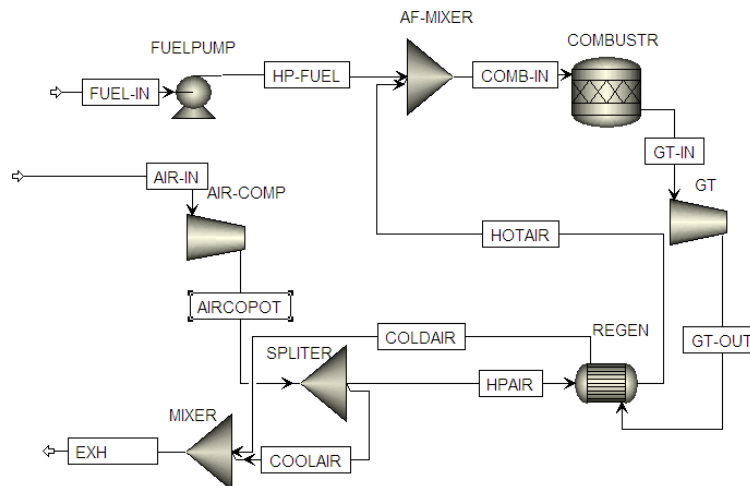


**Figure 96: MGT cycle model configuration**

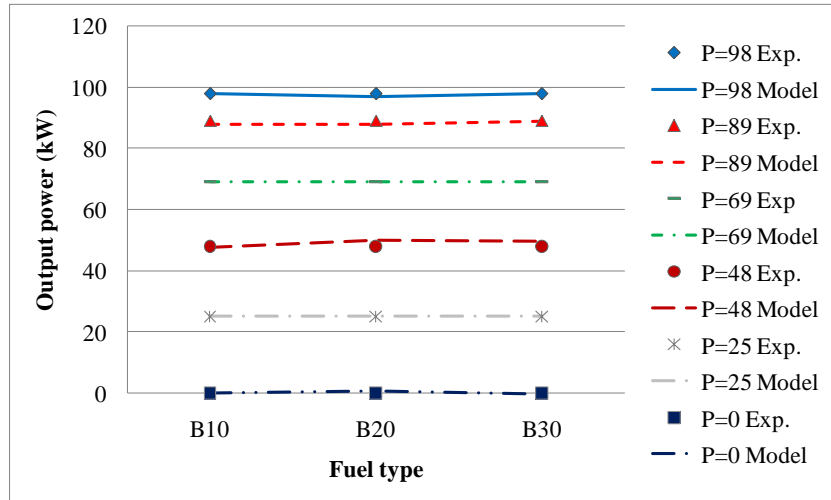
The developed model can be used to estimate all parameters in the cycle. However, before it can be used for any analysis, it should be validated against experimental data. In the following subsection, the experimental setup described in the previous subsections is used for validation of the model.

**Table 53: Input parameters for macro gas turbine model**

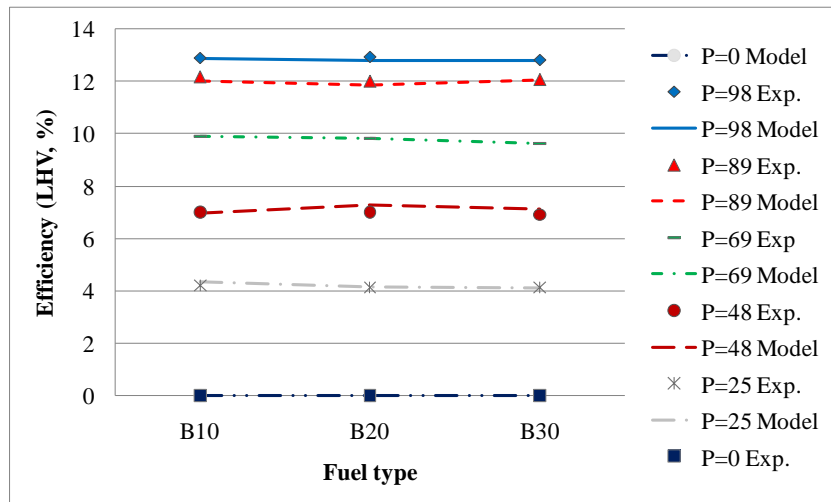
Parameter	Default Value
Inlet fuel temperature and pressure	Ambient conditions
Inlet fuel pump efficiency	80%
Inlet fuel pump discharge pressure	4.1 atm
Inlet air temperature and pressure	Ambient conditions
Inlet air composition	21% O <sub>2</sub> -79% N <sub>2</sub>
Air compressor pressure ratio	3.53
Air compressor isentropic efficiency	80%
Air compressor mechanical efficiency	85%
Gas turbine isentropic efficiency	88%
Gas turbine mechanical efficiency	89%
Gas turbine discharge pressure	1.2 atm
Regenerator effectiveness	89%

### 7.6.2 Model validation

The model's major operating parameters, including output power, system efficiency, TIT, and exhaust temperature, are compared with measurements from the dual-shaft 100 kW Teledyne RGT-3600 micro gas turbine generator set for three types of biodiesel blends: B10, B20, and B30 at various loads in Figures 97a to 97d. The figures indicate a good agreement between the modeling results and experimental measurements for most of the cases, especially for output power and efficiency. However, in a few cases, such as TIT for P25 and exhaust temperature for P98, the error between the model and experiments is significant. This issue should be explained and addressed before the model can be used for prediction of the system performance at a higher concentration of biodiesel.



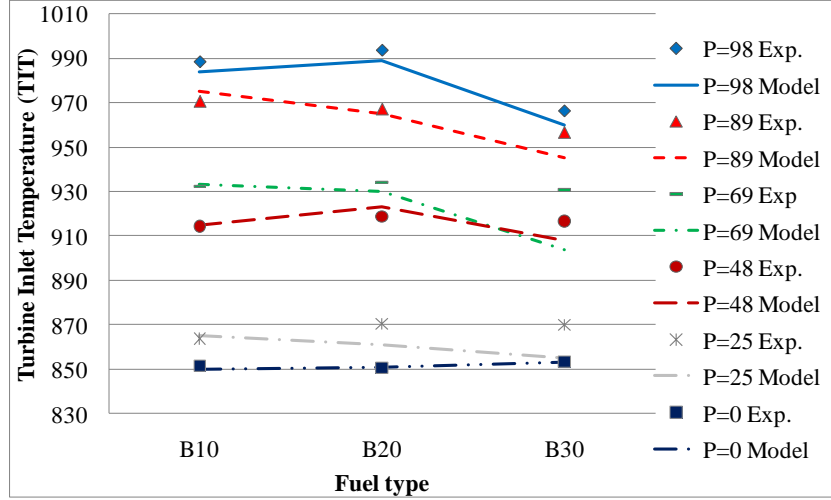
(a)



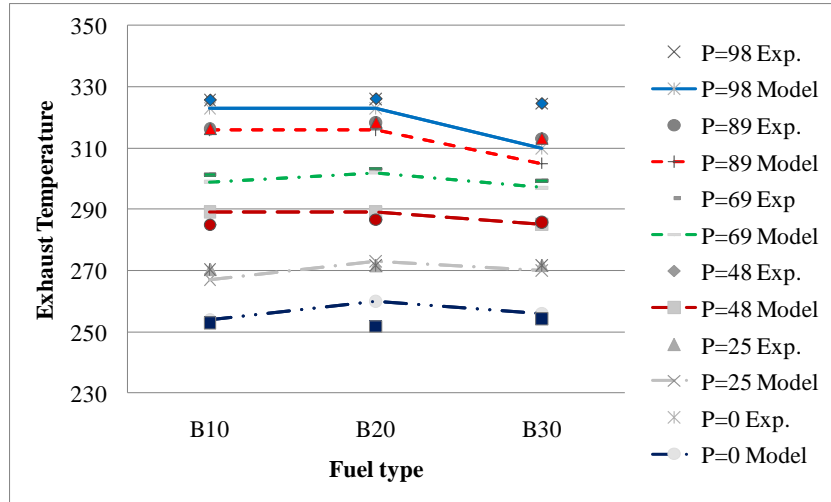
(b)

**Figure 97: Comparison of modeling results with experimental data**

**a) output power b) efficiency**



(c)



(d)

**Figure 97: Comparison of modeling results with experimental data**

**a) output power b) efficiency c) TIT d) exhaust temperature**

## 7.7 Modeling results and discussion

The diagrams in Figures 98 and 99 show how the performance parameters of the MGT model are influenced by the fuel type. In these diagrams, for constant output power, the parameter variations are investigated for three fuels; B10, B20, and B30. In these figures, the lines

represent the modeling result trends. Figure 98 shows that the electrical efficiency of the system is almost constant at most loads, when the concentration of biodiesel increases in the fuel.

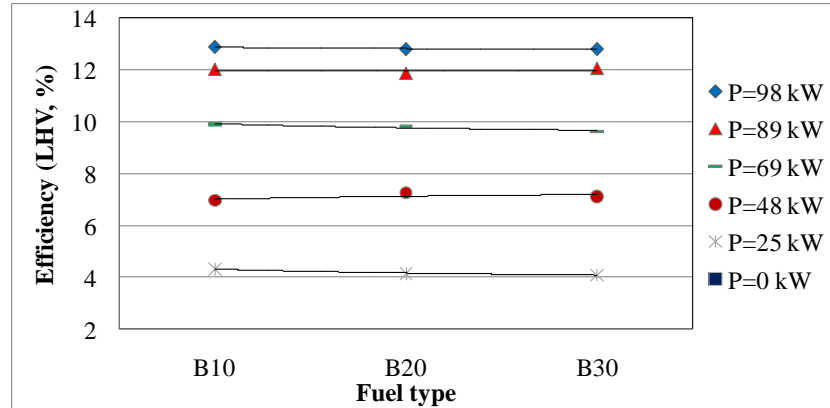
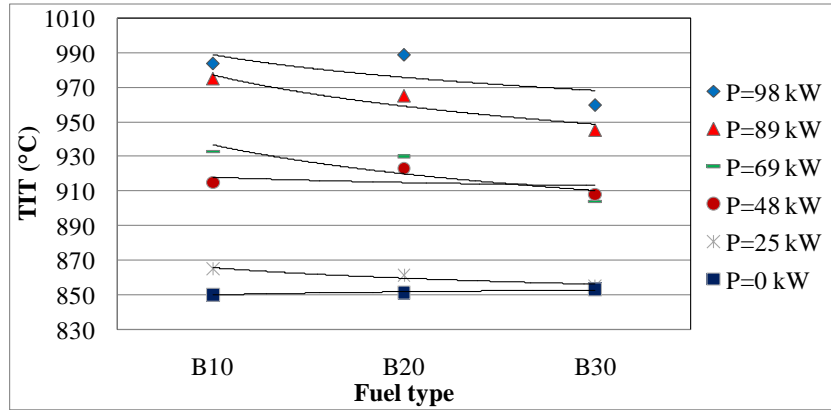


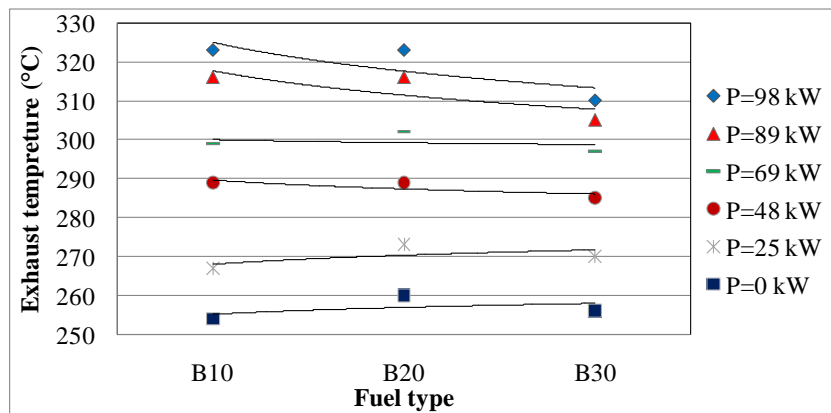
**Figure 98: MGT modeling results for electrical efficiency vs. fuel type for constant output powers**

Figures 99a and 99b show the TIT and exhaust temperature of the MGT. As shown in Figure 99a, at the full load or close to full load operations, the TIT reduces when the concentration of biodiesel increases in the fuel. At lower loads, however, for most cases, the TIT does not change significantly with the fuel composition. Figure 99b indicates that the exhaust temperature follows almost the same trend.





(a)



(b)

Figure 99: Variation of the MGT performance parameters when the system is fuelled by B10, B20, and B30

a) TIT b) exhaust temperature

## 7.8 Conclusion

Biodiesel is an environmentally benign renewable alternative for conventional diesel fuel, and its utilization in MGTs is an interesting option for many applications. The results of experimental works on a dual-shaft 100 kW Teledyne RGT-3600 micro gas turbine generator set were presented in the first part of this chapter. The results indicated that effects of variation in fuel composition were different for various parameters. For instance, the changes in the system electrical efficiency, compressor rotational speed, compressor pressure ratio, and exhaust stream temperature were not significant, whereas the fuel flow rates were considerably affected. The

effect of biodiesel on some parameters, like turbine inlet temperature, depended on the output power.

In the second part of the chapter, the steady-state model of a regenerative micro gas turbine was developed based on the specifications of the experimental micro gas turbine generator set. The model was validated against the experimental performance data. The results of the modeling indicated that most system operational parameters varied, to some extent, when the biodiesel concentration was increased.

The results of the experimental and modeling works in this chapter indicated that the changes in the MGT operating parameters and the effects of these changes in the system performance should be considered for the fuel switching of micro gas turbines from conventional petroleum-based diesel to biodiesel and for designing factory-made biodiesel-fuelled micro gas turbine engines. The fundamental questions about fuel flexibility and its impact on the performance of micro gas turbines should be addressed before this fuel switching can be commercially achieved.

## **7.9 Future work**

For future work, this model will be used to predict the system performance when fuelled by the blends with a higher portion of biodiesel, i.e. B40, and so on. The understanding of the system behaviour when fuelled by the various blends of biodiesel can help to design engines with optimum performance with these fuels. Although the model can predict most of the system operating parameters with an acceptable accuracy, the error level between modeling results and experimental data in a few cases seems high. In order to address this issue, the following suggestion can be helpful.

As stated in Subsection 7.6.1, in this model, it was assumed that for constant output power, the operational characteristics of the system components, such as isentropic and mechanical efficiencies, were fixed, regardless of the input fuel. However, as shown in this chapter, the operating parameters of the system can be affected by the inlet fuel type, which in turn may affect the characteristics of the system components. Therefore, this assumption may be questionable, and these parameters should be found from operating maps of the micro gas turbine. These maps can help to estimate isentropic efficiencies of the compressor and turbine as

a function of mass flow rates, rotational speed, and inlet conditions of these components. Unfortunately, these maps are not available at the moment for this system.

## **CHAPTER EIGHT**

### **Energy Analysis of Gas Turbine-Based Power Plants**

Gas turbine-based cycles generate a significant portion of world's electricity. This chapter presents the modeling of the gas turbine and the cycles based on the gas turbine. First the model of a simple gas turbine cycle with an efficiency of about 40% (LHV) is presented. One of the reasons for the relatively low efficiency of gas turbine cycles is the waste of high-grade energy at their exhaust. A cogeneration power plant is then introduced to use this wasted energy to produce superheated steam for process usage. This cogeneration system model was developed based on the data from the Whitby cogeneration power plant, and its electrical and total (both electrical and thermal) efficiencies were around 40% and 70% (LHV), respectively. The thermal energy of the gas turbine exhaust can also be used to generate steam for the bottoming steam cycle. The model of the combined cycle power plant and its results are then presented with an efficiency of about 47% (LHV). Finally, one of the disadvantages of gas turbine-based cycles is their sensitivity to ambient conditions. In order to minimize the negative impact of high ambient temperature on the performance of the gas turbine cycle, an evaporative fogging compressor inlet air cooling system is introduced, and the results of the modeling for the Whitby cogeneration power plant is presented. In all cases, the models could capture the operation of the systems with an acceptable accuracy.

#### **8.1 Introduction**

Gas turbine cycles theoretically operate based on the Brayton cycle. However, real gas turbine cycles are usually operated based on an open cycle and consist of three main components: compressor, combustor, and gas turbine. Figure 100 shows a schematic of the basic gas turbine

components in a simple gas turbine cycle model developed in Aspen Plus<sup>®</sup>. This model was developed based on the gas turbine part of the Whitby cogeneration power plant (Subsection 8.2). In this cycle, air mass flow rate = 158.2 kg/s, fuel (natural gas) mass flow rate = 3 kg/s, compressor pressure ratio = 34, electrical efficiency = 39.56% (based on LHV), and electrical efficiency = 35.66% (based on HHV).

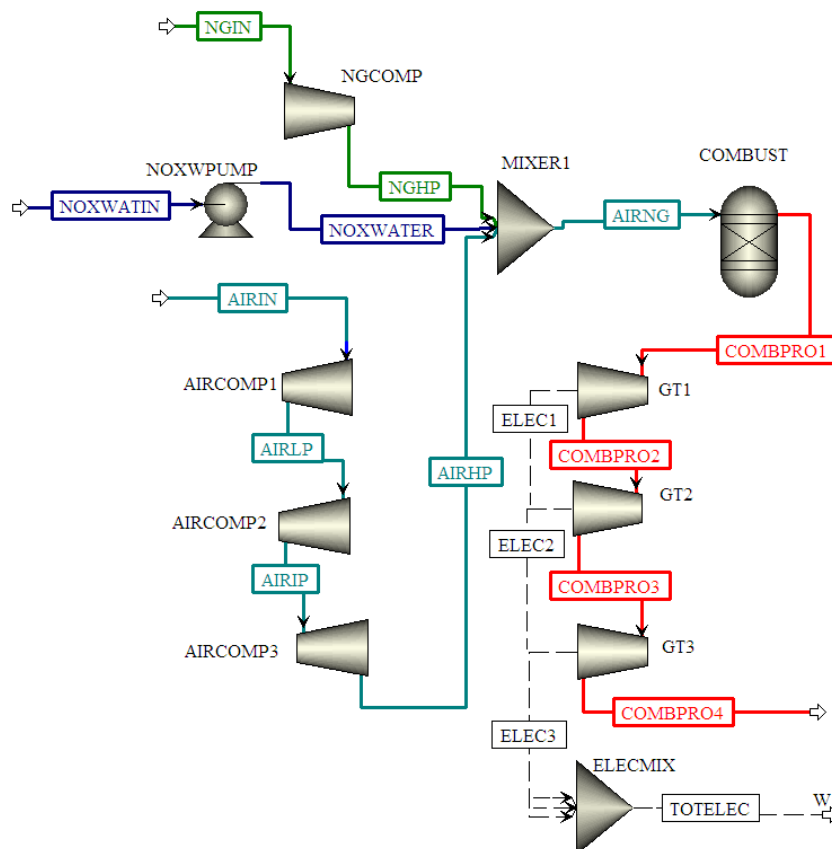


**Figure 100: Schematic of a simple gas turbine cycle model in Aspen Plus<sup>®</sup>**

Gas turbines have been used in the power generation industry for more than a century due to their low capital cost, short installation time, and compact size. Also, the short start-up and shut down time of gas turbines make them a suitable option for peak load operation. Due to their widespread utilization, their technology is mature and very well developed.

Despite their widespread applications, there are three main disadvantages associated with using simple gas turbines for power generation. First, the exhaust temperature of GTs is very high, which means high-grade energy is wasted and results in the low efficiency of the system. Application of gas turbines in cogeneration plants and combined cycle power plants can help to recover some of the wasted thermal energy from the GT exhaust stream to produce further electricity and/or useful thermal energy. Second, the output power and efficiency of GTs and other cycles based on gas turbines strongly depend on ambient conditions, especially ambient temperature, and are reduced with a higher ambient temperature. This problem can be solved by using compressor inlet air cooling systems. Finally, gas turbines cannot be fuelled with solid fuels. This issue can be addressed by using integrated gasification combined cycles. These issues and approaches to deal with them are the topic of this chapter.

## **8.2 Cogeneration**

Cogeneration, also known as combined heat and power (CHP), is a concept to utilize otherwise wasted thermal energy of the thermal engine exhaust stream for some useful applications, such as space heating, generating process steam and/or hot water, and so on. The Whitby cogeneration power plant, located in Whitby, Ontario, is an example of such plants (Figure 101) where the exhaust stream of the gas turbine is used to produce superheated steam in a heat recovery steam generator (HRSG) to provide required steam for a paper manufacturing factory next to the power plant. This plant's configuration and specifications were used to develop a CHP plant model, and the operational data from this power plant were used to validate the model.

The Whitby cogeneration power plant is equipped with a Rolls Royce Trent 60 WLE GT gas turbine with the rated capacity of 58 MW (at the site's standard conditions), and makes use of a once through HRSG to produce superheated steam. It is owned and operated privately and has been operating since 1997. This type of GT was originally designed for aviation applications, and when it was adapted for stationary power generation applications, two types of NO<sub>x</sub> control systems were added: dry system and wet system. In the dry system, the flame temperature is controlled by the flow rate of excess air. But in the wet system, demineralized water is injected to the combustion chamber to control the flame temperature. The gas turbine in this plant was

originally equipped with a dry  $\text{NO}_x$  control system. But due to the high maintenance cost of this system, it was replaced with a wet control system in February 2010.



**Figure 101: General overview of the Whitby cogeneration power plant**

### **8.2.1 Model description**

Figure 102 illustrates the model of the CHP plant developed for this work. Table 54 lists the model constants for the equipment of the gas turbine cogeneration plant. It should be noted that the isentropic and mechanical efficiencies of turbomachinery are proprietary of the equipment manufactures and are not publicly available. In order to determine these constants, the inlet and output stream conditions of compressors and turbines were used to estimate these values by the trial and error process. For instance, to determine the isentropic efficiency of the compressors, it was known that at an ambient temperature of  $10^\circ\text{C}$ , the outlet temperature of the high pressure compressor was  $587^\circ\text{C}$ . It was found that for an isentropic efficiency of 85%, the temperature of the compressor outlet stream from the model matched the actual temperature from the system operation ( $587.3^\circ\text{C}$  vs.  $587^\circ\text{C}$ , respectively). This value was used for the entire range of system operation. The same approach was used to determine the mechanical efficiencies by matching total output power of the system in a particular condition. These values were considered applicable for other conditions as well, and, as will be shown later, these approximations were reasonably accurate.

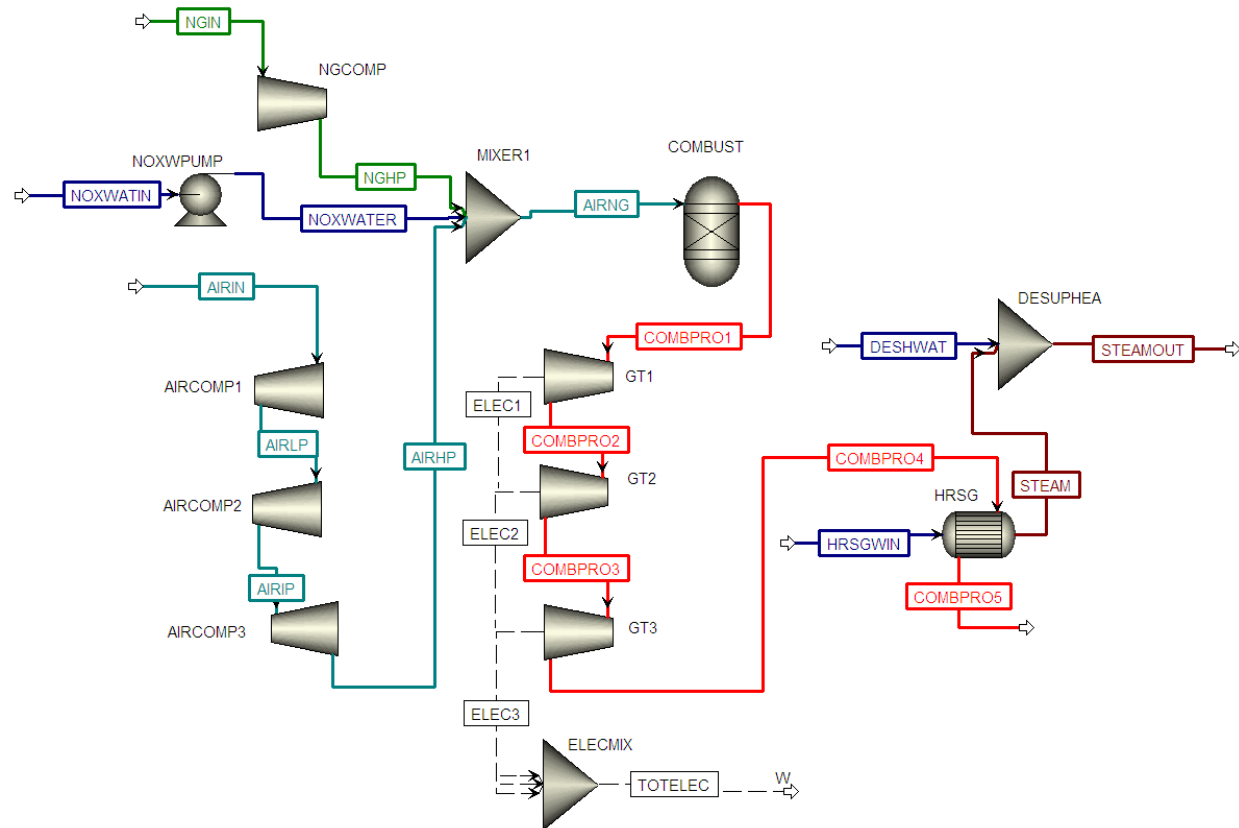


**Figure 102: Schematic of gas turbine cogeneration plant model studied in this chapter**

In this model, which resembles the Whitby cogeneration power plant, the air inlet stream is compressed in three steps through three compressors, with pressure ratio of 1.7, 4.5, and 4.4, respectively, from the low pressure compressor to the high pressure one. The ambient pressure of the site is 1.00232 bar. The pressure of the discharge of the high pressure compressor varies with ambient conditions, but it is about 33 bar. The compressed air stream then mixes with the pressurized natural gas and NO<sub>x</sub> control water streams before being fed to the combustor. The natural gas stream is provided by the gas distribution company at a temperature between 5°C and 15°C (in the model this temperature was fixed at 10°C) and pressure of 28.4 bar. The pressure of the natural gas stream is increased to 55.8 bar at NGCOMP. The composition of the inlet natural gas is presented in Table 55, and its LHV and HHV are 48,832 and 54,168 kJ/kg, respectively. The mass flow rate of natural gas depends on the plant load and operational conditions.



**Table 54: Constants for the gas turbine cogeneration plant model**

<b>Air compressor 1 (AIRCOMP1)</b>	
Pressure ratio	1.7
Isentropic efficiency (%)	85
Mechanical efficiency (%)	98.6
<b>Air compressor 2 (AIRCOMP2)</b>	
Pressure ratio	4.5
Isentropic efficiency (%)	85
Mechanical efficiency (%)	98.6
<b>Air compressor 3 (AIRCOMP3)</b>	
Pressure ratio	4.4
Isentropic efficiency (%)	85
Mechanical efficiency (%)	98.6
<b>Natural gas compressor (NGCOMP)</b>	
Discharge pressure (bar)	56
Isentropic efficiency (%)	85
Mechanical efficiency (%)	98
<b>NO<sub>x</sub> water pump (NOXWPUMP)</b>	
Discharge pressure (bar)	38
Isentropic efficiency (%)	80
Mechanical efficiency (%)	98
<b>Gas turbine 1 (GT1)</b>	
Pressure ratio	2.7
Isentropic efficiency (%)	90
Mechanical efficiency (%)	98.6
<b>Gas turbine 2 (GT2)</b>	
Pressure ratio	2.2
Isentropic efficiency (%)	90
Mechanical efficiency (%)	98.6
<b>Gas turbine 3 (GT3)</b>	
Pressure ratio	5.4
Isentropic efficiency (%)	90
Mechanical efficiency (%)	98.6

**Table 55: Natural gas composition delivered to Whitby cogeneration power plant (mass-based)**

<b>Component</b>	<b>Methane (CH<sub>4</sub>)</b>	<b>Ethane (C<sub>2</sub>H<sub>6</sub>)</b>	<b>Propane (C<sub>3</sub>H<sub>8</sub>)</b>	<b>Nitrogen (N<sub>2</sub>)</b>	<b>Carbon dioxide (CO<sub>2</sub>)</b>	<b>LHV (MJ/kg)</b>	<b>HHV (MJ/kg)</b>
<b>Mass fraction</b>	95.537%	2.064%	0.117%	1.942%	0.34%	48.8	54.2

The NO<sub>x</sub> control water inlet stream is provided from the water treatment plant at a temperature between 5°C and 15°C (in the model this temperature was fixed at 10°C) and pressure around 6.1 bar. The NO<sub>x</sub> control water pump discharge pressure is about 3.4 bar above the discharge of the third compressor. The combustion chamber was assumed fully insulated, and there was no heat loss. After the combustion process in the combustion chamber, the combustion products expand through three gas turbines with pressure ratios of 2.7, 2.2, and 5.4, respectively, from the high pressure turbine to the low pressure one. The combustion chamber temperature is not measured in the plant. The GT3 outlet stream is then guided to the HRSG, where the thermal energy of the stream is utilized to produce superheated steam. The water stream enters the HRSG at the temperature of the deaerator, 108°C, from the discharge of the feedwater pumps at a pressure of about 35 bar with the maximum mass flow rate of 60,330 kg/h at full load cogeneration. The GT exhaust stream cools down in the HRSG to a temperature of about 180°C. The superheated steam produced in the HRSG is then desuperheated in the desuperheater to bring the steam temperature to about 10°C above the saturation temperature of the steam. The mass flow rate of the water inlet stream to the desuperheater at full load cogeneration is about 18,145 kg/h, and the water is at the same conditions as the inlet stream to the HRSG. It should be noted that the operation of the process steam generation system and its load are independent of the power generation system, and depend on the demand from the paper manufacturing factory. In fact, the HRSG of the Whitby cogeneration power plant can be in service in dry conditions even if there is no demand for steam from the factory. Table 56 shows the important thermodynamic properties of the major streams in the cycle at an ambient temperature of 10°C.

**Table 56: Important thermodynamic properties of the major streams in gas turbine cogeneration system**

Streams		AIRHP	AIRIN	AIRIP	AIRLP	AIRNG	COMBPRO1	COMBPRO2	COMBPRO3	COMBPRO4	COMBPRO5
Temperature (°C)		587.3	10.0	274.1	64.5	496.1	1,209.6	937.4	751.4	435.0	180.0
Pressure (bar)		33.7	1.0	7.7	1.7	33.7	33.7	12.5	5.7	1.0	1.0
Mass flow (kg/h)		569,520	569,520	569,520	569,520	592,490	592,490	592,490	592,490	592,490	592,490
Mass flow rate (kg/h)	H <sub>2</sub> O	0	0	0	0	12,177	35,756	35,756	35,756	35,756	35,756
	N <sub>2</sub>	430,272	430,272	430,272	430,272	430,482	430,482	430,482	430,482	430,482	430,482
	O <sub>2</sub>	131,901	131,901	131,901	131,901	131,901	89,892	89,892	89,892	89,892	89,892
	CO	0	0	0	0	0	0	0	0	0	0
	CO <sub>2</sub>	285	285	285	285	321	29,298	29,298	29,298	29,298	29,298
	Argon	7,062	7,062	7,062	7,062	7,062	7,062	7,062	7,062	7,062	7,062
	Methane	0	0	0	0	10,311	0	0	0	0	0
	Ethane	0	0	0	0	223	0	0	0	0	0
	Propane	0	0	0	0	13	0	0	0	0	0

**Table 56: Important thermodynamic properties of the major streams in gas turbine cogeneration system (cont.)**

Streams		DESHWAT	HRSGWIN	NGHP	NGIN	NOXWATER	NOXWATIN	STEAM	STEAMOUT
Temperature (°C)		108.0	108.0	68.3	10.0	10.3	10.0	381.0	242.7
Pressure (bar)		35.5	35.5	56.2	28.6	38.0	6.2	35.5	35.5
Mass flow (kg/h)		18,144	60,328	10,793	10,793	12,177	12,177	60,328	78,471
Mass flow rate (kg/h)	H <sub>2</sub> O	18,144	60,328	0	0	12,177	12,177	60,328	78,471
	N <sub>2</sub>	0	0	210	210	0	0	0	0
	O <sub>2</sub>	0	0	0	0	0	0	0	0
	CO	0	0	0	0	0	0	0	0
	CO <sub>2</sub>	0	0	37	37	0	0	0	0
	Argon	0	0	0	0	0	0	0	0
	Methane	0	0	10,311	10,311	0	0	0	0
	Ethane	0	0	223	223	0	0	0	0
	Propane	0	0	13	13	0	0	0	0

### **8.2.2 Model validation and modeling results**

The results of the developed model were compared against the operational data of the Whitby cogeneration power plant. It should be noted that the mass flow rate of air, fuel, and  $\text{NO}_x$  control water were inputs to the model, and the system output power and low pressure gas turbine outlet temperature were the parameters to compare. The results in Table 57 show that the model can accurately capture the operation of the system with a high accuracy (error of lower than 1%). It should be noted that in order to determine the net output power, the internal power required to run the natural gas compressor and all other auxiliary equipment, about 1 MW all together, should be deducted from the output power.

The turbine inlet temperature is an important parameter for GT design and operation, because it is the highest temperature throughout a specific gas turbine. The turbine inlet temperature (TIT) is limited by turbine blade material and the maximum permitted  $\text{NO}_x$  emission. In this power plant, the TIT is around  $1200^\circ\text{C}$ , and its exact value depends on the ambient conditions and the plant load.

## **8.3 Combined cycle power plant (CCPP)**

In order to improve the efficiency of GTs, combining the gas turbine with a steam cycle is a suitable option. A schematic diagram of a steam cycle, working based on the Rankine cycle, is illustrated in Figure 103.

In a combined cycle power plant, the high temperature exhaust stream of the gas turbine is used to generate required steam for the steam cycle in an HRSG. This is possible because the inlet temperature of the turbine in a gas turbine, higher than  $1200^\circ\text{C}$  for modern GTs, and as a result their exhaust temperature is much higher than that for the steam turbines, between  $500^\circ\text{C}$  and  $600^\circ\text{C}$ . A unit of a CCPP consists of several GTs, usually two or three, a heat recovery steam generator, and a single steam cycle (Figure 104). Very high efficiency, above 60% (LHV), has been reported for recent modern CCPPs (Cengel and Boles, 1998).

**Table 57: Comparison of modeling results with operational data from Whitby cogeneration power plant**

Parameters	Whitby	Model	Error
Ambient temperature (°C)	-10		
Output power (MW)	58	57.99	-0.02%
Temperature of GT3 exhaust (°C)	389.6	391.6	+0.51%
Air mass flow rate (kg/s)	167.4		
Natural gas mass flow rate (kg/h)	10,621		
NO <sub>x</sub> control water mass flow rate (kg/h)	10,881		
Electrical efficiency (LHV)	40.25%		
Electrical efficiency (HHV)	36.29%		
Total (electrical + thermal) efficiency (LHV)	68.25%		
Total (electrical + thermal) efficiency (HHV)	61.53%		
Ambient temperature (°C)	0		
Output power (MW)	58	57.87	-0.22%
Temperature of GT3 exhaust (°C)	409.8°C	411.4	+0.39%
Air mass flow rate (kg/s)	163.7		
Natural gas mass flow rate (kg/h)	11,584		
NO <sub>x</sub> water mass flow rate (kg/h)	10,711		
Electrical efficiency (LHV)	39.83%		
Electrical efficiency (HHV)	35.91%		
Total (electrical + thermal) efficiency (LHV)	69.72%		
Total (electrical + thermal) efficiency (HHV)	62.85%		
Ambient temperature (°C)	10		
Output power (MW)	58	57.91	-0.16%
Temperature of GT3 exhaust (°C)	431.2	434.9	+0.86%
Air mass flow rate (kg/s)	158.2		
Natural gas mass flow rate (kg/h)	10,793		
NO <sub>x</sub> water mass flow rate (kg/h)	12,177		
Electrical efficiency (LHV)	39.56%		
Electrical efficiency (HHV)	35.66%		
Total (electrical + thermal) efficiency (LHV)	71.39%		
Total (electrical + thermal) efficiency (HHV)	64.36%		

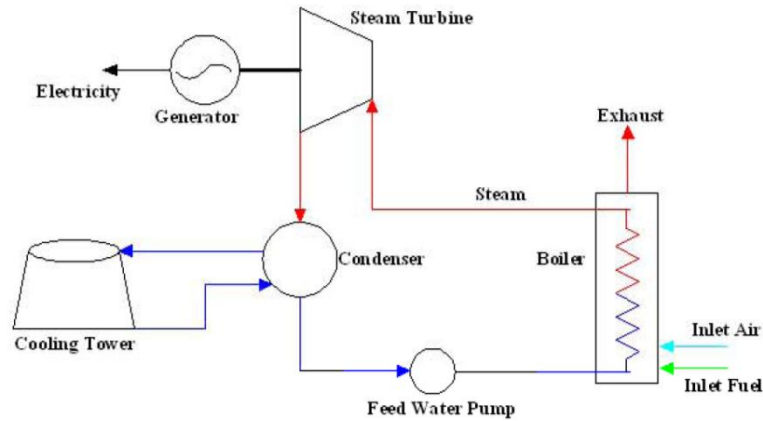


**Figure 103: Schematic of a simple steam power generation (Rankine) cycle**

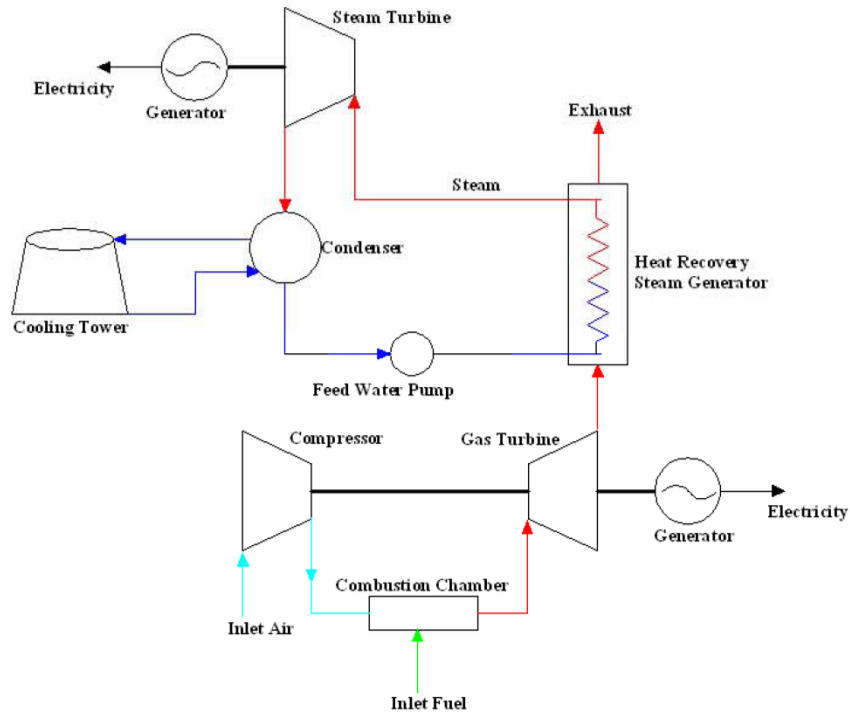


**Figure 104: Schematic of a simple combined cycle power plant**

HRSGs can be designed with or without additional firing. Additional firing, also called duct burning, is used to increase the inlet temperature of the HRSG leading to the higher output power of the steam cycle, although the overall efficiency of the cycle reduces. In the earlier CCPPs,

this configuration was very common due to the low temperature of the GT exhaust stream. However, due to the simplicity of construction and the higher temperature of the exhaust stream of modern GTs, CCPPs with no additional firing in the HRSG, where all fuel is combusted in the GT cycle, is also common. In the CCPPs without additional firing, the efficiency and output power of the bottoming steam cycle is limited by the temperature and flow rate of the gas turbine off-gas and the temperature of the exhaust stream at the stack. The stack temperature is bounded by the exhaust stream dew point to prevent acid corrosions.

Based on the HRSG arrangement, CCPP can be a single-, two-, or three-pressure cycle. In the simplest configuration, the single-pressure cycle, the HRSG can consist of either an economizer, an evaporator, and a superheater or a once-through boiler to generate steam with one pressure. The disadvantage of the single-pressure configuration is its poor waste heat recovery efficiency. To improve this efficiency, a multi-pressure HRSG can be used to produce steam with different pressures. These multiple-pressure steams can drive high- and low-pressure (and possibly intermediate-pressure) steam turbines with a higher efficiency. Figure 105 illustrates an Aspen Plus<sup>®</sup> model of a two-pressure CCPP.

### **8.3.1 CCPP model in Aspen Plus<sup>®</sup>**

Figure 105 illustrates the model of the CCPP cycle developed for this subsection. The gas turbine side of the cycle is exactly identical to the gas turbine side of the Whitby cogeneration power plant. Therefore, the description of the flow diagram of this part of the cycle can be found in Subsection 8.2.1, the model constants in Table 54, important thermodynamic properties in Table 56, and operational parameters in Table 57 at the ambient temperature of 10°C. Table 58 lists the model constants for the equipment of the steam cycle of the plant. Table 59 shows the important thermodynamic properties of the major streams in the steam cycle at the ambient temperature of 10°C.

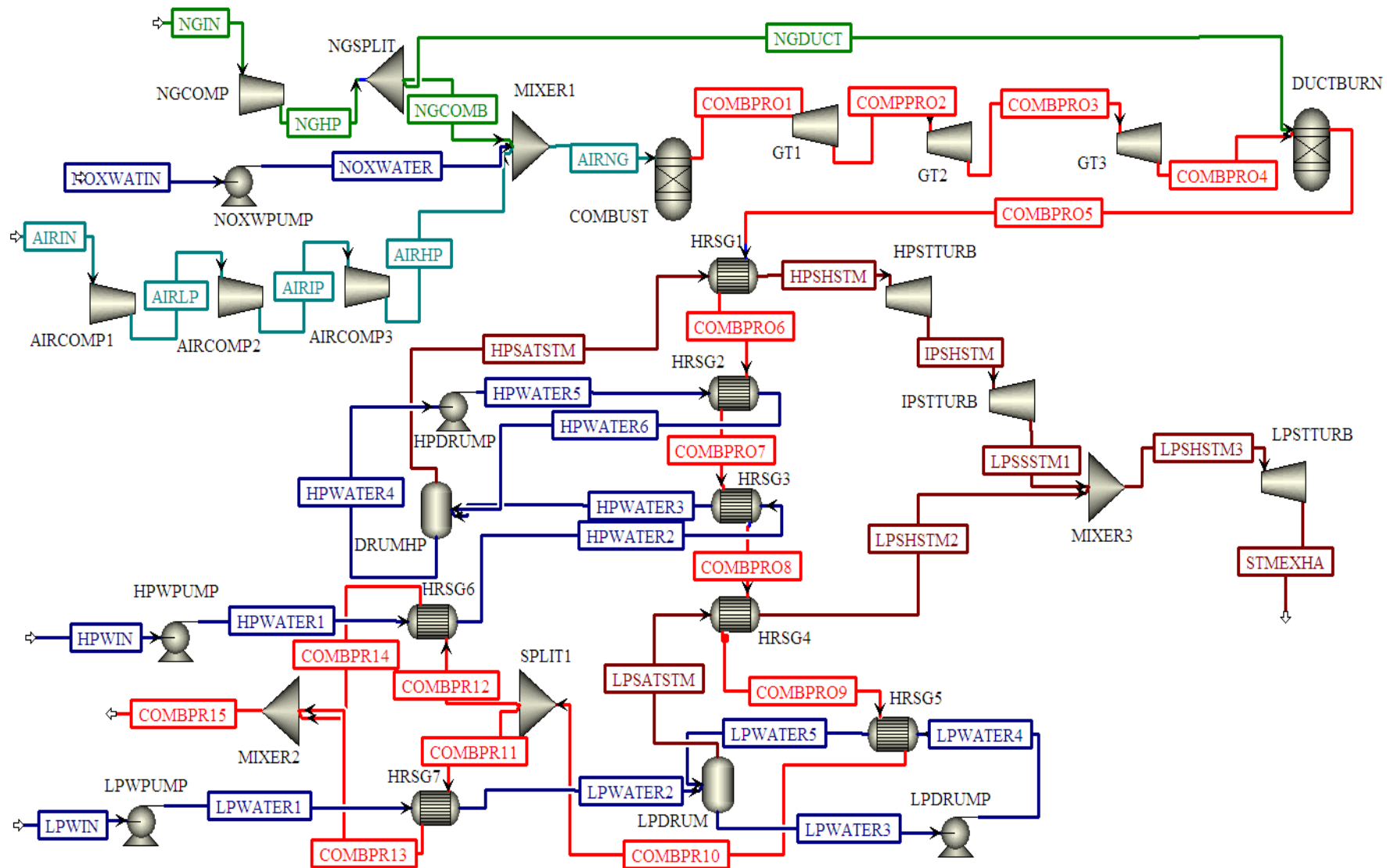


Figure 105: Schematic of an Aspen Plus® model of a two-pressure CCPP



**Table 58: Model constants for the steam cycle of the CCPP**

<b>High pressure steam turbine (HPSTTURB)</b>	
Discharge pressure (bar)	22
Isentropic efficiency (%)	80
Mechanical efficiency (%)	95
<b>Intermediate pressure steam turbine (IPSTTURB)</b>	
Discharge pressure (bar)	5 bar
Isentropic efficiency (%)	80
Mechanical efficiency (%)	98
<b>Low pressure steam turbine (LPSTTURB)</b>	
Discharge pressure (bar)	6.9 bar
Isentropic efficiency (%)	80
Mechanical efficiency (%)	98
<b>High pressure feed water pump (HPWPUMP)</b>	
Discharge pressure	76.5 bar
Isentropic efficiency (%)	80
Mechanical efficiency (%)	98
<b>High pressure drum pump (HPDRUMP)</b>	
Pressure ratio	73.5 bar
Isentropic efficiency (%)	80
Mechanical efficiency (%)	98
<b>Low pressure feed water pump (LPWPUMP)</b>	
Pressure ratio	6.9 bar
Isentropic efficiency (%)	80
Mechanical efficiency (%)	98
<b>Low pressure drum pump (LPDRUMP)</b>	
Discharge pressure (bar)	6
Isentropic efficiency (%)	80
Mechanical efficiency (%)	98

**Table 59: Important thermodynamic properties of the major streams in the steam cycle at the ambient temperature of 10°C**

Streams		COMB PRO5	COMB PRO6	COMB PRO7	COMB PRO8	COMB PRO9	COMB PR10	COMB PR14	COMBP R15	NGDUCT	NGIN	HPSAT STM	HPSH STM
Temperature (°C)		540.2	495.2	362.6	293.2	290.3	240.0	140.6	148.7	151.1	52.0	289.1	500.0
Pressure (bar)		1.0	1.0	1.0	1.0	1.0	1.0	1.0	1.0	56.2	19.5	73.5	73.5
Mass flow (kg/h)		593,990	593,990	593,990	593,990	593,990	593,990	430,643	593,990	1,500	12,293	62,000	62,000
Vapour fraction		1	1	1	1	1	1	1	1	1	1	1	1
Mass flow rate (kg/h)	H <sub>2</sub> O	39,033	39,033	39,033	39,033	39,033	39,033	28,299	39,033	0	0	62,000	62,000
	N <sub>2</sub>	430,511	430,511	430,511	430,511	430,511	430,511	312,121	430,511	29	239	0	0
	O <sub>2</sub>	84,053	84,053	84,053	84,053	84,053	84,053	60,939	84,053	0	0	0	0
	CO	0	0	0	0	0	0	0	0	0	0	0	0
	CO <sub>2</sub>	33,330	33,330	33,330	33,330	33,330	33,330	24,165	33,330	5	42	0	0
	Argon	7,062	7,062	7,062	7,062	7,062	7,062	5,120	7,062	0	0	0	0
	Methane	0	0	0	0	0	0	0	0	1,433	11,744	0	0
	Ethane	0	0	0	0	0	0	0	0	31	254	0	0
	Propane	0	0	0	0	0	0	0	0	2	14	0	0

**Table 59: Important thermodynamic properties of the major streams in the steam cycle at the ambient temperature of 10°C (cont.)**

Streams		HP WATER1	HP WATER3	HP WATER6	HPWIN	IPSHSTM	LP SHSTM3	LP WATER1	LP WATER5	STMEXHA
Temperature (°C)		10.8	291.9	289.1	10.0	343.0	198.2	10.0	158.9	32.9
Pressure (bar)		76.5	76.5	73.5	6.2	22.0	5.0	6.9	6.0	0.1
Mass flow (kg/h)		62,000	62,000	122,437	62,000	62,000	78,000	16,000	31,583	78,000
Vapour fraction		0	0	1	0	1	1	0	1	1
Mass flow rate (kg/h)	H <sub>2</sub> O	62,000	62,000	122,437	62,000	62,000	78,000	16,000	31,583	78,000
	N <sub>2</sub>	0	0	0	0	0	0	0	0	0
	O <sub>2</sub>	0	0	0	0	0	0	0	0	0
	CO	0	0	0	0	0	0	0	0	0
	CO <sub>2</sub>	0	0	0	0	0	0	0	0	0
	Argon	0	0	0	0	0	0	0	0	0
	Methane	0	0	0	0	0	0	0	0	0
	Ethane	0	0	0	0	0	0	0	0	0
	Propane	0	0	0	0	0	0	0	0	0

In this cycle, since the temperature of the GT3 exhaust stream, COMBPRO4 (436.7°C), is not sufficient for steam generation in the HRSG, supplementary firing equipment, also known as the duct burner, is used to increase the temperature of the HRSG inlet stream. For this purpose, the mass flow rate of the inlet natural gas is increased to 12,293 kg/h of which 10,793 kg/h is combusted in the gas turbine combustor, and the rest (1,500 kg/h) is combusted in the duct burner. It should be noted that due to the very high air-to-fuel ratio in the combustion chamber of the gas turbine, there is sufficient oxygen in the duct burner for combustion (89,892 kg/h) such that even after the duct burner, the mass flow rate of oxygen in the stream is 84,053 kg/h. The combustion products at a temperature of 540°C and pressure of 1.048 bar enter the HRSG and pass through seven heat exchangers, each representing different sections of the HRSG and are discharged to the atmosphere at a temperature of 148.7°C.

The HRSG of the cycle is a two-pressure system. For the high pressure section of the HRSG, the feed water with the mass flow rate of 62,000 kg/h is pressurized at HPWPUMP to the pressure of 76.5 bar. Then, it is heated through two economizers (HRSG6 and HRSG3), one evaporator (HRSG2), one drum (HPDRUMP), and one superheater (HRSG1). The superheated steam enters the high pressure steam turbine (HPSTTURB) at a temperature of 500°C and pressure of 73.5 bar. While expanding to a temperature of 343°C and pressure of 22 bar, the steam generates 4.6 MW of power. The steam further expands through the intermediate pressure steam turbine (IPSTTURB) to a temperature of 193.5°C and pressure of 5 bar and generates 4.5 MW of electricity.

For the low pressure section of the HRSG, the water enters the system with a mass flow rate of 16,000 kg/h and is pressurized at LPWPUMP to the pressure of 6.9 bar. Then, it is heated through one economizer (HRSG7), one evaporator (HRSG5), one low pressure drum (LPDRUM), and one superheater (HRSG4). The low pressure superheated steam is then mixed with the IPSTTURB exhaust stream before being fed to the low pressure steam turbine (LPSTTURB). The electricity generated in the low pressure steam turbine is 11.6 MW. This turbine discharges the saturated steam to the condenser at a temperature of 32.9°C and partial vacuum of 0.05 bar. The total output power of the CCPP is 79 MW of which 58.2 MW (73.7%) is generated in the gas turbine and 20.8 MW (26.3%) is generated in the steam cycle. The total efficiencies of the cycle are 42.7% and 47.4%, respectively, based on the HHV and LHV.

## **8.4 Augmentation of gas turbine output power**

The output power and efficiency reduction with a higher ambient temperature is a major problem for gas turbine-based cycles. This problem is more serious in areas with a hot climate because the peak load in these areas is during hot summer days, and GT-based power plants cannot produce their maximum output power (rated power) when it is most needed. This issue has been intensified with the recent global climate change. The reason for this problem can be explained based on the fact that in a single-shaft gas turbine, the rotational speed of the shaft and as a result the volumetric flow rate of the air are constant. On the other hand, high ambient temperature reduces air density. These two facts, constant volumetric air flow rate and lower air density, cause air mass flow rate reduction with increased ambient temperature. This means lower output power from the gas turbine and a higher power requirement in the compressor. Obviously, cooling the inlet air to the compressor can solve the problem. Several methods have been proposed and/or employed to decrease inlet air temperature to the cycle. Generally, these systems can be divided into two main groups: evaporative and non-evaporative systems.

### **8.4.1 Evaporative cooling systems**

In this system, water evaporates in the inlet air stream to the compressor. The heat required for this phase change (the latent heat of evaporation) is gained by cooling down the air. The problem for evaporative systems is that once the air relative humidity reaches 100%, no extra water can be added to the air. Therefore, the cooling capacity of the system is limited by the relative humidity of the air. The evaporative systems are ideal for hot arid regions. The advantages of these systems are their low capital, operating, and maintenance costs, and quick installation. But their operational capacity is limited and highly affected by ambient wet bulb temperature. Also, they require a relatively great amount of water, which is usually a precious commodity in arid regions.

There are two main types of compressor inlet air evaporative cooling: media evaporative cooling and inlet air fogging systems.

#### **8.4.1.1 Media evaporative cooling systems**

In this design, the compressor inlet air passes over a film of water in a carefully designed wetted medium (also known as packing or fill), such as a honey-comb-like medium. This is the first technology employed for gas turbine inlet cooling. The system has the lowest cost among all cooling systems partially because it can operate with less treated and lower quality water. The system also acts as an air washer that cleans air, which in turn can increase the longevity of the gas turbine's filters. However, the water consumption of the system is high, because in each cycle, water is partially evaporated and the remaining water should be partially recycled, with proper control of its chemistry, and the rest should be rejected from the system as blow down. Another disadvantage of the system is that it cannot achieve very high air relative humidity and cannot take advantage of full cooling capacity.

#### **8.4.1.2 Inlet air fogging systems**

In this design, atomized demineralized water is sprayed in the compressor inlet air by high pressure (100 to 200 bar) nozzles, mostly impaction pin type. The GT inlet temperature can be controlled by the amount of water sprayed into the stream. The fogging system can increase the air relative humidity to almost 100%. If more water is sprayed, the excess water will carry over to the compressor in the form of water droplets. These droplets can provide intercooling for the compressor by evaporating while the air temperature increases due to compression. This latter system is called overspraying or wet compression. Figure 106 shows the performance of the nozzles and the water treatment unit (reverse osmosis) of the Zahedan, Iran gas turbine power plant compressor inlet air cooling system.



a



b



c

**Figure 106: Zahedan gas turbine power plant (Iran) compressor inlet air cooling system  
a and b) the performance of the nozzles c) the water treatment unit**

There are also other gas turbine power augmentation methods, such as injection of water or steam to the combustion chamber. The main objective of most of this type of GT augmentation is  $\text{NO}_x$  emission control and reduction. However, due to increase in the GT mass flow rate, higher output power can be achieved as well.

#### **8.4.2 Mechanical refrigeration system cooling**

Alternatively, mechanical refrigeration systems can be used to decrease gas turbine cycle inlet air temperature. These systems are not limited by ambient conditions and can reduce air temperature lower than that of evaporative systems. The refrigeration systems can be either compressor chiller or absorption chiller. The former suffers from high operation cost due to high electricity consumption, and the latter suffers from high capital cost partially due to the required waste heat recovery system.

In order to reduce the cost of electricity and take advantage of the low night time tariff, thermal energy storage systems can also be used. In these systems, ice or chilled water are generated during off-peak hours, usually in the night time, and then used to cool down compressor inlet air in peak hours (Wang, 2007).

#### **8.4.3 Compressor inlet air evaporative cooling system of Whitby cogeneration power plant**

The conventional fogging systems are always installed inside the inlet air duct to the compressor and after the filter house, usually before and sometimes after silencers. However, the inlet evaporative system in the Whitby cogeneration power plant is different from the conventional systems, and it is installed upstream of the filter house, outside of the inlet air duct. The system designer and manufacturer claims that this is the first such system installed in the world. The system consists of an array of nozzles that sprays demineralized water to the inlet air. The system makes use of a droplet collector after the nozzles and before the filter house. The collector is just a packing (fill) to redirect the wet air stream and separate water droplets. It consists of approximately  $76 \times 60 \times 40$  cm blocks that are placed beside each other in order to create a solid packing. The high pressure water nozzles are located around 38 cm from the packing, and there is no housing around the nozzle arrays. The distance between nozzles and the droplet collector was found by trial and error because if the distance is too much, water droplets can be drifted by the wind and if they are too close, there would not be enough time for evaporation of water droplets. Almost 20% of the sprayed water is trapped in the collector. In the original plan, this water should be returned to the water treatment plant, but since the plant is equipped with the



oversized water treatment plant, the collected water is drained to the sewage system. The fogging system has no impact on the air filters because all water droplets are trapped by the collectors, and the filters are able to tolerate above 90% relative humidity (because near Lake Ontario humidity is high during most of the summer). Normally filters should be changed every 3-5 years. For this case, they have not been replaced after the installation of the fogging system. The water electrical conductivity of the demineralized water is 0.1  $\mu\text{S}/\text{cm}$ . However, the fogging system can be operated with a conductivity as high as 0.5  $\mu\text{S}/\text{cm}$ . The flow rate of water injected by the fogging system is normally between 1 to 2  $\text{m}^3/\text{h}$ , with a maximum of 2.5  $\text{m}^3/\text{h}$ .

The operating pressure of the water nozzles is 138 bar (2000 psi). The system (specially the packing) causes some pressure drop, which results in a 200 kW power decrease in the gas turbines. That is why it is designed so that the system can be moved away from the filter house by a couple of metres when it is not in service. Also the droplet collector can be disassembled especially in winter. The system can be reassembled in eight hours, even when the gas turbine is operating.

The system is equipped with ambient temperature and humidity measurement devices. The measured parameters are used to calculate the flow rate of the required water. Two reciprocating pumps, each capable of operating at 50% load, are used to pressurize the demineralized water. As a result, there are four stages of cooling with four sets of arrays of nozzles. The control system is fully integrated with the control system of the power plant, and everything can be monitored and controlled from the plant's control room. An instrument to measure relative humidity is installed inside the filter house, and the actual relative humidity after the filters when the fogging system is in service is normally higher than 95%.

The fogging system was installed in 2007 and was in service May-October 2007, May-October 2008, and April-June 2009. It has not been in service since that time due to the type of contract the power plant signed (based on the new contract they have to produce a fixed amount of electricity; therefore, if the fogging system is used, the plant should be shut down to meet the contractual obligations). The design point of the fogging system is 60% relative humidity and 16°C temperature. But it can be operated with a minimum temperature of 15°C and a maximum relative humidity of 90%. The maximum temperature decrease achieved so far is 9°C. But normally the temperature decrease is much lower, around 3°C (due to the ambient temperature

and high relative humidity of the region). Actually the plant is located very closed to Lake Ontario, so the ambient relative humidity is usually high. According to the plant manager, the system operation has been very satisfactory, and the capital cost of the fogging system was paid back in the first 1.5 year of the system's operation.

The system's advantages over conventional fogging systems can be listed as follows:

- Absolute protection of compressor from any damage;
- No water collection in ducts;
- No changes in the GT system;
- Visual monitoring of the system by walking around the air intake at any time;
- Minimal GT outage during installation;
- No GT outage for system maintenance and re-assembly;
- No modification in the air inlet ducts;
- No pressure drop during winter (when fogging system is disassembled).

However, it has a few disadvantages over conventional fogging systems, namely:

- Lower cooling efficiency (around 95% relative humidity at outlet);
- Drifting of a fraction of sprayed water by wind.

#### **8.4.4 Modeling results of compressor inlet air cooling system of Whitby cogeneration plant**

Table 60 presents the summary of the results of the model of the compressor inlet air cooling system of the Whitby cogeneration power plant for various ambient conditions. The maximum cooling is 8.4°C at an ambient temperature of 30°C and relative humidity of 40%. This much cooling can be achieved with an injection of 2 m<sup>3</sup>/h of water to the inlet air. The results show that the model can simulate the plant and predict the outputs with an acceptable accuracy. In all cases, the model can predict the plant power production with the error level of lower than 3%. Also, the error level of the predicted gas turbine outlet stream temperature is lower than 0.5%. The comparison of the system output power when the plant operates with and without the inlet air cooling system signifies that the fogging system can significantly improve system performance. For example, when the system operates at an ambient temperature of 20°C, its output power is 51 MW. Using the fogging system, in case A with 6.4°C cooling of the inlet air,

the output power can be increased to 55.6 MW. In case B, 1.2°C cooling of the inlet air temperature increases the plant output power to 52.4 MW.

**Table 60: Summary of results of model of compressor inlet air cooling system of Whitby cogeneration plant**

<b>Cases</b>		<b>A</b>	<b>B</b>	<b>C</b>	<b>D</b>	<b>E</b>
<b>Ambient conditions</b>	Temperature (°C)	20	20	25	25	30
	Humidity (%)	40	80	40	80	40
<b>Fogging system water</b>	Flow (m <sup>3</sup> /h)	2.0	1.0	2.0	1.0	2.0
	Pressure (bar)	139	139	139	139	139
	Temperature (°C)	10	10	10	10	10
<b>GT entry conditions (downstream of the fogging system)</b>	Temperature (°C)	13.6	18.8	17.3	23.4	21.6
	Humidity (%)	> 95	> 95	> 95	> 95	> 95
	Air flow (kg/s)	155.2	146.8	149.2	140.1	142.7
<b>GT operational data</b>	Natural gas flow (kg/h)	10,684	10,029	10,219	9,500	9,699
	NO <sub>x</sub> control water flow (kg/h)	12,507	12,021	12,353	11,051	11,424
	Plant power production (MW)	55.6	52.4	53.4	48.9	50.3
	Model power production (MW)	57.0	53.0	54.1	49.9	51.0
	Power production error (%)	2.6	1.1	1.3	2.0	1.4
	Plant GT exhaust temperature (°C)	439	443	442	446	445
	Model GT exhaust temperature (°C)	441	444	442	448	446
	GT exhaust temperature error (%)	0.39	0.14	0.05	0.49	0.27

## 8.5 Future work

As noted in Subsection 8.1, the three disadvantages of gas turbines are their low efficiency due to high temperature exhaust, their vulnerability against high ambient temperature, and their

incapability of consuming solid fuels, mainly coal, as the inlet fuel. The methods to deal with the first two problems and their models were discussed in this chapter. The integrated gasification combined cycle (IGCC) is one of the most environmentally friendly means of producing electricity from coal. Also, CO<sub>2</sub> capture and storage technologies can be used to reduce environmental impacts of fossil fuel-fired power plants in terms of GHG emissions. Since these technologies are considered as immediate future work for this chapter, a brief introduction is presented in the following subsection.

### **8.5.1 Integrated gasification combined cycle (IGCC)**

Coal has been used as a fuel for power generation for a long time. The utilization of coal has been mostly in steam power plants, where coal is combusted in a conventional boiler to produce steam for the power plant. These types of coal-fired power plants are mainly pulverized fuel-fired stations and fluidized bed combustion-based plants. The utilization of coal as fuel in GTs was possible only in externally- or indirectly-fired gas turbines, where coal is burned in an external combustor and then the heat is transferred to the working fluid via a heat exchanger to pass through the gas turbine. On the other hand, coal gasification is a well-developed technology to produce synthesis gas (syngas, mainly hydrogen and carbon monoxide) by gasifying coal with steam together with oxygen or air.

The integrated gasification combined cycle is the combination of coal gasification technology with a gas turbine and steam cycle to generate electricity. The advantages of the technology can be summarized as:

- Higher efficiency, around 40%, in comparison to other coal-fired power generation technologies (Ratafia-Brown et al., 2002);
- Feedstock flexibility, since coal, heavy petroleum products, petroleum coke, biomass, etc. can be used as inlet fuel to the system;
- Low amount of pollutants, such as CO<sub>2</sub>, CO, NO<sub>x</sub>, SO<sub>x</sub>, emissions in comparison to other coal-fired power generation technologies. IGCCs can meet the requirements of the strictest air control regulations (Elseviers, Van, Van, and Verelst, 1996);

- Various potential products, such as electricity, high and low pressure steam, hot water, hydrogen, syngas fuel, other chemicals, sulfur by-products, even valuable solid wastes (Ratafia-Brown et al., 2002), can be generated;
- Capability to be adapted for repowering of old coal-fired power plants.

The main additional equipment in the IGCC, compared to the CCPP, is the gasifier and gas clean up components. In the gasifier, the inlet fuel is converted to high temperature and normally high pressure syngas. The reaction in the gasifier is endothermic, and the required heat can be supplied by partial oxidation of the fuel. The pollutants, such as minerals, ash, slag, particulates, nitrogen, and sulfur compounds, and gaseous mercury are then separated from syngas in different stages of gas clean up. Different carbon dioxide capture technologies can be used to significantly reduce GHG emissions. These CO<sub>2</sub> capture technologies will be briefly explained in the following subsections.

### **8.5.2 CO<sub>2</sub> capture and storage technologies**

As noted in the introduction, the power generation industry is responsible for the majority of GHG emissions from industrial activities. Thus, it is essential to reduce the emissions in light of climate change and environmental concerns. One of the methods to achieve this goal is to increase efficiency in power generation, which has been a main topic of this thesis. Another method is the utilization of CO<sub>2</sub> capture and storage systems in power plants. Potentially, CO<sub>2</sub> capture technologies have already existed for all of the aforementioned power generation technologies, although in most cases they have not been developed particularly for these systems. For different types of power plants fuelled by oil, natural gas, and coal, there are three main techniques that could be applied (Riahi et al., 2003; Metz et al., 2005):

- CO<sub>2</sub> capture after combustion (post-combustion);
- CO<sub>2</sub> capture after concentration of flue gas by using pure oxygen in boilers and furnaces (oxy-fuel power plant);
- CO<sub>2</sub> capture before combustion (pre-combustion).

These technologies will be explained in the following subsections.

### 8.5.2.1 CO<sub>2</sub> capture after combustion (post-combustion)

This method treats plants' flue gases to remove CO<sub>2</sub>. This methodology can be easily applied in the near future. Post-combustion CO<sub>2</sub> capture in conventional power plants is currently too costly and energy consuming. Several methods to capture CO<sub>2</sub> from thermal power stations flue gas are as follows:

*Solvent scrubbing systems:* This method is suitable for CO<sub>2</sub> separation for low concentration of carbon dioxide (5% to 15% by volume) in a stream at low pressure. This low concentration of CO<sub>2</sub> and low pressure is very similar to the condition in the flue gas of conventional power plants.

In this method, the solution of amines is used as solvents to separate CO<sub>2</sub>. Using this process, 90% of CO<sub>2</sub> in the flue gas can be captured. The separation process of carbon dioxide by chemical absorption consists of two steps:

- the absorption of CO<sub>2</sub> by chemical solvents at a low temperature (40°C - 65°C);
- the recovery of CO<sub>2</sub> from chemical solvents by using low temperature (100°C – 150°C) heat sources usually from power plants.

The details of the mechanisms of CO<sub>2</sub> absorption into an amine solution are quite complex (Danckwerts and Sharma, 1966; Versteeg, Van Dijck, and Van Swaaij, 1996). At present, a few coal- and gas-fired power plants utilize this technology to capture CO<sub>2</sub> (IEA, 2003c). However, scrubber-based systems require considerable capital investment as well as remarkable reduction in the overall plant efficiency.

*Cryogenics:* CO<sub>2</sub> can be separated from other gaseous compounds in the flue gas by cooling and condensation. This method is suitable for a high concentration of CO<sub>2</sub> (more than 90%), and the technology is not applied to typical power generation plant exhaust stream. Obviously, a disadvantage of the process is that it requires a significant amount of energy.

*Membranes:* In this method, a separation membrane is used to allow one component to pass more quickly through the membrane. A range of membranes is available for this purpose and all of them are complex and energy consuming with low degree of separation.

*Adsorption:* Some solids can separate CO<sub>2</sub> from gas mixtures. They are not yet considered to be applicable for power plant application because the capacity and CO<sub>2</sub> selectivity of adsorbents is not acceptable yet.

In practice, the most popular technology for CO<sub>2</sub> capture from power generation plants and other industries is the scrubber-based system.

#### **8.5.2.2 CO<sub>2</sub> capture after concentration in the flue gas (oxy-fuel power plants)**

As mentioned, the removal of CO<sub>2</sub> from the exhaust stream of power plants is very energy demanding. The oxy-fuel process is proposed to increase the CO<sub>2</sub> concentration in the flue gas by burning fuel with pure oxygen instead of air. If oxygen is used for the combustion process, the exhaust stream will be mainly composed of CO<sub>2</sub> and steam. An air separation unit (ASU) is required to provide pure oxygen. Also, flue gas should be recycled to reduce temperature in the boiler. With this technology, a CO<sub>2</sub> concentration of above 90% is achievable, which in turn lowers the energy requirement for the separation process. In order to reduce impurities in the off-gas, reduction of excess oxygen from 17% to 5% is proposed (Kather, Mieske, Hermsdorf, Klostermann, Eggers, and Kopke, 2007).

#### **8.5.2.3 CO<sub>2</sub> capture before combustion (pre-combustion)**

In this method, first fuel is gasified and then CO<sub>2</sub> is removed by one of the aforementioned methods. The product fuel gas is almost pure hydrogen. This method is very attractive for the mid-term future in a hydrogen economy. There are different methods to produce hydrogen from decarbonization of fossil fuels, for instance, methane partial oxidation, methane steam reforming, and coal gasification. The latter is mostly being used in IGCC plants. In all these methods, after preparation of a hydrogen-rich stream, CO<sub>2</sub> is usually removed by the chemical absorption method. In all of the above processes, the incorporation of power plants and these systems is complex.

#### **8.5.2.4 CO<sub>2</sub> liquefaction and sequestration**

After CO<sub>2</sub> separation, it should be stored as a liquid. The liquefaction is implemented in various steps by compressing and cooling of the stream. This process is very energy intensive. The use of geologic formations, gas and oil underground fields, old coal seams, and deep-sea sediments, etc. can all be considered as possible methods for CO<sub>2</sub> sequestration. Further research and development are required to determine which is most suitable for each case.

### **8.6 Conclusion**

The results of gas turbine-based power plants were presented in this chapter. The model configuration and specification were based on the Whitby cogeneration power plant. The operational data from this power station were used to validate the models. The modeling confirmed that the electrical efficiency of the plant can be improved from 39.6% (LHV) in the single gas turbine to 47.4% (LHV) in the CCPP. Also, in a cogeneration plant the thermal energy of the gas turbine exhaust can be used to produce steam to achieve a total (electrical and thermal) efficiency of 69.7% (LHV). Also, it was shown that using the compressor inlet air fogging cooling system can significantly increase the system output power.



## **CHAPTER NINE**

### **Conclusion**

Electricity generation plays an important role in maintaining our current standard of living, and fossil fuel-fired power plants are and will remain an inevitable part of this industry. The detailed specific conclusion and recommendation were provided at the end of each chapter. In this section, the generalized conclusion will be made.

In the first part of this work, the methodology to estimate GHG emissions from fossil fuel power plants was presented and applied to the Iranian power generation industry. The GHG emission estimation for the Iranian fossil fuel power generation industry signified that this emission was reduced by 13% between 1995 and 2005, mainly due to the installation of natural gas combined cycle power plants and fuel switching to natural gas in existing power stations. During the same period, the Canadian fossil fuel power generation industry experienced 6% increase in GHG emissions. The detail analysis of the GHG emissions from power plants pointed out that there were remarkable GHG emission reduction potentials. These potentials were evaluated by introducing eight scenarios. The introduced scenarios were implemented for the Canadian and Iranian power generation industries and major reductions were observed. Also, the brief economic evaluation demonstrated that some of these scenarios were practical for mid- and long-term plans.

Then, the steady-state model of the SOFC, hybrid SOFC-GT, micro gas turbine, single gas turbine, gas turbine cogeneration, and combined cycle power plant (CCPP) were presented. These models were used to evaluate the cycles' performance at various conditions and to investigate the effects of different parameters on the systems' performance. Some of these models could achieve high electricity generation efficiency. The methane fuelled SOFC cycle's efficiency was around 58% and 50% (all efficiencies are based on lower heating value, LHV),

with and without anode exhaust recirculation, respectively. The efficiency for the methane fuelled hybrid SOFC-GT cycle was about 74% for both configurations. The efficiencies of the micro gas turbine fuelled with a blend of biodiesel and petrodiesel and natural gas fuelled single gas turbine for stationary power generation were about 13% and 40%, respectively. The efficiency of the latter could be increased to about 47% when the gas turbine was combined with a bottoming steam cycle in a CCPP. Also, the total efficiency of the cogeneration plant that was used to generate process steam, as well as electricity, was about 71%.

Various sensitivity analyses were performed on the models. The effects of various parameters on the SOFC overpotentials and outputs were investigated. The impacts of the hybrid SOFC-GT cycle's design parameters on the system performance were evaluated. It was shown that increasing the system operating pressure and SOFC operating temperature could improve system efficiency, whereas increasing turbine inlet temperature and current density negatively influenced system efficiency. The effect of the SOFC fuel utilization factor on system efficiency, depending on the gas turbine isentropic efficiency, could be positive or negative. The operation of the hybrid SOFC-GT cycle when fuelled with methane and syngas was explained in detail. The results indicated that the method of providing steam for the reactions (with or without anode exhaust recirculation) could influence system operation, especially its specific power. Also, the system configuration (the equipment that participated in the system operation) could be different in two configurations.

The analysis of the impacts of the inlet fuel on the performance of the hybrid SOFC-GT cycle indicated that these impacts could be profound. For instance, the hybrid SOFC-GT cycle efficiency could vary significantly, depending on the inlet fuel type (between 59% and 75%). These effects were discussed in detail for various fuel types and when  $H_2$ ,  $CO_2$ ,  $CO$ , and  $N_2$  replaced the reference fuel, methane. The results signified that the specific work of the cycle with anode exhaust recirculation was always higher than that of the cycle without anode recirculation, which could result in a lower capital cost of the former.

The experimental and numerical analyses of the micro gas turbine fuelled with the blends of biodiesel and petrodiesel (up to B30) demonstrated that, although the system could potentially operate with these fuels at a relatively constant efficiency, before switching the system fuel to biodiesel, the variations of the system operational parameters should be considered.

The modeling of the gas turbine-based power plants indicated that a significant efficiency improvement could be achieved by utilizing the gas turbine in the cogeneration and combined cycle power plants. Also, the compressor inlet air cooling system proved to be an effective technology to offset negative impacts of high ambient temperature on the system performance.

This thesis demonstrated that it is possible to utilize fossil fuels for power generation with a high efficiency and hence lower environmental impacts.

## REFERENCES

- A glance at Iran. (n.d.). In national portal of statistics. Retrieved April 09, 2010, from [http://www.sci.org.ir/portal/faces/public/sci\\_en/sci\\_en.Glance/sci\\_en.pop/](http://www.sci.org.ir/portal/faces/public/sci_en/sci_en.Glance/sci_en.pop/)
- Achenbach, E. (1994). Three-dimensional and time-dependent simulation of a planar solid oxide fuel cell stack. *Journal of Power Sources*, 49(1-3), 333-348.
- Achenbach, E., & Riensche, E. (1994). Methane/steam reforming kinetics for solid oxide fuel cells. *Journal of Power Sources*, 52(2), 283-288.
- Ackmann, T., De Haart, L.G.J., Lehnert, W., & Thom, F. (2000). *Modelling of mass and heat transport in thick-substrate thin-electrolyte layer SOFCs*. Proceedings of Fourth European Solid Oxide Fuel Cell Forum., 1, 431-438.
- Ahmed, K., & Foger, K. (2000). Kinetics of internal steam reforming of methane on Ni/YSZ-based anodes for solid oxide fuel cells. *Catalysis Today*, 63(2-4), 479-487.
- Ahmed, S., McPheeters, C., & Kumar, R. (1991). Thermal-hydraulic model of a monolithic solid oxide fuel cell. *Journal of the Electrochemical Society*, 138, 2712-2718.
- Appleby, A. J., & Foulkes, F.R. (1989). *Fuel cell handbook*. New York: Van Nostrand Reinhold.
- Aras, H., & Balli, O. (2008). Exergoeconomic analysis of a combined heat and power system with the micro gas turbine (MGTCHP). *Energy Exploration & Exploitation*, 26-1, 53-70.
- Baker, B. S. (1984). Molten carbonate fuel cell technology - the past decade. *The Electrochemical Society Proceedings*, 84-13: 2-19.
- Bauer, N. (2005). Carbon capturing and sequestration an option to buy time?, Doctor Politicorum, University Potsdam Faculty of Economics and Social Sciences.
- Beausoleil-Morrison, I., Weber, A., Marechal, F., & Griffith, B. (2004). Model specifications for a fuel cell cogeneration device. *IEA / ECBCS Annex 42 working document*.
- Bevc, F. (1997). Advances in solid oxide fuel cells and integrated power plants. *Proceedings of the Institution of Mechanical Engineers, Part A (Journal of Power and Energy)*, 211(A5), 359-366.
- Biyikoglu, A. (2005). Review of proton exchange membrane fuel cell models. *International Journal of Hydrogen Energy*, 30, 1181-1212.
- Bolland, O., & Stadaas, J. F. (1993). *Comparative evaluation of combined cycles and gas turbine systems with water injection, steam injection and recuperation*. Proceeding of the international Gas Turbine and Aeroengine congress and exposition, Ohio, USA.
- Borbely, A. M., & Kreider, J. F. (2001). *Distributed generation: The power paradigm for the new millennium*, CRC Press.
- Bove, R., Lunghi, P., & Sammes, N. M. (2005). SOFC mathematic model for systems simulations. Part one: from a micro-detailed to macro-black-box model. *International Journal of Hydrogen Energy*, 30, 181-187.

- Bove, R., & Ubertini, S. (2006). Modeling solid oxide fuel cell operation: Approaches, techniques and results. *Journal of Power Sources*, 159, 543-559.
- Braun, R. J., Klein, S. A., & Reindl, D. T. (2006). Evaluation of system configurations for solid oxide fuel cell-based micro-combined heat and power generators in residential applications. *Journal of Power Sources*, 158, 1290-1305.
- Bustamante, F., Enick, R.M., Cugini, A.V., Killmeyer, R.P., Howard, B.H., & Rothenberger, K.S., (2004). High-temperature kinetics of the homogeneous reverse water-gas shift reaction. *AIChE Journal*, 50(5), 1028-1041.
- Calise, F., Palombo, A., & Vanoli, L. (2006a). Design and partial load exergy analysis of hybrid SOFC–GT power plant. *Journal of Power Sources*, 158, 225-244.
- Calise, F., Dentice d'Accadia, M., Palombo, A., & Vanoli, L. (2006b). Simulation and exergy analysis of a hybrid Solid Oxide Fuel Cell (SOFC)–Gas Turbine System. *Energy*, 31, 3278-3299.
- Calise, F., Dentice d'Accadia, M., Vanoli, L., & Von Spakovsky, M. R. (2007). Full load synthesis/design optimization of a hybrid SOFC–GT power plant. *Energy*, 32, 446-458.
- Calise, F., Dentice d'Accadia, M., Palombo, A., & Vanoli, L. (2008). One-dimensional model of a tubular solid oxide fuel cell. *Journal of Fuel Cell Science and Technology*, 5(2), 021014-1-021014-15.
- Campanari, S. (2000). Full load and part-load performance prediction for integrated SOFC microturbine systems. *Journal of Engineering for Gas Turbines and Power*, 122, 239–246.
- Campanari, S. (2001). Thermodynamic model and parametric analysis of a tubular SOFC module. *Journal of Power Sources*, 92, 26-34.
- Campanari, S. (2002). Carbon dioxide separation from high temperature fuel cell power plants. *Journal of Power Sources*, 112, 273–289.
- Campanari S., & Macchi, E. (1998). *Thermodynamic analysis of advanced power cycles based upon solid oxide fuel cells, gas turbines and Rankine bottoming cycles*, Proceedings of International Gas Turbine & Aeroengine Congress, Sweden, Stockholm.
- Campanari, S., & Chiesa, P. (2002). *Potential of solid oxide fuel cells (SOFC) based cycles in low-CO<sub>2</sub> emission power generation*. Proceedings of the 6th International Conference on Greenhouse Gas Control Technologies, Kyoto, Japan.
- Canada inactive on climate front. (2009). In the Toronto Star. Retrieved April 09, 2010, from <http://www.thestar.com/opinion/editorials/article/735079--canada-inactive-on-climate-front>.
- Canada's population estimates. (2010). In Statistics Canada. Retrieved April 09, 2010, from <http://www.statcan.gc.ca/daily-quotidien/100325/dq100325a-eng.htm>
- Cengel, Y. A., & Boles, M. A. (1998). *Thermodynamics: An engineering approach (third ed.)*. McGraw-Hill.
- Chan, S. H., Ho, H. K., & Tian, Y. (2002a). Modelling of simple hybrid solid oxide fuel cell and gas turbine power plant. *Journal of Power Sources*, 109, 111-120.
- Chan, S. H., Low, C. F., & Ding, O. L. (2002b). Energy and exergy analysis of simple solid-oxide fuel-cell power systems. *Journal of Power Sources*, 103(2), 188-200.

- Chan, S. H., Ho, H. K., & Tian, Y. (2003a). Multi-level modeling of SOFC–gas turbine hybrid system. *International Journal of Hydrogen Energy*, 28(8), 889-900.
- Chan, S. H., Ho, H. K., & Tian, Y. (2003b). Modelling for part-load operation of solid oxide fuel cell-gas turbine hybrid power plant. *Journal of Power Sources*, 114, 213-227.
- Chiang, I. C. (1995). Performance and emission study of a turbogenerator fueled by biodiesel, Master of Science thesis, National Tsing Hua University, Under supervision of Dr. Hsiao-Wei Chiang, Hsinchu, Taiwan.
- Chiang, H. W. D., Hong, W. T., & Lee, C. H. (2007). Microturbine performance testing with twin rotating disk regenerators. *International journal of turbo & jet engines*, 24 (3-4), 149-160.
- Chiang, H. W. D., Chiang, I.C., & Li, H. L. (2009). Microturbine performance testing using biodiesel. *International journal of turbo & jet engines*, 26 (2), 168-178.
- Colpan, C. O., Dincer, I., & Hamdullahpur, F. (2008). A review on macro-elevel modeling of planar solid oxide fuel cells. *International Journal of Energy Research*, 32, 336-355.
- Connelly, L., & Koshland, C. P. (2001). Exergy and industrial ecology, Part 2: a non-dimensional analysis of means to reduce resource depletion. *International Journal Exergy*, 1, 234–255.
- Costamagna, P., Magistri, L., & Massardo, A. F. (2001). Design and part-load performance of a hybrid system based on a solid oxide fuel cell reactor and a micro gas turbine. *Journal of Power Sources*, 96, 352-368.
- Costamagna, P., Selimovic, A., Del Borghi, M., & Agnew, G. (2004). Electrochemical model of the Integrated Planar Solid Oxide Fuel Cell (IP-SOFC). *Chemical Engineering Journal*, 102(1), 61-69.
- Cunel, C., Pangalis, M. G., & Martinez-Botas, R. F. (2002). Integration of solid oxide fuel cells into gas turbine power generation cycles. Part 2: hybrid model for various integration schemes. *Proceedings of the Institution of Mechanical Engineers, Part A: Journal of Power and Energy*, 216, 145-154.
- Danckwerts, P.V., & Sharma, M.M. (1966). The absorption of Carbon Dioxide into solutions of alkalis and amines, *The Chemical Engineer*, 37, 244-280.
- Dicks, A. L., Pointon, K. D., & Siddle, A. (2000). Intrinsic reaction kinetics of methane steam reforming on a nickel/zirconia anode. *Journal of Power Sources*, 86(1-2), 523-530.
- Dincer, I., & Rosen, M. A. (2004). Exergy as a driver for achieving sustainability. *International Journal of Green Energy*, 1, 1–19.
- Dokiya, M. (2002). SOFC system and technology. *Solid State Ion*, 152-153, 383–392.
- Donitz, W., Erdle, E., Schafer, W., Schamm, R., & Spah, R. (1991). *Status of SOFC development at dornier*. Proceeding of 2nd international on SOFCs, Athens, Greece.
- Dunbar, W. R., & Gaggioli, R. A. (1988). *Computer simulation of solid electrolyte fuel cells*. Proceedings of the 23rd Intersociety Energy Conversion Engineering Conference. Denver, USA.

- Dunbar, W. R., Lior, N., & Gaggioli, R. (1990). Exergetic advantages of topping rankine power cycles with fuel cell units. *American Society of Mechanical Engineers, Advanced Energy Systems Division (AES)*, 21, 63-68.
- Dunbar, W. R., Lior, N., & Gaggioli, R. (1991). Combining fuel cells with fuel-fired power plants for improved exergy efficiency. *Energy (Oxford)*, 16, 1259-1274.
- Dunbar, W. R., Lior, N., & Gaggioli, R. (1993). Effect of the fuel-cell unit size on the efficiency of a fuel-cell-topped Rankine power cycle. *Journal of Energy Resources Technology*, 115, 105-107.
- Ellis, M. W., & Burak Gunes, M. (2003). Evaluation of energy, environmental, and economic characteristics of fuel cell combined heat and power systems for residential applications. *Journal of Energy Resources Technology*, 125, 208-220.
- Elseviers, W. F., Van, M. T., Van, D. V. M. J. F., & Verelst, H. (1996). Thermodynamic simulations of lignite-fired IGCC with in situ desulfurization and CO<sub>2</sub> capture. *Fuel*, 75(12), 1449-1456.
- El-Wakil, M.M. (2002). *Powerplant technolog*, U.S.A.: The McGraw-Hill Companies, Inc.
- Environment Canada. (1997). Electricity generation greenhouse gas emissions data- Canada (unpublished Excel file). Greenhouse Gas Division Environment Canada, Canada.
- Environment Canada. (2005). *Canada's greenhouse gas inventory 1990–2003*. Greenhouse Gas Division Environment Canada, Canada.
- Environment Canada. (2006). *Canada's greenhouse gas inventory 1990–2004*. Greenhouse Gas Division Environment Canada, Canada.
- Environment Canada. (2008). *Canada's greenhouse gas inventory 1990–2006*. Greenhouse Gas Division Environment Canada, Canada.
- EU climate package explained. (2009). In BBC. Retrieved April 09, 2010, from <http://news.bbc.co.uk/2/hi/europe/7765094.stm>
- Finnerty, C., Tompsett, G. A., Kendall, K., & Ormerod, R. M. (2000). SOFC system with integrated catalytic fuel processing. *Journal of Power Sources*, 86(1), 459-463.
- Fontell, E., Kivisaari, T., Christiansen, N., Hansen, J. B., & Pålsson, J. (2004). Conceptual study of a 250kW planar SOFC system for CHP application. *Journal of Power Sources*, 131, 49-56.
- Franzoni, A., Magistri, L., Traverso, A., & Massardo, A. F. (2008). Thermoeconomic analysis of pressurized hybrid SOFC systems with CO<sub>2</sub> separation. *Energy*, 33, 311-320.
- Freeh, J. E., Pratt, J. W., & Brouwer, J. (2004). *Development of a solid oxide fuel cell/gas turbine hybrid system model for aerospace applications*. Turbo Expo, Vienna, Austria.
- Freeh, J. E., Steffen, Jr. C. J., & Larosiliere, L. M. (2005). *Off-design performance analysis of a solid-oxide fuel cell/gas turbine hybrid for auxiliary aerospace power*. Proceedings of the 3rd International Conference on Fuel Cell Science. Ypsilanti, United States.
- Fuel Cell Handbook (7th ed.). (2004). *EG&G Technical Services, Inc.* Prepared for the US Department of Energy, Office of Fossil Energy, Morgantown, WV.

- Gale, J. (2002). *Overview of sources, potential, transport and geographical distribution of storage possibilities*, IPCC Workshop on Carbon Capture and Storage, Regina, Canada, 15–29.
- Ghezel-Ayagh, H., Lukas, M. D., & Junker, S. T. (2004). Dynamic modeling and simulation of a hybrid fuel cell/gas turbine power plant for control system development. *Fuel Cell Science, Engineering and Technology*, 325-329.
- Gopalan, S., & DiGiuseppe, G. (2003). Fuel sensitivity test in tubular solid oxide fuel cells. *Journal of Power Sources*, 125, 183-188.
- Granovskii, M., Dincer, I., & Rosen, M. A. (2007a). Performance comparison of two combined SOFC–gas turbine systems. *Journal of Power Sources*, 165, 307-314.
- Granovskii, M., Dincer, I., & Rosen, M. A. (2007b). *Exergetic performance analysis of a gas turbine cycle integrated with solid oxide fuel cells*. Proceedings of the Energy Sustainability Conference. Long Beach, United States.
- Granovskii, M., Dincer, I., & Rosen, M. A. (2008). Exergy and industrial ecology: an application to an integrated energy system. *International Journal Exergy*, 5, 52–63.
- Graven, W. M., & F. J. Long. (1954). Kinetics and mechanisms of the two opposing reactions of the equilibrium  $\text{CO} + \text{H}_2\text{O} = \text{CO}_2 + \text{H}_2$ . *Journal of the American Chemical Society*, 76, 2602–2607.
- Haberman, B.A., & Young, J.B. (2006). Diffusion and chemical reaction in the porous structures of solid oxide fuel cells. *Journal of Fuel Cell Science and Technology*, 3(3), 312-21.
- Haraldsson, K., & Wipke, K. (2004). Evaluating PEM fuel cell system models. *Journal of Power Sources*, 126, 88-97.
- Harvey, S. P., & Richter, H. J. (1993). Improved gas turbine power plant efficiency by use of recycled exhaust gases and fuel cell technology. *American Society of Mechanical Engineers, Advanced Energy Systems Division (AES)*, 30, 199-207.
- Harvey, S. P., & Richter, H. J. (1994a). Gas turbine cycles with solid oxide fuel cells. Part I: Improved gas turbine power plant efficiency by use of recycled exhaust gases and fuel cell technology. *Journal of Energy Resources Technology*, 116, 305-311.
- Harvey, S. P., & Richter, H. J. (1994b). Gas turbine cycles with solid oxide fuel cells. Part II: A detailed study of a gas turbine cycle with an integrated internal reforming solid oxide fuel cell. *Journal of Energy Resources Technology*, 116, 312-318.
- Hengyong, T., & Stimming, U. (2004). Advances aging mechanisms and lifetime in solid-oxide fuel cells. *Journal of Power Sources*, 127, 284-293.
- Hoogers, G. (2002). *Fuel Cell Technology Handbook*. New York: CRC Press.
- Hussain, M. M., Dincer, I., & Li, X. (2004). *Energy and exergy analysis of an integrated SOFC power system*. CSME 2004 Forum 10.
- IEA (International Energy Agency). (2000). *Leading options for the capture of CO<sub>2</sub> emissions at power stations*. IEA Greenhouse Gas R&D Programme, UK.
- IEA (International Energy Agency). (2003). *Potential for improvements in gasification combined cycle power generation with CO<sub>2</sub> capture*. IEA Greenhouse Gas R&D Programme, UK.
- IEA. (2003b). *Energy technology: facing the climate challenge*. IEA Governing Board.



- IEA. (2003c). CO<sub>2</sub> Capture at power stations and other major point sources. *Working party on fossil fuels international energy agency, zero emissions technologies for fossil fuel*.
- IEA (International Energy Agency). (2004). *Improvements in power generation with post-combustion capture of CO<sub>2</sub>*. IEA Greenhouse Gas R&D Programme, UK.
- IEA (International Energy Agency). (2005). *World Energy Outlook 2005: Middle East and North Africa Insights*. IEA, Paris, France.
- IEA (International Energy Agency). (2006). *World Energy Outlook 2006*. IEA, Paris, France.
- Inui, Y., Yanagisawa, S., & Ishida, T. (2003). Proposal of high performance SOFC combined power generation system with carbon dioxide recovery. *Energy Conversion and Management*, 44, 597-609.
- Iora, P., & Campanari, S. (2007). Development of a three-dimensional molten carbonate fuel cell model and application hybrid cycle simulations. *Journal of Fuel Cell Science and Technology*, 4, 501-510.
- IPCC (Intergovernmental Panel on Climate Change). (1996). *Scientific assessments: consideration of the second assessment report of the intergovernmental panel on climate change*. Working group I of the IPCC, Geneva, Switzerland.
- IPCC (Intergovernmental Panel on Climate Change). (1997). *Revised 1996 IPCC guidelines for national greenhouse inventories*. IPCC, Paris, France.
- IPCC (Intergovernmental Panel on Climate Change). (2005). *IPCC special report on carbon dioxide capture and storage*. Working Group III of the Intergovernmental Panel on Climate Change, Cambridge University Press, UK.
- IPCC (Intergovernmental Panel on Climate Change). (2006). IPCC guidelines for national greenhouse gas inventories (2006)-Energy (vol. 2). IPCC, The National Greenhouse Gas Inventories Programme, Hayama, Japan.
- IPCC (Intergovernmental Panel on Climate Change). (2007a). *Climate Change 2007: Synthesis Report, An assessment of the Intergovernmental Panel on Climate Change*. IPCC, UK.
- IPCC (Intergovernmental Panel on Climate Change). (2007b). Highlights from Climate Change 2007: The Physical Science Basis, Summary for Policy Makers, Contribution of Working Group I to the Fourth Assessment Report of the Intergovernmental Panel on Climate Change. In *pewclimate*. Retrieved May 01, 2011, from <http://www.pewclimate.org/docUploads/Pew%20Summary%20of%20IPCC%20WGI%2020207.pdf>.
- Iran Power Generation Co. (2007). *Detailed statistic of Iran's electricity industry (2005 and 06)*. Second Volume, Electricity Generation Sector, Iran Power Generation, Transmission, Distribution, Management Co. Tehran, Iran.
- Jansen, D., van der Laag, P. C., Oudhuis, A. B. J., & Ribberink, J. S. (1994). Prospects for advanced coal-fuelled fuel cell power plants. *Journal of Power Sources*, 49, 151-165.

Japan vows big climate change cut. (2009). In BBC. Retrieved April 09, 2010, from <http://news.bbc.co.uk/2/hi/science/nature/8241016.stm>.

Jiang, W., Fang, R., Dougal, R. A., & Khan, J. A. (2008). Thermoelectric model of a tubular SOFC for dynamic simulation. *Journal of Energy Resources Technology, Transactions of the ASME*, 130(2), 0226011-02260110.

Judkoff, R. D., & Neymark, J. S. (1995). Procedure for testing the ability of whole building energy simulation programs to thermally model the building fabric. *Journal of Solar Energy Engineering*, 117, 7-15.

Kakac, S., Pramuanjaroenkij, A., & Zhou, X. Y. (2007). A review of numerical modeling of solid oxide fuel cells. *International Journal of Hydrogen Energy*, 32, 761-786.

Karra, P. K., Veltman, M. K., & Kong, S. C. (2008). Characteristics of engine emissions using biodiesel blends in low-temperature combustion regimes. *Energy and Fuels*, 22 (6), 3763-3770.

Kather, A., Mieske, K., Hermsdorf, C., Klostermann, M., Eggers, R., & Kopke, D. (2007). Oxyfuel process for hard-coal power plants with CO<sub>2</sub> removal, *Clean Air*, 8(3), 273-286.

Kee, R. J., Zhu, H., Sureshini, A. M., & Jackson, G. S. (2008) Solid oxide fuel cells: operating principles, current challenges, and the role of syngas. *Combustion Science and Technology*, 180 (6), 1207 – 1244.

Kemm, M., Hildebrandt, A., & Assadi, M. (2004). *Operation and performance limitations for solid oxide fuel cells and gas turbines in a hybrid system*. Proceedings of the ASME Turbo Expo. Vienna, Austria.

Kim, J., Lee, S. M., Srinivasan, S., & Chamberlin, C. E. (1995). Modeling of proton exchange membrane fuel cell performance with an empirical equation. *Journal of the Electrochemical Society*, 142(8), 2670-2674.

Kikuchi, R., & Eguchi, K. (2004). Solid oxide fuel cell as a multi-fuel applicable power generation device. *Journal of Japan petroleum institute*, 47(4), 225-238.

Kimijima, S., & Kasagi, N. (2002). *Performance evaluation of gas turbine-fuel cell hybrid micro generation system*. Proceedings of the ASME TURBO Expo. Amsterdam, Netherlands.

Kivisaari, T., Björnbohm, P., Sylwan, C., Jacquinet, B., Jansen, D., & de Groot, A. (2004). The feasibility of a coal gasifier combined with a high-temperature fuel cell. *Chemical Engineering Journal*, 100, 167-180.

Kuchonthara, P., Bhattacharya, S., & Tsutsumi, A. (2003a). Energy recuperation in solid oxide fuel cell (SOFC) and gas turbine (GT) combined system. *Journal of Power Sources*, 117, 7-13.

Kuchonthara, P., Bhattacharya, S., & Tsutsumi, A. (2003b). Combinations of solid oxide fuel cell and several enhanced gas turbine cycles. *Journal of Power Sources*, 124, 65-75.

Kuchonthara, P., Bhattacharya, S., & Tsutsumi, A. (2005). Combination of thermochemical recuperative coal gasification cycle and fuel cell for power generation. *Fuel*, 84, 1019-1021.

Lai, W. H., Hsiao, C. A., Lee, C. H., Chyou, Y. P., & Tsai, Y. C. (2007). Experimental simulation on the integration of solid oxide fuel cell and micro-turbine generation system. *Journal of Power Sources*, 171, 130-139.

- Larminie, J., & Dicks, A. (2003). *Fuel cell systems explained* (2nd Edition). England: John Wiley & Sons Ltd.
- Lazzaretto, A., Toffolo, A., & Zanon, F. (2004). Parameter setting for a tubular SOFC simulation model. *Transactions of the ASME. Journal of Energy Resources Technology*, 126(1), 40-46.
- Li, X. (2006). *Principles of Fuel Cells*. Great Britain: Taylor & Francis Group.
- Li, C. H. (2010). Performance and emission study of a turbogenerator fueled by biodiesel, Master of Science thesis, National Tsing Hua University, Under supervision of Dr. Hsiao-Wei Chiang, Hsinchu, Taiwan.
- Lin, P. H., & Hong, C. W. (2006). On the start-up transient simulation of a turbo fuel cell system. *Journal of Power Sources*, 160, 1230-1241.
- Lobachyov, K., & Richter, H. J. (1996). Combined cycle gas turbine power plant with coal gasification and solid oxide fuel cell. *Journal of Energy Resources Technology*, 118, 285-292.
- Lundberg, W. L., Veyo, S. E., & Moeckel, M. D. (2003). A high-efficiency solid oxide fuel cell hybrid power system using the Mercury 50 advanced turbine systems gas turbine. *Journal of Engineering for Gas Turbines and Power*, 125, 51-58.
- Magistri, L., Bozzo, R., Costamagna, P., & Massardo, A. F. (2004). Simplified versus detailed solid oxide fuel cell reactor models and influence on the simulation of the design point performance of hybrid systems. *Journal of Engineering for Gas Turbines and Power*, 126, 516-523.
- Magistri, L., Traverso, A., Cerutti, F., Bozzolo, M., Costamagna, P., & Massardo, A. F. (2005). Modelling of pressurised hybrid systems based on integrated planar solid oxide fuel cell (IP-SOFC) technology. *Fuel Cells*, 5, 80-96.
- Massardo, A. F., & Lubelli, F. (2000). Internal reforming solid oxide fuel cell- gas turbine combined cycles (IRSOFC-GT): Part A- Cell model and cycle thermodynamic analysis. *Journal of Engineering for Gas Turbines and Power*, 122, 27-35.
- Massardo, A. F., & Bosio, B. (2002). Assessment of molten carbonate fuel cell models and integration with gas and steam cycles. *Journal of Engineering for Gas Turbines and Power*, 124, 103-109.
- Matsuzaki, Y., & Yasuda, I. (2000). Electrochemical oxidation of H<sub>2</sub> and CO in a H<sub>2</sub>-H<sub>2</sub>O-CO-CO<sub>2</sub> system at the interface of a Ni-YSZ cermet electrode and YSZ electrolyte. *Journal of the Electrochemical Society*, 147(5), 1630-1635.
- Mench, M. M. (2008). *Fuel Cell Engine*. New Jersey: John Wiley & Sons, Inc.
- Metz, B., Davidson, O., de Coninck, H. C., Loos, M., & Meyer, L. A. (2005). *IPCC Special report on carbon dioxide capture and storage*. Working Group III of the Intergovernmental Panel on Climate Change. Cambridge University Press, UK.
- MHI achieves Japan's first SOFC-MGT combined-cycle power generation. (2006). In MHI. Retrieved December 20, 2010, from <http://www.mhi.co.jp/en/news/sec1/200608041128.html>
- Möller, B. F., Arriagada, J., Assadi, M., & Potts, I. (2004). Optimisation of an SOFC/GT system with CO<sub>2</sub>-capture. *Journal of Power Sources*, 131, 320-326.

- Moran, M. J., & Shapiro, H. N. (2004). *Fundamentals of engineering thermodynamics*. 5<sup>th</sup> edition, John Wiley & Sons, Inc., USA.
- Mueller, F., Jabbari, F., Brouwer, J., Roberts, R., Junker, T., & Ghezel-Ayagh, H. (2007). Control design for a bottoming solid oxide fuel cell gas turbine hybrid system. *Journal of Fuel Cell Science and Technology*, 4, 221-230.
- Na, J. I., Park, S. J., Kim, Y. K., Lee, J. G., & Kim, J. H. (2003). Characteristics of oxygen-blown gasification for combustible waste in a fixed-bed gasifier. *Applied Energy*, 75, 275-285.
- Natural gas prices – historical and forecast. (2009). In Energy shop. Retrieved April 09, 2010, from <http://www.energyshop.com/es/homes/gas/gaspriceforecast.cfm?>
- Noren, D. A., & Hoffman, M. A. (2005). Clarifying the Butler-Volmer equation and related approximations for calculating activation losses in solid oxide fuel cell models. *Journal of Power Sources*, 152, 175-181.
- Nsakala, N., Liljedahl, G., Marion, J., Bozzuto, C., Andrus, H., & Chamberland, R. (2003). *Greenhouse gas emissions control by oxygen firing in circulating fluidised bed boilers*. Proceedings of Second National Conference on Carbon Sequestration, USA, 1–21.
- NRC (Natural Resources Canada). (2006). *Canada's Energy Outlook: The Reference Case 2006*. Canada.
- OAG (Office of the Auditor General of Canada). (2006). *Report of the Commissioner of the Environment and Sustainable Development*. Canada.
- Obama vows greenhouse gas emissions cuts. (2009). In BBC. Retrieved April 09, 2010, from <http://news.bbc.co.uk/2/hi/8378890.stm/>
- Obara, S., & Kudo, K. (2005). Study of a small-scale fuel cell cogeneration system with methanol steam reforming considering partial load and load fluctuation. *Journal of Energy Resources Technology*, 127, 265-271.
- Omosun, A. O., Bauen, A., Brandon, N. P., Adjiman, C. S., & Hart, D. (2004). Modeling system efficiencies and costs of two biomass-fuelled SOFC systems. *Journal of Power Sources*. 131, 96-106.
- Padulle's, J., Ault, G. W., & McDonald, J. R. (2000). An integrated SOFC plant dynamic model for power systems simulation. *Journal of Power Sources*, 86, 495-500.
- Palsson, J., Selimovic, A., & Sjunnesson, L. (2000). Combined solid oxide fuel cell and gas turbine systems for efficient power and heat generation. *Journal of Power Sources*, 86, 442-448.
- Pangalis, M. G., Martinez-Botas, R. F., & Brandon, P. (2002). Integration of solid oxide fuel cells into gas turbine power generation cycles. Part 1: fuel cell thermodynamic modelling. *Journal of Power and Energy*, 216, 129-144.
- Parsons, E. L., Shelton, W. W., & Lyons, J. L. (2002). *Advanced fossil power systems comparison study*, Final Report Prepared for NETL, USA.

- Peters, R., Riensche, E., & Cremer, P. (2000). Pre-reforming of natural gas in solid oxide fuel-cell systems. *Journal of Power Sources*, 86(1-2), 432-441.
- Peters, R., Dahl, R., Kluttgen, U., Palm, C., & Stolten, D. (2002). Internal reforming of methane in solid oxide fuel cell systems. *Journal of Power Sources*, 106(1-2), 238-244.
- Petruzzi, L., Cocchi, S., & Fineschi, F. (2003). A global thermo-electrochemical model for SOFC systems design and engineering. *Journal of Power Sources*, 118(1-2), 96-107.
- Pfafferodt, M., Heidebrecht, P., Stelter, M., & Sundmacher K. (2005). Model-based prediction of suitable operating range of a SOFC for an Auxiliary Power Unit. *Journal of Power Sources*, 149, 53-62.
- Popovic, P. (2002). Integration of microturbine with single-effect exhaust-driven absorption chiller and solid wheel desiccant system. *ASHRAE Transactions*, 108 (2), 660-669.
- Raak, H., Diethelm, R., & Riggensbach, S. (2002). *The Sulzer Hexis story: from demonstrators to commercial products*. Proceedings of the Fuel Cell World. Lucerne, Switzerland.
- Rajashekara, K. (2005). Hybrid fuel-cell strategies for clean power generation. *IEEE Transactions on Industry Applications*, 41, 682-689.
- Rao, A. B., & Rubin, E. S. (2002). A technical, economic, and environmental assessment of amine-based CO<sub>2</sub> capture technology for power plant greenhouse gas control. *Environmental Science and Technology*, 36, 4467-4475.
- Rao, A. D., & Samuelsen, G. S. (2003). A thermodynamic analysis of tubular solid oxide fuel cell based hybrid systems. *Journal of Engineering for Gas Turbines and Power*, 125, 59-66.
- Rao, A. D., Verma, A., & Samuelsen, G. S. (2005). *Engineering and economic analyses of a coal-fueled solid oxide fuel cell hybrid power plant*. Proceedings of the ASME Turbo Expo. Reno-Tahoe, United States.
- Ratafia-Brown, J. A., Manfredo, L. M., Hoffmann, J. M., Ramezan, M., & Stiegel, G. J. (2002). *An environmental assessment of IGCC power systems*, Proceedings of Nineteenth Annual Pittsburgh Coal Conference, USA, 1-16.
- Riahi, K., Rubin, E. S., & Schrattenholzer, L. (2003). *Prospects for carbon capture and sequestration technologies assuming their technological learning*. Proceedings of 6th International Greenhouse Gas Control Technologies, Kyoto, Japan.
- Riensche, E., & Fedders, H. (1993). *Parameter study on SOFC plant operation for combined heat and power generation*. Proceedings of SOFC International Symposium, Honolulu.
- Riensche, E., Stimming, U., & Unverzagt, G. (1998a). Optimization of a 200 kW SOFC cogeneration power plant Part I: Variation of process parameters. *Journal of Power Sources*, 73, 251-256.
- Riensche, E., Meusinger, J., Stimming, U., & Unverzagt, G. (1998b). Optimization of a 200 kW SOFC cogeneration power plant Part II: Variation of the flowsheet. *Journal of Power Sources*, 71, 306-314.
- Riensche, E., Achenbach, E., Froning, D., Haines, M. R., Heidug, W. K., Lokurlu, A., & von Andrian, S. (2000). Clean combined-cycle SOFC power plant — cell modelling and process analysis. *Journal of Power Sources*, 86, 404-410.

- Roberts, R., Brouwer, J., Jabbari, F., Junker, T., & Ghezel-Ayagh, H. (2006). Control design of an atmospheric solid oxide fuel cell/gas turbine hybrid system: Variable versus fixed speed gas turbine operation. *Journal of Power Sources*, 161, 484-491.
- Rubin, E. S., Chen, C., & Rao, A. B. (2007). Cost and performance of fossil fuel power plants with CO<sub>2</sub> capture and storage. *Energy Policy*, 35, 4444-4454.
- Rubin, E. S., Rao, A. B., & Chen, C. (2005). *Comparative assessments of fossil fuel power plants with CO<sub>2</sub> capture and storage*. Proceedings of 7<sup>th</sup> International Conference on Greenhouse Gas Control Technologies, UK, 1-9.
- Selimovic, A., & Palsson, J. (2002). Networked solid oxide fuel cell stacks combined with a gas turbine cycle. *Journal of Power Sources*, 106, 76-82.
- Senatore, A., Cardone, M., Rocco, V., & Prati, M. V. (2000). A comparative analysis of combustion process in DI diesel engine fueled with biodiesel and diesel fuel. SAE Tech. Pap. Ser. 2000-01-0691.
- Shimada, T., Kato, T., & Tanaka, Y. (2007). Numerical analysis of thermal behavior of small solid oxide fuel cell systems. *Journal of Fuel Cell Science and Technology*, 4, 299-307.
- Sieros, G., & Papailiou, K. D. (2007). *Gas turbine components optimised for use in hybrid SOFC-GT systems*. Proceedings of 7th European conference on turbomachinery fluid dynamics and thermodynamics. Athens, Greece.
- Siemens. (2010) The principle behind the technology. Retrieved December 20, 2010, from <http://www.energy.siemens.com/fi/en/power-generation/fuel-cells/principle-behind-technology.htm#content=Operation%20Principle/>
- Simbeck, D. R. (2002). *New power plant CO<sub>2</sub> mitigation costs*. USA.
- Singhal, S. C. (2000a). Advances in solid oxide fuel cell technology. *Solid State Ionics*, 135, 305-313.
- Singhal, S. C. (2000b). Science and technology of solid oxide fuel cells. *MRS Bulletin*, 25, 16-21.
- Singhal, S. C. (2002). Solid oxide fuel cells for stationary, mobile, and military applications. *Solid State Ionics*, 152-153, 405-410.
- Singhal, S. C., & Kendall, K. (2003). *High temperature solid oxide fuel cell, fundamental, design and applications*, UK: Elsevier.
- Song, T. W., Sohn, J. L., Kim, J. H., Kim, T. S., Ro, S. T., & Suzuki, K. (2005). Performance analysis of a tubular solid oxide fuel cell/micro gas turbine hybrid power system based on a quasi-two dimensional model. *Journal of Power Sources*, 142, 30-42.
- Song, T. W., Sohn, J. L., Kim, T. S., & Ro, S. T. (2006). Performance characteristics of a MW-class SOFC/GT hybrid system based on a commercially available gas turbine. *Journal of Power Sources*, 158, 361-367.
- Sousa, J. R., & Gonzalez, E. R. (2005). Mathematical modeling of polymer electrolyte fuel cells. *Journal of Power Sources*, 147, 32-45.

Spath, P.L., & Mann, M.K. (2000). *Life cycle assessment of a natural gas combined – cycle power generation system*. National Renewable Energy Laboratory (NREL), Department of Energy Laboratory, USA.

Status of Ratification of the Kyoto Protocol. (2010). In UNFCCC. Retrieved April 09, 2010, from [http://unfccc.int/kyoto\\_protocol/background/status\\_of\\_ratification/items/2613.php](http://unfccc.int/kyoto_protocol/background/status_of_ratification/items/2613.php)

Steffen, Jr. C. J., Freeh, J. E., & Larosiliere, L. M. (2005). *Solid oxide fuel cell/gas turbine hybrid cycle technology for auxiliary aerospace power*. Proceedings of the ASME Turbo Expo. Reno-Tahoe, United States.

Stiller, C., Thorud, B., Seljeb, S., Mathisen, O., Karoliussen, H., & Bolland, O. (2005). Finite-volume modeling and hybrid-cycle performance of planar and tubular solid oxide fuel cells. *Journal of Power Sources*, 141, 227-240.

Stiller, C., Thorud, B., Bolland, O., Kandepu, R., & Imsland, L. (2006a). Control strategy for a solid oxide fuel cell and gas turbine hybrid system. *Journal of Power Sources*, 158, 303-315.

Stiller, C., Thorud, B., & Bolland, O. (2006b). Safe dynamic operation of a simple SOFC/GT hybrid system. *Journal of Engineering for Gas Turbines and Power*, 128, 551-559.

Stiller, C., Thorud, B., & Bolland, O. (2006c). *Shutdown and startup of a SOFC/GT hybrid system*. Proceedings of 4th International ASME Conference on Fuel Cell Science. Irvine, United States.

Stobbs, R., & Clark, P. (2005). *Canadian clean power coalition: the evaluation of options for CO<sub>2</sub> capture from existing and new coal-fired power plants*. Proceedings of 7th International Conference on Greenhouse Gas Control Technologies, UK, 1–4.

Sucipta, M., Kimijima, S., & Suzuki, K. (2007). Performance analysis of the SOFC–MGT hybrid system with gasified biomass fuel. *Journal of Power Sources*, 174, 124-135.

Sucipta, M., Kimijima, S., & Suzuki, K. (2008a). Solid oxide fuel cell-micro gas turbine hybrid system using natural gas mixed with biomass gasified fuel. *Journal of the Electrochemical Society*, 155(3), B258-63.

Sucipta, M., Kimijima, S., Song, T. W., & Suzuki, K. (2008b). Biomass solid oxide fuel cell-microgas turbine hybrid system: Effect of fuel composition. *Journal of Fuel Cell Science and Technology*, 5, 1-8.

Suther, T. (2006). *Simulation of a solid oxide fuel cell-gas turbine system using Aspen plus*. Master of Applied Science thesis, Dalhousie University.

Suther, T., Fung, A. S., Koksai, M., & Zabihian, F., (2010a). Macro level modeling of a tubular solid oxide fuel cell. *Sustainability*, 2(11), 3549-3560.

Suther, T., Fung, A. S., Koksai, M., & Zabihian, F. (2010b). Effects of operating and design parameters on the performance of a solid oxide fuel cell-gas turbine system. *International Journal of Energy Research*, Articles online in advance of print.

Suwanwarangkul, R., Croiset, E., Pritzker, M. D., Fowler, M. W., Douglas, P. L., & Entchev, E. (2006). Mechanistic modelling of a cathode-supported tubular solid oxide fuel cell, *Journal of Power Sources*, 154(1), 74-85.



Tanaka, K., Wen, C., & Yamada, K. (2000). Design and evaluation of combined cycle system with solid oxide fuel cell and gas turbine. *Fuel*, 79, 1493-1507.

Tao, W. Q., Min, C. H., Liu, X. L., He, Y. L., Yin, B. H., & Jiang, W. (2006). Parameter sensitivity examination and discussion of PEM fuel cell simulation model validation. Part I. Current status of modeling research and model development. *Journal of Power Sources*, 160, 359-373.

The world factbook: Canada. (n.d.). In the work of a nation. Retrieved April 09, 2010, from <https://www.cia.gov/library/publications/the-world-factbook/geos/ca.html>

The world factbook: Iran. (n.d.). In the work of a nation. Retrieved April 09, 2010, from <https://www.cia.gov/library/publications/the-world-factbook/geos/ir.html>

Topper, J. (2006). *IEA energy technology day coal fired power and efficiency*. IEA Clean Coal Centre, New York.

Tucker, D., Lawson, L., & Gemmen, R. (2005). *Characterization of air flow management and control in a fuel cell turbine hybrid power system using hardware simulation*. Proceedings of the ASME Power Conference. Chicago, United States.

UNFCCC (United Nations Framework Convention on Climate Change). (1992). *The United Nations Framework Convention on Climate Change (Article 2)*. Japan.

UNFCCC (United Nations Framework Convention on Climate Change). (1998). *Kyoto Protocol to the United Nations Framework Convention on Climate Change (UNFCCC)*. Japan.

UNFCCC (United Nations Framework Convention on Climate Change). (2009). Copenhagen Accord, In UNFCCC. Retrieved April 09, 2010, from <http://unfccc.int/resource/docs/2009/cop15/eng/l07.pdf>.

U.S. Department of Energy. (2000). *Advanced microturbine systems, Program plan for fiscal years 2000 through 2006*. U.S.A.

Van Der Drift, A., Van Doorn, J., & Vermeulen, J. W. (2001). Ten residual biomass fuels for circulating fluidized-bed gasification. *Biomass and Bioenergy*, 20, 45-56.

Van herle, J., Marechal, F., Leuenberger, S., & Favrat, D. (2003). Energy balance model of a SOFC cogenerator operated with biogas. *Journal of Power Sources*, 118, 375-383.

Van herle, J., Marechal, F., Leuenberger, S., Membrez, Y., Bucheli, O., & Favrat, D. (2004). Process flow model of solid oxide fuel cell system supplied with sewage biogas. *Journal of Power Source*, 131, 127-141.

Versteeg, G. F., Van Dijck, L. A. J., & Van Swaaij, W. P. M. (1996). On the kinetics between CO<sub>2</sub> and alkanolamines both in aqueous and non-aqueous solutions. *An overview, Chemical Engineering Community*, 144, 113-158.

Veyo, S. E., Shockling, L. A., Dederer, J. T., Gillett, J. E., & Lundberg, W. L. (2002a). Tubular solid oxide fuel cell/gas turbine hybrid cycle power systems: Status. *Journal of Engineering for Gas Turbines and Power*, 124, 845-849.



- Veyo, S. E., Vora, S. D., Litzinger, K. P., & Lundberg, W. L. (2002b). *Status of pressurized SOFC/GAS turbine power system development at Siemens Westinghouse*. Proceedings of the ASME Turbo Expo. Amsterdam, Netherlands, 823–829.
- Vielstich, W., Gasteiger, H. A., & Lamm, A. (2003). *Handbook of Fuel Cells – Fundamentals, Technology and Applications. Volume 1: Fundamentals and Survey of Systems*. John Wiley & Sons.
- Wang, C. Y. (2004). Fundamental models for fuel cell engineering. *Chemical Reviews*, 104, 4727-4765.
- Wang, P. Y. (2007). *Combined cycle power augmentation study*, PhD thesis, National Tsing Hua University, Taiwan.
- WECD (World Commission on Environment and Development). (1987). Our Common Future, Chapter 2: Towards Sustainable Development. In UN Documents, UN Documents. Retrieved May 01, 2011, from <http://www.un-documents.net/ocf-02.htm#III.4>.
- Where countries stand on Copenhagen. (2009). In British Broadcasting Corporation (BBC). Retrieved April 09, 2010, from <http://news.bbc.co.uk/2/hi/science/nature/8345343.stm>
- Williams, M. C., Strakey, J. P., Surdoval, W. A., & Wilson, L. C. (2006). Solid oxide fuel cell technology development in the USA, *Solid State Ionics*, 177, 2039-2044.
- Winkler, W., & Lorenz., H. (2002). The design of stationary and mobile solid oxide fuel cell-gas turbine systems. *Journal of Power Sources*, 105, 222-227.
- Winkler, W., Nehter, P., Williams, M. C., Tucker, D., & Gemmen R. (2006). General fuel cell hybrid synergies and hybrid system testing status. *Journal of Power Sources*, 159, 656-666.
- Yakabe, H., Ogiwara, T., Hishinuma, M., & Yasuda, I. (2001). 3-D model calculation for planar SOFC. *Journal of Power Sources*, 102(1-2), 144-154.
- Yi, Y., Rao, A. D., Brouwer, J., & Samuelsen, G. S. (2004). Analysis and optimization of a solid oxide fuel cell and intercooled gas turbine (SOFC-ICGT) hybrid cycle. *Journal of Power Sources*, 132, 77-85.
- Young, J. B. (2007). Thermofluid modeling of fuel cells. *Annual Review of Fluid Mechanics*, 39, 193-215.
- Zabihian, F., Fung, A., Koksai, M., Malek, S., & Elhebshi, M. (2008). *Sensitivity analysis of a SOFC-GT based power cycle*. Proceedings of the 6th ASME Fuel Cell Conference. Denver, United States.
- Zhang, X., Li, J., Li, G., & Feng, Z. (2006). Dynamic modeling of a hybrid system of the solid oxide fuel cell and recuperative gas turbine. *Journal of Power Sources*, 163, 523-531.
- Zhu, Y., & Tomsovic, K. (2002). Development of models for analyzing the load-following performance of microturbines and fuel cells. *Electric Power Systems Research*, 62, 1-11.